University of Southampton

Faculty of Medicine

Clinical and Experimental Sciences

The role of extracellular vesicle miRNA released in response to influenza A virus

by

Laura Reid

ORCID ID 0000-0002-9994-4639

Thesis for the degree of DOCTOR OF PHILOSOPHY

June 2023

University of Southampton

Abstract

Faculty of Medicine

Clinical and Experimental Sciences

Doctor of Philosophy

The role of extracellular vesicle miRNA released in response to influenza A virus

by

Laura Reid

Introduction: Influenza A virus (IAV) is a common respiratory pathogen that has caused millions of deaths throughout history. Airway epithelial cells are the first line of defence and primary target against IAV. Recently, airway epithelial cells have been shown to release lipid bilayer particles, termed extracellular vesicles (EVs). EVs provide a stable capsule for the transfer of biological molecules such as microRNAs (miRNAs). MiRNAs are small, non-coding regulatory RNAs that have been shown to be altered in response to respiratory stimuli, including viral infections and have recently emerged as an EV cargo with the potential as novel biomarkers and therapeutics.

Aim: This thesis investigates the hypothesis that the miRNA profile of EVs released from bronchial epithelial cells is altered in response to infection with IAV, promoting the anti-viral immune response.

Methods: IAV infection of air-liquid interface (ALI) differentiated epithelial cells was characterised by analysing the expression of antiviral genes, cell barrier permeability and cell death. EVs were isolated by filtration and size exclusion chromatography from the apical surface wash of ALI cultured bronchial epithelial cells (BCi-NS1.1). The EV miRNA profile was then sequenced, and reads were mapped to miRBase. The sequencing results were validated by RT-qPCR using healthy and COPD primary epithelial cells. Functional analyses of the miRNAs was completed by *in silico* analyses and transfection of BCi with miRNA mimics and inhibitors.

Results: Infection of ALI cultured epithelial cells with IAV at 3.6 x 10^6 IU/ml for 24 hours was determined to be a suitable condition for EV analyses due to the detection of significant upregulation of anti-viral genes without high levels of cell death or loss of barrier integrity. The presence of EVs released from ALI cultured bronchial epithelial cells was confirmed by visualisation using electron microscopy and detection of known EV markers such as CD9, CD63 and CD81 using western blot and the ExoView R100 platform. Differential expression analyses

identified 13 miRNAs that were differentially expressed between EVs released from IAV infected BCi compared to uninfected BCi (FDR <0.01). Of these 5 had a fold change of >1.5: miR-155-5p, miR-122-5p, miR-378a-3p, miR-7-5p and miR-146a-5p and 1 had a fold change of <-1.5: miR-505-5p. Differences between EV, non-EV and cellular levels of these miRNA were detected. Furthermore, the EV miRNA response to IAV was reduced for PBECs obtained from COPD patients and was altered with participant age. miRNA target prediction and functional analysis was performed using miRNet to identify biological processes and pathways that were enriched for the target genes of these miRNAs. Target genes were found to be associated with immune and damage response further suggesting that these miRNAs are involved in immune response to IAV.

Conclusion: EV miRNA may be a key mechanism in modulating the response to IAV and therefore are potential targets for future therapies. However further work to determine transfer of EV miRNA and fully characterise the function of EV miRNA in response to IAV is required.

Table of Contents

Table of Tables

Table of Figures

Research Thesis: Declaration of Authorship

Print name: Laura Reid

Title of thesis: The role of extracellular vesicle miRNA released in response to influenza A virus

I declare that this thesis and the work presented in it are my own and has been generated by me as the result of my own original research.

I confirm that:

1. This work was done wholly or mainly while in candidature for a research degree at this University;

2. Where any part of this thesis has previously been submitted for a degree or any other qualification at this University or any other institution, this has been clearly stated;

3. Where I have consulted the published work of others, this is always clearly attributed;

4. Where I have quoted from the work of others, the source is always given. With the exception of such quotations, this thesis is entirely my own work;

5. I have acknowledged all main sources of help;

6. Where the thesis is based on work done by myself jointly with others, I have made clear exactly what was done by others and what I have contributed myself;

7. Parts of this work have been published in the following:

Reid LV, Spalluto CM, Watson A, Staples KJ, Wilkinson TM. The role of extracellular vesicles as a shared disease mechanism contributing to multimorbidity in patients with COPD. Frontiers in Immunology. 2021;12.

Reid LV, Spalluto CM, Staples KJ, Wilkinson TM. Influenza infection of epithelial cells alters extracellular vesicle microRNA involved in viral replication and the immune response. ERJ Open Research Mar 2022, 8 (suppl 8) 77

Signature: ..... Date:.....

Acknowledgements

Firstly, I would like to thank my supervisors Dr Mirella Spalluto, Dr Karl Staples and Professor Tom Wilkinson for giving me the opportunity to complete such a fascinating research project and for providing essential support and guidance. Furthermore, this opportunity would not have been possible without the Medical Research Council (MRC)-funded Doctoral Training Partnership.

I would also like to thank the numerous individuals involved in ensuring the maintenance and smooth running of equipment and facilities that have been essential for the work in this thesis. Namely, I need to thank Dr.Carolann McGuire, Dr Laurie Lau, Dr.Regina Teo and Dr Anton Page.

I must thank all the participants and study staff involved in the MICA III study that provided me with valuable samples. I must also thank NanoView for their analyses of EVs using ExoView system and the team at Qiagen for completing and providing advice and support regarding the sequencing.

I would also like to thank everyone else from the Wilkinson group for their help and encouragement. Special thanks must go to Hannah Burke for her advice and support in the field of microRNA and extracellular vesicles. For both academic and emotional support, I would also like to thank Dr Jodie Ackland, Sruthymol Lukose, Lee Page, Claire Simms and Jake Weeks. It was an absolute pleasure working with all of you. Your technical help in the laboratory has been invaluable as well as providing much needed relief in the form of both academic and non-academic chats.

Of course, thanks must go to my family and friends for their love and support throughout my PhD.

Abbreviations

AAT	Alpha-1 antitrypsin
ACTB	Actin Beta
AF4	Asymmetric flow field-flow fractionation
AGO	Argonaute
ALI	Air-liquid interface
ApoE	Apolipoprotein E
B2M	Beta-2-Microglobulin
BALF	Bronchoalveolar lavage fluid
BCi-NS1.1	Immortalised human bronchial cell line generated via telomerase integration
BSA	Bovine Serum Albumin
CCL	C–C motif ligand chemokine
cDNA	Complementary DNA
COPD	Chronic obstructive pulmonary disease
CPM	Counts per million
Ct	Cycle threshold
CXCL	C-X-C motif ligand chemokine
DAMP	Damage associated molecular pattern
DPBS	Dulbecco's Phosphate Buffered Saline
EGFR	Epidermal growth factor receptor
ELISA	Enzyme-Linked Immunosorbent Assay
EV	Extracellular vesicles
FDR	False Discovery Rate
FEV1	Forced expiratory flow in 1 second
FVC	Forced vital capacity

HA	Hemagglutinin
HBSS	Hanks' Balanced Salt solution
hTERT	Telomerase reverse transcriptase
IAV	Influenza A virus
IBV	Influenza B virus
ICV	Influenza C virus
IDV	Influenza D virus
IFN	Interferon
IFITM3	IFN-induced transmembrane protein 3
IL	Interleukin
ISEV	International Society of Extracellular Vesicles
ISGs	Interferon Stimulated Genes
ISG15	Interferon Stimulated Gene 15
LDH	Lactate Dehydrogenase
lncRNA	Long noncoding RNAs
M1	Matrix protein
M2	Proton channel protein
MHC	Major histocompatibility molecules
miRBase	Mature miRNA database
miRISC	MicroRNA induced silencing complex
miRNA	MicroRNA
MOI	Multiplicity of Infection
mRNA	Messenger RNA
Mx	Myxovirus resistance protein
NA	Neuraminidase
NLR	NOD-like receptor

NLRP3	NLR family pyrin domain containing 3
NP	Nucleoprotein
NSP	Non structural protein
PAMP	Pattern-associated molecular patterns
PCA	Principal component analysis
piRNA	Piwi RNA
Pre-miRNA	Precursor microRNA
Pri-miRNA	Primary microRNA
PRR	Pattern recognition receptor
PVDF	Polyvinylidene difluoride
RdRp	RNA-dependant RNA polymerase
RNA	Ribonucleic acid
rRNA	Ribosomal RNA
RSV	Respiratory syncytial virus
RT-qPCR	Real-time quantitative polymerase chain reaction
SA	Sialic acid
SDS-PAGE	Sodium dodecyl sulphate-polyacrylamide gel electrophoresis
SEC	Size exclusion chromatography
SOCS	Suppressor of cytokine signalling
SOD2	Superoxide dismutase 2
SP-IRIS	Single particle interferometric reflectance imaging sensing
TCID50	Tissue Culture Infectious Dose required to kill 50% of cells
TEER	Trans epithelial electrical resistance

TEM	Transmission Electron Microscopy
TLR	Toll-like receptors
TMM	Trimmed Mean of M-values
TNF	Tumour Necrosis Factor
tRNA	Transfer RNA
vRNA	Viral RNA
vRNP	Viral ribonucleoprotein

1 Introduction

1.1 Influenza

1.1.1 Burden

Throughout history, the world has witnessed a series of respiratory viral outbreaks with devastating consequences to human life. These outbreaks are due to the highly transmissible nature of respiratory viruses either directly through inhalation of airborne particles or indirectly via contact with contaminated objects. In 1918, the crowding and movement of soldiers in the First World War provided ideal conditions for a novel influenza strain to spread, infecting one-third of the world population, and killing an estimated 50 million people (1). Influenza strains are classified into subtypes based on the antigenic properties of the surface glycoproteins. The 1918 influenza pandemic was caused by H1N1 subtype. Further influenza pandemics occurred in 1957 and 1968, by H2N2 and H3N2 subtypes respectively, as a result of genetic reassortment with low-pathogenic avian influenza (2). In 2009 a novel influenza reassortant derived from swine influenza viruses caused the "swine flu" pandemic (3). Furthermore, the global impact of respiratory viral outbreaks is exemplified by the recent SARS-CoV-2 pandemic that has caused millions of deaths, life changing morbidity and severe economic damage (4). The possibility of another influenza pandemic through the evolution of highly pathogenic influenza viruses, such as H5N1, is a major concern for public health (5). H5N1 has been associated with high mortality rates (approximately 60%), but has so far shown limited transmissibility from person to person.

Even in the absence of pandemics, countries with temperate climates, such as the UK, experience strong seasonal cycles of respiratory infections, peaking in the winter months. Influenza virus continues to be one of the most common seasonal human respiratory tract infections and causes seasonal epidemics (6). The H1N1 and H3N2 influenza subtypes currently circulate in humans and are responsible for seasonal influenza. A broad spectrum of clinical disease severity, from asymptomatic infection to death is observed in individuals with seasonal influenza. In severe cases, influenza can damage the airway and alveolar epithelium leading to potentially fatal diffuse alveolar damage complicated by secondary bacterial infections and pneumonia (7). While the majority of individuals infected with influenza will experience symptoms such as a sore throat, cough and fever that do not require hospitalisation, it is associated with high levels of loss of working days and productivity contributing to the substantial financial burden of the disease to society (8). On the other hand, in populations including the young, the elderly and those who have chronic illnesses such as chronic obstructive pulmonary disease (COPD) and heart disease,

seasonal influenza causes substantial morbidity that often requires hospitalization and can be fatal. Annual seasonal influenza epidemics are responsible for an estimated 291,000 – 646,000 deaths a year worldwide (9). Epidemiological studies have revealed hospitalisation rate due to influenza is highest among people aged ≥65 year. Approximately 47% of reported influenza-associated hospitalisations and over 90% of influenza-related deaths occur in older adults (10).

Vaccination remains the most cost-effective method currently available for reducing the morbidity and mortality associated with influenza infection. Although vulnerable populations are vaccinated annually against influenza, the vaccination relies on antibody responses that are often short-lived and directed against specific influenza strains and thus they are not protective against novel influenza viruses (9). Furthermore, the diminished influenza-vaccine response and protection observed in the elderly is a major challenge. A better fundamental understanding of the interplay between influenza and the host immune response is required for the development of novel anti-viral therapeutics to reduce the socioeconomic burden of influenza. In particular, further research is required to unravel the mechanisms modulating the anti-viral immune response to limit damage and promotion of chronic disease.

1.1.2 Influenza and COPD

COPD impacts the lives of hundreds of millions of people worldwide and is the third leading cause of death (11,12). It causes progressive and irreversible lung function decline associated with chronic persistent inflammation that promotes narrowing of airways, impaired mucociliary clearance and emphysema (13,14). Non-reversible airflow obstruction observed in COPD can be quantified by spirometry by measuring the postbronchodilator forced expiratory flow in 1 second (FEV1) and forced vital capacity (FVC). An FEV1/FVC ratio of less than 0.70 is required for the diagnosis of COPD (15). Furthermore, the FEV1 percentage predicted informs the severity of lung function impairment, which is classified as mild (FEV1 ≥80% of predicted), moderate (FEV1 of 50%–79% of predicted), severe (FEV1 of 30%–49% of predicted), or very severe (FEV1 <30% of predicted).

The main pathological driver of COPD is sustained exposure to noxious stimuli such as cigarette smoke that damages the airways and promotes a chronic inflammatory cascade and a defective pulmonary immune response (16). An association between COPD genetic determinants and COPD-related phenotypes has also been suggested (17). The most well-established genetic risk factor is the hereditary deficiency of alpha-1 antitrypsin (AAT) (18). However, the molecular mechanisms driving disease progression in COPD, even following removal of environmental risk factors including smoking cessation, remain poorly understood.

COPD individuals are more susceptible to respiratory infections due to the physiological abnormalities including compromised mucociliary and barrier functions observed (19). Virus-infected COPD airway epithelial cells have been reported to display defective antiviral responses and induce disproportionate cytokine expression (20,21). Respiratory infections are a common cause of COPD exacerbations, which lead to worsening of symptoms and increased risk of hospitalisation and morbidity (22–25). Systemic inflammation and endothelial dysfunction driven by respiratory infections have also been associated with a higher incidence of acute cardiovascular events following exacerbation of COPD (26,27). A longitudinal multicentre COPD cohort study revealed respiratory viral infections account for around 30% of exacerbation cases. Influenza was the second most common virus identified associated with COPD exacerbations, with a prevalence ranging from 2.5 to 11.6%, the first one being rhinovirus (prevalence 7.2 to 27.3%) (28). Recently influenza has been reported to significantly increase the risk of ischemic stroke, pneumonia, respiratory failure, and COPD acute exacerbations among COPD patients (29). Other studies have shown a reduced number of exacerbations, hospitalisation and mortality in COPD patients vaccinated against influenza (30). Influenza infection results in airway epithelial barrier disruption and downregulates the host immune response promoting secondary bacterial infections. Colonisation of the airways of COPD patients by bacteria such as *Haemophilus influenzae, Streptococcus pneumoniae* and *Moraxella catarrhalis* is also common during both stable disease and exacerbations (31–33). In particular, the acquisition of new bacterial strains appears to be associated with an increased risk of COPD exacerbations (34,35).

Overall, the underlying molecular mechanisms of the dysregulated airway inflammatory response induced by influenza in COPD patients remain unclear. Further work is required to understand the mechanism of deficient airway innate immunity involving epithelial cells observed in COPD and their contribution to disease exacerbations. Therapeutic approaches to boost innate antimicrobial immunity in the lung could be a useful strategy for the prevention and treatment of frequent exacerbations. However, it will be important to uncouple the mechanisms that are essential for anti-viral defence from those that also contribute to immunopathology.

1.1.3 Influenza structure and mechanism

Influenza has been classified into four genera (A, B, C and D) that together with *Thogotovirus*, *Quaranjavirus*, and *Isavirus* form the *Orthomyxoviridae* family (36). Members of the *Orthomyxoviridae* family are characterized by 80–120 nm enveloped virions with single-stranded, negative-sense, segmented ribonucleic acid (RNA) genomes. The four influenza virus genera differ in structure, host species and pathogenicity (36). Influenza A virus (IAV) infects humans as well as a wide variety of other mammals including, cats, dogs, birds and pigs (37). On the other hand,

influenza B virus (IBV) only infects humans and influenza C virus (ICV) infects humans and pigs (38). Most recently identified, influenza D virus (IDV) infects cattle, pigs and small ruminants (39). Both IAV and IBV can cause severe upper respiratory disease and seasonal flu epidemics (37). In contrast, ICV infections are generally mild and rarely reported. Furthermore, IAV strains of zoonotic origin have historically caused sporadic and unpredictable global pandemic outbreaks (37). Given its role in seasonal epidemics and global pandemics in the human population, this study investigates the IAV genera and therefore the characteristics of other genera will not be discussed further in this literature review.

The viral genome of IAV is composed of eight segments of nucleoprotein-enwrapped single-stranded RNA in the negative sense (40,41). These eight genome segments encode viral proteins including the RNA-dependent RNA polymerase (RdRp) consisting of PB1, PB2 and PA, two surface glycoproteins (hemagglutinin (HA) and neuraminidase (NA)), the nucleoprotein (NP), the matrix protein (M1), the proton channel protein (M2), and two nonstructural proteins NS1 and NS2. The eight viral RNA (vRNAs) are found as individual viral ribonucleoprotein (vRNP) complexes that is wrapped around numerous copies of the NP. The outcome of the influenza virus entry into the host cell is to release the eight viral genome segments into the nucleus to initiate virus transcription and replication (**Figure 1.1**).

IAV preferentially targets polarised respiratory epithelium from the apical surface. Airway epithelial cells possess surface glycoconjugates that contain sialic acid (SA) residues that function as binding sites for IAV major surface protein, HA. In general, the HA of human adapted IAVs preferentially recognises α2,6 linked SA (α2,6-SA) whereas avian IAVs preferentially binds to α2,3 linked SA (α2,3-SA)(42). In humans, α2,6-SA are predominantly present on ciliated airway epithelial cells from the nose to respiratory bronchioles. In contrast, α2,3-SA are mainly present on bronchiolar non-ciliated cuboidal cells and alveolar type II pneumocytes of the lower respiratory tract.

IAV attachment to a host cell induces endocytosis using the clathrin-dependent mechanism (43). IAV can also be taken up through the actin-dependent formation of large endocytic vesicles called macropinosomes (43). Influenza viruses exploit the transport system via distinct endosomal stages and simultaneously occurring changes in pH in the late lysosome to release their vRNPs into the cytoplasm (44). The low pH of endosomes triggers a conformational change in the HA glycoprotein that exposes a fusion peptide and fusion of viral and endosomal membranes. In addition, it opens the M2 proton channel for proton flux into the virus and triggers uncoating including the detachment of M1 from the vRNPs, resulting in the release of the vRNPs into the cytoplasm (45). The vRNPs are imported to the nucleus by interacting with the cellular importin-

α/β (43). RdRp initiates RNA synthesis including transcription and replication of the viral RNA. Nuclear export of vRNPs via nuclear export protein is mediated by bridge formed by M1 (46). The vRNPs along with newly translated viral proteins including HA, NA, and M2 are transported to the plasma membrane and virus particles bud from the cells. NA cleaves sialic acid residues from glycoproteins and glycolipids enabling the particle to be released (43).

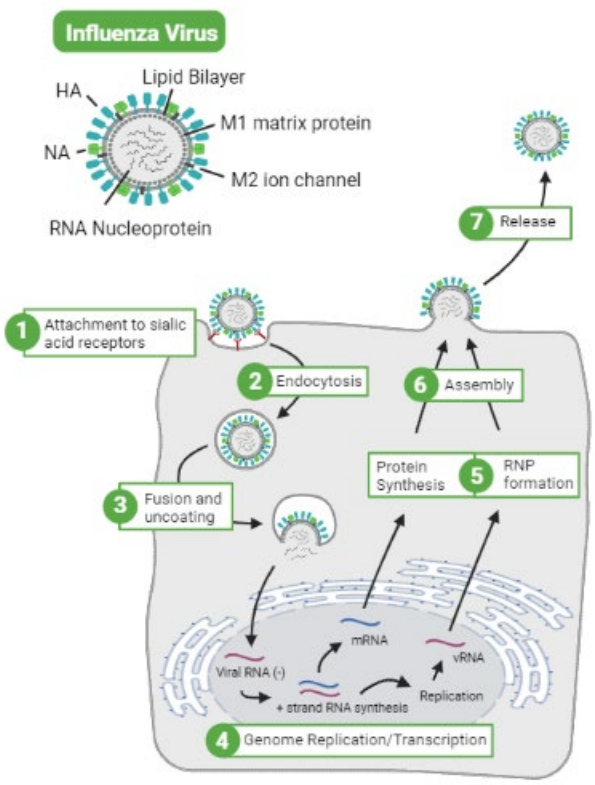

Figure 1.1 Influenza structure and replication mechanisms

Replication of influenza A viruses in the lung epithelium. 1. Attachment of haemagglutinin (HA), expressed on the surface of the influenza virion, with sialic acid residues linked to cell surface glycans on the plasma membrane of the target cell. 2. The virus then enters the cell via endocytosis or micropinocytosis. 3. Acidification activates the proton selective matrix protein-2 viral channel (M2), inducing membrane fusion and uncoating of the viral ribonucleoprotein (RNP) core. 4. RNP is then transported to the nucleus where viral RNA transcription and replication occurs. 5. Progeny viral RNP cores are generated in the cytosol and viral protein synthesised. 6. RNP along with the viral surface proteins, HA and neuraminidase (NA), and other viral proteins, are assembled at the plasma membrane. 7. Budding of these plasma membrane regions releases the influenza virion. Created with BioRender.

1.2 Host immune response against influenza

A dynamic interplay between the immune system and viral anti-immune strategies exists. Bronchial epithelial cells that line the airway lumen are the first line of defence at the lung

interface and perform a crucial role in maintaining normal airway function (47,48). The bronchial epithelium is composed of several different cell types including roughly 50-70% ciliated cells, 25% goblet cells, 11% club cells, 30% basal cells and 1-2% recently discovered ionocytes (49–53). Undifferentiated basal cells have stem cell properties and can differentiate into ciliated cells, club cells or goblet cells in normal tissue turnover as well as in tissue repair (51). Lung epithelial cells are not only the first physical barrier against respiratory viruses, but they also rapidly recognise the viral antigens with a variety of pattern recognition receptors, trigger the immune and inflammatory responses by releasing cytokines, and regulate potentially harmful inflammation. Furthermore, the lung has a unique set of immune cells such as lung resident dendritic cells, alveolar macrophages and interstitial macrophages, as well as basophils and mast cells which, together with epithelial cells, form an interconnected network that orchestrates lung immunity. Innate immunity is critical for host survival by the containment of viral spread and subsequent activation of the adaptive immune response.

1.2.1 Innate Immunity

1.2.1.1 First line of defence

Bronchial epithelial cells that line the airways provide a physical barrier against the entry of pathogens via strong intercellular junctions such as tight junctions, adherens junctions and gap junctions (54). In addition, the surface of the trachea and bronchioles is coated in a layer of mucus secreted by goblet cells that trap inhaled pathogens. The mucus is then cleared by motile cilia on the apical surface of ciliated epithelial cells protecting the lungs against infection. In COPD, mucus overproduction and decreased mucociliary clearance are observed due to structural and functional changes to the airway epithelium (16). Mucus is composed of a mixture of mucin proteins (predominantly mucin 5AC and mucin 5B) that are decorated by a diverse repertoire of carbohydrate moieties, including sialic acid and sulphate residues. Therefore, not only do mucins form a physical barrier preventing IAV from accessing the airway surface, but also can act as decoys for the sialic acid receptors on the respiratory epithelium. In support of this, plaque assay experiments demonstrated that purified MUC5AC reduced IAV infection in a murine model (55).

Bronchial epithelial cells secrete a range of other antimicrobial factors including β-defensins that disrupt the viral envelope and inhibit viral entry into the cell (56). The β-defensin 1 isoform is expressed constitutively by human airway epithelial cells whereas expression of β-defensin 2, 3 and 4 is inducible (57). Using a murine model influenza infection has been shown to increase the expression of β-defensin 3 and 4 in the airway epithelium and β-defensin deficient mice have been shown to have a worse outcome from IAV infection (58,59).

1.2.1.2 Recognition of IAV

The antiviral response depends on the ability of host cells to rapidly sense the invasion of foreign pathogens. Infected bronchial epithelial cells along with alveolar macrophages and dendritic cells detect IAV by pathogen recognition receptors (PRRs) that bind viral conserved components called pathogen associated molecular patterns (PAMPs) or damage-associated molecular patterns (DAMPs) (56). Viral RNA are major PAMPs for RNA viruses including IAV and can be detected by several PRRs including Toll-like receptors (TLRs), RIG-I-like receptors and NOD-like receptors (**Figure 1.2**). Unlike mammalian messenger RNA (mRNA), the IAV viral genome contains uncapped RNA segments with phosphate groups at their 5'-termini (60). This allows receptors to distinguish viral from mammalian RNA (60). These pattern-recognition receptors are important sensors that recognise infectious pathogens and activate downstream signalling cascades that drive host defence responses.

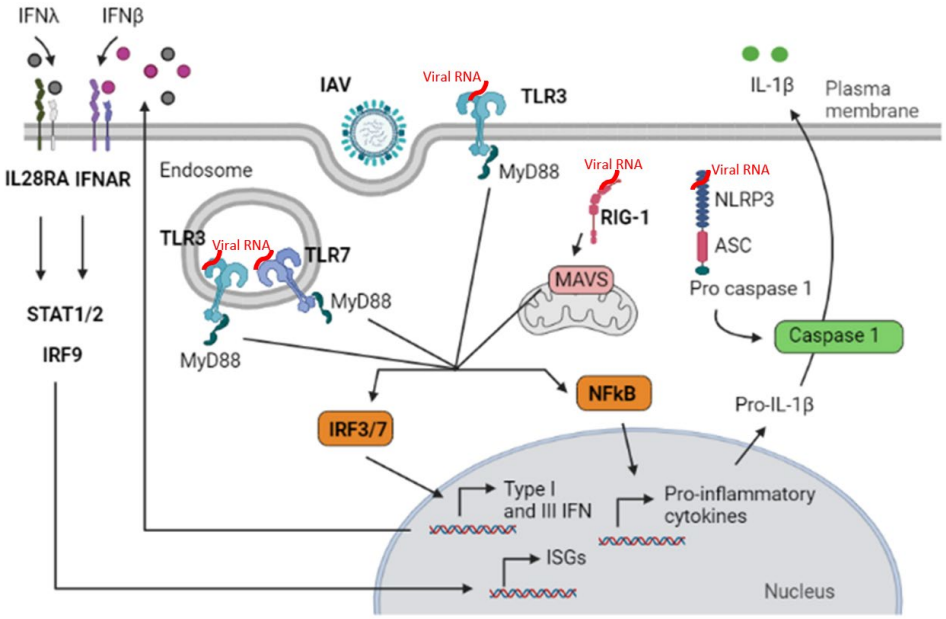

Figure 1.2 IAV innate immune recognition

TLR3 and TLR7 sense viral PAMPs within the endosome and cell membrane. RIG-I recognizes cytosolic viral RNA and by interacting with MAVS, induces type I and III IFN responses through the transcriptional factors NF-κB and IRF. These cytokines bind to the epithelial cells own IFNAR/IL28RA receptors or that expressed by other cells causing expression of Interferon Stimulated Genes (ISGs) and an antiviral state. In parallel, cytosolic single-stranded RNA and damage associated molecular patterns (DAMPs) can also interact with NLRP3 of the inflammasome complex to cause cleavage and activation of caspase-1 and induction of IL-1β and IL-18. Made in BioRender.

The expression of antiviral TLRs, including TLR3 and TLR7, have been detected intracellularly and on the apical cell surface of epithelial cells (61,62). This is distinct from antigen-presenting cells in which antiviral TLRs are typically located on endosomal membranes. While TLR3 has typically been described to recognise double-stranded RNA, its ability to recognise influenza is currently not clear given that viral double-stranded RNA is not generated in influenza infected cells due to the activity of RNA helicase (63). However, it has been suggested that TLR3 recognises virus-derived single-stranded RNA with mismatched stems, host cell mRNA and RNA from necrotic cells during influenza infection (64). On the other hand, TLR7 has widely been shown to sense single-stranded RNA from viruses including IAV (65). In addition, when the IAV RNA exits the endosomal compartment into the cytoplasm it is detected by RIG-I-like receptors via the 5'-triphosphate-containing panhandle structure. The panhandle structure formed from viral RNA primary function is to serve as the viral promoter for transcription and replication (66).

During IAV infection, TLR3 has been reported to induce the secretion of cytokines that can aid viral clearance but also lead to pathology (62). This has been demonstrated by the increased survival rate of TLR3 knockout mice (67). TLR7 and RIG-I also contribute to the production of type I interferons (IFNs) (68). Mice deficient in the RIG-I downstream adapter molecules mitochondrial antiviral-signaling protein (MAVS) and TLR7 failed to induce type I IFNs and increased mortality in response to IAV (69). IAV-induced disease and mortality in *Tlr7*$^{-/-}$ and *Mavs*$^{-/-}$ mice appeared to be due to caspase and neutrophil-dependent tissue damage that increased secondary bacterial infection (69). Crotta et al. demonstrated that in alveolar epithelial cell lines, knocking out TLR7 or MyD88 had little effect on type I or III IFN production in response to IAV, but MAVS ablation greatly reduced IFN levels (70). Therefore, the MAVS sensing pathway may function as the dominant mechanism of IAV sensing and IFN induction in alveolar epithelial cells. NOD-like receptors (NLRs) form part of the multi-protein inflammasome complexes that process caspase 1 and induces the cleavage of pro-interleukin (IL)-1β into its active form IL-1β. In the setting of IAV infection, the NLR family pyrin domain containing 3 (NLRP3) is the most studied NLR family member (71). NLRP3 is expressed in the cytosol and recognises single-stranded RNA and DAMPs. Human airway epithelial cells have been shown to express NLRP3 and secrete IL-1β when challenged with IAV (72).

Apart from TLR3, which signals through TRIF adaptor molecule, all other TLRs utilize their cytoplasmic toll-interleukin-1 receptor domain to regulate cellular responses via their adaptor protein, MyD88, and kinases to initiate innate inflammatory responses (73). In addition, multiple TLRs in airway epithelial cells produce innate immune responses by activating epidermal growth

factor receptor (EGFR) pathway via an epithelial cell signalling cascade. TLR activation upregulates signalling via the reactive oxygen species -TNFα-converting enzyme -EGFR pathway, which results in IL-8 and vascular endothelial growth factor production (74).

1.2.1.3 Immune regulatory molecules

Recognition of viral components by PRRs leads to activation of the fast but nonspecific innate immune response which is critical given components of the adaptive immune response are not detected until around 5 days after infection (75). Bronchial epithelial cells along with resident alveolar macrophages and dendritic cells, orchestrate the recruitment of immune cells including monocytes, neutrophils and natural killer cells to the lung (**Figure 1.3**). These immune cells contribute to the further release of cytokines and chemokines mediating inflammation as described below.

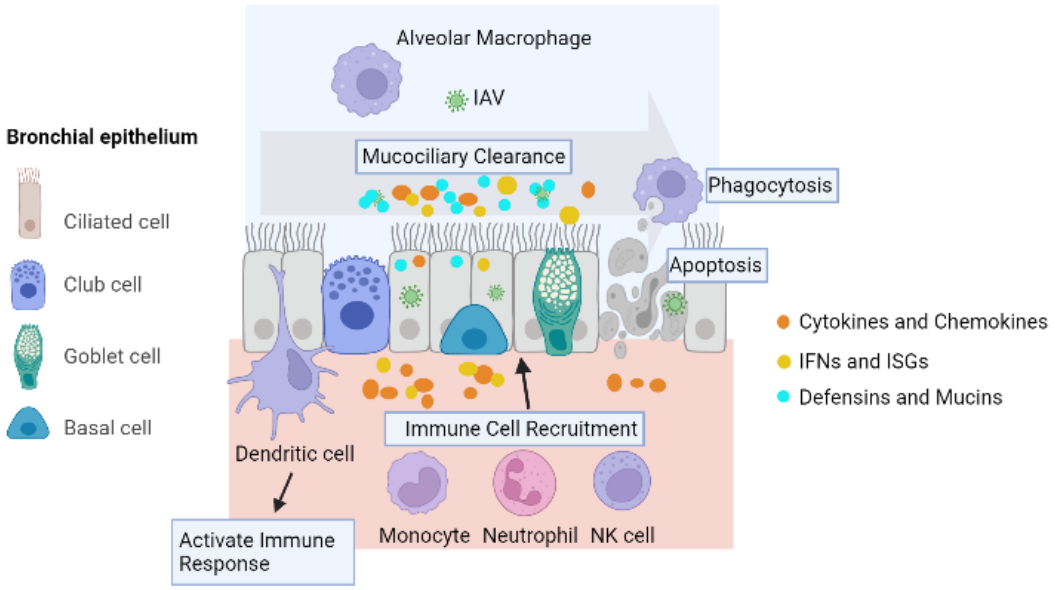

Figure 1.3 The respiratory epithelium, immune cells and immune factors involved in IAV infection. *Bronchial epithelial cells that line the airways provide a physical barrier and release mucus that is then cleared by motile cilia on the apical surface of ciliated epithelial cells. IAV infected cells undergo apoptosis that promotes removal of infected cells. Macrophages clear apoptotic cells via phagocytosis. Bronchial epithelial cells along with resident alveolar macrophages and dendritic cells, orchestrate the recruitment of immune cells including monocytes, neutrophils and natural killer cells to the lung. These immune cells contribute to the further release of immune mediating molecules that promote viral clearance. Created in BioRender.*

Upon viral recognition specific transcription factors, NF-κB, IRF3 and IRF7 are activated and translocate into the nucleus where they initiate the transcription of genes encoding IFNs, chemokines and pro-inflammatory cytokines. An increase in the concentration of cytokines and

chemokines, such as IL-6, IL-8/C-X-C motif ligand (CXCL)-8, CXCL10 and C-C motif ligand (CCL)-2 can be detected within a few hours of IAV infection (56). The role of IL-6 during inflammation is complicated, in addition to its well-known pro-inflammatory properties, it also elicits anti-inflammatory effects under certain situations. IL-6 has been suggested as crucial for lung repair after influenza-induced lung injury by reducing fibroblast accumulation, promoting epithelial cell survival, increasing macrophage recruitment to the lung and enhancing phagocytosis of viruses by macrophages (76). CXCL9, CXCL10 and CXCL11 are involved in T cell recruitment in the anti-viral immune response. However, of these three, CXCL10 is most highly upregulated in epithelial cells in response to IAV (77). CXCL10 induces monocyte stimulation, natural killer and activated T cell migration and modulation of adhesion molecule expression (78). CXCL8 and CCL2 are potent neutrophil and monocyte chemoattractants respectively (79,80). Traditionally, Tumour Necrosis Factor (TNF)-α has been considered a pro-inflammatory cytokine with mice deficient in TNF receptor exhibiting prolonged survival, reduced morbidity, and pulmonary infiltration following infection with IAV (81). Despite strong evidence supporting a pro-inflammatory role for TNF-α, it is becoming increasingly clear that TNF-α is also capable of exerting immunoregulatory effects during infection. Soluble, but not transmembrane, TNF-α is required during influenza infection to limit the magnitude of immune responses and the extent of immunopathology (82).

Type I interferons (IFN-α/β) and the recently discovered type III IFNs (IFN-λ1, -λ2, -λ3) are central players in innate antiviral responses. Once released, type I and type III IFNs bind to their respective receptors IFNAR2 and IL-28Rα/IL-10Rβ on the same and/or neighbouring cells, and this initiates the expression of hundreds of genes, grouped as IFN-stimulated genes (ISGs). These ISGs have a variety of functions including inducing immune responses in neighbouring cells and limiting viral replication and spread. Key ISGs in IAV infection include myxovirus resistance protein (Mx), IFN-induced transmembrane protein 3 (IFITM3) and interferon-stimulated gene 15 (ISG15) (83). Mx proteins interact with the IAV nucleocapsid preventing its entry into the nucleus, thereby inhibiting viral genome transcription and replication (84). IFITM3 is a small, conserved transmembrane protein that was among the first ISGs identified and restricts the proliferation of a broad range of viruses. By modulating endosomal cholesterol, IFITM3 blocks pH-dependent fusion in the late endosome and so impairs viral entry to the cytoplasm. ISG15 is a ubiquitin-like protein that restricts viral replication by interfering with virus release and translation of viral protein.

Furthermore, detection of PAMPs by cytoplasmic PRRs results in priming of the inflammasome pathway through increased expression of caspase 1, pro–IL-1β, and pro–IL-18 (85). Subsequent activation of inflammasome complex assembly is also required through several diverse signals such as, potassium efflux, lysosomal damaging factors and mitochondrial damage. IAV M2 ion

channel activity in the Golgi apparatus activates inflammasome formation. This results in the secretion of the mature IL-1β that both stimulates release of other cytokines and chemokines by the epithelium and increases adhesion molecule expression, enhancing immune cell recruitment to the lungs.

Immune cells aid in the destruction and clear up of IAV infected epithelial cells. Macrophages and dendritic cells phagocytose and destroy IAV-infected cells limiting viral release and initiating adaptive immune responses including B cell-mediated humoral immunity by presenting viral antigens to T cells (54). NK cells are important cytotoxic lymphocytes of the innate immune system that can eliminate IAV infection. Expression of IAV-HA on the surface of infected cells is a recognition signal for NK cells, that then lyse the infected cells (54).

1.2.2 Adaptive immunity

Adaptive immune memory from previous IAV infection or immunisation can prevent infection or limit the development of symptoms or severe complications. Hence why young children who are immunologically naive to influenza virus are at greater risk of severe disease. In addition, the age-related declines of both the innate and adaptive immune systems result in increased susceptibility and severity of infection in older adults.

Dendritic cells are specialised antigen-presenting cells that bridge the innate and adaptive immune responses during the IAV infection (54). Dendritic cells migrate from lungs to lymph nodes leading to T-cell proliferation and differentiation of naïve CD8 T cells into cytotoxic T effector cells. Upregulation of MHC I on infected respiratory epithelial cells and dendritic cells results in the presentation of viral antigens to CD8+ cytotoxic T lymphocytes (54). This activates them to kill virally infected cells through the release of pore forming proteins like perforin. In addition, presentation of viral antigens via MHC II activates antigen-specific CD4+ helper T lymphocytes (75). The activated helper T lymphocytes (specifically the T helper 1 phenotype) produce IL-2 and proliferate, which promotes cytotoxic T lymphocyte activity, and IFN-γ, which promotes differentiation of B lymphocytes and the production of antiviral antibodies (75). Immunosenescence, characterized by impaired humoral responses and reduction in T cell receptor diversity and T cell function are thought to contribute to the increased disease severity witnessed in elderly populations (86).

1.2.3 Influenza immune evasion

Despite several immune mechanisms to neutralize invasive pathogens or restrict viral replication, IAVs have evolved diverse strategies to evade host immunity and establish successful infection

(87–89). Several influenza virus proteins have a direct role in inhibiting the IFN system, including the influenza NS1, which suppresses the type I IFN response. In addition, NS1 can trigger the apoptosis of human airway epithelial cells via a caspase-dependent mechanism during the IAV infection. IAV has also been shown to take advantage of specific cellular negative regulators of IFN to further decrease the antiviral effects of IFN including upregulation of suppressor of cytokine signalling (SOCS) factors (69). In addition, IAV has adapted neuraminidase activity to help penetrate mucins via the degradation of sialic acids and evade antiviral treatments such as oseltamivir (90).

IAV can also undergo a process termed “antigenic drift” that involves the accumulation of mutations in the viral surface glycoproteins that can be rapidly selected for if they present an evolutionary advantage to escape the host immune response (41). The low fidelity of influenza RNA polymerase and exonuclease proofreading capability promotes the accumulation of mutations and antigenic drift. This alters the structure of antigenic surfaces recognised by the humoral responses and the ability of the virus to infect. The 1918 pandemic was thought to be caused by the antigenic drift of a fully avian virus to a form that could infect humans efficiently. In addition, HA (and to a lesser extent NA) gene segments can undergo genetic re-assortment in a process termed “antigenic shift”. Genetic re-assortment of two different strains of influenza originating from different species can occur after simultaneously infecting a host (41). This leads to the formation of novel strains of influenza to which most people have little or no immune protection and therefore usually leads to a global pandemic.

1.3 Extracellular Vesicles

The immune and inflammatory response must be tightly regulated. Although the host response is essential in viral clearance in some cases IAV induces excessive inflammation or unbalanced production of inflammatory mediators that can be detrimental to the organism via the amplification of tissue damage, injury and increased susceptibility to fatal secondary infection (91). This communication has been widely studied in terms of cytokines, chemokines and other soluble mediators. However, in recent decades, research into the role of extracellular vesicles (EVs) in cellular communication modulating disease pathology has increased dramatically.

1.3.1 Introduction to extracellular vesicles

EVs are highly heterogeneous lipid bilayer particles produced by most cell types. Based on the mechanism of biogenesis, EVs can be categorised into three distinct subgroups; exosomes, microvesicles and apoptotic bodies (**Figure 1.4**) (92). Exosomes are the smallest subclass of EVs

with a diameter ranging from 30 nm to 100 nm (93). They are formed as intraluminal vesicles by inward budding of the endosomal membrane and are then released into the extracellular space (94). Several molecules are involved in the biogenesis of intraluminal vesicles, such as the ESCRT machinery, lipids (such as ceramide) and the tetraspanins (such as CD9, CD63, CD81) (94). Furthermore, RAB proteins (RAB11, RAB27 and RAB35) have been shown to be involved in the transport of multivesicular bodies to the plasma membrane and in exosome secretion. In contrast, MVs are 50 nm to 1000 nm in diameter and are formed by direct budding from the plasma membrane (94). Lastly, apoptotic bodies have the broadest range of diameters (50–5000 nm) and are produced by cells undergoing apoptosis (95).

Our understanding of the role of specific EV subgroups remains limited due to the technical challenges associated with isolating pure subgroups, including EV size overlap and the current lack of subgroup specific markers (96). These challenges have been recognised by the International Society of Extracellular Vesicles (ISEV). The 2018 ISEV guidelines now advise referring to EVs as a whole or EV subtypes based on their physical characteristics, such as size for example “small EVs” (sEVs) (92). Therefore, in this report EVs will be considered as a whole, rather than specific subgroups.

Currently reported EV isolation techniques include ultracentrifugation, size-exclusion chromatography (SEC), ultrafiltration, precipitation, immunoaffinity capture and more recently asymmetric flow field-flow fractionation (AF4) has been used to fractionate EV subpopulations (97). Using AF4 non-vesicular nanoparticles that are 20–50 nm in diameter, were identified and given the name exomeres (98). However, ultracentrifugation and size exclusion chromatography (SEC) are still the most commonly used EV separation method. Several studies have also demonstrated the superiority of SEC over conventional EV separation techniques, such as ultracentrifugation and precipitation with chemical agents in terms of removal of contaminating particles and less compositional and structural alteration (97). SEC consists of a column filled with porous beads that separates particles based on their size. Smaller particles are able to diffuse into the beads and therefore are eluted later than larger particles. In addition, SEC allows high recovery rate without the need for expensive specialised equipment such as a high-power centrifuge or AF4.

Originally considered to be cell debris, EVs have since been shown to transfer lipids, proteins and nucleic acids as a form of intercellular communication (99,100). EV cargo varies depending on the cellular origin or pathophysiological conditions. Comprehensive ‘omics’ approaches including proteomic (mass spectrometry) and transcriptomic (RNA sequencing) analysis have successfully enabled profiling of EV cargo. The role of EVs has been widely implicated in many chronic lung

diseases (101). In response to environmental stress, EVs are enriched in surface proteins with immunoregulatory functions, such as heat shock proteins and the major histocompatibility molecules (MHC) class I and II (102,103). Other inflammatory mediators such as cytokines, chemokines and proteolytic enzymes have also been shown to be transferred in EVs modulating the behaviour of the recipient cells (104). This study focuses on the role of microRNA (miRNA) as EV cargo.

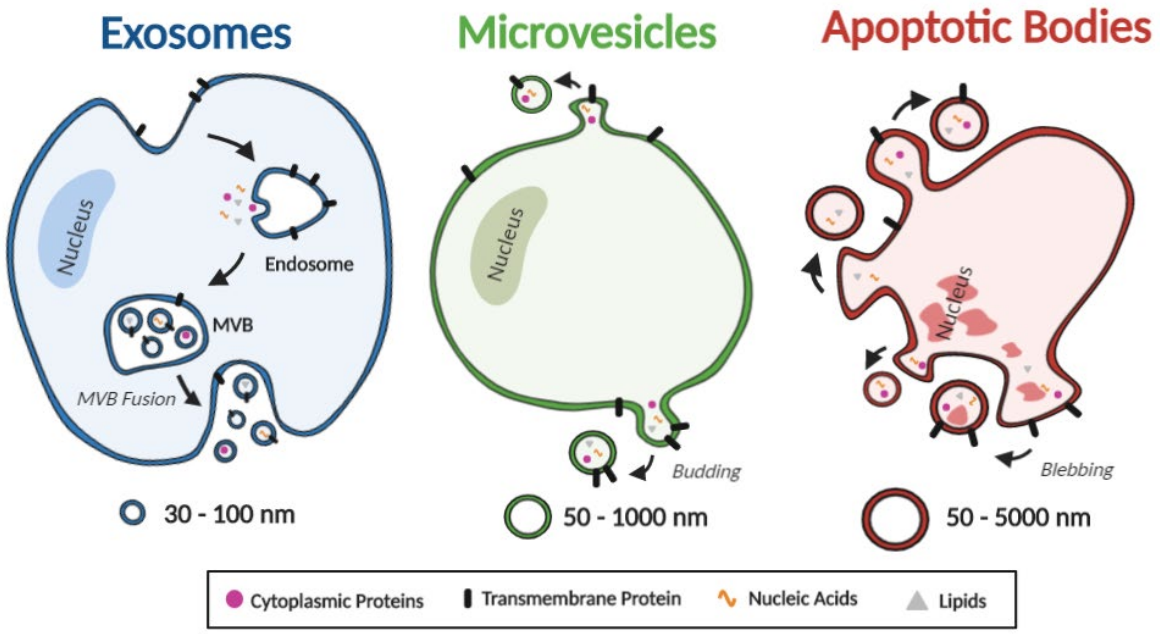

Figure 1.4 Schematic depiction of EV subtypes, including exosomes, microvesicles, and apoptotic bodies *Based on the mechanism of biogenesis, EVs can be categorised into three distinct subgroups; exosomes, microvesicles and apoptotic bodies. Exosomes are the smallest subclass of EVs with a diameter ranging from 30 nm to 100 nm. They are formed as intraluminal vesicles by inward budding of endosomal membrane to form multivesicular bodies (MVB) and are then released into the extracellular space. In contrast, MVs are 50 nm to 1000 nm in diameter and are formed by direct budding from the plasma membrane. Lastly apoptotic bodies have the broadest range of diameters (50–5000 nm) and are produced by cells undergoing apoptosis. Created in BioRender.*

1.3.2 Extracellular vesicle miRNA

1.3.3 Introduction to miRNAs

Originally discovered around 30 years ago, microRNAs (miRNAs) are the most abundant class of small non-coding RNAs. Biosynthesis of miRNAs involves a series of complex mechanisms that begins with the generation of long primary transcripts called pri-miRNA by RNA polymerase II (**Figure 1.5**) (105). This pri-miRNA is then cleaved by the RNase III enzyme Drosha and its partner

DGCR8 Microprocessor Complex Subunit to form precursor miRNAs (pre-miRNAs). These pre-miRNAs are then exported from the nucleus to the cytoplasm by exportin-5-Ran-GTP complexes (106). In the cytoplasm, pre-miRNAs are cleaved by the endonuclease DICER to generate a short "active" molecule of mature miRNA approximately 22 nucleotides in length. The mature miRNA duplex is loaded into the Argonaute (AGO) family of proteins to form a miRNA-induced silencing complex (miRISC) (105). This miRISC anneals to the 3'-untranslated region of target mRNAs, silencing the corresponding gene post-transcriptionally by inducing mRNA degradation or repressing protein production. MiRNAs have been reported to be involved in most biological pathways and cellular processes including cell proliferation, differentiation, autophagy, metabolism and immune responses (107–109). They are suggested to regulate over 60% of all protein-coding genes in multicellular organisms at the post-transcriptional level (110). Furthermore, dysregulation of miRNAs has been reported in a wide range of diseases such as viral infections, COPD, cardiovascular disease and cancer (111–113).

The miRNA content of EVs is markedly different from the RNA content of the parent cell. It has therefore been suggested that cells are capable of altering the concentration of EV RNAs through sorting mechanisms. Several mechanisms have been reported for sorting miRNA into EVs and have recently been extensively reviewed by Groot et al (114). These mechanisms broadly include RNA-binding proteins such as hnRNPA2B1, membranous proteins involved in EV biogenesis such as Caveolin-1 and posttranscriptional RNA modifications such as 3'-end uridylation (115,116). Despite the knowledge that cells can selectively sort miRNA into EVs, the different mechanisms and purpose of this sorting is still under debate.

Distinct EV-associated miRNA signatures have been reported for various diseases (117). EV miRNA has therefore been implicated in the development of pathophysiological processes (including inflammation or fibrosis), resulting in the promotion of disease (118). In some cases, selective loading of miRNAs into EVs has been directly implicated in the pathological process of the disease (118). Furthermore, there is evidence that secreted EVs including miRNA cargo can be endocytosed by recipient cells (119). Once inside the recipient cells, EV miRNA has been shown to regulate cellular functions by altering gene expression. Another theory is that cells might secrete EVs to eliminate RNAs, including miRNAs and therefore mediate gene expression in the parent cell (120). Cells may use EV miRNA sorting mechanisms for both intercellular communication and disposal. Furthermore, given miRNAs are protected by EVs in biofluid, the identification of distinct signatures across diseases has been proposed for the identification of novel biomarkers.

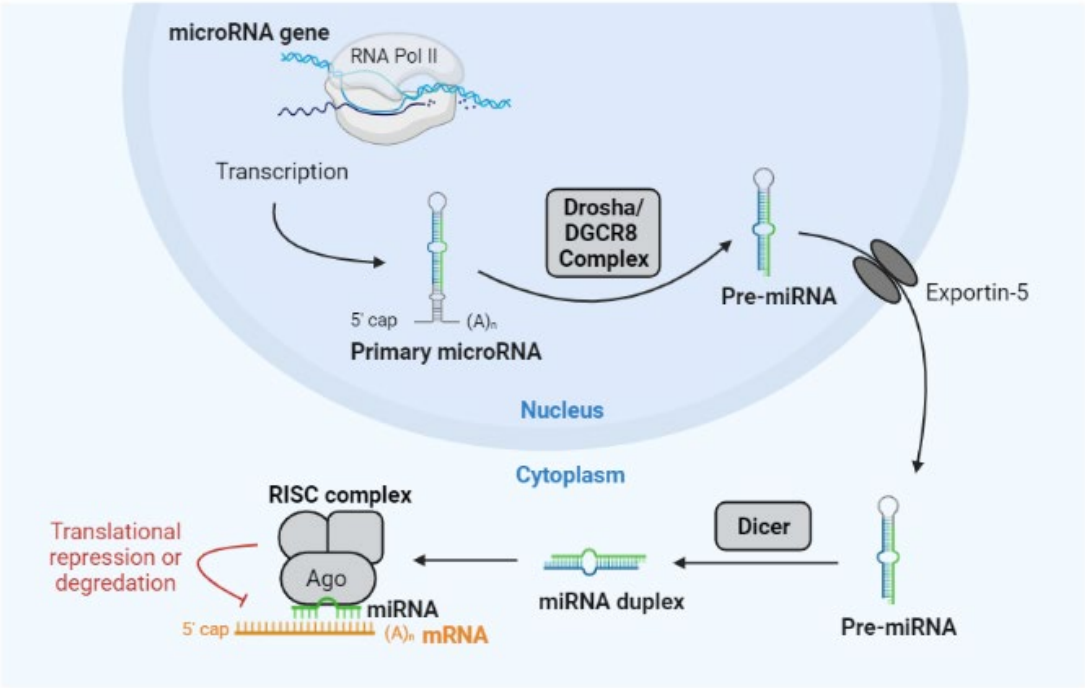

Figure 1.5 The biogenesis of miRNAs

Primary miRNA transcripts are transcribed by RNA polymerase II and processed by DGCR8/Drosha complex into precursor stem-loop miRNAs in the nucleus. Precursor miRNAs (pre-miRNAs) are exported into the cytoplasm by Exportin-5 and are cleaved by Dicer to produce mature miRNAs. Mature miRNAs recognize their respective target mRNAs and mediate post-transcriptional repression of their targets through translational repression or degradation. Created in BioRender.

1.3.4 The immune regulatory role of microRNAs in response to influenza

Over the last ten years there are a wide number of studies that report the expression of miRNA to be altered in response to IAV infection. Many studies support a key role of miRNAs in mediating viral replication by directly targeting IAV mRNAs and host immune responses to IAV such as increased IFN response or alteration of cell fate as summarised in **Table 1.1**. A few miRNAs have also been reported to facilitate virus replication.

miRNAs	Model	Expression/ variation	Target genes or associated genes	Function/mechanism	Ref
miR-323, miR-491, miR-654	Madin-Darby canine kidney (MDCK) cells	NA	PB1 subunit of viral RNA-dependent RNA polymerase	Negatively regulates IAV replication by targeting the PB1 gene	(121)
miR-3145	A549	NA	PB1 subunit of viral RNA-dependent RNA polymerase	Negatively regulates IAV replication by targeting the PB1 gene	(122)
miR-584-5p, miR-1249	A549	Up	PB2 subunit of viral RNA-dependent RNA polymerase	Negatively regulates IAV replication by targeting the PB2 gene	(123)
miR-9	A549	Up	Monocyte Chemotactic Protein-Induced Protein 1 (MCPIP1)	Promotes IAV replication by downregulating expression of MCPIP1 an inhibitor of viral M and NP genes expression	(124)
miR-146a	A549	Up	Interleukin-1 receptor-associated kinase 1 (IRAK1) TNF Receptor Associated Factor 6 (TRAF6) NFκB	Negatively regulates genes involved in the innate immune and inflammatory response by targeting TRAF6 and IRAK1, which are important components in TLR/IL-R mediated NF-κB activation pathways.	(125)
miR-144	Primary mouse lung epithelial cells	Up	TRAF6	Negatively regulates TRAF6 involved in the innate immune and inflammatory response	(126)
miR-7, miR-132, miR-187, miR-200c, miR-1275	A549, BEAS-2B, Primary differentiated human airway epithelial cells	Up	MAPK3, IRAK1	Negatively regulates genes involved in the innate immune and inflammatory response including IRAK1 and MAPK3	(127)
miR-302c	A549	Down	Mitogen-Activated Protein Kinase Kinase Kinase 14 (MAP3K14)	Negatively regulates kinases resulting in reduced type I IFN expression to promote virus replication	(128)

miR-29	A549, PBMCs	Up	DNA Methyltransferase 1 (DNMT)	Negatively regulates DNMT activity and thus induces expression of COX2 that enhances expression of antiviral protein IFN-λ1	(129)
miR-29c	A549	Up	A20	Negatively regulates NF-κB activation by enhancing deubiquitinating enzyme A20 (also known as TNFAIP3) expression and therefore decreases expression of antiviral and proinflammatory cytokines	(130)
miR-29c	A549	Up	BCL2 Like 2 (BCL2L2)	Negatively regulates BCL2L2 to promote cell death	(131)
miR-449b	A549	Up	Histone Deacetylase 1 (HDAC1)	Negatively regulates HDAC1 expression and therefore increases IFN expression	(132)
miR-21-3p	A549	Down	Histone Deacetylase 1 (HDAC8)	Promotes IAV replication by suppressing HDAC8 expression	(133)
miR-26a	A549	Down	Ubiquitin Specific Peptidase 3 (USP3)	Negatively regulates USP3, a negative regulator of type I IFN signalling	(134)
miR-34a	A549	Down	Bcl-2 Associated X-protein (Bax)	Negatively regulates the expression of pro-apoptotic Bax	(135)
miR-4276	Primary human bronchial epithelial cells, A549	Down	Cytochrome C Oxidase Subunit 6C (COX6C)	Downregulates the expression of COX6C to induce apoptotic protein caspase-9	(136)
miR-548	A549	Down	NS1A Binding Protein (NS1ABP)	Downregulates NS1ABP to promote apoptosis	(137)
miR-33a	A549	Up	Archain 1 (ARCN1)	Negatively regulates ARCN1 expression and weakens viral ribonucleoprotein activity in an ARCN1-independent manner to inhibit influenza virus	(138)

miR-302a	A549, PBMCs, human throat swab	Down	IRF5	Negatively regulates IRF5 expression, resulting in increased expression of IAV RNA and NP and M1 viral proteins	(139)
miR-451	Murine myeloid (mDC, CD11c+PDCA1−) and plasmacytoid (pDC, PDCA1+) dendritic cells were	Up	Tyrosine 3-Monooxygenase/Tryptophan 5-Monooxygenase Activation Protein Zeta (YWHAZ)	Negatively regulates YWHAZ which mediates signal transduction including decreases negative regulation of IL-6 and TNF expression by ZFP36 and FOXO3	(140)
miR-221	A549	Down	SOCS1	Downregulates SOCS1 promoting activation of the NF-κB signaling pathway and the type-I IFN-mediated immune response	(141)
miR-30	A549, primary human alveolar epithelial cells	Down	SOCS1, SOCS3, NEDD4	Downregulates SOCS1 and SOCS3 expression, and thus relieved their inhibiting effects on IFN/JAK/STAT signalling pathway. In addition inhibited the expression of NEDD4, a negative regulator of IFITM3, which is important for host defence against influenza viruses	(142)
miR-206	A549, primary human bronchial tracheal epithelial cells	Down	Tankyrase 2 (TNKS2)	Inhibited IAV infection through the activation of anti-viral innate immunity via type I IFNs	(143)
miR-193b	A549	Down	β-catenin	Downregulates β-catenin inducing cell cycle arrest	(144)

miR-1290	A549, primary human bronchial epithelial cells	Up	Vimentin	Downregulates vimentin that is necessary for the release of vRNPs to the cytoplasm	(145)
miR-132-3p	A549	Up	IRF1	Suppresses type I IFN response through targeting IRF1	(146)
miR-93	MLE-12, A549	Down	Janus kinase 1 (JAK1)	Downregulates JAK1 reducing antiviral type I IFN immune response	(147)
let-7	A549, BEAS-2B	Down	Ribosomal protein 16 (RPS16)	Targets RPS16 gene and increases the expression of type I interferon and inhibits viral replication	(148)

Table 1.1 Summary of studies investigating the role of miRNAs in response to influenza

Table includes name of miRNA, cell type used in study, whether the particular miRNA investigated was either up or down regulated in response to IAV and the suggested target and function of the miRNA. Table adapted from reference (149).

1.3.5 Role of miRNA in viral COPD exacerbations

Several recent studies have investigated the role of miRNA as a molecular mechanism mediating immune dysregulation and more severe symptoms observed in COPD in response to IAV. Lung tissue from COPD patients shows a constitutive decreased expression of IFN-β, IRF-7 and RIG-I, suggesting that this deficiency contributes to increased susceptibility of the COPD epithelium to RNA virus infection (150). A recent study investigating IAV infection responses in PBECs revealed exaggerated inflammatory but deficient antiviral responses in PBECs from COPD patients. IAV infection increased the expression of miR-125a or -b, which directly reduced the expression of A20 (an important negative regulator of NF-κB–mediated inflammation) and MAVS. This caused exaggerated inflammation and impaired antiviral responses (151). Similarly, the association between miR-125a/b and the expression of A20 deubiquitinase was observed in a mouse model of COPD. Furthermore another study using PBEC has shown hypersusceptibility of airways and inflammatory response via activation of TUG1/miR-145–5p/NF-κB axis (152). Long noncoding RNAs (lncRNA) TUG1 was shown to regulate cigarette smoke induced airway remodelling by suppressing miR-145-5p in COPD patients. In addition, they demonstrated an earlier activation of the NF-κB pathway in COPD PBEC after IAV infection, accompanied with increased lncRNA TUG1 and decreased miR-145-5p. Knockdown of lncRNA TUG1 significantly attenuated airway inflammation by inhibiting the NF-κB pathway and its downstream proinflammatory cytokines IL-1β and TNF-α. These results may partially explain the reason why COPD patients are more susceptible to IAV and have earlier and more severe symptoms than normal people. Thus, miRNA may be targeted therapeutically to inhibit excessive inflammatory responses and enhance antiviral immunity in IAV infections and in COPD.

1.3.6 The role of extracellular vesicles in the immune response to respiratory infections

There are a growing number of studies that report the isolation and characterisation of lung-derived EVs from bronchoalveolar lavage fluid (BALF) (20). Airway epithelial cells and alveolar macrophages are thought to be the major producers of EVs in the lung. Using cell type-specific membrane tagging and single vesicle flow, Pua et al reported that 80% of murine lung-derived EVs were of epithelial origin (153). Given their ability to transfer cargo it is possible airway epithelial EVs may be an important mechanism in modulating the anti-viral immune response (47,154).

Previous studies have reported that respiratory infections trigger an increased release of lung-derived EVs from alveolar macrophages and epithelial cells (155,156). The exact mechanism for biogenesis of EVs in response to infection is not fully understood. However, there is accumulating

evidence to support the release of EVs in response to viral infections are induced by activation of TLRs. Mills et al. recently reported an increase in pro-inflammatory EVs following TLR3 stimulation of the BEAS-2B bronchial epithelial cell line with the viral mimetic poly (I:C) (157). Furthermore, TLR3-activated human brain microvascular endothelial cells to release EVs that contain multiple antiviral factors as a defence mechanism against HIV-1 infection (158).

EVs may act as part of the first line of defence binding to viral particles in the lung mucosa and blocking its attachment to the lung epithelium. Studies have demonstrated EVs released from human ciliated epithelial cells bear α-2,6-linked sialic acid on their surface that bind and neutralises human influenza virus particles (159). This neutralising effect was lost when the sialic acid was removed from the vesicles. The effect of EVs to act as viral decoys has been demonstrated for other viruses. For example, ACE2-EVs were reported to block SARS-CoV-2 Spike-dependent infection in a much more efficient manner than soluble ACE2 (160).

In addition, there is evidence that EVs released in response to respiratory viruses have molecular content that can contribute to the antiviral immune response in recipient cells. A recent study reported significant differences in small RNA EV cargo released by the human alveolar epithelial A549 cell line when infected with respiratory syncytial virus (RSV) (161). These EVs were shown to activate the innate immune response through increasing the release of cytokines and chemokines including CXCL10, CCL5 and TNF in other A549 cells and human monocytes (161). In addition, EVs released from influenza infected macrophages have been shown to directly transfer cytokines, including IL-6, IL-18, and TNF (111).

EVs have also been shown to upregulate type I IFNs, a key mediator of anti-viral responses. Liu et al demonstrated that EVs produced by influenza infected A549 cells induced IFN production to inhibit viral replication through upregulation of miR-1975 (162). Similarly, BALF EVs from a murine model of highly pathogenic avian influenza have also been reported to have an increased level of miR-483-3p and to potentiate IFN immune response (163). Another study reported EVs derived from the bronchoalveolar lavage of patients infected with the influenza virus have increased levels of miR-483-3p, mir-374-5p, and miR-446i-5p. These EVs promoted the expression of IFN-β, proinflammatory cytokines, and interferon-stimulated genes, including IL-6, TNF-α, CCL2, and SP100 (164).

In addition, EVs play key roles in both direct and indirect antigen presentation. It has been demonstrated EVs transfer hemagglutinin epitopes in complex with MHCII molecules, increasing the efficiency of antigenic determinant presentation to immune cells (165). Furthermore, some studies have demonstrated host cell EVs released following infection contain PAMPs that can

stimulate a proinflammatory response in macrophages through TLR and enhance T cell activation (166,167).

1.3.7 Pro-viral role of extracellular vesicles

On the other hand, pathogens may use EVs to promote immune suppression facilitating the establishment of persistent infections. A549 cells infected with IAV were reported to increase levels of miR-17-5p in EVs and promote enhanced IAV replication through downregulation of the antiviral factor Mx1 (168). It was also recently suggested that EVs may provide shelter for host and viral proteins and genome, facilitating viral escape from immune surveillance, and favour viral entry into the recipient cells (169). In recent years, an accumulating body of data has emerged suggesting that some viruses can also manipulate the vesicular trafficking machinery for their assembly and transmission. Several negative strand RNA viruses, such as IAV, hantavirus, and RSV, have all been reported to utilize the Rab pathway for their transport to the plasma membrane for exit (170). High-throughput analysis has discovered that IAV integrates with EV proteins or markers such as annexin A3, CD9, CD81, and ICAM1, which may protect IAV and promote viral spreading (171).

Overall based on current studies EVs may play a role in both activating host immune response against respiratory pathogens or facilitating infection (**Figure 1.6**). In addition, many experiments investigating airway epithelial EVs are based on simple *in vitro* cell culture systems that utilise undifferentiated, nonpolarized respiratory epithelial cells. Further studies using better *in vitro* models are required to fully elucidate the mechanisms in which lung epithelial EV cargo including miRNA modulate the immune response of recipient cells to IAV.

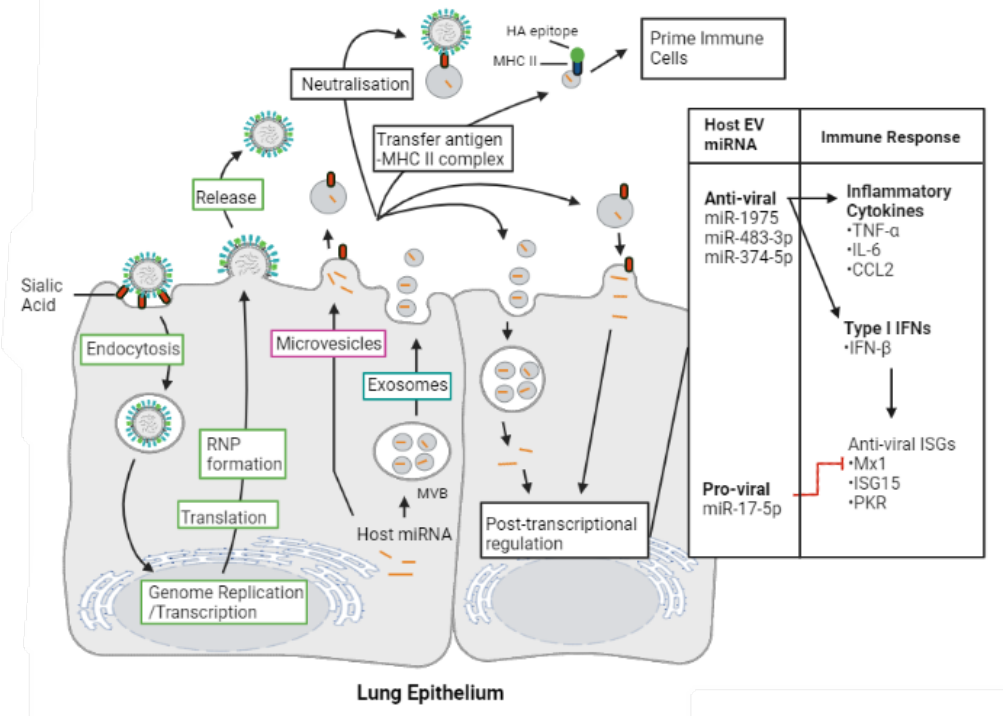

Figure 1.6 Schematic diagram of epithelial EV release in response to influenza

Epithelial cells infected with influenza release EVs that contain sialic acid neutralising the virion, antigens to prime immune cells or host miRNA that can act to alter expression of immune genes in recipient cell. Created in BioRender.

1.3.8 The role of extracellular vesicle miRNA in COPD

Alteration of EVs in COPD has been widely investigated in terms of response to cigarette smoke or particulate matter. EVs released in response to cigarette smoke or particulate matter upregulate inflammatory pathways that result in increased immune cell recruitment and release of pro-inflammatory mediators. For example, cigarette smoke extract-stimulated BEAS-2B cells release EVs that promote adhesion of monocytes to endothelial cells (172). Furthermore, EVs released from BEAS-2B cells under oxidative stress were shown to activate macrophages and promote expression of TNF, IL-1β, and IL-6 through increased EV levels of miR-320a and miR-221 (173). EVs released in response to cigarette smoke have also been shown to promote cytokine release in epithelial cells. Heliot et al. reported EVs isolated from the BAL of smokers increased the secretion of IL-6 by the BEAS-2B cells (174).

Damage caused to the lung by exposure to cigarette smoke results in airway remodelling. EVs have been reported to play a role in airway remodelling by mediating fibrosis through epithelial-mesenchymal transition and myofibroblast differentiation. Cigarette smoke extract was shown to increase miR-210 in human bronchial epithelial cell EVs, leading to suppression of autophagy and promotion of myofibroblast differentiation (112). He et al. reported that EVs from cigarette

smoke extract-treated BEAS-2B cells had reduced miR-21 which indirectly modulated epithelial-mesenchymal transition by alleviating the polarization of M2 macrophages (175).

Our group have recently found 23 miRNAs differentially expressed between lung derived EVs of COPD and healthy ex-smokers (176). Network-based analysis identified miRNA targeted genes as central to pro-inflammatory pathways (176). One of the top differentially expressed miRNA was miR-223 which has been widely reported in modulating inflammation. Neudecker et al. reported transfer of miR-223 from neutrophils to alveolar epithelial cells via EVs attenuates lung inflammation (177). On the other hand, Ismail et al. reported macrophage EVs with increased levels of miR-223 induce macrophage differentiation promoting inflammation (178). This functional variation may be due to different cell types. Another more recent study suggested removal of miR-223 from alveolar macrophages via EVs releases suppression of the NLRP3 inflammasome thereby promoting activation (120). In support of this selective export of miR-223 and some tRNA in EVs were also shown to promote T cell activation (179). These studies suggest EVs may have a dual function in selectively removing suppressive molecules to promote immune cell activation as well as intercellular communication, though this requires further investigation.

1.3.9 The role of extracellular vesicles in vaccine and therapeutics

Common anti-inflammatory treatments are often non-specific such as steroids and therefore can worsen the long-term outcome of influenza infection via general immune suppression. Identifying specific EV miRNA that could be used to target specific pathways responsible for damaging immunopathology observed in acute influenza may be useful novel therapeutics. Compared to artificial drug delivery systems (e.g., liposomes, polymers), EVs could minimise immunogenicity, prolonging the *in vivo* circulation time and decreasing the distribution to the liver and spleen.

Tsukamoto et al. reported circulatory EVs enriched in miR-192 as an anti-inflammatory factor able to target the lung to reduce chronic inflammation upon stimulation with inactivated influenza whole virus particles (180). Additionally, miR-192 in EVs improved the efficacy of vaccination in aged mice (180). These investigators therefore suggested a therapeutic potential for miR-192 EVs wherein they could be used to reduce adverse reactions and improve vaccine efficacy in the elderly (180). Furthermore, the potential of IFN treatment in the prevention of virally induced exacerbations in COPD is currently being investigated (181,182). Given EVs have been shown to modulate IFN response they may therefore also have useful anti-viral therapeutic applications. However, the use of miRNA in therapeutics requires a full understanding of target genes given that miRNA commonly have multiple targets and therefore could lead to damaging off target effects.

1.4 Aims and Objectives

Hypothesis

This project investigates the hypothesis that the microRNA cargo of extracellular vesicles released from bronchial epithelial cells is altered following infection with influenza A virus promoting the anti-viral immune response.

This will be tested by the following aims:

1) Establish air-liquid interface bronchial epithelial cell model for IAV infection and isolation of EVs
2) Compare EV miRNA released from IAV infected bronchial epithelial to non-infected control
3) Compare EV miRNA of healthy and COPD primary epithelial cells in response to influenza A virus
4) Identify the biologically significant targets of these differentially expressed miRNA and validate these *in-vitro*

2 Methods

2.1 Epithelial Cell Culture

2.1.1 Epithelial Cell Submerged Culture

Immortalized human bronchial epithelial cells (BCi-NS1.1), kindly provided by Prof Ronald Crystal from Cornell Institute New York, were defrosted after storage at -80°C and maintained in Pneumacult-Ex Complete Medium (**Table 2.1**) (Stemcell Technologies, Cambridge, UK). BCi cells were cultured in a T75 flask coated with 1:10 dilution of PureCol® Type I Bovine Collagen (Advanced BioMatrix, California, USA) at 37°C and 5% CO_2. Cells were expanded until 70% confluence and passaged with trypsin-EDTA solution 1X (Sigma-Aldrich, Poole, UK). The cells were pelleted by centrifugation at 400 g for 5 minutes and seeded in a collagen coated T75 flask. Cells were used passages 20-25.

2.1.2 Epithelial Cell Air-Liquid Interface Cultures

Air-liquid interface (ALI) BCi cell cultures were generated by seeding submerged cultured BCi cells at 100,000 cells/insert for 24 well plates or 300,000 cells/insert for 12 well plates on collagen coated Transwell permeable polyester membrane inserts (Corning Costar, High Wycombe, UK) with a 0.4 µm pore size. Pneumacult-Ex Plus Complete Medium (**Table 2.1**) was added to both the apical and basal compartments. After 5 days the media was replaced in apical and basal compartments with Pneumacult™-ALI Medium (Stemcell Technologies) prepared the manufacturer's instructions (**Table 2.1**). After a further 2 days the media was removed from the apical chamber. The Pneumacult™-ALI Medium was replaced in the basal compartment every 2-3 days. ALI cultures were maintained for around 28 days until a pseudostratified epithelium was observed. Differentiation was confirmed by the observation of a homogeneous layer of cells and presence of cilia using a Leica DM-IL microscope (Leica, Milton Keynes, UK) with phase-contrast and a transepithelial electrical resistance (TEER) greater than 500 Ω cm^2 measured using a Millicell ERS-2 Voltohmmeter (Merk Millipore, Watford, UK).

Reagent	Components
Pneumacult-Ex Complete Medium	*PneumaCult-Ex Basal Medium (Stemcell Technologies)* *Pneumacult-Ex Supplement 1X (Stemcell Technologies)* *Hydrocortisone 1X (Stemcell Technologies)* *0.125 µg/ml amphotericin B (Sigma-Aldrich)* *25 µg/ml gentamicin (Gibco, Paisley, UK)*
Pneumacult-Ex Plus Complete Medium	*PneumaCult-Ex Basal Medium (Stemcell Technologies)* *Pneumacult-Ex Plus Supplement 1X (Stemcell Technologies)* *Hydrocortisone 1X (Stemcell Technologies)* *0.125 µg/ml amphotericin B (Sigma-Aldrich)* *25 µg/ml gentamicin (Gibco)*
Pneumacult-ALI Complete Medium	*PneumaCult-ALI Basal Medium (Stemcell Technologies)* *Pneumacult-ALI Supplement 1X (Stemcell Technologies)* *Pneumacult-ALI Maintenance Supplement 1X (Stemcell Technologies)* *Hydrocortisone 1X (Stemcell Technologies)* *Heparin Solution (Stemcell Technologies)* *100 U/ml penicillin (Sigma-Aldrich)* *100 µg/ml streptomycin (Sigma-Aldrich)*
Pneumacult-ALI Infection Medium	*45 ml PneumaCult-ALI basal media* *5 ml PneumaCult-ALI supplement* *100 U/ml penicillin (Sigma-Aldrich)* *100 µg/ml streptomycin (Sigma-Aldrich)* *0.02 % Bovine Serum Albumin (BSA) (Sigma-Aldrich)*
Pneumacult-Ex Infection Medium	*45 ml PneumaCult-Ex Basal Medium* *100 U/ml penicillin (Sigma-Aldrich)* *0.02 % Bovine Serum Albumin (BSA) (Sigma-Aldrich)*

Table 2.1 Composition of cell culture media

2.1.3 Primary Bronchial Epithelial Cells

2.1.3.1 Ethics

All subjects gave written informed consent for the study Microbiology and Immunology of the Chronically-Inflamed Airway (MICA) III (ID: 15/5C/0528).

2.1.3.2 MICA III study design

Inclusion and exclusion criteria for the MICA III study (**Table 2.2**).

Inclusion Criteria	Exclusion Criteria
Written informed consent obtained from the participant	A confirmed diagnosis of asthma or other respiratory diseases.
Patients with COPD and healthy ex-smokers with a history of ≥10 pack-years of cigarette smoking	History of lung surgery.
Male or female aged 40–85 years	AAT deficiency as underlying cause of COPD.
COPD subjects must have a confirmed diagnosis of mild/moderate COPD based on post bronchodilator spirometry with FEV1 >50% of predicted normal and FEV1/FVC <0.7.	Immunocompromised patients.
Healthy subjects must have an FEV1/FVC >0.7.	Moderate or severe COPD exacerbation not resolved at least 1 month prior to enrolment and less than 30 days following the last dose of oral corticosteroids and/or antibiotics.
Subjects must be fit to undergo bronchoscopy	Use of any antibacterial, antiviral or respiratory investigational drug or vaccine within 30 days of the enrolment visit
	Presence of other conditions that the principal investigator judges may interfere with the study findings.

Table 2.2 Inclusion and exclusion criteria for the MICA II study

2.1.3.3 Bronchial Brushes

PBECs were isolated from bronchial brushes collected as part of the MICA III study and grown in culture using PneumaCult™-Ex Plus Medium, (STEMCELL Technologies, Cambridge, UK) in T75 flasks coated with collagen (PureCol, Nutacon, the Netherlands) (**Table 2.3**). When cells were confluent, they were trypsinised with trypsin EDTA solution and transferred to ALI culture as per section 2.1.2.

Patient	Healthy/COPD	Lobe
304	COPD	RUL
305	Healthy	RUL
320	COPD	RUL/RLL
326	Healthy	RUL/RLL
331	Healthy	RUL/RLL
340	COPD	RUL

Table 2.3 Bronchial brushes phenotype

Right upper lobe (RUL), right lower lobe (RLL).

2.2 Extracellular vesicle isolation

EVs were recovered from ALI BCi apical secretions by two sequential washes completed as follows. HBSS (Sigma-Aldrich) was added to the apical compartment, incubated for 30 minutes at 37°C and 5% CO_2 and then collected. Samples were then centrifuged at 300 g for 10 minutes. The supernatant was then collected and centrifuged at 1200 g for 20 minutes. The supernatant was then filtered through a 0.22 µm PES sterilised filter (Merck Millipore), to remove any larger particles. The sample was then loaded onto an equilibrated Amicon® Ultra-15 (10,000 Molecular weight cut-off) spin filter (Merck Millipore) and centrifuged at 3200 g, 4°C for 15 minutes to further purify and concentrate the sample. The filter device was washed with DPBS (Sigma-Aldrich) and centrifuged at 3200 g, 4°C for at least a further 15 minutes or until the sample was concentrated.

Separation of EVs based on size was completed using PURE-EVs™ size exclusion columns (HansaBioMed Life Sciences®, Tallinn, Estonia). Prior to use, columns were washed with 30 ml of DPBS to eliminate any preservative buffer residues. Up to 2 ml of the concentrated sample was then added to the column. In total, 24 fractions each of 500 µL in volume were collected. The initial fractions contain the void volume in which buffer within the column prior to sample application is eluted. EVs are the first particles to be eluted at around fractions 6-11 as has previously been confirmed by the manufacturer. Based on the manufacturer's instructions and previous work completed by Burke et al, EVs have been demonstrated to be eluted in fractions 6-11 (elution volume 2.5-5.5 ml) (176). Fractions were then combined to form 4 groups as follows; fractions 1-5 termed SEC#1, fractions 6-11 termed SEC#2, fractions 12-17 termed SEC#3 and fractions 18-24 termed SEC#4 (176). These grouped fractions were concentrated using an equilibrated Amicon® Ultra-4 (10,000 Molecular weight cut-off) spin filter, centrifuged at 3200 g, 4°C for at least 30 minutes. The sample was then recovered from the filter device and stored frozen at -80°C for analyses.

2.3 Measurement of protein concentration

Protein concentration was determined by the Pierce BCA Protein Assay kit (Thermo Fisher Scientific®, Basingstoke, UK) according to the manufacturer's instructions. The absorbance was measured at 550 nm using a ThermoMax Microplate Reader (Molecular Devices, Berkshire, UK). The average 550 nm absorbance measurement of the Blank standard replicates was subtracted from the 550 nm measurement of all the other standards and unknown sample replicates. A standard curve was plotted using the Blank-corrected 550 nm measurement for each BSA standard versus the concentration (µg/ml). This was then used to determine the concentration of each unknown sample.

2.4 RNA isolation

Briefly, 1000 µl of QIAzol Lysis Reagent (Qiagen®) was added directly to cells or concentrated 200 µl SEC elution sample. The samples were then stored at -80°C.

2.4.1 miRNeasy Micro Kit

RNA was isolated from cells and SEC elution samples using miRNeasy Micro kit (Qiagen®) according to the manufacturer's instructions. Once accumulated the samples were then defrosted on ice and 200 µl of chloroform (Sigma) was added. The samples were shaken vigorously for 15 seconds and

incubated at room temperature for 5 minutes. Samples were then centrifuged for 15 minutes at 12, 000 g at 4°C. The upper aqueous phase was combined with 1.5 volumes of 100% ethanol then added in a RNeasy MinElute spin column in a 2 ml collection tube. The samples were then centrifuged in RNeasy MinElute spin column at 8000 g for 15 seconds at room temperature. For SEC elution samples DNase digestion was completed according to Appendix B of miRNeasy Micro kit protocol for samples containing <1µg total RNA. The sample was then rinsed with 700 µl of Buffer RWT then 500 µl Buffer RPE by centrifugation at 8000 g for 15 seconds. Then 500 µl of 80% ethanol was added to the RNeasy MinElute spin column and centrifuged for 2 minutes at 8000 x g. The spin column was then centrifuged at 12 000 g for 5 min to dry the membrane and 14 µl of RNase-free water was added and centrifuged at 12 000 g to elute RNA.

2.4.2 Isopropanol precipitation

RNA was isolated from transfected samples through isopropanol precipitation. The samples were vortexed and left at room temperature for 8 minutes before centrifugation at 12,000 g, 4°C for 10 min. RNA was precipitated in 0.5 ml isopropanol (Sigma) and 4 µl Glyco Blue (Applied Biosystems, Paisley, UK), followed by two 75% ethanol (Sigma) washes. Excess ethanol was removed by air-drying and the subsequent pellet was resuspended in RNase free water (sigma).

2.4.3 Nanodrop

Concentrations of RNA were determined by NanoDrop 1000 spectrophotometer (Thermo Fisher Scientific®). The Nanodrop calculates RNA concentration from 1.5 µl of sample using the Beer-Lambert law, which predicts a linear change in absorbance with concentration. The A260/A280 ratio is used to assess RNA purity.

2.5 cDNA synthesis

Synthesis of cDNA was carried out using Taqman Advanced miRNA cDNA synthesis kit (Applied Biosystems) using following manufacturer's instructions summarised in **Table 2.4.**

2.6 Real-time quantitative PCR

The cDNA was then diluted 1:10 with RNase free water (Sigma-Aldrich). The real-time quantitative polymerase chain reaction (RT-qPCR) was performed using a PCR reaction mix containing 2.5 µl

TaqMan Universal Master Mix II no UNG (Applied Biosystems), 1.25 µl RNase-free water and 0.25 µl TaqMan Advanced miRNA Assays (Applied Biosystems) (**Table 2.5**). 1 µl of diluted cDNA was combined with 4 µl of a PCR reaction mix and the RT-qPCR was performed using a 7900HT Fast Real-Time PCR System (Thermofisher). The reaction mix was incubated at 95°C for 10 minutes to activate enzyme and then completed 40 cycles of denaturing at 95°C for 15 seconds and annealing/ extending at 60°C for 1 minute.

Taqman Advanced miRNA and mRNA synthesis	Reaction Mix	Thermal Cycles
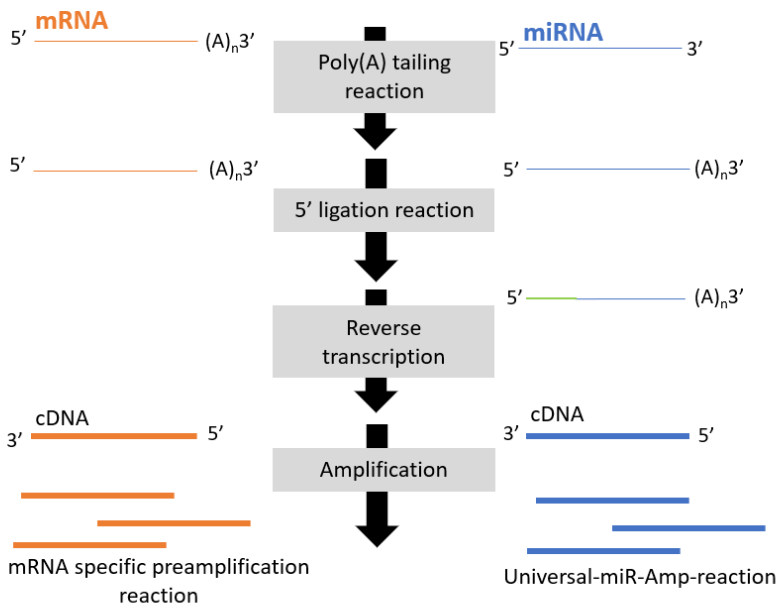	5 µl in volume made up of: 10 ng RNA sample, 1X Poly(A) Buffer, 1 mM ATP, 0.3 U/µl Poly(A) Enzyme and RNase-free water	• Polyadenylation: 37°C for 45 minutes • Stop Reaction: 65°C for 10 minutes • Hold: 4°C
	15 µl in volume made up of: poly(A) tailing reaction product, 1X DNA Ligase Buffer, 15% PEG 8000, 1X Ligation Adaptor, 1 U/µl RNA Ligase and RNase-free water	• Ligation: 16°C for 60 minutes • Hold: 4°C
	30 µl in volume made up of: adaptor ligation reaction product, 1X RT Buffer, 4 mM dNTP Mix, 1X Universal RT Primer, 1X RT Enzyme Mix, 50 µM random hexamers and RNase-free water	• Reverse transcription: 42°C for 15 minutes • Stop reaction: 85°C for 5 minutes • Hold: 4°C
	50 µl in volume made up of: 5 µl RT reaction product, 1X miR-Amp Master Mix, 1X miR-Amp Primer Mix, 0.05 X pooled TaqMan Assays, and RNase-free water	• Enzyme activation: 95°C for 10 minutes • Denature: 95°C for 15 seconds • Anneal/Extend: 60°C for 4 minutes • Repeat steps 2 and 3 for 14 cycles • Stop reaction: 99°C for 10 minutes • Hold: 4°C

Table 2.4 Summary **of TaqMan Advanced cDNA synthesis protocol (Applied Biosystems, Germany)**

Listed are the reaction mix and thermal cycles for each of the four stages of TaqMan Advanced cDNA synthesis (Applied Biosystems) including Poly(A) tailing reaction, Adaptor ligation reaction, Reverse transcription reaction and miR-AMP reaction.

Assay Name	Assay ID
hsa-miR-16-5p	477860_mir
hsa-miR-24-3p	477992_mir
hsa-miR-138-5p	477905_mir
hsa-miR-182-5p	477935_mir
hsa-miR-26b-5p	478418_mir
hsa-miR-155-5p	483064_mir
hsa-miR-122-5p	477855_mir
hsa-miR-146a-5p	478399_mir
hsa-miR-378a-3p	478349_mir
hsa-miR-7-5p	483061_mir
B2M	Hs00984230_m1
ACTB	Hs99999903_m1
FLUWINSCONSIN15	1655416 A7
CXCL10	Hs00171042_m1
IL6	Hs00174131_m1
SOCS1	Hs00705164_s1
IFNB	Hs01077958_s1
ISG15	Hs01921425_s1
SOD2	Hs00167309_m1

Table 2.5 TaqMan Assay IDs (Applied Biosystems)

2.7 Apolipoprotein E ELISA

The presence of contaminating lipoproteins was determined using a Human Apolipoprotein E (ApoE) Enzyme-Linked Immunosorbent Assay (ELISA) (ab108813) (abcam, Cambridge, UK) as per the manufacturer's instructions. Briefly, standards or test samples were added to the wells of an anti-ApoE antibody 96-well plate. Subsequently, an ApoE specific biotinylated detection antibody was added and washed with the provided wash buffer. Streptavidin-Peroxidase Complex was then added and 3,3',5,5'-Tetramethylbenzidine was used to generate a reaction with the colorimetric signal quantified by ThermoMax Microplate Reader.

2.8 RIPA lysis

Particles from SEC eluted samples were lysed by adding 10X RIPA (abcam) to a final concentration of 1X. Samples were vortexed and incubated on ice for 30 minutes.

Cells were lysed following removal of the culture media and a wash with DPBS. Lysis was completed by adding 1 ml of 1X RIPA (ThermoFisher Scientific) combined with Halt Protease inhibitor (ThermoFisher Scientific) to the apical face. Cells were then incubated on ice for 15 minutes and then collected into a 1.5 ml microcentrifuge tube. Samples were then stored at -80°C

2.9 SDS-PAGE

Reduced sodium dodecyl sulphate-polyacrylamide gel electrophoresis (SDS-PAGE) was completed using NuPAGE® 12 % Bis-Tris Protein Gels (Invitrogen, Paisley, UK) according to manufacturer's instructions. Analyses of CD9, STCH and calnexin was completed under reducing conditions with NuPAGE® LDS Sample Buffer (Invitrogen) and NuPAGE® Reducing Agent (Invitrogen) added to samples. Analyses of CD63 was completed under non-reducing conditions with NuPAGE® LDS Sample Buffer added to the samples. The samples were incubated at 70°C for 10 minutes. The sample was then centrifuged for 10 minutes at 12 000 g and loaded onto the protein gel alongside 5 µl of PageRuler Prestained Protein Ladder (ThermoFisher Scientific). Electrophoresis was completed at 200 V (110mA) for 50 minutes.

2.10 Western Blotting

Proteins were transferred to a Polyvinylidene difluoride (PVDF) membrane using an iBlot Dry Blotting System with an iBlot Transfer Stack (PVDF) (Invitrogen), according to manufacturer's instructions. Membranes were blocked in Tris-buffered saline (TBS) with 0.1% Tween-20 (wash buffer) containing 5% (w/v) skimmed milk for 1 hour rocking at room temperature. Primary antibodies CD9 (ab92726, abcam), CD63 (ab59479, abcam), STCH (ab127750, abcam) and calnexin (C5C9, cell signalling) diluted 1:1000 were applied seperately to the membrane and incubated overnight. Membranes were then washed three times with wash buffer before being incubated with relevant secondary antibody either horse radish peroxidase-conjugated goat α-mouse IgG antibody (ab205719) or horse radish peroxidase-conjugated goat α-rabbit IgG antibody (ab205718) diluted 1:2000. The membranes were then washed three times with wash buffer. To visualise the protein, SuperSignal™ West Pico PLUS Chemiluminescent Substrate (Thermo Scientific) was used with reagents mixed 1:1 ratio and then applied to the surface of the membrane. A ChemiDoc MP Imaging System (BioRad, Hertfordshire, UK) with was then used to detect the luminescent signal visualised using ImageLab software.

2.11 Transmission electron microscopy

Transmission electron microscopy (TEM) was completed as previously reported (183). Briefly, 5 µL of EVs in 1X PBS was layered onto individual formvar-carbon coated 200 mesh copper grids (Agar Scientific Ltd, Stansted, UK). After 1 minute the grid was blotted to remove excess liquid. The samples were then contrasted in a solution of 5% ammonium molybdate (w/v) plus 1% trehalos. TEM micrographs were obtained with the FEI Tecnai T12 instrument at Biomedical Imaging Unit,

University Hospital Southampton with an 11-megapixel side mounted camera (Morada® G2, EMSIS Ltd, Muenster, Germany).

2.12 ExoView

Single particle interferometric imaging measurement was performed by NanoView Biosciences using the ExoView R100 platform. CD9, CD63 and CD81-positive EVs were immunocaptured on a tetraspanin microarray chip and imaged as single particles. Particle size was analyzed using single particle interferometric reflectance imaging sensing (SP-IRIS) using the ExoView Human Tetraspanin Kit (NanoView Biosciences, Malvern, UK). Co-expression of tetraspanin proteins were then assessed by labelling the captured EVs with a cocktail of fluorescence antibodies conjugated to CD81-Alexa555, CD63-Alexa647 and CD9-Alexa488. The chips were then imaged with the ExoView R100 reader with sizing thresholds set to 50-200nm diameter. A 150-µm-diameter area of each capture spot was selected for analysis using an automated circle finding algorithm. The particles within this area were counted, producing a particle value that represents normalization of particle count to spot area. Each chip has the antibody capture spots in triplicate.

2.13 Cytotoxicity

Cell death was analysed by the release of Lactate Dehydrogenase (LDH) into supernatants using the CytoTox 96® Non-Radioactive Cytotoxicity Assay (Promega, Southampton, UK) following the manufacturer's instructions. Briefly, 50 µl of the CytoTox 96® Reagent was to 50 µl of cell supernatant or cell lysate then incubated in the dark for 30 minutes at room temperature. Following this 50 µl of Stop Solution to each well and the absorbance was measured at 490 nm using a ThermoMax Microplate Reader (Molecular Devices). The following formula was used to compute percent cytotoxicity:

Percent cytotoxicity = 100 × Experimental LDH Release (OD490) / Maximum LDH Release (OD490)

2.14 Influenza A virus infection

2.14.1 ALI Culture

Differentiated ALI culture BCi cells were washed with Hanks' Balanced Salt solution (HBSS) (Sigma-Aldrich) and ALI infection medium (**Table 2.1**) was added to basal lateral side. Influenza A/Wisconsin/67/2005 (Virapur, San Diego, CA) at a TCID50 (Tissue Culture Infectious Dose required to kill 50% of cells) of 3.6 x 10^8 IU/ml (infectious units/ml) was diluted 1/100 or 1/1000 in

HBSS and applied apically at a TCID50 of 3.6 x 10^6 IU/ml (multiplicity of infection (MOI) 0.3) or 3.6 x 10^5 IU/ml (MOI 0.03) respectively. An uninfected control with HBSS added apically was also completed. Cells were then incubated at 37°C and 5% CO_2 for 2 hours. After this the apical side was washed twice with HBSS. The cells were returned to incubate at 37°C and 5% CO_2 for a further 22 hours or 46 hours with TEER recorded and compared between the 0 hour, 24 hour and 48 hour time points. Infected cells were collected at either 24 or 48 hours for qPCR analyses in 1 ml of QIAzol (Qiagen, Manchester, United Kingdom) and stored at -80°C. Apical wash was collected at 24 and 48 hours for analysis.

2.14.2 Submerged Culture

Submerged cultured BCi cells were washed with Hanks' Balanced Salt solution (HBSS) (Sigma-Aldrich) and Pneumacult-Ex infection medium (**Table 2.1**) was added. Influenza A/Wisconsin/67/2005 (Virapur, San Diego, CA) at a TCID50 of 3.6 x 10^8 IU/ml (infectious units/ml) was diluted and applied at a TCID50 of 3.6 x 10^6 IU/ml (multiplicity of infection (MOI) 0.3). An uninfected control was also completed. Cells were then incubated at 37°C and 5% CO_2 for 2 hours. After this the cells were washed twice with HBSS. The cells were returned to incubate at 37°C and 5% CO_2 for a further 22 hours. Infected cells were collected at either 24 for qPCR analyses in 1 ml of QIAzol (Qiagen, Manchester, United Kingdom) and stored at -80°C. Media was collected at 24 hours for analysis.

2.15 miRNA Sequencing

2.15.1 RNA isolation

RNA isolated for miRNA sequencing was completed by Qiagen using the miRNeasy Mini Kit (Qiagen) according to manufacturer's instructions. Briefly, EVs (suspended in 150 µl of 1X DPBS) were lysed using QIAzol Lysis Reagent (Qiagen). To assess the quality of RNA isolation across samples, QIAseq miRNA Library Quality control (QC) Spike-Ins (Qiagen) were added to each of the lysed EV samples. RNA was extracted, using phenol/chloroform-based phase separation and silica membrane–based purification, with an elution volume of 14 µl.

2.15.2 Library preparation and miRNA sequencing

The library preparation was performed by Qiagen using the QIAseq miRNA Library Kit (Qiagen) as per the manufacturer's instructions (**Figure 2.1**) A total of 5 µl total RNA was converted into

miRNA Next Generation Sequencing libraries. Briefly, library preparation included adapter ligation, reverse transcription with the introduction of Unique Molecular Index's (UMIs), library amplification using PCR (22 cycles), addition of sample indices and sample purification. Library preparation was quality controlled using capillary electrophoresis (Agilent DNA 1000 Chip).

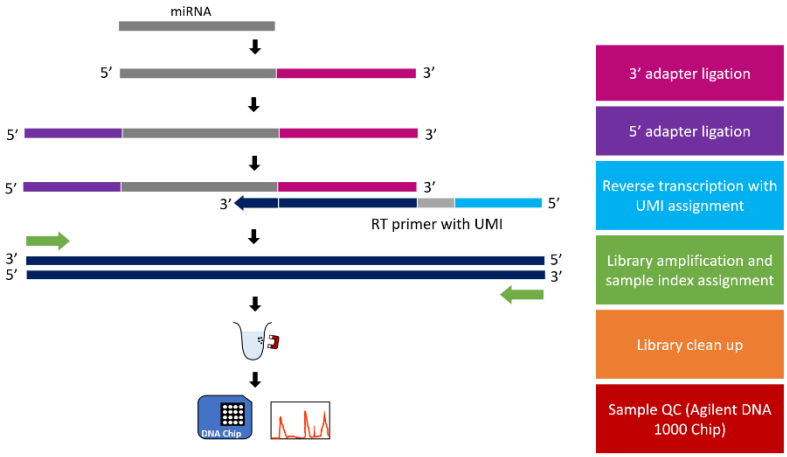

Figure 2.1 Schematic of miRNA QIAseq miRNA library preparation

Specially designed 3' and 5' adapters are ligated to mature miRNAs. The ligated miRNAs are then reverse transcribed to cDNA with assignment of Unique Molecular Index's (UMI). Library amplification occurs with indexing. Following a final library cleanup using magnetic bead-based method, the miRNA library is then ready for quality control (QC) and subsequent sequencing.

The libraries were then pooled in equimolar ratios, based on quality and concentration measurements, and then sequenced by Qiagen on a NextSeq (Illumina Inc.) sequencing instrument according to the manufacturer instructions. The following sequencing parameters were used:

- Read type - Single-end read
- Number of sequencing cycles (read length) - 75 nucleotides
- Average number of reads - 12 million reads/sample

The NextSeq500 sequencing system generates raw data files in binary base call (BCL) format. Qiagen® used bcl2fastq conversion software v2.20 (Illumina Inc) to demultiplex data and convert BCL files to standard FASTQ file format that stores both raw sequence data and quality scores. The sequencing resulted in 20 million reads per sample on average (**Figure 2.2**).

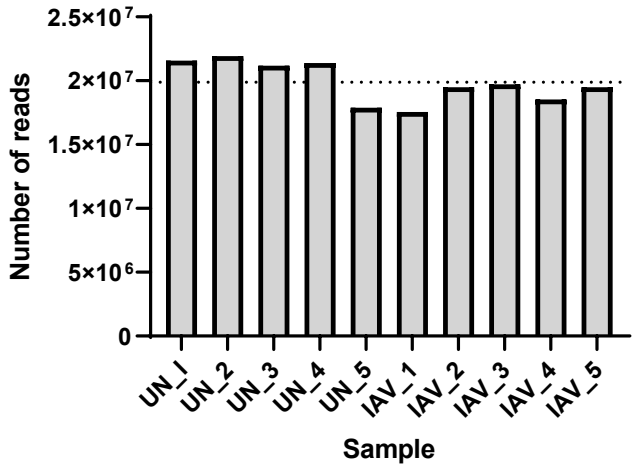

Figure 2.2 Sequencing resulted in 20 million reads per sample on average

Samples are EVs isolated from uninfected ALI BCi (UN) and EVs isolated from IAV infected ALI BCi (IAV). The dotted horizontal line indicates the mean number of reads.

2.15.3 Quality control of sequenced data

FASTQ files were analysed by Qiagen using FastQC, a quality control tool for high throughput sequencing data. The quality of a given base call is measured as a Phred quality score and indicates the probability of the base being called correctly. **Figure 2.3** displays the distribution of median Phred quality scores over all reads at each read position for each sample. The Phred scores are categorised into poor (red, 0 to <20), medium (yellow, 20 to <28) and good (green, 28 and higher). The sequencing data is of excellent sequencing quality as can be seen by a high PHRED score over the whole read length for all samples.

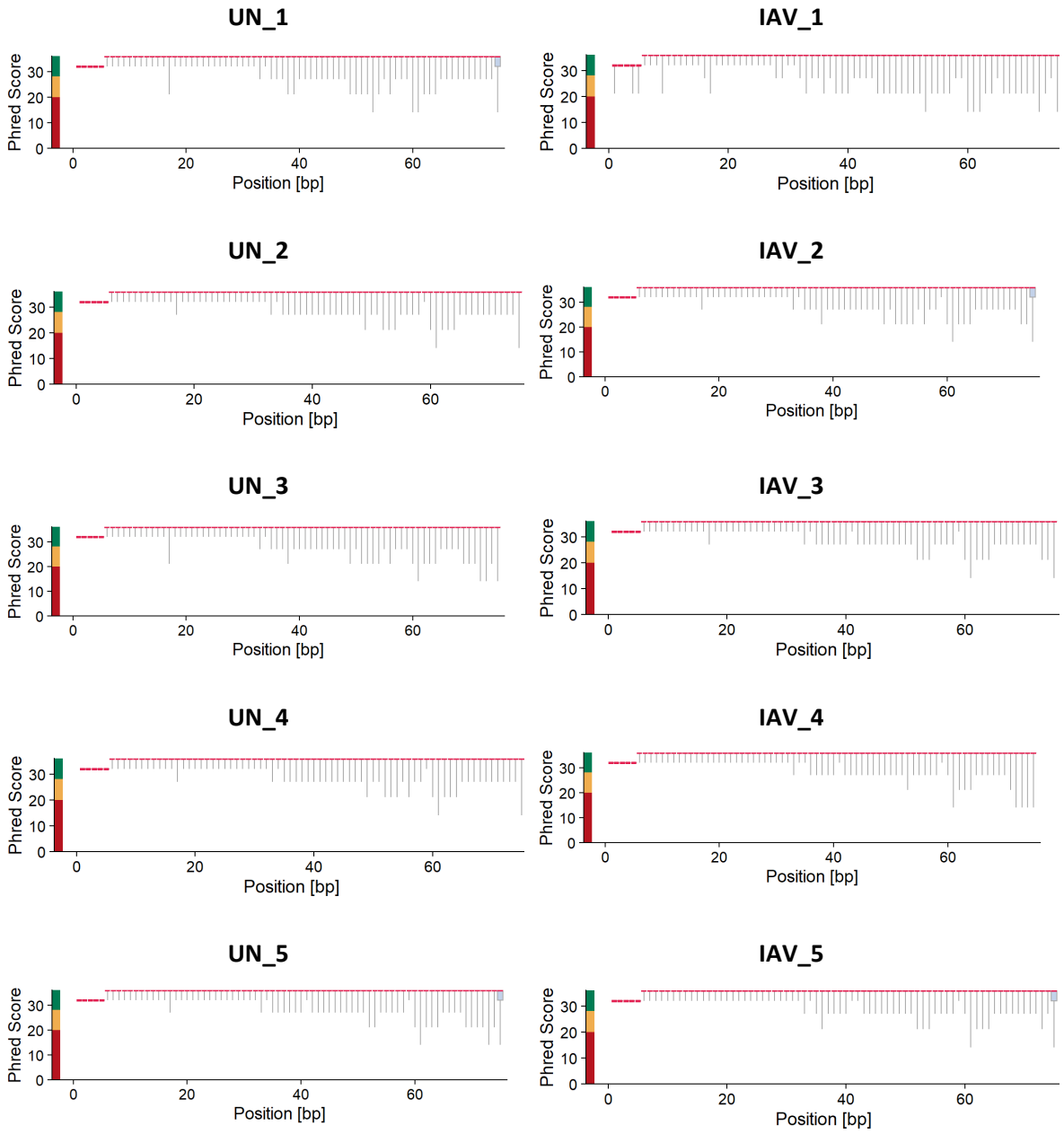

Figure 2.3 Sequencing data is of excellent quality

Samples are EVs isolated from uninfected ALI BCi (UN) and EVs isolated from IAV infected ALI BCi (IAV). The boxplots represent the 5th, 25th, 75th and 95th percentile and the median. The coloured bar classifies the Phred scores into three quality categories: poor (red, 0 to <20), medium (yellow, 20 to <28) and good (green, 28 and higher).

2.15.4 Read processing

Read processing was carried out by Qiagen using CLC Genomics Server 21.0.4. In summary, the reads were processed by trimming the common sequence, UMI and adapters. In addition, reads with length < 15 nt or > 55 nt were filtered out and deduplicated using the UMI. Reads were grouped into UMI groups when they start at the same position based on the end of the read to which the UMI is ligated, are from the same strand or have identical UMIs. Groups that contain only one read (singletons) are merged into non-singleton groups if the singleton's UMI can be converted to a UMI of a non-singleton group by introducing a single nucleotide polymorphism. The distribution of the processed reads is displayed in **Figure 2.4**. Trimmed read length distributions depict that all samples have a peak at the expected miRNA read length of around 21 nucleotides.

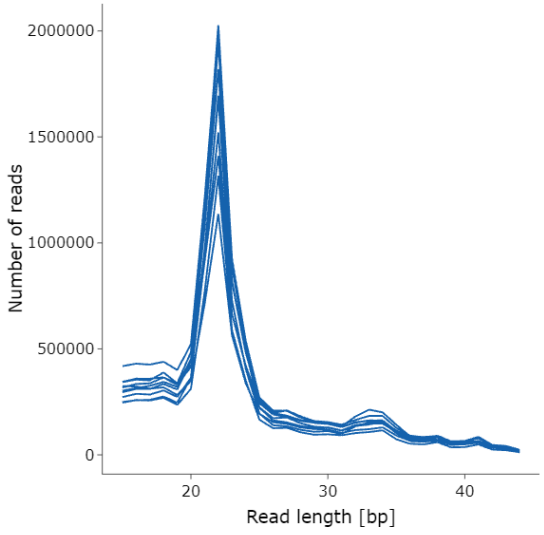

Figure 2.4 All samples have a peak at the expected miRNA read length

Reads were processed by trimming of the common sequence, UMI and adapters, and keeping reads with lengths of 15 to 55 nt.

2.16 Read Mapping

Qiagen mapped the reads to human miRBase version 22 using the workflow "QIAseq miRNA Quantification" of CLC Genomics Server with standard parameters. Reads were also mapped by Qiagen to the human piwi RNA (piRNA) database hsa.v1.7.6. All reads that didn't map to miRBase or piRNA database were mapped by Qiagen to the human genome GRCh38 with ENSEMBL

GRCh38 version 97 annotation. This was carried out using the “RNA-Seq Analysis” workflow of CLC Genomics Server with standard parameters.

2.17 Spike in analyses

QIAseq miRNA Library QC Spike-Ins were used to track technical variation in the samples. Spearman correlation analysis of the RNA-spike-in was performed across the samples. The following correlation matrix demonstrates excellent correlation of counts corresponding to the spike-in between the samples which indicates a minimal proportion of variation from technical sources (**Figure 2.5**).

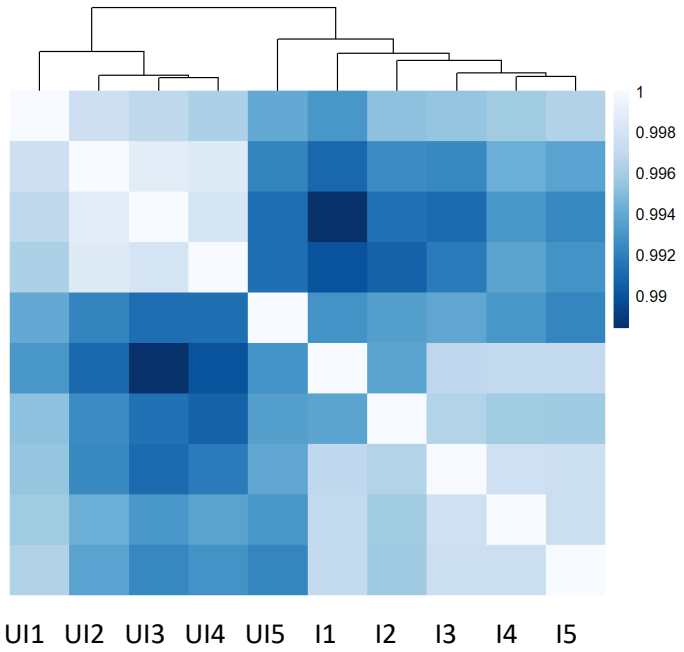

Figure 2.5 High correlation of spike-in counts

miRBase counts were normalised as counts per million. Spearman correlation was used as distance metric for hierarchical clustering with complete-linkage as the agglomeration method for correlation matrix. Samples are EVs isolated from uninfected ALI BCi (UI) and EVs isolated from IAV infected ALI BCi (I).

2.18 Data Filtering

Unsupervised filtering, data analysis and differential expression analysis was performed by me in RStudio®, using R (v 4.1.1). The code can be found in the Appendix. The methods were adapted from the Bioconductor package, “Empirical analysis of digital gene expression in R” (edgeR).

Lowly-expressed miRNA were filtered out given that they are likely to below minimal level to have biological effect or may interfere with downstream analysis (**Figure 2.6**). A conservative value of 10 counts in a minimum of 5 samples was chosen as a cut-off margin for filtering to ensure maximum differential expressed miRNA were captured.

Violin plots were used to visualise the distribution of the data before and after unsupervised filtering of low counts. Data is presented as counts per million (CPM). The distribution was consistent between samples and no outliers were detected.

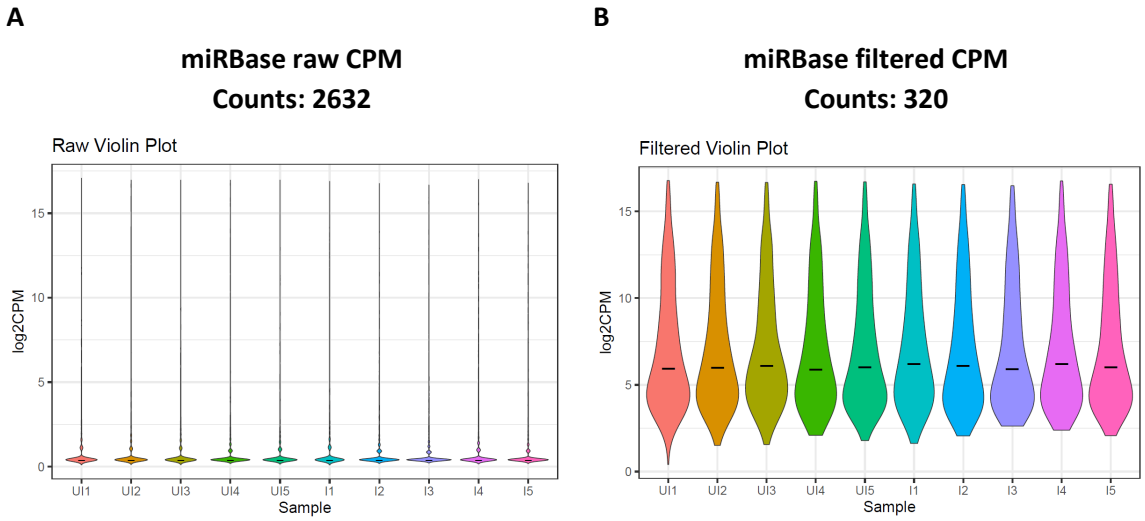

Figure 2.6 Unsupervised filtering to remove low counts

Violin plots showing the median and distribution of A) miRBase raw log2CPM (counts per million) and B) miRBase filtered log2CPM across samples. Samples are EVs isolated from uninfected ALI BCi (UI) and EVs isolated from IAV infected ALI BCi (I).

2.19 Detection of outliers - Interquartile range vs median plot

The presence of outliers was further investigated using IQR/Median plots. No samples were observed outside of ±2SD and therefore no outliers were removed (**Figure 2.7**).

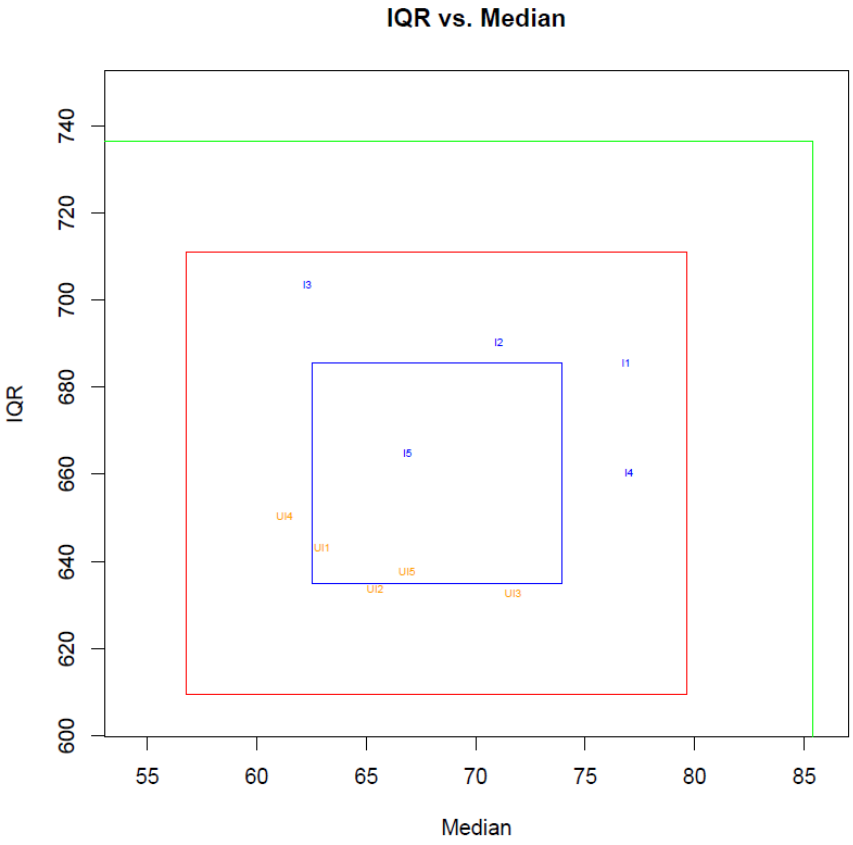

Figure 2.7 No outliers were detected.

Interquartile range/median plots of CPM data for miRbase. Blue perimeters represent ±1SD from the mean. Red perimeters represent ±2SD from the mean. Green perimeters represent ±3SD. Samples are EVs isolated from uninfected ALI BCi (UN) (orange data points) and EVs isolated from IAV infected ALI BCi (I) (blue data points).

2.20 Data normalisation

The filtered data was normalised using "Trimmed Mean of M-values" normalisation (TMM) implemented in the calcNormFactors function in the edgeR package (184,185). Under the TMM method of normalisation the TMM factor is computed by considering one sample as a reference sample and the others as test samples. This method is based on the hypothesis that most genes are not differentially expressed.

2.21 Principal component analysis

Principal component analysis (PCA) was used to transform the multi-dimensional sequencing dataset to smaller, discrete sets of orthogonal principal components. The first principal component specifies the direction with the largest variability in the data and then the variation decreases over the principal components. The PCA and plots were generated using the rgl package in R (v 3.8.2) using the function "prcomp" on the filtered CPM.

2.22 Differential expression analysis

Differential expression analysis was completed using edgeR method. EV miRNAs that were most stably expressed across all samples from the miRNA sequencing results were also investigated using NormFinder software (186).

2.23 miRNet

In silico miRNA target network analyses was conducted using miRNet 2.0 (www.mirnet.ca) and miRNA gene target database miRTarBase (https://bio.tools/mirtarbase). MiRNet was used to visualise the complex underlying networks between the miRNA and their target genes. The functional roles of the miRNA target gene network were also investigated in miRNet using gene ontology (GO) and Kyoto Encyclopedia of Genes and Genomes (KEGG) pathway analysis, where p-values < 0.05 were regarded as statistically significant for the functional analysis. Functional analyses of miRNA target genes identified by miRTarBase was also completed using ToppFun function of ToppGene an online biological information database that performs GO and KEGG pathway analysis (https://toppgene.cchmc.org/enrichment.jsp).

2.24 Transfection

Submerged BCi cells were seeded 6 x 10^4 cells per well in a 24 well plate with 500 µl of Pneumacult-Ex Complete Medium. The following day the media was changed to 450 µl of Pneumacult-Ex Complete Medium. Transfection was completed with Lipofectamine™ 3000 Transfection Reagent and 20 nM of either miRVana miR-155-5p mimic, miRVana miR-155-5p inhibitor, miRVana control mimic or miRVana control inhibitor per well as per manufacturer instructions. Briefly 1 µl of Lipofectamine™ 3000 Transfection Reagent was diluted in 25 µl of Opti-MEM Medium. In addition, 10 pmol of RNA was diluted in 25 µl of Opti-MEM Medium. The

diluted RNA was then added to diluted Lipofectamine™ 3000 in 1:1 ratio. The RNA Lipofectamine mixture was then incubated at room temperature for 15 minutes. Then 50 µl of the RNA Lipofectamine complex was added to the cells. The cells were the incubated at 37°C for 48 hours.

ALI BCi cells were transfected with 100 nM of miRVana miR-155-5p mimic or miRVana control mimic. Briefly 5 µl of Lipofectamine™ 3000 Transfection Reagent and 100 pmol of RNA were combined in 500 µl of Opti-MEM Medium. From this 100 µl of transfection mixture was added to the apical surface and 400 µl of the transfection mixture was added to basolateral compartment. The cells were then incubated at 37°C for 4 hours and then returned to Pneumacult ALI media.

2.25 Statistical Analyses

GraphPad Prism version 9 (GraphPad Software Inc., San Diego, USA) was used for analyses. Statistical test used for analyses will be described where appropriate. Normality determined by Shapiro-Wilk test. Normally distributed data displayed with mean and analysed using unpaired t-test. Normally distributed uninfected vs infected PBEC data displayed with mean and analysed using paired t-test. Non-parametric data displayed with medium and analysed using Mann-Whitney test. Non-parametric uninfected vs infected PBEC data displayed with medium and analysed using Wilcoxon test. Significance was determined by $p<0.05$.

3 Characterisation of BCi-NS1 epithelial model for IAV infection and isolation of EVs

3.1 Introduction

This chapter addresses the first aim of this thesis which was to establish an ALI cultured bronchial epithelial cell model for IAV infection and isolation of EVs. This was completed using the BCi-NS1.1 immortalised cell line kindly provided by Ronald Crystal. The BCi cell line has been generated from bronchial airway epithelial cells taken from a clinically normal donor and infected with a retrovirus expressing human telomerase (hTERT) (187). A cell line was chosen over primary cells as it was more easily accessible, especially during the COVID-19 pandemic.

Most studies to date have used submerged basal airway epithelial cells to investigate influenza infection. Submerged basal airway epithelial models have limitations regarding recapitulating the differentiated epithelium observed *in vivo* (188). ALI differentiated epithelial cells have been proposed as a superior model system to investigate the pathogenesis of respiratory infections (189). The BCi cell line has been shown to retain characteristics of original primary cells over 40 passages and has the capacity to differentiate into a pseudostratified layer including tight junction formation and the presence of motile cilia (187).

Previous studies have shown EVs isolated 24 h post viral-infection contain significantly different levels of immune regulatory miRNA compared to uninfected controls (161). There are currently no studies that describe the response of ALI cultured BCi to IAV or that characterise the EV miRNA cargo released from ALI cultured epithelial cells in response to IAV. Given the time and costs involved in RNA-sequencing and bioinformatics analysis it was important to first establish suitable infection conditions. IAV strain H3N2 was chosen for analyses given it routinely circulates in humans and has been associated with increased risk of hospitalisation in COPD patients (190). The immune response, cell death and barrier integrity of BCi was investigated following infection with IAV at TCID50 of 3.6 x 10^5 IU/ml (MOI 0.03) or 3.6 x 10^6 IU/ml (MOI 0.3) for either 24 or 48 h.

Furthermore, this chapter reports the isolation and characterisation of EVs from BCi cells. EV characterization is a key first step in order to understand the function of EVs as described in the MISEV 2018 guidelines (92). EVs were isolated from the apical air-exposed surface of ALI BCi to

investigate the role of EVs in immune signal propagation in the lung. SEC was used to isolate EVs from other soluble proteins that can bind miRNA (191).

3.2 Results

3.2.1 Analysis of immune response, cell death and barrier integrity of ALI BCi following infection with IAV

ALI cultured BCi cells were infected by adding IAV diluted in HBSS at either TCID50 of 3.6×10^5 IU/ml or 3.6×10^6 IU/ml to the apical compartment for 2 hours. The cells were then washed with HBSS to remove any external virus and returned to ALI for 24 h or 48 h. Uninfected controls were incubated with HBSS without IAV. Uninfected and IAV infected samples were considered as unpaired samples given a single cell line was used and the experiments were carried out in separate wells.

To investigate viral infection of BCi, analysis of viral RNA encoding IAV HA gene via qPCR was completed. ΔCT values of viral RNA were calculated for each sample from Ct values of gene of interest minus Ct value of housekeeping gene (*ACTB*). Following infection with 3.6×10^5 IU/ml, low levels of viral RNA were detected at 24 h (**Figure 3.1A**). However, the level of viral RNA was greatly increased by 48 h. A greater level of viral RNA was observed at 24 h for BCi infected with higher dose of IAV (3.6×10^6 IU/ml) compared to lower dose (3.6×10^5 IU/ml). Furthermore, the level of viral RNA was similar between 24 and 48 hours for 3.6×10^6 IU/ml.

The MISEV 2018 guidelines outline the importance for EV studies to indicate the levels of cell death, since even a small percentage of cell death could release cell membranes that outnumber true released EVs. However, establishing a condition in which there is IAV infection but no cell death would not be possible in this circumstance, given it has been widely demonstrated that IAV induces apoptosis and necrosis of airway epithelial cells (91,192).

To analyse IAV induced cell death, a LDH assay was performed on the apical wash supernatant harvested from differentiated BCi cells cultured at ALI. LDH is a soluble cytoplasmic enzyme that is released from the cytoplasm upon damage to the cellular membrane. Cytotoxicity was calculated as a percentage of LDH release of the total LDH measured following lysis of cells at each condition. Analyses of the data revealed a slight but not significant increase in LDH release by BCi cells infected with IAV at the 24 h time point for either infectious dose (***Figure 3.1B***). However, at the

48 h timepoint there was a large significant increase in LDH release from the BCi-ALI cultures that were infected with IAV at either infectious dose.

To further understand the effect of IAV damage to the 3D architecture within the pseudostratified epithelium the integrity of the barrier formed by ALI cultured BCi cells was investigated by measuring the TEER. The electrical resistance of the epithelial layer was measured in ohms by placing one electrode in the apical compartment and the other in the basal compartment. The data presented is the TEER measurement of a particular well as a percentage of TEER measurement at time point 0 (***Figure 3.1C***). At 24 h post-infection, there was no significant difference in percentage TEER values for BCi infected with IAV at 3.6×10^5 IU/ml. On the other hand, at 24 h post-infection for BCi infected with IAV at 3.6×10^6 IU/ml there was a significant 15% decrease in TEER. At 48 h there was a dramatic 75% reduction in TEER for 3.6×10^5 IU/ml and 85% for 3.6×10^6 IU/ml IAV infected BCi. Despite this reduction in TEER no visible leakage of media to the apical face was observed.

The innate immune response of ALI BCi to IAV was also investigated by analysing expression of *CXCL10*, *IFNB1*, *ISG15*, *IL6* and *SOCS1* (**Figure 3.2**). ALI BCi cultures infected with IAV at 3.6×10^5 IU/ml showed slight upregulation of these innate immune genes at 24 h, with a more robust upregulation by 48 h. On the other hand, ALI BCi infected with IAV at 3.6×10^6 IU/ml showed a greater upregulation of these genes by 24 h. The most upregulated gene in response to IAV at 3.6×10^6 IU/ml for both 24 and 48 h was *CXCL10* followed by *IFNB1*, *ISG15*, *SOCS1* and then *IL6*.

Infection of ALI cultured BCi with IAV at 3.6×10^6 IU/ml for 24 h was decided as the most suitable condition to take forward for EV miRNA-sequencing due to the significant increase in the immune response but with low potential for confounding by factors associated with cell death.

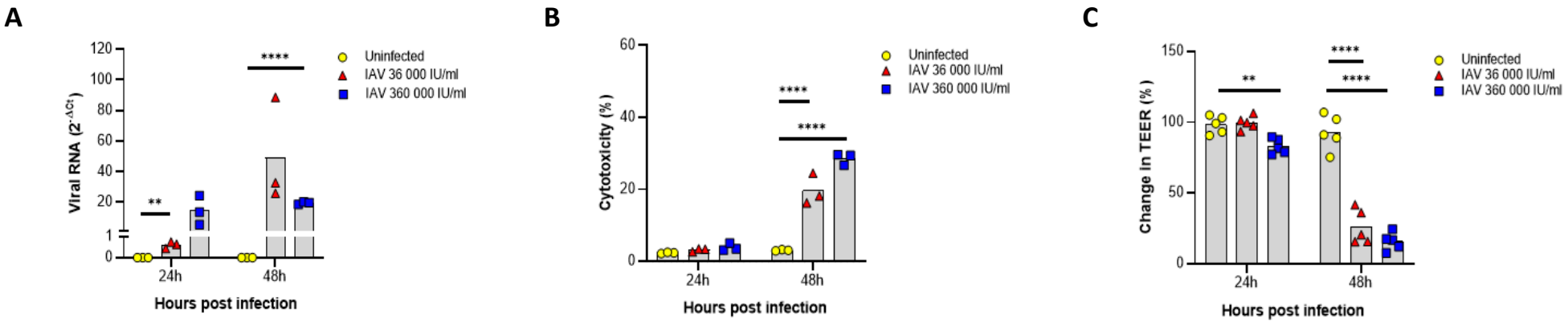

Figure 3.1 ALI BCi infection with IAV results in cell death and reduced barrier integrity

Analysis was completed for IAV infected BCi (3.6 x 10^5 IU/ml (red symbols) or 3.6 x 10^6 IU/ml (blue symbols)) and uninfected BCi (yellow symbols) at the 24 h or 48 h post infection timepoints. A) The intracellular level of viral RNA encoding IAV HA was analysed via qPCR. ΔCT values of viral RNA was calculated as Ct values of IAV HA minus Ct value of housekeeping gene (ACTB). B) Cytotoxicity was calculated as LDH release as a percentage of the total LDH measured following cell lysis. C) TEER measurement as a percentage of TEER measurement at time point 0. Fold change was calculated for IAV infected sample compared to uninfected sample. Normality determined by Shapiro-Wilk test. Data displayed with mean and analysed using unpaired t-test. *P<0.05, **p<0.01, ***p<0.001, ****p<0.0001

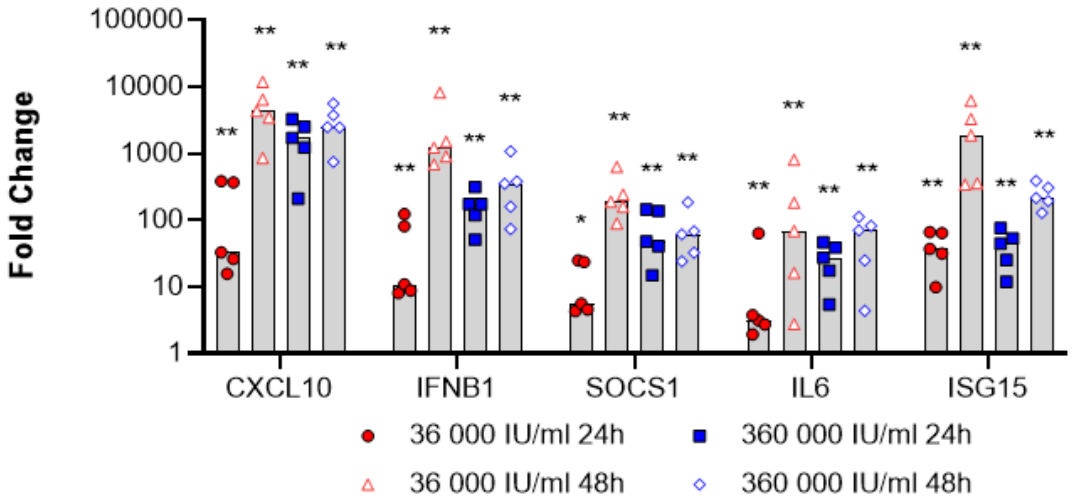

Figure 3.2 ALI BCi infection with IAV results increased anti-viral gene expression

*Analysis was completed for IAV infected BCi (3.6 x 105 IU/ml (red symbols) or 3.6 x 106 IU/ml (blue symbols)) and uninfected BCi (yellow symbols) at the 24 h or 48 h post infection timepoints. The expression of CXCL10, IFNB1, ISG15, IL6 and SOCS1 was analysed via qPCR. ΔCT values were calculated from the Ct values of gene of interest minus Ct value of housekeeping gene (ACTB). Fold change was calculated for IAV infected sample compared to uninfected sample. Normality determined by Shapiro-Wilk test. Data displayed with medium and analysed using Mann-Whitney test. *P<0.05,**p<0.01, ***p<0.001, ****p<0.0001*

3.2.2 Characterisation of SEC isolated EVs - Protein concentration

EVs were collected from ALI BCi by completing a HBSS wash of the apical surface. A multi-step process including filtration and SEC was then used to isolate EVs, based on size, from other soluble protein-miRNA complexes in the apical wash. EV isolation was completed using 5 ml of apical wash collected and concentrated from 12 x 0.33 cm^2 BCi ALI transwells. The SEC elution was collected as 24 x 0.5 ml fractions immediately after loading the sample (**Figure 3.3A**). Based on the manufacturer's instructions EVs were expected to be eluted in fractions 6-11. The protein concentration across the first 17 SEC fractions were analysed (**Figure 3.3B**). This showed a clear peak in protein concentration of around 100 µg/mL at fraction 8. A second protein peak was also observed in the later fractions. The fractions were then combined and concentrated to form 4 groups as follows: fractions 1-5 termed SEC#1, fractions 6-11 termed SEC#2, fractions 12-17 termed SEC#3 and fractions 18-24 termed SEC#4. The protein concentration of the grouped fractions was analysed. Once concentrated, around 300 µg/mL of protein could be detected in the SEC#2 grouped EV fraction and around 900 µg/mL in the later fraction's termer SEC#4 (**Figure 3.3C**). Protein was not detected in the SEC#1 void volume samples. No significant difference in protein concentration of SEC#2 grouped EV fraction was detected between uninfected and IAV infected samples (**Figure 3.3D**).

3.2.3 Characterisation of SEC isolated EVs - Lipoprotein detection

One of the main limitations of SEC is that EVs have been shown to be co-isolated with lipoprotein particles due to a similarity in size (193). Unlike EVs, lipoproteins are composed of a surface monolayer of phospholipid, cholesterol and apolipoproteins. While there is evidence that lipoproteins are present in the lung, previous studies have reported the release of lipoproteins from cell types including macrophages and alveolar epithelial cells rather than ciliated bronchial epithelial cells (194). Furthermore, bronchial epithelial cells have not been shown to express typical apolipoproteins required for the formation of lipoprotein (195). To confirm the absence of lipoprotein released from ALI BCi an ApoE ELISA was completed. Indeed, ApoE was not detected even in the concentrated apical wash prior to isolation (data not shown). A signal was detected from the positive control supporting this result was due to no ApoE or extremely low concentrations of ApoE released by BCi and not an error in the experimental technique.

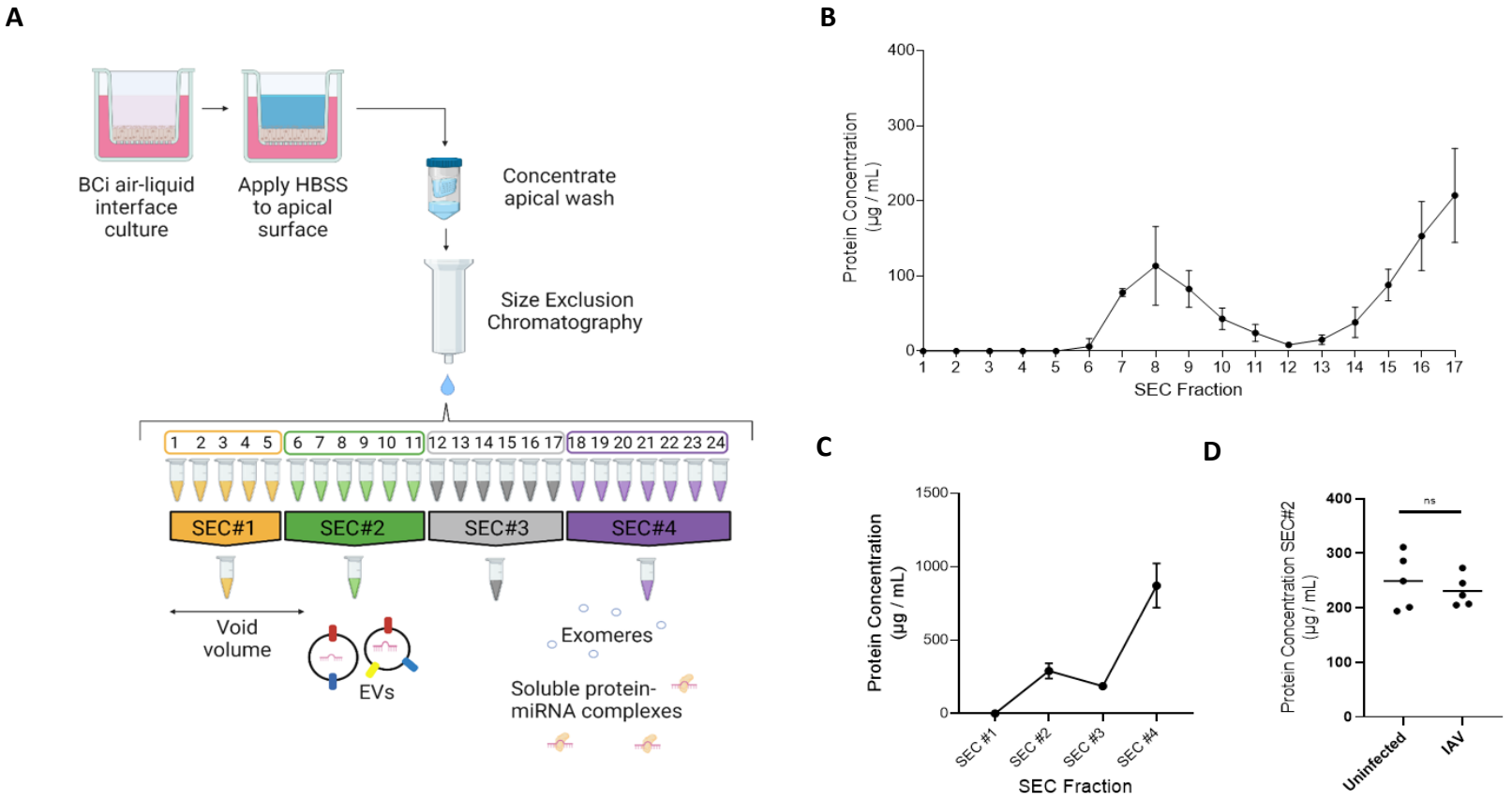

Figure 3.3 EVs separated from other soluble protein using SEC

A) Schematic of SEC EV isolation protocol from ALI BCi. Protein concentration (µg/ml) measured by BCA assay of B) 1-17 fractions obtained from SEC separation of ALI BCi apical wash (n=3). C) Concentrated fractions SEC#1 (fractions 1-5), SEC#2 (fractions 6-11), SEC#3 (fractions 12-17) and SEC#4 (fractions 18-24) from SEC separation of ALI BCi (n=4). Mean displayed with standard deviation. D) Protein concentration SEC#2 for uninfected and IAV infected ALI. Normality determined by Shapiro-Wilk test. Normally distributed data displayed with mean and analysed using unpaired t-test. Statistical analyses completed with unpaired t-test. ns=not significant.

3.2.4 Characterisation of SEC isolated EVs - Transmission electron microscopy

To provide further confirmation that EVs were present in the SEC#2 isolated sample from the apical wash of ALI BCi, the SEC concentrated fractions were visualised using TEM. Visualisation of grouped SEC fraction SEC#2 revealed particles with expected size (<200 nm) and "cup shaped" morphology previously observed for EVs under TEM (**Figure 3.4A**). Particles with the typical EV morphology were not visualised in the SEC#3 isolated sample (**Figure 3.4B**). Other small particles around <50 nm in size with no clear membrane structure were observed in both SEC#2 and SEC#3. These may be non-vesicular particles, EVs that are too small to observe clear membrane structure or an artefact of the method as the EVs appear to be ruptured releasing their content.

3.2.5 Characterisation of SEC isolated EVs - Western blot analyses

Western blot analyses was used to further demonstrate the presence of EVs and lack of contaminating particles and other molecules in SEC#2 isolated samples from ALI BCi cultures (**Figure 3.5**). Concentrated SEC fractions (#1, #2, #3 and #4) and ALI BCi cell lysate were loaded onto the same gel. The same volume of each of the concentrated SEC fractions (#1, #2, #3 and #4) was loaded. The different SEC fractions were not standardised to equal protein concentrations prior to loading. Tetraspanin CD63 commonly used as an EV marker was predominantly detected in SEC#2 and to a lesser extent in SEC#3. Furthermore, CD63 appears to be enriched in SEC#2 compared to cell lysate. Tetraspanin CD9, also commonly used as an EV marker, was only detected in SEC#2. In addition, the molecular weight of CD9 was lower for SEC#2 compared to the cell lysate. Given smaller particles were observed by TEM the presence of STCH (Heat Shock Protein Family A (Hsp70) Member 13) previously associated with small non membrane particle was investigated (98). This was shown to be only present in the later fractions SEC#3 and SEC#4. In addition, the absence of endoplasmic reticulum protein calnexin in any of the SEC fractions was demonstrated. On the other hand, calnexin was strongly detected in the cell lysate.

A

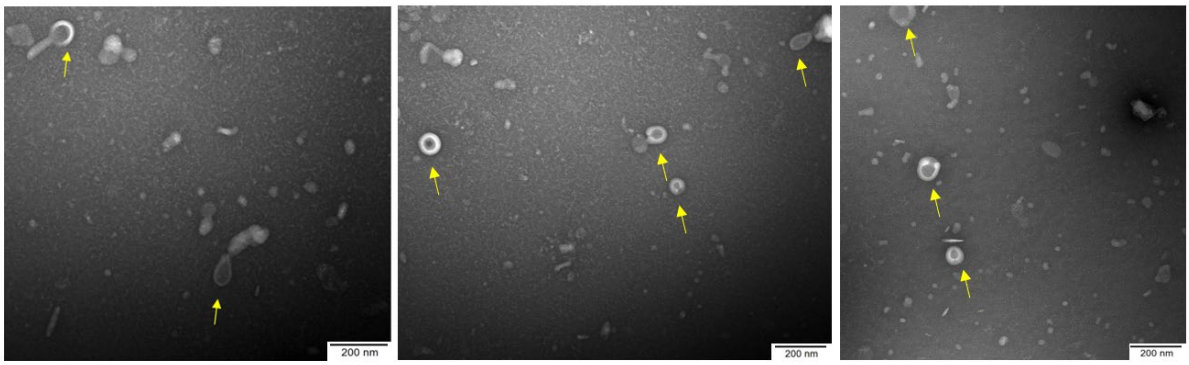

B

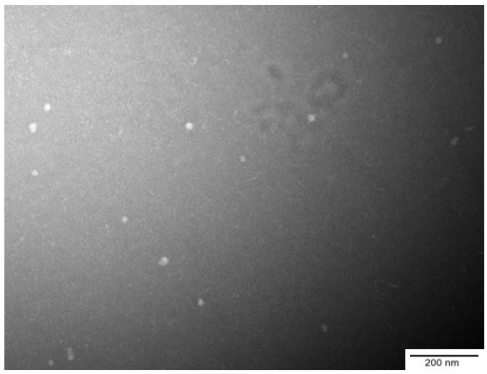

Figure 3.4 Particles with typical size and morphology of EVs visualised in SEC#2 sample by TEM

TEM images of A) SEC#2 (multiple images from single sample) and B) SEC#3 isolated samples from apical wash of ALI BCi. Yellow arrows indicate example of particles typical of EVs. Scale bar shown in bottom right-hand corner. n=1.

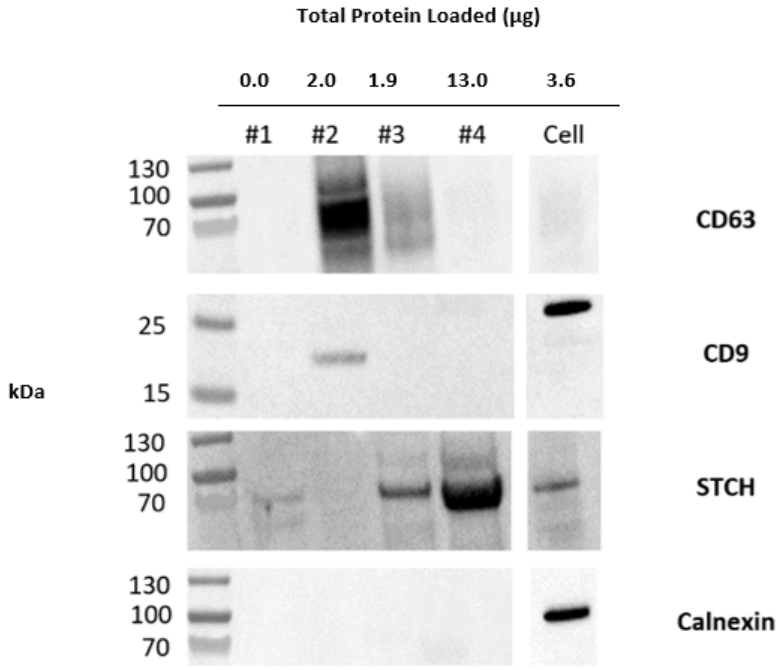

Figure 3.5 Presence of EV proteins (CD63 and CD9) and absence of non-EV proteins (STCH and Calnexin) detected in SEC#2 sample

Left lane contains prestained protein ladder with protein size indicated in kDa. Samples and total protein loaded include SEC#1 (0 µg), SEC#2 (2 µg), SEC#3 (1.9 µg), SEC#4 (13 µg) isolated from apical wash of ALI BCi and ALI BCi cell lysate (3.6 µg).

3.2.6 Characterisation of SEC isolated EVs - ExoView

To further characterize the EV population, 200 µl of concentrated SEC#2 sample was sent for analyses by NanoView Biosciences using the ExoView R100. A 200 µl non-isolated sample concentrated from 10 ml of apical wash prior to filtration or SEC was also analysed. The ExoView system and antibodies have been optimised to allow comparison between different EV markers. The mean size of CD9, CD63 or CD81 positive particles was obtained by interferometry-based label free measurements on particles captured by either CD9, CD63 or CD81 antibodies based on three technical replicates (**Figure 3.6A**). The mean particle size was determined to be relatively similar across the capture antibodies at 59 nm for CD9 capture, 61 nm for CD63 capture and 65 nm for CD81 capture. This was comparable to non-isolated sample supporting that SEC does not bias a particular population. One limitation of this method is that it has a lower limit cut-off of 50 nm and therefore any EVs smaller than 50 nm would not be detected potentially skewing the mean particle

size to be greater than it is (**Figure 3.6B**). This technology also allows quantification of all tetraspanin positive particles using fluorescent antibodies. The highest concentration of particles in both the isolated and non-isolated samples were CD9 positive followed by CD63 and CD81 (**Figure 3.6C**). In addition, the data suggests around 50% yield of EVs from the isolation protocol. The co-localisation of tetraspanins on particles in the SEC#2 sample was also investigated (**Figure 3.6D**). This demonstrated a heterogenous population with around half of CD9+ particles only containing CD9, with the remainder containing two tetraspanins and only a small percentage containing all three. CD63+ particles again predominantly only contained one tetraspanin however CD63+ is more commonly found co-isolated with CD9 compared to CD81. Lastly, CD81+ particles predominantly also contained CD9. A similar number of particles contained only CD81 or all three tetraspanins with little co-localisation observed with just CD63. Unfortunately it was not possible to complete ExoView analysis on EVs from IAV infected BCi as the company would not accept infected samples for analyses.

A

Sample	Average Vesicle Size (nm)		
	CD9	CD63	CD81
EV Sample (SEC#2)	59	61	65
Non-isolated	58	57	61

B

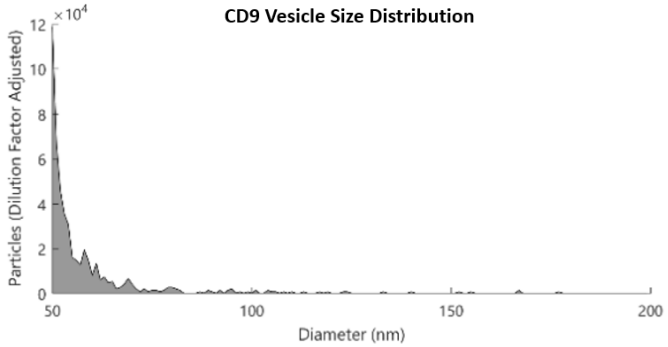

C

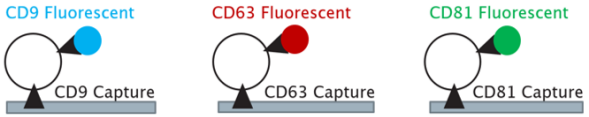

D

Sample	Average Vesicle Concentration (particles/ml)		
	CD9	CD63	CD81
EV Sample (SEC#2)	4.60×10^{11}	2.37×10^{11}	8.23×10^{10}
Non-isolated	8.66×10^{11}	4.30×10^{11}	1.73×10^{11}

E

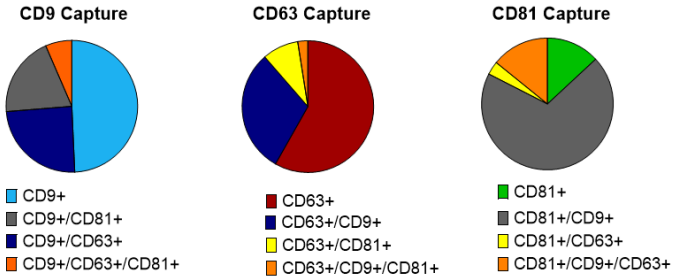

Figure 3.6 Analyses using ExoViewR100 platform reveal heterogenous population of ALI BCi EVs based on CD9, CD63 and CD81 EV markers

A) Mean size of CD9, CD63 and CD81 captured particles for SEC#2 (n=1) and non-isolated samples (n=1) from ALI BCi apical wash. B) Size histogram SEC#2 isolated CD9 capture. C) Diagram of ExoView immunocapture of EVs and fluorescent detection of CD9, CD81 and CD63. D) Concentration of particles with either CD9, CD63 or CD81 markers for SEC#2 and non-isolated supernatants. E) Co-localisation of CD9, CD63 and CD81 markers for particles captured by either CD9, CD63, CD81 antibodies. Average based on three technical replicates.

3.3 Discussion

Bronchial epithelial cells are vital mediators of the immune response at the lung interface (47). Recently it has been proposed that epithelial cells use EVs to communicate within the lung (196). There is limited existing literature on the miRNA cargo of airway epithelial EVs released in response to IAV. This chapter addresses the first aim of this thesis that was to establish a suitable *in vitro* culture model for the characterisation of EVs released by bronchial epithelial cells into the lung in response to IAV. The majority of previous studies investigating IAV infection of epithelial cells use monolayer, basal epithelial models. However in this thesis, epithelial cells were cultured under ALI to allow them to differentiate into a pseudostratified layer and that more closely mimics *in vivo* infection conditions (122,127,197). Furthermore EVs released apically from ALI cultured bronchial epithelial cells have been suggested to be reflective of those present in the airways and provide a relevant model of studying the role of EVs in immune signal propagation in the lung (198,199).

A number of immortalised respiratory epithelial cell lines have been developed including BEAS-2B, Calu-3, A549 (200). Cell lines offer many advantages including that they are easily accessible and can be used at high passage. However, many cell lines such as, A549 and Calu-3 are carcinogenic in origin and likely to have altered genetic and phenotypic characteristics compared with non-carcinogenic cells (201). BEAS-2B was the first cell line developed from non-carcinogenic human epithelium via transfection with an adenovirus 12-SV40 hybrid virus and have been used widely to in epithelial studies (202). However, BEAS-2B have limited ability to differentiate and do not form functional tight junctions (201). This study utilises the BCi immortalised human bronchial cell line that has been generated via expression of hTERT (187). BCi were used in this thesis due to the fact they can be more easily obtained and can be passaged for longer compared to primary epithelial cells. Furthermore, they were suitable for the preliminary nature of the research completed in this thesis. However, immortalised cell lines have limitations including the fact they have altered characteristics and do not capture the varying characteristics of the human population. Therefore, according to the third aim of this thesis, research will initially be completed using BCi and then validated using primary epithelial cells.

Epithelial cells are the primary target for IAV infection. Infection of host cells is required for IAV to propagate. In live cells 5.8% for 3.6×10^5 IU/ml and 7.3% for 3.6×10^6 IU/ml were IAV NP1 positive. In dead cells 16% for 3.6×10^5 IU/ml and 21.4% for 3.6×10^6 IU/ml were IAV NP1 positive. The results of this chapter also support IAV infection of ALI cultured BCi cells. An increase in the level of IAV RNA between 24 h and 48 h combined with the observation that a higher level of viral RNA was detected at 48 h after infection with the lower dose of IAV compared to the higher dose suggests IAV can

efficiently replicate in BCi. In addition, the results support that the level of IAV infection reaches a plateau.

IAV infection has been widely shown to induce apoptosis or necrosis of airway epithelial cells (192). Although studies have suggested that apoptotic bodies may also transfer miRNA and play a role in antigen presentation in immunoregulation or harbour viral materials that contribute to the progression of IAV infection, they are not the focus of this study (203,204). Low infectious doses were chosen for this study to minimise cell death as this thesis aimed to investigate EVs released by epithelial cells in response to IAV rather than apoptotic bodies as a result of cell death (205).

The results in this chapter suggest that infection of ALI cultured BCi with either 3.6×10^5 IU/ml or 3.6×10^6 IU/ml IAV result in a high level of LDH release and disruption of the epithelial barrier function at 48 h. In addition, a slight increase in LDH release and barrier function was observed at 24 h following infection with IAV at 3.6×10^6 IU/ml but not following infection with IAV at 3.6×10^5 IU/ml. This is most likely due to the much higher levels of viral infection detected for 3.6×10^6 IU/ml IAV infection compared to 3.6×10^5 IU/ml IAV infection at 24 h. These observations align with a previous study that demonstrated that IAV results in damage of the epithelium both in terms of cell death and break down of epithelial cell barriers. A recent study demonstrated damage to *in vitro* cultures of alveolar epithelium 30 hours after H1N1pdm09 infection at MOI of 1, as characterized by a reduced TEER and increased cell death (77).

Epithelial cells have been widely demonstrated to express and release a range of anti-viral proteins. In this chapter increased expression of a range of immune genes including *CXCL10*, *IFNB1*, *ISG15*, *IL6* and *SOCS1* was demonstrated in response to IAV. These genes have previously been reported to be upregulated in response to IAV infection (206–210). Substantial immune gene expression was observed for 3.6×10^5 IU/ml at 48 h or 3.6×10^6 IU/ml IAV at 24 and 48 h. Again, this is most likely due to the higher levels of viral infection detected for 3.6×10^6 IU/ml IAV infection compared to 3.6×10^5 IU/ml IAV infection at 24 h. *CXCL10* was the most upregulated gene followed by *IFNB1*. This aligns with another study that reported a dramatic 13,000-fold increase in *CXCL10* expression and 5500-fold increase in *IFNB1* expression in ALI cultured airway epithelial cells following infection with IAV (77). Furthermore, ISG15 has previously been shown to be one of the most strongly and rapidly induced ISGs, with the ability to directly inhibit viral replication and modulate host immunity by the induction of natural killer cell proliferation and dendritic cell maturation as well as recruitment of neutrophils (211). In addition previous *in vitro* studies report increased SOCS expression in IAV-infected human bronchial epithelial cells as a key regulator of the innate immune response (212). *IL6* was the least upregulated gene of those investigated. IL6 has been reported to be required for virus

clearance through modulating neutrophil release and recruitment, and pivotal for the antibody production by promoting the differentiation of B cells (213). Furthermore, an increase in *IL6* expression has been strongly associated with IAV disease severity in humans (214).

Over the last 10 years there has been a rapid increase in the number of studies investigating the structure and function of EVs. This has been accompanied by the development of a wide range of techniques for the separation of EVs from other extracellular particles with some of the most common techniques including ultracentrifugation, SEC and density gradient separation. Given the lack of a gold standard it is currently accepted in the EV field to select a technique most suitable for the purpose of the study and provide evidence to support the successful isolation of EVs (92). SEC was selected for this study given it does not require any specialised equipment that could not be affordably purchased. In addition, this method has previously been shown to isolate a high yield compared to other techniques while separating EVs from other soluble proteins such as AGO2 that can bind miRNA (191). SEC uses porous beads to separate particles based on size with the largest particles being eluted first as they are unable to diffuse into the beads. Ultrafiltration combined with SEC has previously been shown to efficiently isolate EVs from cell culture for compositional and functional studies (172).

The release of EVs from ALI cultured BCi was investigated. On review of the literature, previous studies have required around 4 x T75 flasks of submerged basal epithelial cell culture conditioned media to isolate enough EVs for analyses (172). Therefore, experiments with basal epithelial EVs require a large quantity of culture plates that are more challenging to process. Furthermore another study using primary human bronchial epithelial ALI models reported that EVs are primarily released from the apical face opposed to the basolateral compartment (198). This thesis therefore focused on EVs released apically from differentiated epithelial cells as a model of EVs present in the lung.

The presence of EVs in the SEC#2 isolated sample from the ALI BCi apical wash was demonstrated by a range of methods. A distinct peak in protein concentration was detected in the SEC#2 EV fractions isolated from the apical wash. EV samples were visualised with TEM and shown to contain membrane bound vesicles with typical morphology as previously described for lung derived EVs (215). In addition, it was not possible to observe any EVs greater than 200 nm supporting the absence of apoptotic bodies. Particles with typical EV morphology were also not observed in the later SEC#3 fraction. In support of this, the tetraspanins CD9 and CD63, known to be enriched in EVs, were predominantly detected in the SEC#2 EV sample (92). On detection of EV CD9 the band was at a lower molecular weight compared to CD9 from cell lysate. Potentially CD9 could be cleaved in EVs or this may be an artefact of western blot analyses. The ExoView platform demonstrated the

presence of particles with a mean diameter of around 60 nm that contain tetraspanins CD9, CD63 and CD81. EVs isolated from apical face of bronchial epithelial cells appear to fall into previously reported small EV category (98).

Furthermore, the ExoView platform has been optimised with fluorescent antibodies to compare the presence of EV markers. The results in this chapter are the first to my knowledge that quantify EV markers from ALI cultured BCi via the ExoView platform. ALI cultured BCi EVs were shown to predominantly contain CD9 followed by CD63 and then CD81. In line with the data presented in this chapter, a previous study investigating EVs released from epithelial cells demonstrated that CD9 was the most prominently expressed EV marker followed by CD63 and CD81 (216). In addition, this chapter reports the co-localisation of CD9, CD63 and CD81 tetraspanins on isolated EVs. A heterogeneous population of EVs with a range of one or more tetraspanins was detected supporting previous studies that have demonstrated the heterogeneity of EVs (217).

Other studies have found differences in the presence of EV markers in response to viral infection. Plasma EV markers have been shown to be altered by infection with SARS-CoV-2 (218). A recent study also using the ExoView platform showed diverse populations of human epithelial EVs with opposite functions during Herpes Simplex Virus 1 infection (216). This previous study also reported that CD63+ EVs significantly increased with infection and became present in higher levels than CD9 (216). Unfortunately, it was not possible to complete analyses of EVs from IAV infected BCi in this thesis as NanoView Biosciences did not accept infected samples for analyses. This study will continue to investigate the EV population as a whole, given the additional technical difficulty and amount of sample required to separate different populations. Future work is required to determine differences in the miRNA content and function between EV populations.

The absence of other extracellular particles in the SEC#2 EV sample was also demonstrated. The presence of other smaller particles without clear membrane structures were visualised in the EV sample using TEM. These particles are likely to be an artefact of the method as the EVs appear to be ruptured releasing their content. Other studies have shown one limitation of SEC is that due to similarity in size, EVs can be co isolated with lipoprotein particles that have also been associated with miRNA (193,219). However, the absence of lipoproteins in the EV sample is supported by absence of ApoE, an important protein for the formation of lipoproteins and the fact many apolipoprotein have been shown not to be expressed by bronchial epithelial cells (220). In addition, the absence of STCH, supports the absence of non-membrane particles termed exomeres that are ~30nm and have also been associated with miRNA (221). Furthermore, the absence of endoplasmic

reticulum protein calnexin in these ALI culture-derived SEC#2 EV samples indicates no contamination with non-EV associated intracellular proteins (222).

3.4 Summary

In this chapter infection of ALI cultured BCi with IAV at 3.6 x 10^6 IU/ml for 24 h was decided as the most suitable condition to take forward for EV miRNA-sequencing due to significant increase in immune response but with low potential for confounding by factors associated with cell death. Overall, successful isolation of EVs from the apical surface of ALI cultures BCi was demonstrated by visualisation of EVs via TEM and detection of EV markers via western blot and ExoView system. Furthermore, ELISA and western blot analyses support the absence of typical contaminating factors.

4 Bronchial epithelial cell EV miRNA profile in response to IAV

4.1 Introduction

The previous chapter determined suitable IAV infection conditions for ALI BCi and demonstrated the successful isolation of EVs from the apical wash of ALI cultured BCi. This chapter addresses the aim to compare EV miRNA released from uninfected and IAV infected BCi cells.

RNA sequencing has previously demonstrated significant differences in EV miRNA released from RSV infected A549 monoloyer cultures at MOI 1 for 24 hours compared to non-infected controls (161). There are a few previous studies that have reported changes in epithelial EV miRNA in response to influenza. For example, EVs produced by influenza infected A549 epithelial cells induced IFN production to inhibit viral replication through upregulation of miR-1975 (162). However, these studies are limited by the fact they use submerged monolayer basal cell culture systems. To my knowledge there are currently no studies that characterise the EV miRNA cargo released from ALI cultured epithelial cells in response to influenza.

EVs were isolated from the apical wash of uninfected ALI cultured BCi (n=5) and IAV infected BCi (n=5) using filtration and SEC as previously described in Chapter 3. Infection was completed with IAV at TCID50 of 3.6 x 10^6 for 24 h as optimised in Chapter 3. EV samples were sent to Qiagen for RNA extraction, library preparation and sequencing using optimised, robust miRNA specific methods developed by Qiagen as described in section 2.15.

Qiagen completed the initial stages of processing the sequencing data for analyses including aligning the sequencing reads to the human mature miRNA database (miRBase). Reads were also mapped to another small RNA called piRNA. Reads not mapped to miRBase or piRNA database were mapped to the human genome. Differential expression analysis of EV miRNA between uninfected and IAV infected epithelial EVs was completed. The sequencing results were validated using RT-qPCR. The level of cellular and non-EV miRNA was also investigated to better understand if the changes in EV miRNA were specific to EVs.

Given BCi cells have been modified to immortalise them it was also important to validate these finding using primary cells. Furthermore, one of the benefits of primary cells is it is possible to investigate the impact of chronic disease such as COPD on the EV miRNA response to IAV. As

previously described in Chapter 1 patients with COPD are more susceptible to influenza infections though the exact molecular mechanism responsible for dysfunction of anti-viral immune response remains unclear. Therefore, EV miRNA released following infection were compared between healthy (n=3) and COPD (n=3) PBEC.

4.2 Results

4.2.1 Distribution of read biotypes

Reads obtained from miRNA sequencing of uninfected (n=5) and IAV infected (n=5) BCi EVs were mapped by Qiagen to the mature miRNA database (miRBase). Reads were also mapped to the piRNA database (piRNAdb). Both piRNA and miRNA have been reported as regulators of gene expression and piRNA are of a similar size compared to miRNA, at 26-31 nt compared to 21-24 nt (223). However, while miRNA have been demonstrated to be ubiquitously expressed and their ability to repress target transcripts has been widely reported, piRNA have been predominantly identified in germline cells, where they serve essential roles in transposon silencing (109,224,225).

The average proportion of reads mapped to miRBase was 31.8% for EVs released from uninfected BCi and 34.8% for EVs released from IAV infected BCi (**Figure 4.1A**). The average proportion of reads mapped to piRNA database was much lower at 2.7% for uninfected BCi EVs and 3.2% for IAV infected BCi EVs. A large proportion of the reads were not mapped to these small RNA databases. These reads were mapped to the human genome. For both the uninfected BCi EVs and IAV infected BCi EVs the majority of the genome mapped reads were either lncRNA or protein coding RNA (**Figure 4.1B**). Uninfected and IAV infected samples were considered as unpaired samples given a single cell line was used and the experiments were carried out in separate transwells. Overall, the percentage of mapped reads was not significantly different between uninfected BCi EVs and IAV infected BCi EVs with the exception of miscellaneous RNA (miscRNA) which was significantly higher in IAV infected BCi EVs. MiscRNA is a non-coding RNA that cannot be classified by known RNA types. Other RNA biotypes including ribosomal RNA (rRNA), small nuclear RNA, mitochondrial (Mt) rRNA, small nucleolar RNAs, Mt tRNA were detected at very low levels at less than 1% of total.

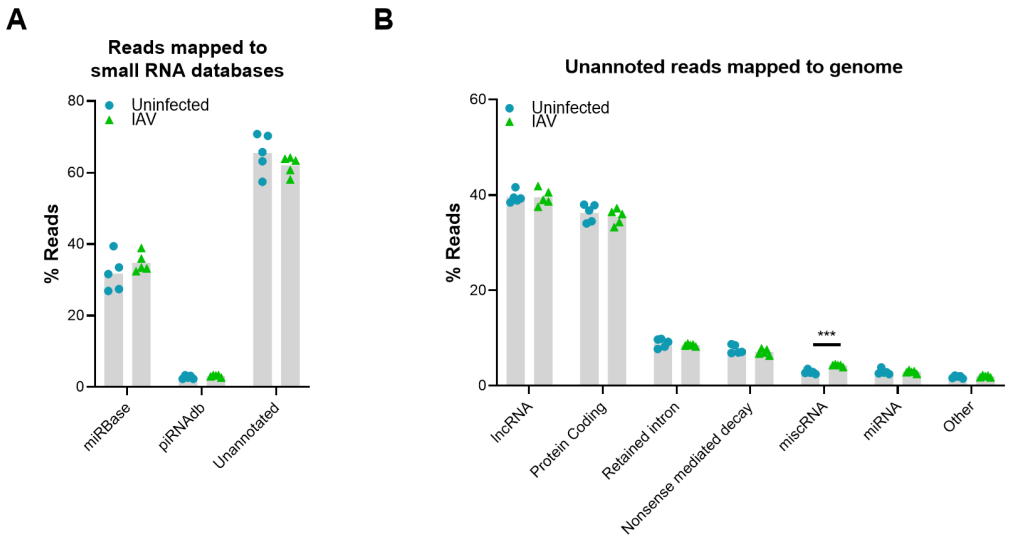

Figure 4.1 Proportions of EV reads mapped to miRBase is not altered following infection with IAV.

*A) Percentage of reads, from miRNA sequencing of uninfected BCi and IAV infected BCi EVs, mapped to miRBase and piRNAdb. B) Figure display unannotated reads (reads not mapped to miRBase or piRNAdb) mapped to the human genome. Other group includes ribosomal RNA (rRNA), small nuclear RNA, mitochondrial (Mt) rRNA, small nucleolar RNAs, Mt tRNA. Individual data points displayed. Normality determined by Shapiro-Wilk test. Bar-graph display mean. t-test ***p<0.001.*

4.2.2 Separation of uninfected and IAV infected samples by EV miRNA

One way to visualise variation in the data is to use dimensional reduction techniques such as principal component analysis (PCA). PCA is a statistical procedure that looks for a small set of orthogonal principal components. PCA plot performed for TMM normalised miRBase mapped data reveals separate clustering across PC1 of uninfected and infected BCi EVs based on miRNA except for one influenza data point (I4) that appears to cluster with the uninfected data points (**Figure 4.2**). The influenza datapoint (I4) was therefore determined to be an outlier and removed from the dataset for differential expression analysis.

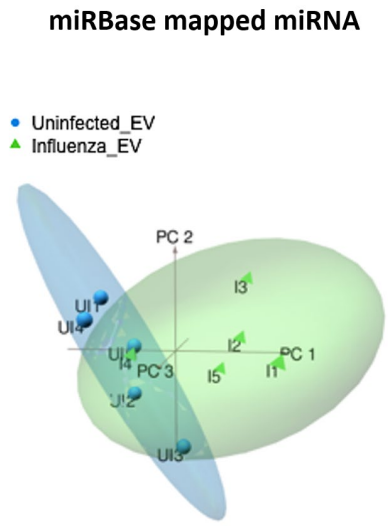

Figure 4.2 PCA reveals variation between IAV and uninfected EV miRNA

Three-dimensional principal component analysis (PCA) plot of filtered and TMM normalised miRBase mapped reads. EV samples were isolated from uninfected ALI BCi (Blue) (UI1-5) or IAV infected ALI BCi (green) (I1-5).

4.2.3 EV miRNA identified by sequencing to be altered in response to IAV

Differential expression analysis of uninfected and IAV infected BCi EVs was performed using methods outlined in section 2.15.4. Uninfected and IAV infected samples were considered as unpaired samples given a single cell line was used and the experiments were carried out in separate wells. The results are summarised in the heat map in **Figure 4.3A**, showing 13 significantly differentially expressed miRNA with p value adjusted using false discovery rate (FDR) correction, whereby by significance is demonstrated with an FDR of less than 0.01. These 13 significantly differentially expressed miRNA were then further reduced to 6 miRNA by applying a logFC > 0.6 or < -0.6 cut-off to identify miRNA altered above the minimal level of change of miRNA previously reported to have a significant impact on the biology of the cell (**Figure 4.3B**) (226). Of these, 5 miRNA were identified to be upregulated for IAV infected BCi EVs with logFC > 0.6 (miR-122-5p, miR-155-5p, miR-146a-5p, miR-7-5p, miR-378a-3p) and 1 downregulated with logFC < -0.6 (miR-505-5p). Three of these miRNAs had a relatively high degree of difference between uninfected and IAV infected BCi EVs with a logFC > 1 (miR-155-5p and miR-122-5p) or logFC < -1 (miR-505-5p). However, these three miRNAs were also only present at low levels with an average CPM <100. On the other hand, miR-146a-5p was the most highly abundant miRNA of these 6 differentially expressed miRNA wqqqith an

average CPM of 18,500. In addition, the top five miRNA that were most stably expressed across both IAV and uninfected BCi EVs were determined to be miR-26b-5p, miR-25-3p, let-7f-5p, miR-200b-5p and miR-148b-3p (**Figure 4.3C**). These were identified using the NormFinder software (186).

Visualisation of the differentially expressed miRNA CPM revealed IAV EV sample I4, that clustered with the uninfected samples on PCA, did not have elevated levels of miR-146 as observed for the other IAV EV samples (**Figure 4.3D**). However, levels of miR-505, miR-378a, miR-7, miR-155 and miR-122 were altered in sample I4.

A

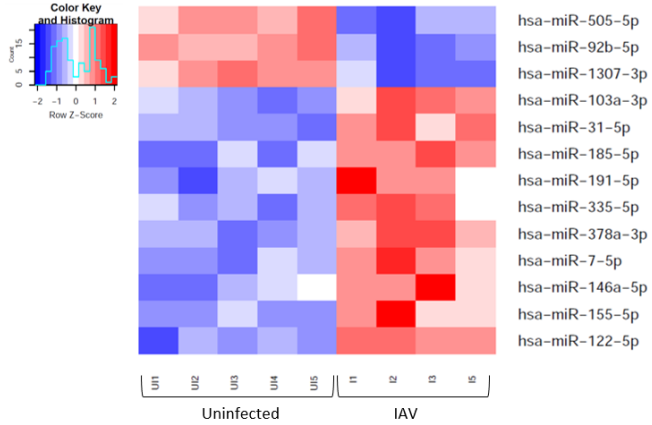

B

miRNA	logFC	logCPM	FDR
miR-505-5p	-1.47	3.70	0.0039
miR-378a-3p	0.60	9.82	0.0019
miR-7-5p	0.84	8.06	0.0036
miR-146a-5p	0.84	14.23	0.0097
miR-155-5p	1.8	6.11	0.001934
miR-122-5p	2.1	2.86	0.004146

C

	GroupDif	GroupSD	Stability
miR-26b-5p	0.02	0.04	0.04
miR-25-3p	0.00	0.09	0.06
let-7f-5p	0.04	0.07	0.06
miR-200b-5p	0.09	0.04	0.06
miR-148b-3p	0.07	0.05	0.07

D

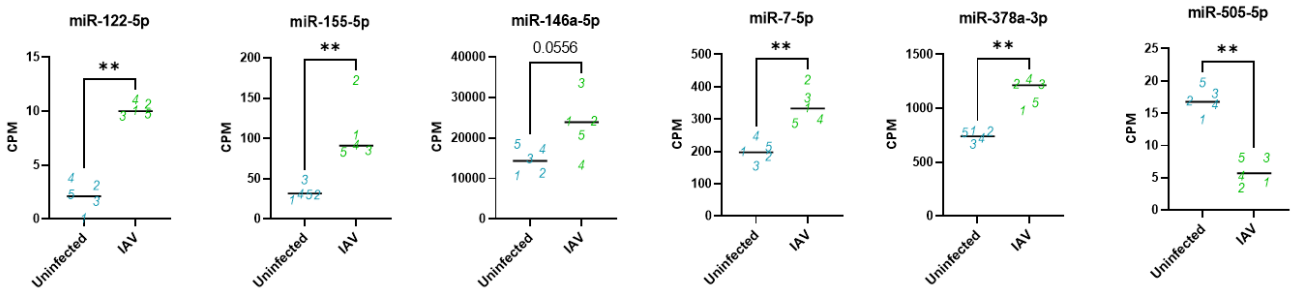

Figure 4.3 Differential expression analyses reveals miRNA altered in IAV infected BCi EVs compared to uninfected BCi EVs

*Comparison of EV samples isolated from uninfected ALI BCi or IAV infected ALI BCi. A) Heatmap, created using heatmap.2 function, of differential expressed miRNA (FDR<0.01) (Samples UI1-5 and I1-3,5) B) Table displaying logFC, logCPM and FDR of differential miRNA with logFC > 0.6 (red) or logFC< -0.6 (blue). C) NormFinder analysis of miRNA sequencing data to detect the most stably expressed miRNA across both IAV and uninfected BCi EVs. NormFinder uses a model-based approach which calculates the stability of reference genes based on two parameters–the intergroup variation (GroupDif) and the intragroup variation (GroupSD). D) Graphs displaying CPM of differential miRNA with logFC > 0.6 or logFC< -0.6 for uninfected EV (blue) (UI1-5) and IAV infected EVs (green) (I1-5). Line indicates median. Normality determined by Shapiro-Wilk test. Mann-Whitney. *=P<0.05, **p<0.01*

4.2.4 Most abundant BCi EV miRNA

Previous studies have suggested that miRNA abundance may be an important factor for miRNA-mediated gene regulation. Therefore, the most abundant EV miRNAs were investigated. Abundant miRNAs were identified by visualising miRNA with a mean count (n=5) greater than 3 SD from the mean count of all the miRNA (**Figure 4.4A**). In total 17 miRNA were identified for uninfected EVs and 19 miRNA were identified for IAV EVs. Several of these miRNAs including miR-191-5p, miR-146a-5p and miR-103a-3p were identified in section 4.2.3 to be significantly increased in IAV infected EVs compared to uninfected EVs. Though miR-191-5p and miR-103a-3p had a very low log2 fold change <0.6. Most of the abundant miRNAs were not significantly altered between uninfected and IAV infected BCi EVs. Furthermore, several miRNAs, including miR-26a-5p and let-7f-5p, were miRNA identified in section 4.2.3 to be the most stable miRNA. The top 10 most abundant miRNA were shared between uninfected and IAV infected EVs and form a distinct cluster over 9 SD above the mean count of all miRNA (**Figure 4.4B**). Of these 10 miRNAs, only miR-191-5p was also shown to be significantly increased in IAV infected EVs (section 4.2.3). The average amount of the top 10 miRNA (n=5) was calculated as a percentage of the total miRNA counts. This revealed for both uninfected and IAV infected EVs these top 10 miRNA make up a large proportion (around 60%) of the total counts (**Figure 4.4C**).

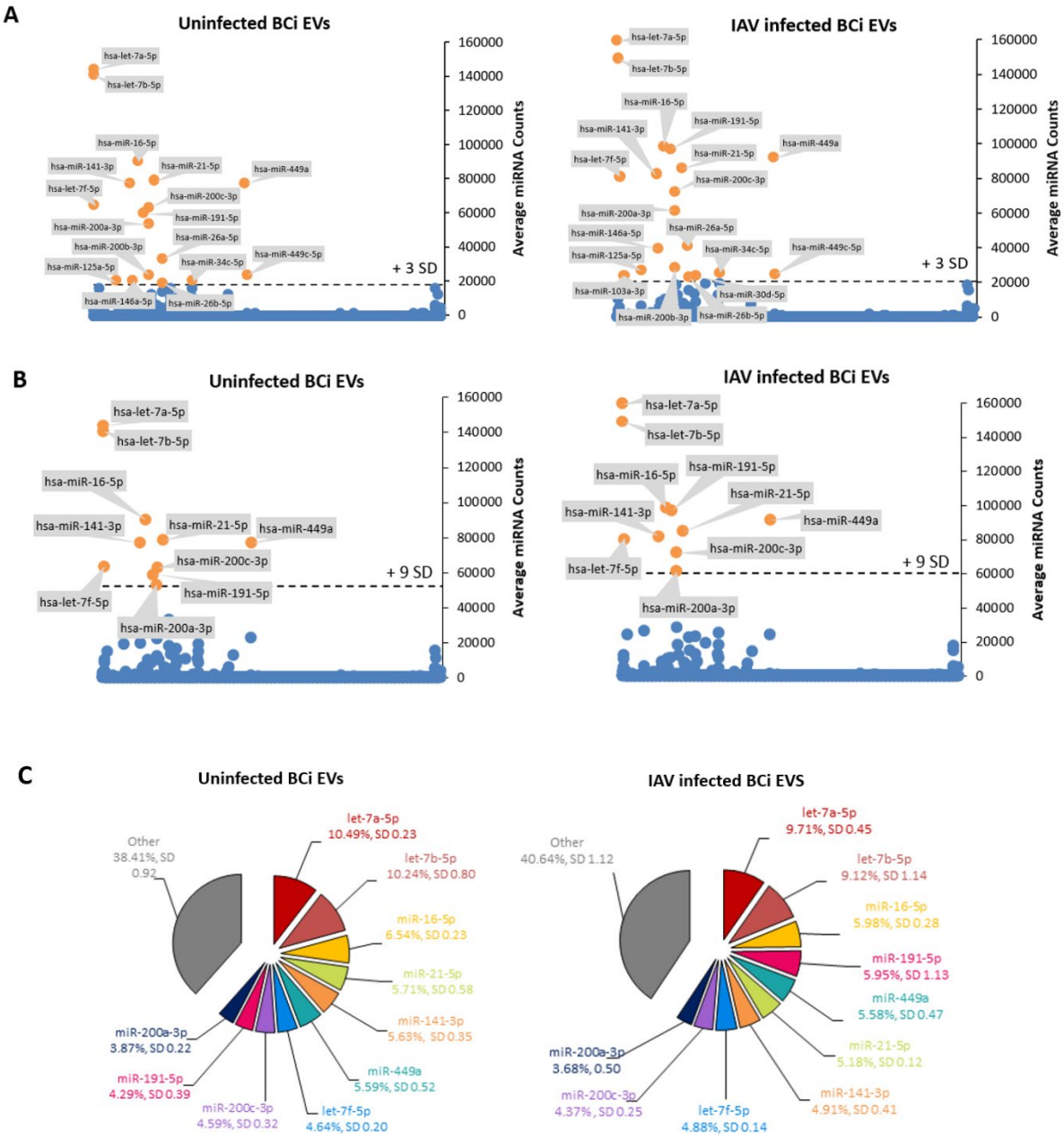

Figure 4.4 Top ten most abundant EV miRNA make up a large proportion of total EV miRNA

A) Scatter plot for uninfected and IAV infected BCi EV miRNA average counts. miRNA with an average count above 3 SD (indicated by line) of the total miRNA average counts are labelled. B) Scatter plot for uninfected and IAV infected BCi EV miRNA average counts. miRNA with an average count above 9 SD (indicated by line) of the total miRNA average counts are labelled. C) Graphs show miRNA counts as an average percentage of total miRNA counts for EVs released from either uninfected or IAV BCi. MiRNA outside of top 10 grouped together in category "other". Standard deviation (SD) labelled.

4.3 Validation of BCi EV miRNA altered in response to IAV using qPCR

Analyses of the levels of miR-122, miR-155, miR-146a, miR-7, miR-378a and miR-505 relative to housekeeping miRNA (miR-26b-5p) was completed by qPCR to validate sequencing results that showed these miRNAs to be altered in BCi EVs at 24 hours post infection (hpi) with IAV. Uninfected and IAV infected samples were considered as unpaired samples given a single cell line was used and the experiments were carried out in separate wells. Given RT-qPCR is cheaper, analyses could also be expanded to include 48 hpi as well as the cellular and non-EV miRNA. It was therefore possible to analyse if miRNA changes in response to IAV were EV specific. Non-EV samples at 48 hpi was not analysed due to an issue with one of the samples and insufficient time to generate additional samples. The most upregulated EV miRNA in response to IAV was miR-122-5p. However, as demonstrated in section 4.2.3, miR-122-5p was also very lowly abundant with CPM <15. miR-122-5p was not detected by qPCR across all the samples including EVs, non-EVs and cells supporting the low abundance of bronchial epithelial miR-122-5p (**Figure 4.5A**).

The next most elevated miRNA in response to IAV, as demonstrated in section 4.2.3, was miR-155 which was slightly more abundant with an average CPM <50 in uninfected EV samples and CPM <200 in IAV infected EV samples. Due to the low abundance of miR-155, it could not be detected by qPCR in many of the uninfected EV samples and some of the IAV infected EV samples (**Figure 4.5B**). Despite this qPCR supported increase in EV and non-EV miR-155 at 24 hpi. Furthermore a 10-fold increase in both EV and cellular miR-155 was observed between 24 and 48 hpi. Sequencing suggested miR-146a to be the most abundant of the miRNA shown to be altered in response to IAV. Analyses via qPCR also showed miR-146a to be the most abundant extracellular miRNA both in EV and non-EV samples as well as on the cellular level (**Figure 4.5C**). Furthermore, qPCR analyses revealed a small increase in miR-146a levels relative to miR-26b in EVs at both 24 hpi and 48 hpi.

A significant increase in the relative levels of miR-7-5p was detected by qPCR at 48 hpi but not at 24 hpi in both EVs and cells (**Figure 4.5D**). On the other hand, a small but non-significant increase in the relative levels of EV miR-378a-3p but not cellular miR-378a-3p was demonstrated by qPCR at 24 hpi (**Figure 4.5E**). No significant change in relative levels of miR-505 was detected for all samples (**Figure 4.5F**).

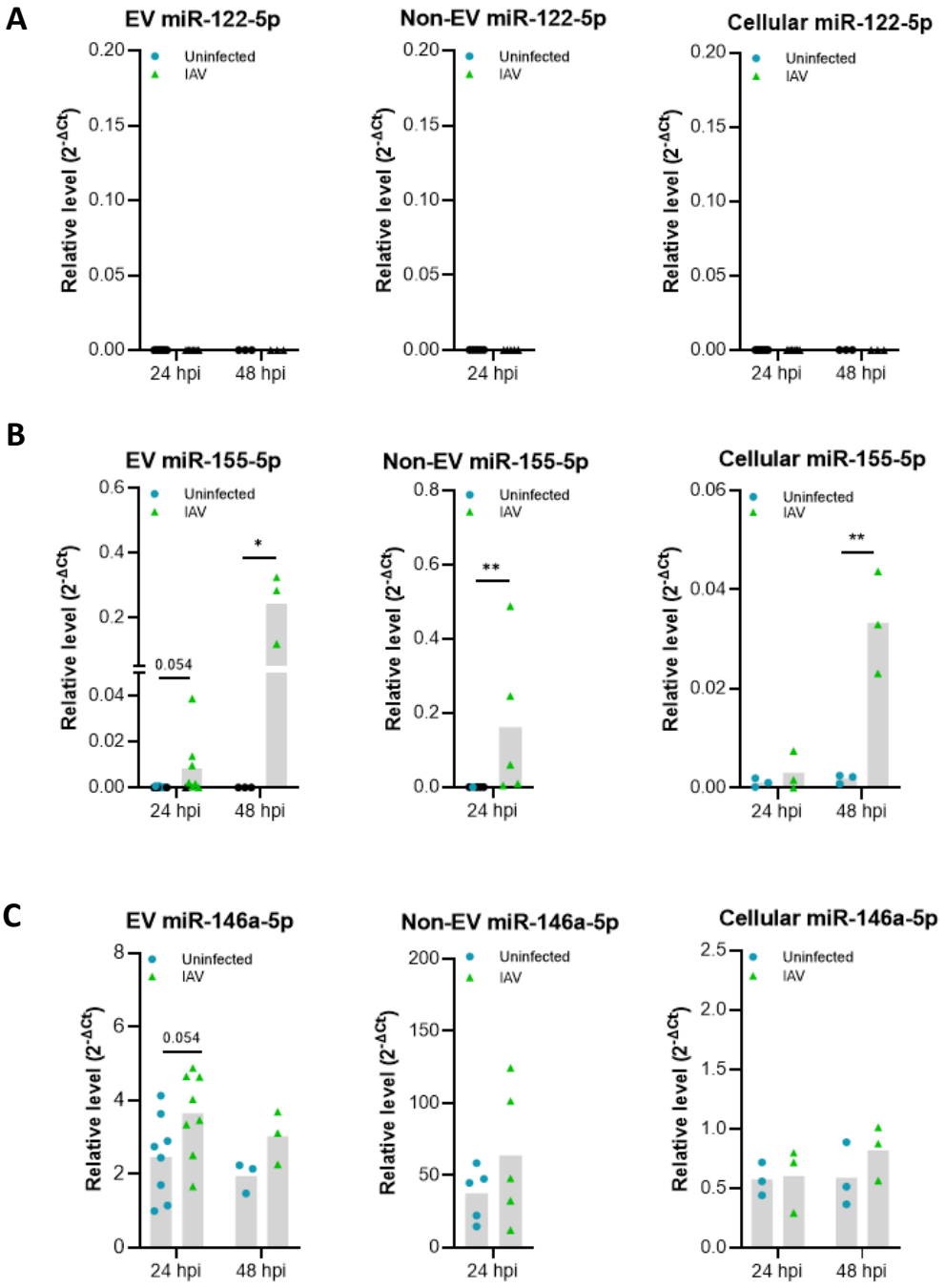
A
EV miR-122-5p
Non-EV miR-122-5p
Cellular miR-122-5p
Uninfected
IAV
Relative level (2-ΔCt)
0.20
0.15
0.10
0.05
0.00
24 hpi
48 hpi
B
EV miR-155-5p
Non-EV miR-155-5p
Cellular miR-155-5p
0.6
0.4
0.2
0.04
0.02
0.8
0.06
0.054
*
**
C
EV miR-146a-5p
Non-EV miR-146a-5p
Cellular miR-146a-5p
8
6
4
2
0
200
150
100
50
2.5
2.0
1.5
1.0
0.5
0.0

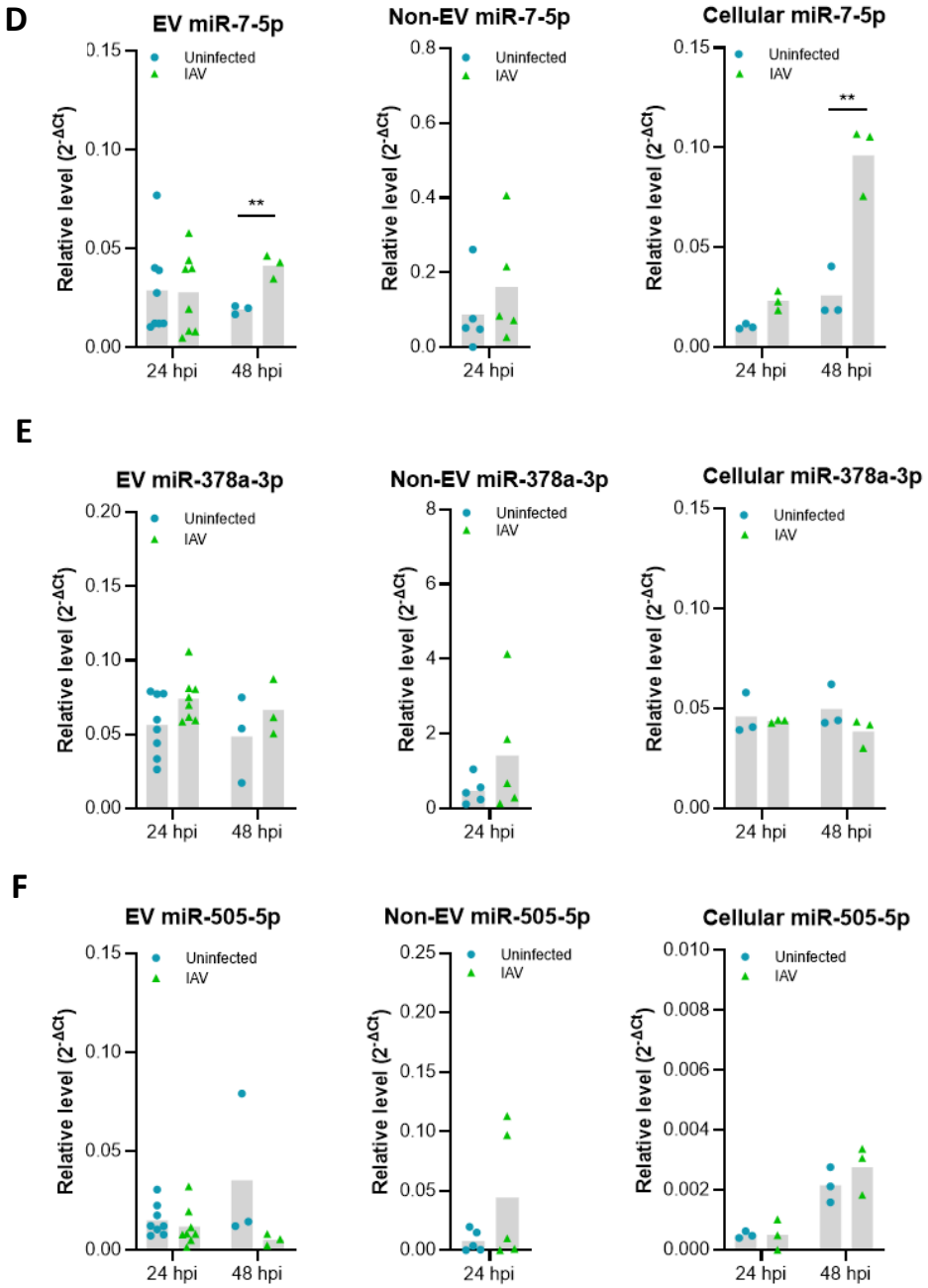

Figure 4.5 Validation of miRNA altered in IAV infected BCi EVs compared to uninfected BCi EVs via qPCR

*Relative level of A) miR-122-5p, B) miR-155-5p, C) miR-146a-5p, D) miR-7-5p, E) miR-378a-3p and F) miR-505-5p compared to miR-26b-5p for EV, Non-EV and cellular samples from uninfected or IAV infected BCi at either 24 hours post infection (hpi) or 48 hpi. Blue circle= Uninfected, Green triangle=infected. Black data points=Not detected. Normality determined by Shapiro-Wilk test. Normally distributed data displayed with mean and analysed using unpaired t-test. *=P<0.05, **p<0.01*

4.4 Validation of healthy and COPD PBEC EV miRNA altered in response to IAV using qPCR

PBEC were then used to further validate changes in EV miRNA in response to IAV given that the modification of cells to generate cell lines, such as the BCi cells used in this study, can alter cell characteristics. Furthermore, by using primary cells it was possible to compare response in healthy and COPD PBECs. This is particularly of interest given that patients with COPD are more susceptible to IAV with more severe symptoms, yet the underlying molecular mechanisms of the hypersusceptibility of airway inflammatory response remain unclear (152).

An postbronchodilator FEV1/FVC ratio of less than 70% quantified by spirometry was required for the diagnosis of COPD (**Table 4.1**). Furthermore, COPD patients were either mild (FEV1 ≥80% of predicted) or moderate (FEV1 of 50%–79% of predicted). These samples were age and gender matched. However further replicates are required to include female samples to remove any gender bias. Furthermore, COPD patients had a significantly higher number of smoking pack years that may bias results and therefore further replicates are also required to remove this bias. Unfortunately, it was not possible to achieve a greater number of replicates due to availability of primary samples in the designated time frame.

PBEC from healthy ex-smokers (n=3) or COPD ex-smoker donors (n=3) were cultured at ALI. The comparison of ex-smokers was chosen to investigate mechanism by which some smokers develop COPD while others do not as this remains a pertinent question in the study of COPD. IAV infection and EV isolation was completed as detailed in previous section for BCi (TCID50 of 3.6 x 10^6 for 24 h). Uninfected and IAV infected samples from a single donor were considered as paired samples. Uninfected and IAV infected EV samples from healthy and COPD PBEC were confirmed to be enriched in CD63 EV marker while non-EV protein calnexin was shown to be absent (**Figure 4.6A**). In addition, a greater level of CD63 was observed in infected EV sample for both healthy and COPD EVs. However future experiments are required to validate this.

Gene expression was calculated as ΔCT value for each sample from Ct values of gene of interest minus Ct value of housekeeping gene (*ACTB*). An increase in expression of immune genes including *CXCL10*, *IFNB1*, *ISG15* and *SOCS1* was detected for PBECs in response to IAV (**Figure 4.6B**). Furthermore, viral RNA was detected. The average immune gene expression was similar between healthy and COPD PBECs. In addition, there was no difference in the level of IAV RNA detected and barrier formation as determined by TEER measurement between healthy and COPD PBECs (**Figure**

4.6C-D). Due to the spread of the data and low number of replicates there was not enough power to determine statistical significance.

4.4.1 Subject/sample characteristics

Subject/sample characteristics	COPD ex-smoker (n=3)	Healthy ex-smoker (n=3)	P value
Age, mean ±SD	62±9	57±14	0.617
Male, (%)	100	100	-
Smoking pack years, mean ±SD	42±9	26±4	0.047
BMI, mean ±SD	29.6±2.6	28.5±5.1	0.756
Lung Physiology			
FEV1 (% predicted), mean ±SD	74±12	93±13	0.141
FVC (% predicted), mean ±SD	96±10	94±13	0.895
FEV1/FVC%, mean ±SD	59±10	77±3	0.038

Table 4.1 Characteristics of PBEC subjects

BMI, body mass index; FEV1, forced expiratory volume in 1 sec, FVC, forced vital capacity ; FEF, Forced expiratory flow rate. SD, standard deviation. T-test.

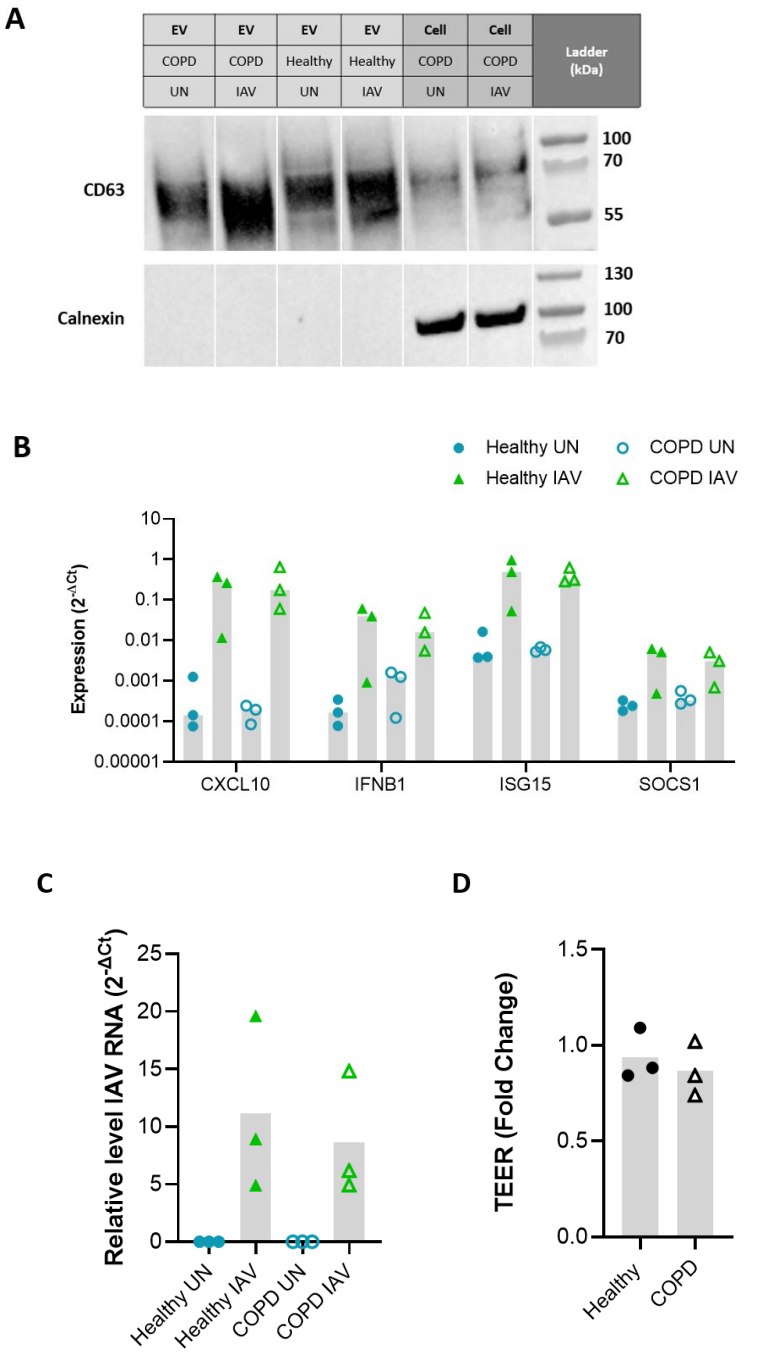

Figure 4.6 Characterisation of healthy and COPD PBEC infection model

*Healthy and COPD PBEC either uninfected or IAV infected at TCID50 of 3.6 x 10^6 for 24 hours. A) Western Blot of EV protein marker CD63 and non-vesicular protein calnexin. PBEC cell lysate included. Molecular weight protein ladder displayed in kDa. B) Expression of CXCL10, IFNB1, ISG15 and SOCS1. Gene expression was calculated as ΔCT value for each sample from Ct values of gene of interest minus Ct value of housekeeping gene (ACTB). C) level of IAV RNA or D) TEER fold change in healthy or COPD PBEC in response IAV infection. Normality determined by Shapiro-Wilk test. Normally distributed data displayed with mean and analysed using paired t-test (C and D). Non-parametric data displayed with medium and analysed using Wilcoxon test (B). *P<0.05*

Levels of EV miRNA (miR-122-5p, miR-155-5p, miR-146a-5p, miR-7-5p, miR-378a-3p and miR-505-5p) found by sequencing to be altered in response to IAV were investigated by qPCR in healthy and COPD PBECs. Infection conditions were as described for BCi (IAV at TCID50 of 3.6 x 10^6 for 24 h). As was observed for BCi miR-122-5p could not be detected in EVs, non-EVs or cells (data not shown). Furthermore, as observed for BCi, miR-155 could not be detected in the uninfected EV samples (**Figure 4.7A**). An increase in the relative levels of EV miR-155 was detected for healthy PBEC. On the other hand, a smaller increase in the relative levels of EV miR-155 was detected for COPD PBEC. Increased relative levels of miR-155 was also detected for non-EV and cell samples. An increase in the relative levels of miR-146a, miR-7 and miR-378a was also detected for healthy EVs but not COPD EVs in response to IAV (**Figure 4.7B-D**). On the other hand, no difference in the relative levels of miR-146a, miR-7 or miR-378a was detected for both healthy and COPD non-EV and cell samples in response to IAV. As observed for BCi, miR-146a was observed to be the most abundant miRNA of those altered in response to IAV for both EV and non-EV samples as well as on the cellular level for PBECs. No change in the relative levels of miR-505 was detected for all samples (**Figure 4.7E**). Due to the spread of the data and low number of replicates there was not enough power to determine statistical significance. Unfortunately, it was not possible to achieve a greater number of replicates due to availability of primary samples during designated time frame.

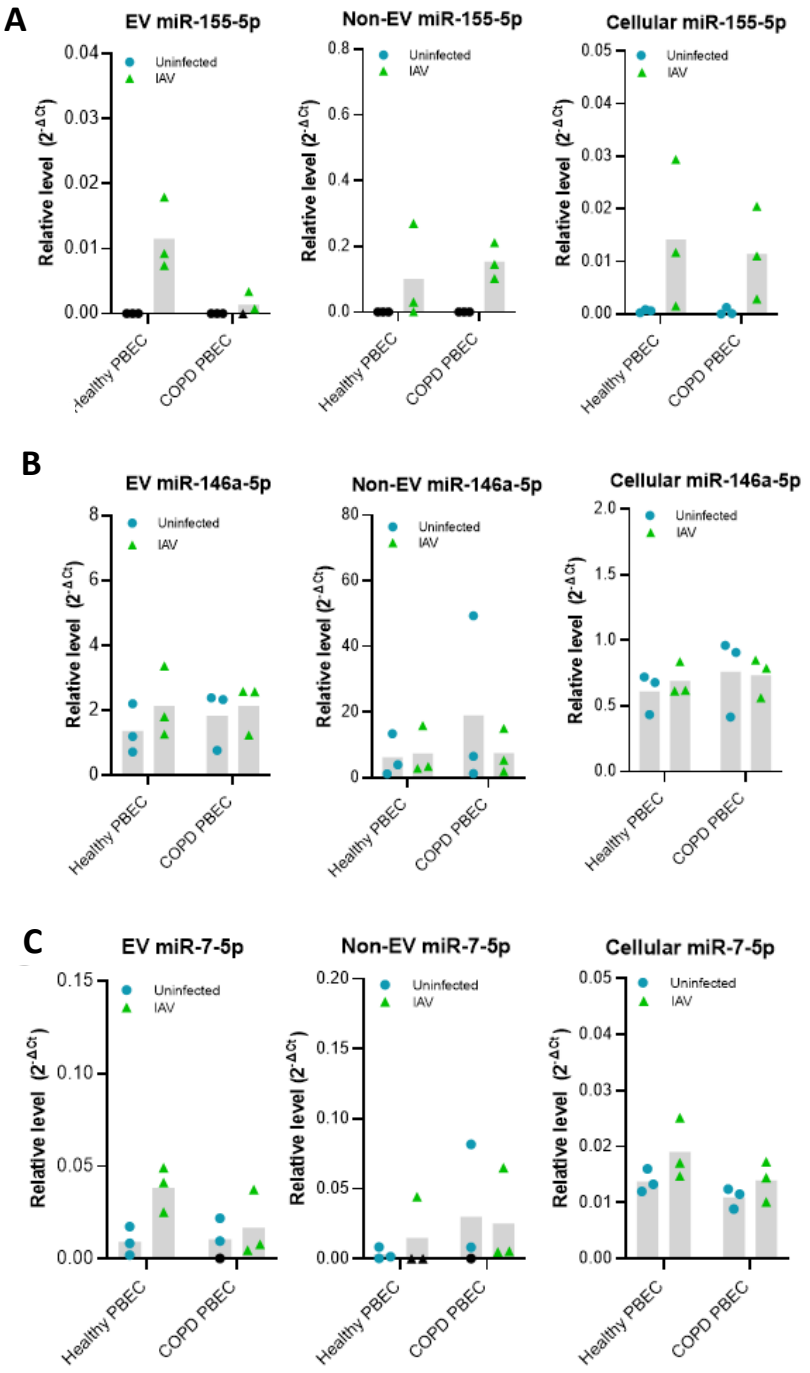
A
EV miR-155-5p
Non-EV miR-155-5p
Cellular miR-155-5p
Uninfected
IAV
Relative level (2-ΔCt)
Healthy PBEC
COPD PBEC
B
EV miR-146a-5p
Non-EV miR-146a-5p
Cellular miR-146a-5p
C
EV miR-7-5p
Non-EV miR-7-5p
Cellular miR-7-5p

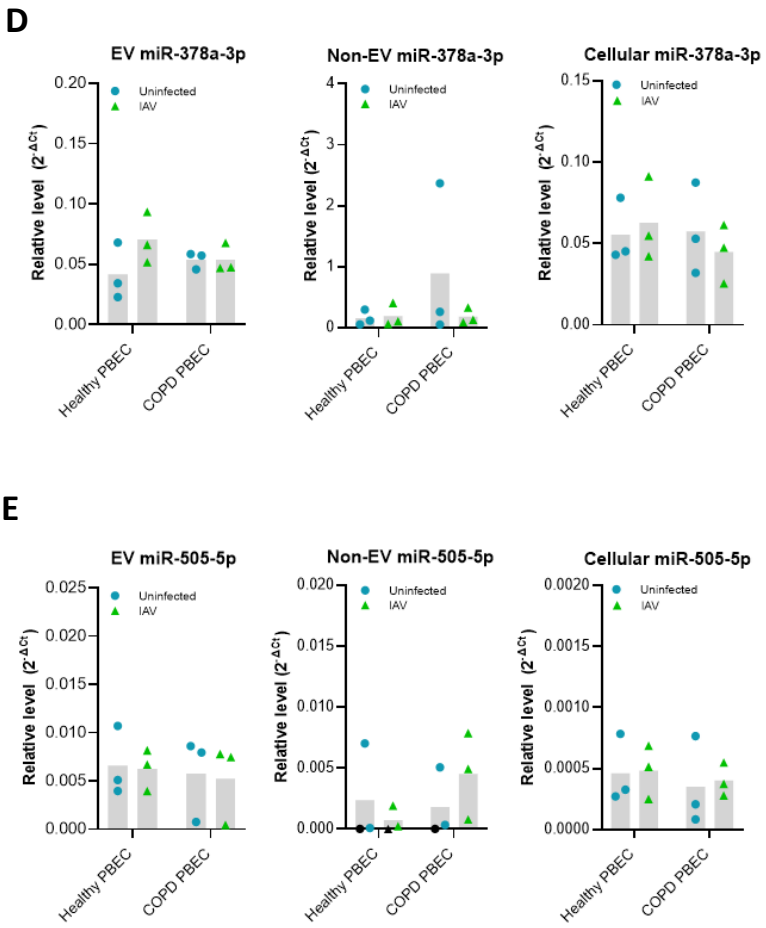

Figure 4.7 Validation miRNA altered in IAV infected healthy and COPD PBECs via qPCR

*Relative level of A) miR-155-5p, B) miR-146a-5p, C) miR-7-5p, D) miR-378a-3p, E) miR-505-5p compared to miR-26b-5p for EV, Non-EV and cellular samples from healthy and control PBECs uninfected or IAV infected at TCID50 of 3.6 x 10^6 for 24 hours. Blue circle= Uninfected, Green triangle=infected. Black data points=Not detected. Normality determined by Shapiro-Wilk test. Non-parametric data displayed with medium and analysed using Wilcoxon test. *P<0.05*

4.4.2 Analyses of impact of ageing on PBEC EV miRNA response to IAV

Given that ageing has been shown to impact the anti-viral immune response to influenza, the primary samples were grouped into those obtained from 41-65 years old (under 65) compared to 66-85 years old (over 65) to assess impact of age as a confounding factor for comparison of healthy and COPD samples. Uninfected and IAV infected samples from a single donor were considered as paired samples. Interestingly the PBEC isolated from the over 65 group displayed lower immune gene expression in response to IAV compared to the younger group (**Figure 4.8A**). This may be at

least partly explained by the fact that a lower level of infection, as measured by IAV RNA, was also observed for over 65 PBEC samples (**Figure 4.8B**). PBEC barrier formation as determined by TEER measurements showed no difference between age groups (**Figure 4.8C**). As previously stated unfortunately due to the spread of the data and low number of replicates there was not enough power to determine statistical significance and it was not possible to achieve a greater number of replicates in designated time frame.

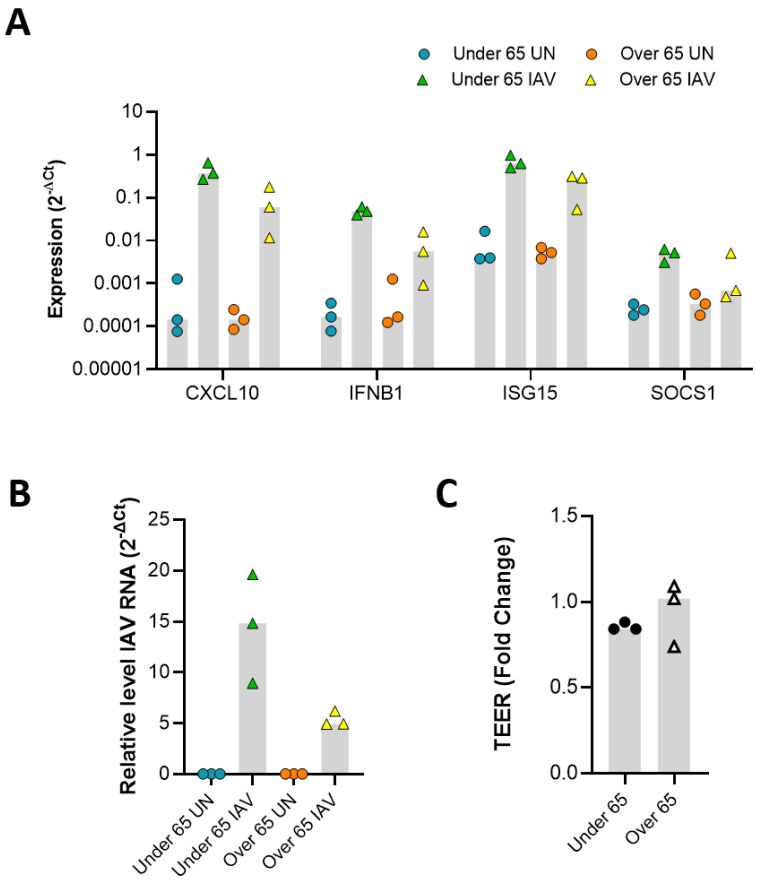

Figure 4.8 Characterisation of PBEC infection model grouped into under 65 and over 65 year old participants

*Under 65 and over 65 year old participant PBEC either uninfected or IAV infected at TCID50 of 3.6 x 10^6 for 24 hours. A) Fold change of expression of CXCL10, IFNB1, ISG15 and SOCS1. Gene expression was calculated as ΔCT value for each sample from Ct values of gene of interest minus Ct value of housekeeping gene (ACTB). B) level of IAV RNA or C) TEER fold change in under 65 or over 65 PBEC in response to IAV infection. Normality determined by Shapiro-Wilk test. Non-parametric data displayed with medium and analysed using Wilcoxon test. *=P<0.05*

Analyses of EV miRNA from PBEC of under 65 and over 65 years old participant PBEC samples revealed age related differences in EV miRNA (**Figure 4.9**). The relative level of miR-146a-5p was higher in EVs isolated from PBEC of participants over the age of 65, compared to the under the age of 65 for both the uninfected and IAV infected samples. On the other hand, in the over 65 group a lower level of miR-7-5p was detected in response to IAV. Due to the spread of the data and low number of replicates there was not enough power to determine statistical significance. Unfortunately, it was not possible to achieve a greater number of replicates due to availability of primary samples and time available to complete the work.

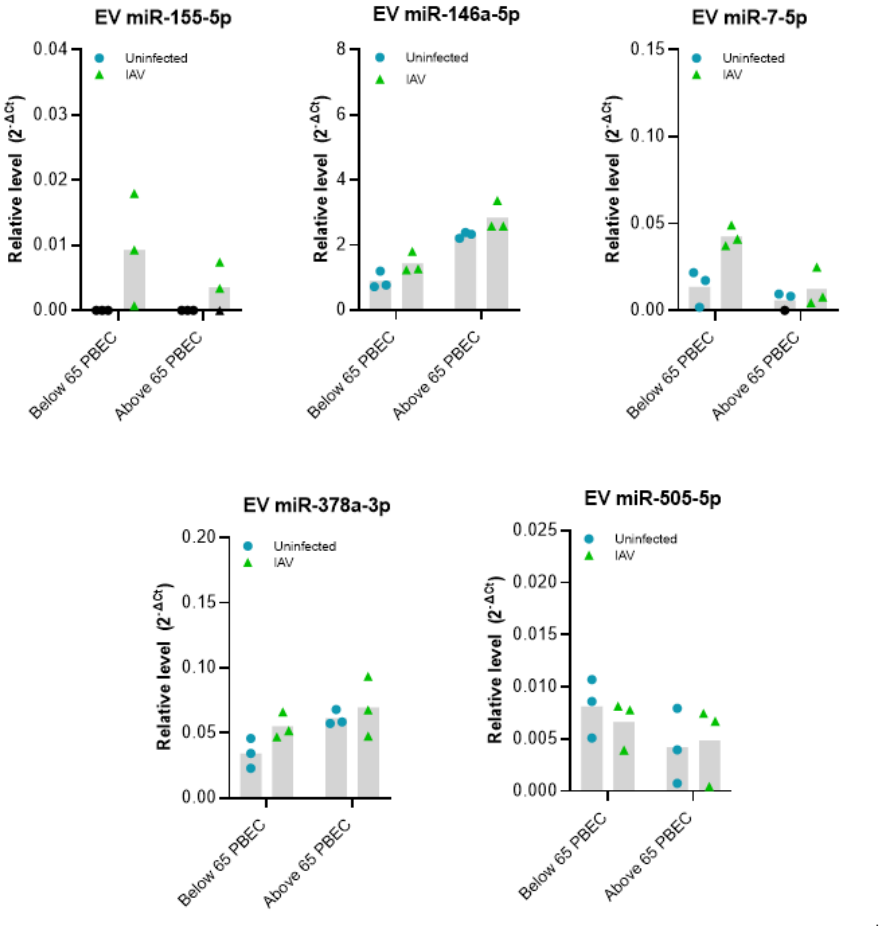

Figure 4.9 Ageing impacts EV miRNA released by PBECs

*Relative level of miR-155-5p, miR-146a-5p, miR-7-5p, miR-378a-3p and miR-505-5p compared to miR-26b-5p for EV from under 65 and over 65 year old participant PBEC uninfected or IAV infected at TCID50 of 3.6 x 10^6 for 24 hours. Blue circle= Uninfected, Green triangle=infected. Black data points=Not detected. Normality determined by Shapiro-Wilk test. Non-parametric data displayed with medium and analysed using Wilcoxon test. *=P<0.05*

4.4.3 Relative abundance of extracellular and cellular miRNA

The relative levels of the EV and non-EV miRNA detected to be altered in response to IAV were investigated as a ratio to cellular miRNA levels. The ratio was calculated using miRNA normalised to housekeeping miRNA. COPD and healthy samples were combined to increase the number of replicates. Given miR-155 was not detected in uninfected samples it was not possible to complete the analyses in these samples. In samples obtained from IAV infected PBEC the median ratio of EV miR-155 to cellular miR-155 was 0.6 whereas the median ratio of non-EV miR-155 to cellular miR-155 was 9.2 suggesting miR-155 to be enriched in the non-EV extracellular space compared to EVs (**Figure 4.10**). Furthermore, there was significantly higher levels of miR-146a in the non-EV samples compared to EV samples cells in uninfected PBEC and IAV infected PBEC. The medium ratio of miR-7 was 1 and 0.7 respectively for EVs and non-EVs in uninfected PBECs and 1.7 and 1.3 respectively for EVs and non-EVs in infected PBECs suggesting no extracellular enrichment. Enrichment of miR-378a in non-EV samples was observed for both uninfected (median 3.7) and IAV infected (median 3.7) PBEC. Lastly miR-505 was the most enriched EV miRNA with cell ratio of 13.0 and 12.8 in uninfected and IAV infected samples respectively. A greater number of PBEC samples are required to meaningfully compare possible differences between healthy and COPD EV miRNA expression.

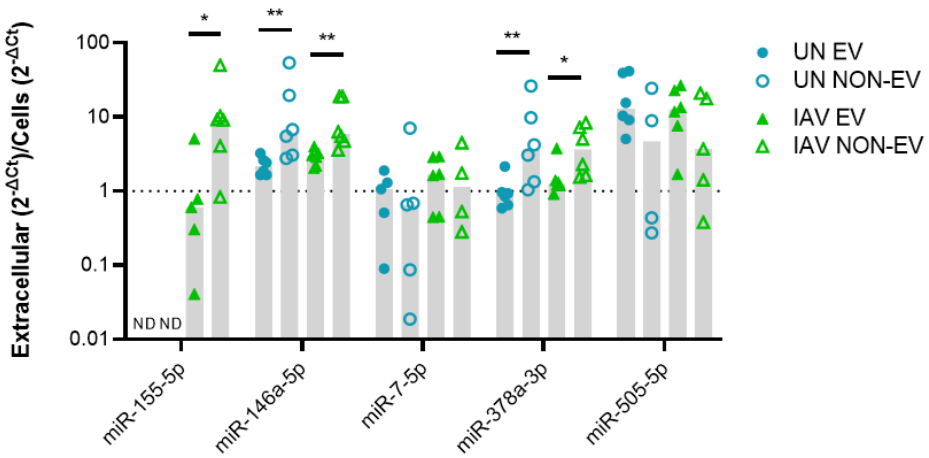

Figure 4.10 Relative abundance of extracellular and cellular miRNA

*A) EV to cell ratio or non-EV to cell ratio of the relative level of miR-155-5p, miR-146a-5p, miR-7-5p, miR-378a-3p and miR-505-5p compared to miR-26b-5p. Samples from PBECs uninfected or IAV infected at TCID50 of 3.6 x 10^6 for 24 hours. Normality determined by Shapiro-Wilk test. Non-parametric data displayed with medium and analysed using Wilcoxon test. *=P<0.05, **=P<0.01*

4.5 Discussion

The presence of RNAs, including miRNAs, within EVs was published 15 years ago (119). Since then studies have demonstrated EV miRNA, released from cells *in vitro* or obtained from biofluids, are altered in response to a range of stimuli including viral infection (161,227). Furthermore it is now widely accepted that miRNA are transferred by EVs and can induce functional effects in a recipient cell (228). This chapter addresses the aim of completing small RNA sequencing to characterise miRNA cargo of EVs released from ALI cultured bronchial epithelial cell line in response to infection with IAV. To our knowledge, this is the first study to complete small RNA sequencing of EVs released from IAV infected bronchial epithelial cells cultured at ALI. Specific EV miRNA signatures hold the potential for being used as disease biomarkers and may provide novel targets for underlying pathological mechanisms.

Analysis of EVs released from the apical face of BCi revealed the RNA composition to be on average 32% miRNAs. Other predominant RNA biotypes were lncRNAs (26%) and protein coding RNA (23%). On the other hand, a low percentage of piRNA were detected (3%). This is comparable to previous literature. Another study that investigated EVs released from the apical face of bronchial epithelial cells reported a high proportion of miRNA (37%) and lncRNA (33%) but a low abundance of piRNA (1%) (229)**.** The proportion of RNA biotypes was not significantly altered in response to IAV except for miscRNA. An increase in miscRNA that include RNA types such as Y-RNA and Vault RNA was detected for EVs released from IAV infected BCi. These RNA types have been found to be enriched in EVs and modulated in response to range of immune-related stimuli (230,231). However the biotype and function of these miscRNA was outside the scope of the research and therefore was not further investigated in this thesis.

Analyses of the sequencing data, mapped to miRBase, found that IAV infection significantly impacts the miRNA EV profile of ALI BCi. A logFC > 0.6 or logFC < -0.6 cut-off was applied to identify miRNA altered above the minimal level of change of miRNA previously reported to have a significant impact on the biology of the cell (226). This revealed 5 miRNAs to be upregulated in EVs of IAV infected BCi with logFC > 0.6 (miR-122-5p, miR-155-5p, miR-146a-5p, miR-7-5p, miR-378a-3p) and 1 downregulated with logFC < -0.6 (miR-505-5p). Overall, the levels of fold change observed in this chapter were relatively low. Only three of these miRNAs had a logFC > 1 (miR-155-5p and miR-122-5p) or logFC < -1 (miR-505-5p). However, these three miRNAs were also only present at low levels with an average CPM <100. This may be due to the low infectious dose used in this study. A recent study reported altered EV microRNA with LogFC > 1 or < -1 from A549 human epithelial lung cells in response to influenza A/H1N1pdm09 infection (232). They showed that the expression levels of five

EV miRNAs (hsa-miR-572, hsa-miR-141, hsa-miR-196b, hsa-miR-24, hsa-miR-483) to be significantly up-regulated and five EV miRNAs (hsa-miR-194, hsa-let-7d, hsa-miR-361, hsa-miR-223, hsa-miR- 671-3p) to be significantly down-regulated in influenza virus-infected group as compared with control. There does not seem to be any overlap in miRNA detected in this previous study and this thesis. However, these differences can be attributed to the use of a different epithelial cell model and EV isolation techniques including the use of a different cell type and isolation of EVs from submerged cell conditioned media using CD63 Isolation/Detection Reagent. This highlights the sensitivity of the EV miRNA profile to different *in vitro* models and the importance of validating these findings *in vivo*.

Sequencing identified miR-122 as the miRNA with the greatest fold change in response to IAV. Other studies have reported elevated levels of miR-122-5p in EVs in response to Hepatitis C virus and suggested it plays a key role in HCV replication and lymphocytes' activation (233). However, miR-122 was present at very low levels in BCi and PBEC cells and EVs. This aligns with other research that have reported miR-122 to be predominantly detected in the liver (234). Interestingly other miRNA found in this thesis to be altered in EVs in response to IAV, including miR-146a and miR-378a-3p, were also found to be enriched in EVs of HCV patients. The study suggested the shared common targets of these miRNA to have key roles in immune response and were markedly reduced following antiviral therapy (233).

The second most increased miRNA in EVs in response to IAV identified in this chapter was miR-155. This miRNA was observed to be dramatically increased extracellularly in EVs and non-EV samples as well as within the cells 48 hpi. Therefore, the increase in EV miRNA may be attributed to cellular increase rather than EV specific mechanism. An increase in cellular and EV miR-155 has been previously shown to be induced by IAV as well as in response to a wide range of other viruses such as RV and other non-viral stimuli observed in the lung including cigarette smoke and hypoxia (235–238). Furthermore miR-155 has been widely reported as a multifunctional miRNA enriched in cells of the immune system with a role in regulating a variety of biological processes including cell proliferation, apoptosis, inflammation and cell development (239). Given that miR-155 has been described as critical for immune regulation its presence may suggest that epithelial EVs release miR-155 in EVs as an immune regulatory signals (199). On the other hand, increased expression of microRNA-155-5p by alveolar type II (ATII) cells but not immune cells has been shown to contribute to the development of lethal acute respiratory distress syndrome (ARDS) in H1N1 IAV-infected mice without affecting viral replication (235). Some of the other miRNA identified from analysis of sequencing data, such as miR-378a and miR-7 have also been associated with regulating damage and cell death. One study reported miR-7-5p as a tumour suppressor, participates in various biological

processes including cell proliferation and apoptosis regulation by repressing expression of specific oncogenic target genes including through inhibiting the ability of DNA damage repair (240). In addition macrophage-derived EVs enriched in miR-378a-3p have been shown to regulate cell death by blocking activation of the NLRP3/Caspase-1/GSDMD pathways in cardiomyocytes after myocardial infarction (241). As observed for miR-155, an increase in cellular and EV miR-7 in response to IAV was validated by qPCR in this chapter. However, while miR-155 appeared to be enriched in the non-EV samples, the levels of miR-7 were comparable between the EV and non-EV samples. Changes in the level of miR-378a were not validated in BCi EVs or cells by qPCR and only showed a slight trend of increasing in IAV infected PBECs. Further work is required to determine the function of EV miRNA and if it varies depending on the cellular source and target.

The results of this chapter also showed miR-146a to be the most abundant miRNA altered in response to IAV. Indeed, previous studies have shown miR-146a to be abundantly expressed in various mammalian cell types and play a role in inflammation, differentiation, and function of adaptive and innate immune cells. Downregulation of miR-146a has been suggested to inhibit IAV replication by enhancing the type I interferon response *in vitro* using A549 cells lung epithelial cells (242). Furthermore, the authors reported inhibition of miR-146a alleviated IAV-induced mice lung injury and increased survival rates by promoting type I antiviral activities (242). The results of this thesis suggest a low increase of miR-146 in EVs but not cells in response to IAV. Based on the functional results of previous studies it may be miR-146a EVs act to dampen the anti-viral immune response. However, this requires further investigation.

The top 10 most abundant EV miRNA were shared between uninfected and IAV infected EVs. These included let-7a-5p, let-7b-5p, miR-16-5p, miR-449a, miR-21-5p, miR-141-3p, miR-191-5p, let-7f-5p, -miR-200c-3p and miR-200a-3p. Furthermore, they make up around 60% of all miRNA reads. This supports previous studies that have shown, a small number (<20) of miRNAs accounts for > 80% of all cellular miRNAs (243). The majority of abundant miRNA, defined as miRNA present in levels of more than 3 SD above average, were not significantly altered with IAV infection. The exception being miR-103a-3p, miR-191-5p and miR-146a-5p. These miRNAs had a very small log2 fold change of 0.4, 0.5 and 0.8 respectively. However, given the abundance of these miRNAs, even a small change may have a significant impact on target protein levels.

The miRNA found to be abundant in EVs in this thesis have also been widely detected in lung samples and EVs in previous literature. Multiple members of the highly conserved let-7 miRNA family were shown to be highly abundant lung miRNAs (244). Furthermore miR-16 is abundantly expressed in across many sample types and is therefore frequently used as a normalisation factor for

miRNA studies (245). Studies have shown let-7 and miR-21 are thought to have a proinflammatory role in allergic lung disease (244,246). However, the function of the most abundant EV miRNA were not investigated for purpose of this study.

COPD causes significant morbidity and mortality worldwide (247). It is a major social and economic burden with patients typically having impaired quality of life that deteriorates considerably with exacerbation frequency (248). COPD exacerbations are associated with increased airway inflammation usually triggered by bacterial and viral infections (249). Recognition of the importance of viral infection in COPD exacerbations has increased over recent years due to the development of technology for the detection of respiratory viruses (250). A recent study showed the prevalence of viral infection was 28.1% in hospitalised patients (249). Exacerbations triggered by viral infections are usually associated with hypersusceptibility of greater airway inflammatory response, more severe symptoms, and delayed recovery compared to those without viral infections (152). However, the underlying molecular mechanisms of the hypersusceptibility of airway inflammatory response induced by IAV in COPD patients remain unclear. EVs have been identified as a novel mechanism of intercellular signalling involved in COPD pathogenesis (215). Burke et al recently reported altered profile of miRNA from EVs isolated from BALF of 20 patients with COPD compared to 15 well-matched healthy ex-smokers (176).

Furthermore, EV miRNA are altered following exposure to noxious stimuli that are a risk factor for COPD such as ambient particulate matter <2.5 μm (PM2.5). Oxidative stress in PM2.5-stimulated bronchial epithelial cells has been shown to be regulated by miR-155/ forkhead box class O3a (FOXO3a) pathway. *In vitro* transfection of miR-155 mimic into Beas-2B epithelial cells significantly decreased FOXO3a protein expression, accompanied by the reduced superoxide dismutase 2 (SOD2) and catalase expressions, promoting PM2.5-evoked oxidative stress (251).

In addition, a number of miRNA investigated in this thesis have been reported to be altered in COPD patients. A study screening serum miRNAs for as potential biomarkers for COPD reported upregulation of miR-7 (252). Serum levels of miR-146a have been shown to be down regulated in AECOPD patients compared with stable COPD patients and healthy controls (253). Furthermore, in AECOPD patients, levels of miR-146a in AECOPD patients have been negatively associated with inflammatory cytokines including TNF-α, IL-6 and IL-8 expression. Another study demonstrated increased miR-155 expression by RT-qPCR in lung tissue of smokers without airflow limitation and patients with COPD compared to never smokers (237). Differences in EV or cellular miR-155, miR-146a, miR-378a, miR-7 and miR-505 were not detected in this thesis between healthy and COPD PBECs. Though further studies using larger sample sizes are required to determine the statistical

significance. The cellular origin and stimuli resulting in changes in the level of miRNA in COPD requires further investigation.

This chapter also investigated whether changes in EV miRNA in response to IAV were altered in COPD epithelial cells compared to healthy epithelial cells. It was observed that changes in EV miRNA were dysregulated in COPD epithelial cells in response to IAV. A lower miR-155 EV response was observed for COPD PBECs compared to healthy PBECs. Furthermore, miR-146, miR-378 or miR-7 appeared to increase in EVs in healthy PBECs in response to IAV but this increase was not observed for COPD PBECs. These observations may suggest a potential mechanism for immune dysfunction that is observed in COPD resulting in increased susceptibility to infection. However, these changes require validation using larger sample size to enable analyses of statistical significance.

There is accumulating evidence that ageing induces a state of chronic inflammation and immune dysfunction that may simultaneously contribute to the development of multiple age-related chronic diseases such as COPD (254–256). Infected patients who are older have higher risks of developing severe complications and higher mortality from influenza. Interestingly, the PBEC isolated from the over 65 age group displayed a lower level of IAV infection and lower immune gene expression in response compared to 41-65 age group. Furthermore, elevated levels of EV miR-146a and miR-378 were observed in PBEC of the over 65 patient group in the uninfected samples compared to 41-65 age group. In addition, an increase in miR-7 in response to IAV was observed for the 41-65 age patient group but not the over 65 patient group. One recent study identified four miRNAs (miR-7-5p, miR-24-3p, miR-145-5p and miR-223-3p) that were downregulated in elderly people and associated with anti-viral response to SARS-CoV-2 (257). In addition, they showed that EVs from the serum of young people can significantly inhibit SARS-CoV-2 infection and reduce viral load. These observations suggest EV miRNA altered with age may contribute to altered immune response and may be useful in the development of therapeutics. However, these observations require further investigation in a larger cohort that can separate patients based on age and disease status.

Variation in the EV miRNA vs cell miRNA ratio reported in this chapter supports mechanisms involved in selective miRNA packaging into EVs (258). In addition, the results suggest that much of the extracellular miRNA may not be associated with EVs. Indeed previous studies have suggested extracellular miRNAs are in the most part by-products of dead cells that remain in extracellular space (259). However, alterations observed in EV miRNA in response to IAV were not always reflected in non-vesicular miRNA suggesting potential function of EV miRNA over non-vesicular miRNA. The mechanisms behind EV miRNA packaging are complex and still under investigation. The potential mechanisms for miRNA packaging were not investigated as part of this study.

4.6 Summary

The COVID-19 pandemic has brought to the forefront the threat that viral pathogens present and the challenges of developing effective countermeasures. The study of EV miRNAs during IAV infection will help to further understand the mechanisms of virus-host interactions. RNA sequencing of EV miRNA released from IAV infected BCi compared to uninfected BCi revealed 5 miRNA to be upregulated with logFC > 0.6 (miR-122-5p, miR-155-5p, miR-146a-5p, miR-7-5p, miR-378a-3p) and 1 downregulated with logFC < -0.6 (miR-505-5p). These miRNAs may present potential biomarkers of IAV infection or therapeutic targets however this requires further research. Furthermore, the results of this chapter suggest regulation of EV miRNA in response to IAV may be dysregulated in COPD or due to ageing as summarised in **Table 4.2**.

	Summary of miRNA Results - IAV infected epithelial cells vs Uninfected epithelial cells		
miRNA	**BCi EVs - Sequencing**	**BCi EVs and Cells - qPCR**	**PBEC EVs and Cells - qPCR**
miR-122	• Upregulated	• Not detected	• Not detected
miR-155	• Upregulated	• Highly upregulated in EVs and cells in response to IAV	• Upregulated in EVs and cells in response to IAV • Upregulated less in COPD PBEC EVs compared to healthy PBEC EVs in response to IAV
miR-146a	• Upregulated	• Lowly upregulated in EVs but not cells in response to IAV	• Lowly upregulated in EVs but not cells in response to IAV • Upregulated in healthy PBEC EVs but not COPD PBEC EVs in response to IAV • Levels were higher in 66+ age group PBEC EVs compared to 41-65 age group PBEC EVs
miR-7	• Upregulated	• Upregulated in EVs and cells in response to IAV	• Upregulated in EVs and cells in response to IAV • Upregulated in healthy PBEC EVs but not COPD PBEC EVs in response to IAV • Upregulated in 41-65 age group PBEC EVs but not in 66+ age group PBEC EVs in response to IAV
miR-378a	• Upregulated	• No differences	• Lowly upregulated in EVs but not cells in response to IAV • Upregulated in healthy PBEC EVs but not COPD PBEC EVs in response to IAV • Levels were higher in 66+ age group PBEC EVs compared to 41-65 age group PBEC EVs
miR-505	• Downregulated	• No differences	• No differences

Table 4.2 Summary of miRNA results in Chapter 4

5 *In silico* functional analyses of microRNA altered in epithelial EVs in response to IAV

5.1 Introduction

The previous chapter addressed the aim of identifying and validating changes in the miRNA profile of bronchial epithelial cell EVs in response to IAV. MiRNAs identified to be altered in IAV infected BCi EVs by logFC greater than 0.6 or less than -0.6 were miR-122-5p, miR-155-5p, miR-146a-5p, miR-7-5p, miR-378a-3p and miR-505-5p. However, understanding the impact of these miRNA on gene expression is key to understanding whether these differences have biological significance and relevance to disease pathology.

Chapter 5 explores the interactions between the EV miRNA altered in response to IAV and their predicted gene targets. Furthermore, investigates the function of these target genes. This was completed using the miRNA target protein analysis platform miRNet, which uses experimentally identified gene targets. miRNet allows visualisation of the well-established complexity of miRNA-mRNA interactions given that a single miRNA can target multiple genes and one gene is often regulated by many miRNAs.

5.2 Results

5.2.1 Bioinformatic analyses of function of target genes of EV miRNA altered in response to IAV

The results of the *in silico* analysis identified 2348 target genes for the six EV miRNA altered in response to IAV. The biological function of the identified gene targets was investigated using GO and KEGG pathway analysis (**Figure 5.1**). As shown in **Figure 5.2A**, the top significantly associated GO biological processes were ageing, response to UV, epidermal growth factor receptor signalling pathway and negative regulation of cell proliferation. From the network diagrams in **Figure 5.2B** it is apparent that the top biological processes were targeted by all the miRNA investigated. However, the genes identified to be involved in the ageing biological process were shown to be predominantly targeted by miR-155. On the other hand, genes involved in the response to UV were more evenly distributed between the miRNAs. Furthermore, there were some target genes that were shared amongst the top biological processes. These include genes involved in the apoptotic response to DNA damage such as, MSH2, MSH6, BCL2, TP53, PML, AURKB and CAT.

Given that the purpose of this research was to investigate the viral response and that cancer terms are over-represented in curated bioinformatic datasets, cancer terms were removed from analysis KEGG analyses (**Figure 5.3A**). Many of the top KEGG pathways observed were viral pathways including Hepatis C, Influenza A and Epstein-Barr. In addition, there were several KEGG pathways related to the immune response including T cell receptor signalling and toll-like receptor signalling. Furthermore, apoptosis appears in both the top KEGG pathways and GO biological process. Genes enriched in the top KEGG pathways were predominantly targeted by miR-155 and miR-7 (**Figure 5.3B**). This can at least be partially attributed to the fact these miRNAs are more widely studied and therefore have more identified gene targets.

The KEGG influenza pathway was significantly enriched for the predicted gene targets of miRNA altered in EVs in response to IAV. Visualisation of the KEGG pathway using DAVID bioinformatic tool revealed that EV miRNA altered in response to IAV, target genes involved in a range of IAV related processes including the detection of IAV through pattern recognition receptors such as TLR4 and related downstream signalling cascade (**Figure 5.4**). In addition, many of the target gene were identified to be involved in the innate immune response to IAV such as *IFN*, *NFKB*, *IL8*, *IL6* and genes involved in apoptosis such as *CASP3*, *CASP9* and *BAX*. Other genes important for viral replication including viral protein export and nucleoplasmic transport such as Importin were also identified as targets of the EV miRNA altered in response to IAV. While the Influenza A KEGG map is very useful for initial analysis and visualisation of miRNA targets associated with IAV infection it is in no way an exhaustive list of all genes regulated in response to IAV.

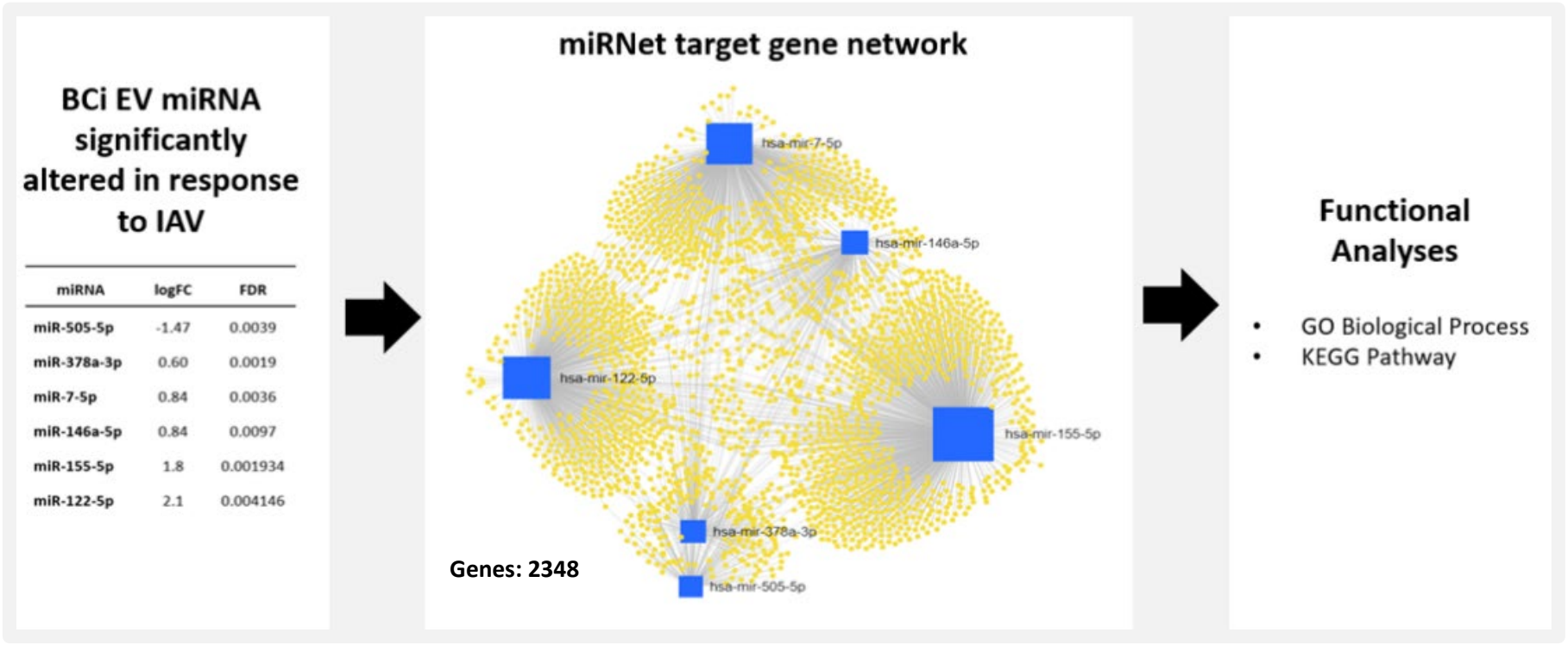

Figure 5.1 Gene network for EV miRNA altered in response to IAV

Diagram of functional analyses steps of significantly different miRNA (miR-505-5p, miR-378a-3p, miR-7-5p, miR-146a-5p, miR-155-5p and miR-122-5p). Target genes were identified using miRTarBase v8.0. A network of all potential target genes were visualised and functionally analysed in miRNet.

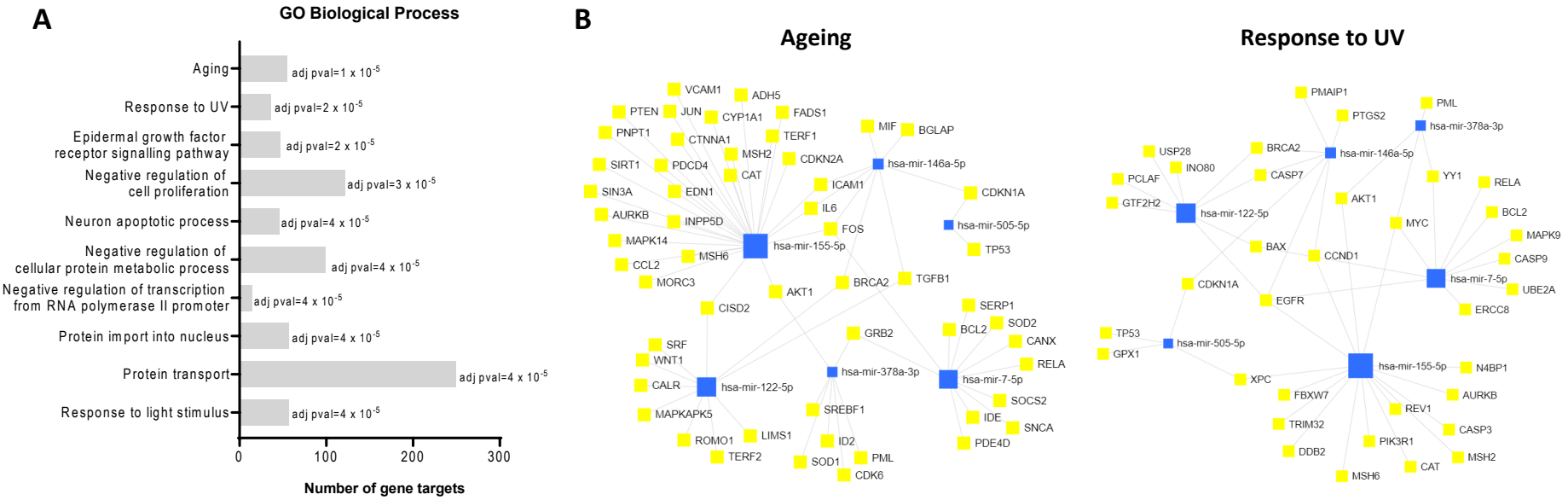

Figure 5.2 EV miRNA altered in response to IAV, target genes enriched in biological processes associated with ageing and response to UV

A) Top ten GO biological processes associated with target genes based on miRNet analyses. C) Gene network of top two GO biological processes.

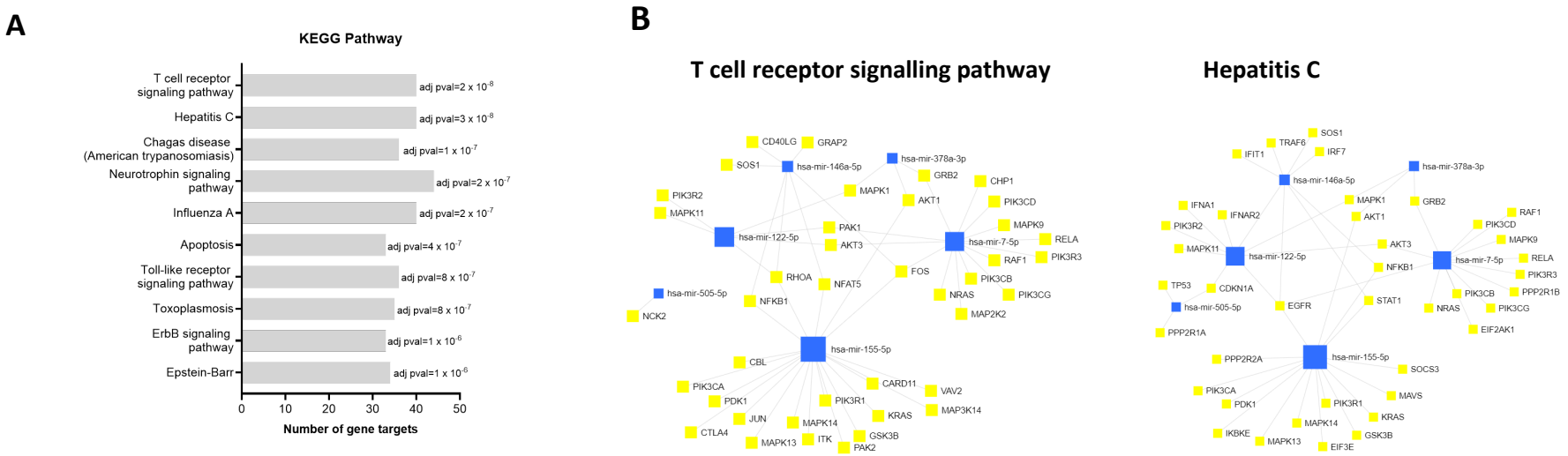

Figure 5.3 EV miRNA altered in response to IAV, target genes involved in viral response

A) Top ten KEGG pathways associated with target genes based on miRNet analyses without cancer terms. B) Gene network of top two KEGG pathways excluding cancer terms.

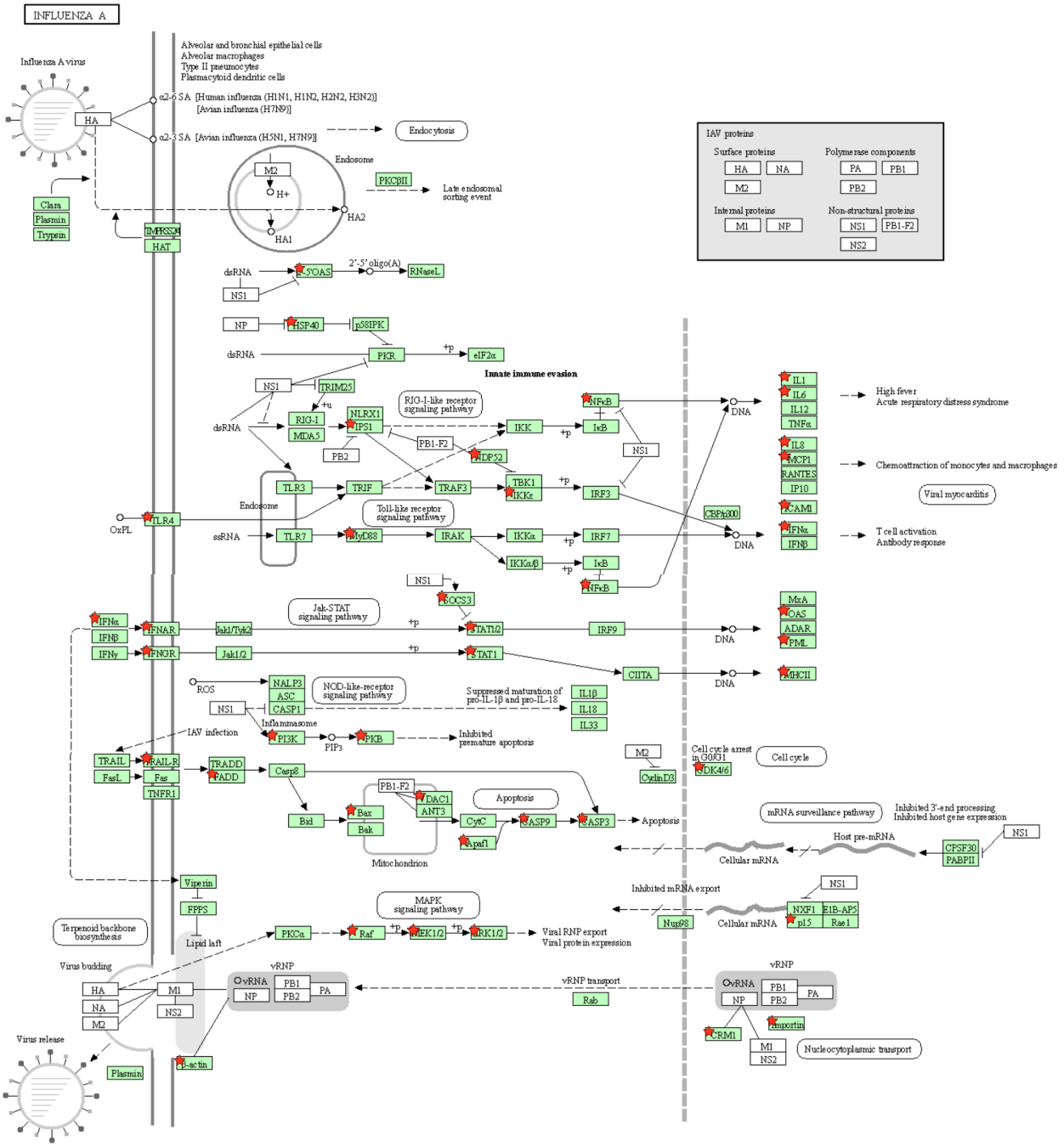

Figure 5.4 Target genes associated with Influenza A KEGG pathway

KEGG pathway analysis using DAVID bioinformatic tool with predicated target genes from miRNAs altered in EV in response to IAV. Green boxes with red star represent the potential genes targeted by selected miRNAs.

5.2.2 Reporter assay verified target genes of EV miRNA altered in response to IAV

Reporter assays provide strong evidence to verify the interaction between miRNA and potential target genes. For example, luciferase reporter assays can be used to investigate the interaction of miRNA with 3' UTR of a predicted target gene by cloning the 3' UTR of mRNA into luciferase reporter constructs that generate light output from luciferase enzyme (260). By measuring the light released it is possible to determine the effect of miRNA on transcription. To increase the confidence of the *in silico* functional analyses of miRNA target genes, the list of target genes for EV miRNA altered in response to IAV (miR-122-5p, miR-155-5p, miR-146a-5p, miR-7-5p, miR-378a-3p and miR-505-5p) was reduced to those validated by reporter assays.

The biological function of the gene targets validated by reporter assays were then investigated using GO and KEGG pathway analysis function of ToppFun platform (**Figure 5.5**). As shown in **Figure 5.6*A***, the top significantly associated GO biological processes were positive regulation of developmental process, positive regulation of multicellular organismal process, immune system development, hematopoietic or lymphoid organ development and regulation of apoptotic process. The results show, genes targeted by miR-155 make up the largest proportion of the top GO biological processes again highlighting the potential bias towards miR-155 given that it has been widely studied. On the other hand, there were no target genes that have been verified by reporter assays for miR-505.

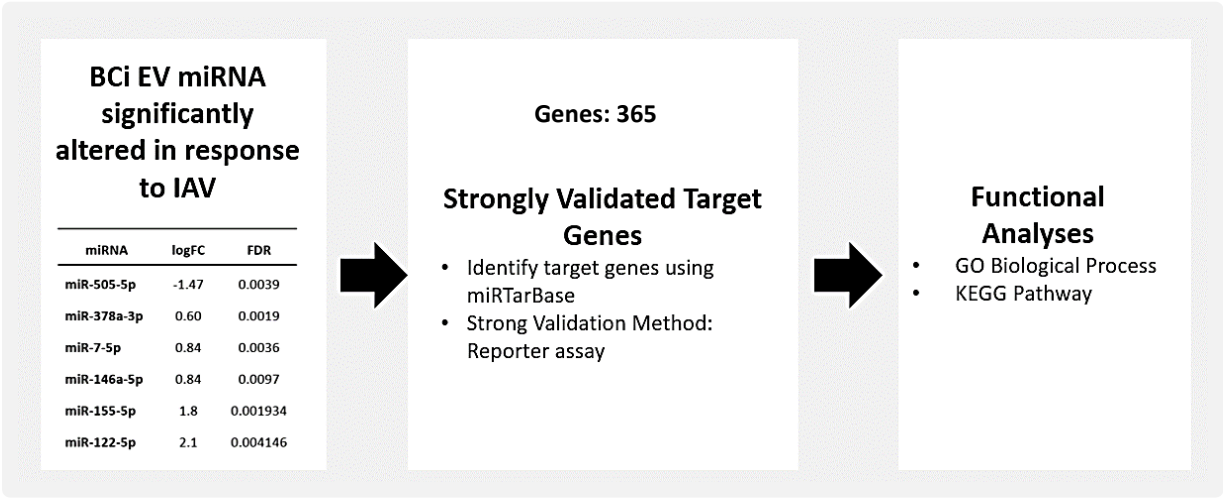

Figure 5.5 Verified target genes for EV miRNA altered in response to IAV

A) Diagram of functional analyses steps of significantly different miRNA (miR-505-5p, miR-378a-3p, miR-7-5p, miR-146a-5p, miR-155-5p and miR-122-5p). Reporter assay verified target genes were identified using miRTarBase v8.0. Functional analyses of strongly validated target genes was completed using ToppFun function of ToppGene.

Interestingly, as observed when investigating all the target genes in the previous section, hepatitis viral pathway appears as one of the top KEGG pathways (excluding cancer terms). Furthermore, genes in this pathway are predominantly targets of miR-155 and miR-7. Other top KEGG pathways were AGE-RAGE signalling pathway, TNF signalling pathway, signalling pathway regulating pluripotency of stem cells and PI3K-Akt signalling pathway. It was also observed that some of these target genes that have been validated are shared targets for more than one of the miRNAs altered in EVs in response to IAV. Visualisation of shared gene network in **Figure 5.6B** revealed several key cell signalling genes involved in cell development, immune response and apoptosis that are targeted by two or more the miRNA.

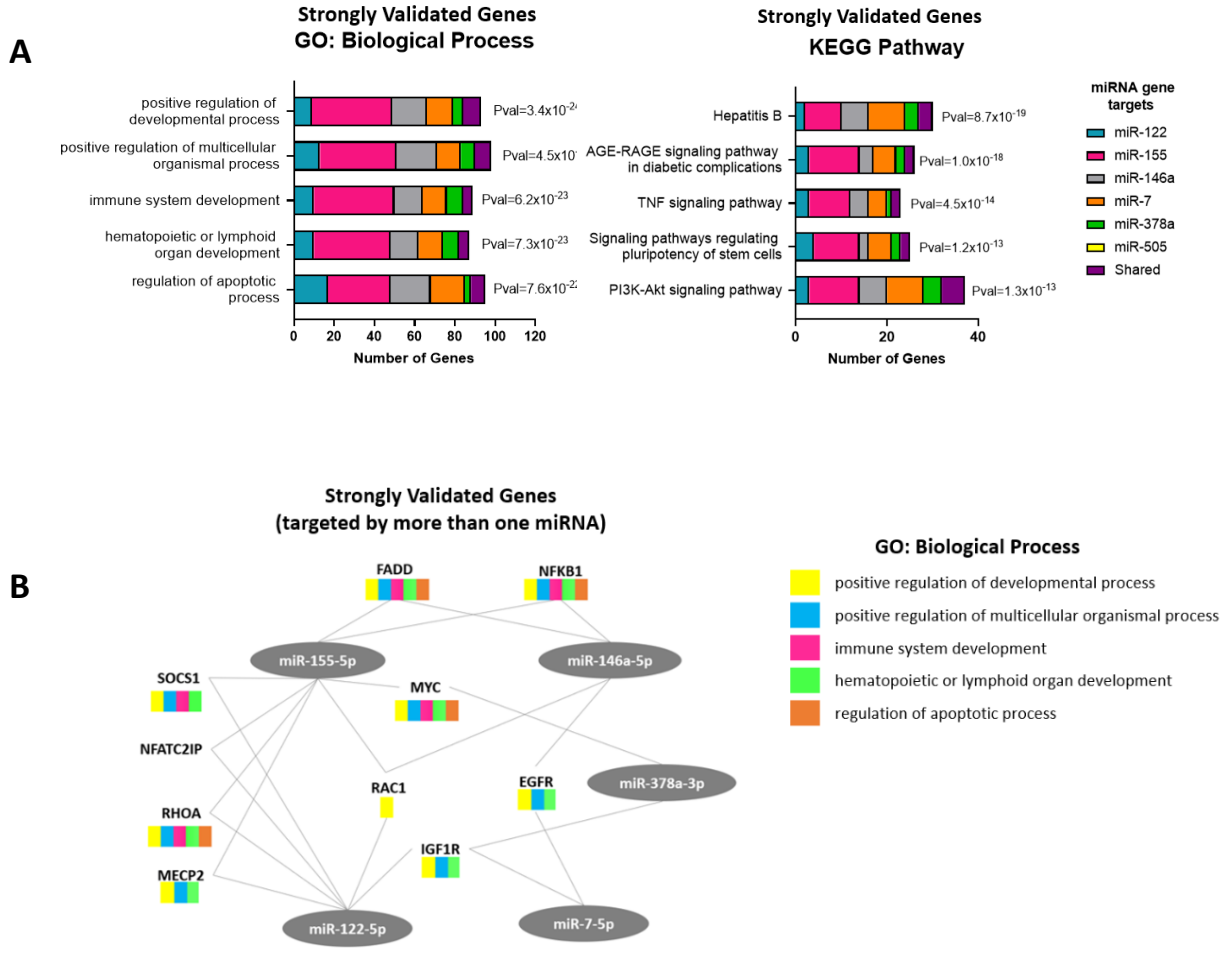

Figure 5.6 EV miRNA altered in response to IAV have been verified to target genes involved in viral immune response

A) Top ten GO biological processes and KEGG pathways associated with validated target genes. B) Gene network of verified target genes regulated by two or more of the significantly different miRNA.

5.2.3 Function of upregulated EV miRNA in response to IAV

There are a growing number of studies that suggest miRNA work cooperatively to regulate expression of a gene (261). Therefore, shared gene targets of the miRNA upregulated in EVs in response to IAV were investigated. This was completed in miRNet using all target genes identified by miRTarBase. Filters were then applied to select target genes associated with at least two miRNA or at least three miRNAs. The biological function of the gene targets was then investigated using GO and KEGG pathway analysis function (**Figure 5.7A**).

The top significantly enriched biological process for genes targeted by at least two miRNA was wound healing and the top KEGG pathway was focal adhesion (**Figure 5.7B**). Focal adhesions are specialized structures in which many of the biological responses to external forces are originated. These large multiprotein complexes mechanically link the extracellular matrix to the cytoskeleton via integrin membrane receptors (262). Furthermore, miRNet identified 16 genes to be targeted by three or more of the upregulated miRNA (**Figure 5.7C**). Only one gene, EGFR, was targeted by 4 miRNA and no genes were targeted by greater than 4 miRNA. EGFR regulates focal adhesion and cellular responses to the environment (263). Genes targeted by at least 3 miRNA were identified to be involved in functions such as response to stimulus and focal adhesion (**Figure 5.7D**).

A

BCi EV miRNA significantly increased in response to IAV

miRNA	logFC	FDR
miR-378a-3p	0.60	0.0019
miR-7-5p	0.84	0.0036
miR-146a-5p	0.84	0.0097
miR-155-5p	1.8	0.001934
miR-122-5p	2.1	0.004146

→ **miRNet target gene network**

→ **Filter genes targeted by at least 2 miRNA**

→ **Filter genes targeted by at least 3 miRNA**

→ **Functional Analyses**

- GO Biological Process
- KEGG Pathway

B

Genes targeted by at least two miRNA
Top GO Biological Process

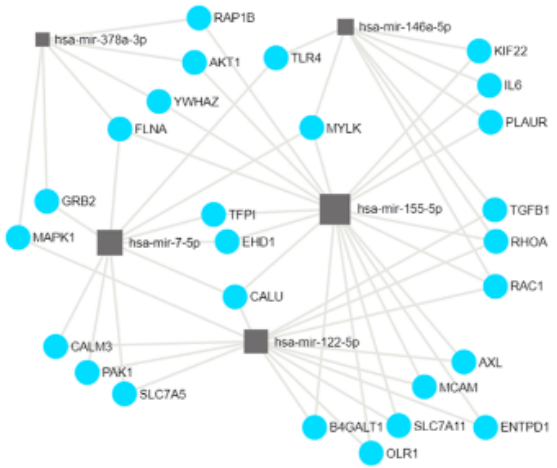

Wound healing Adj Pval: 0.0000366

Genes targeted by at least two miRNA
Top KEGG pathway

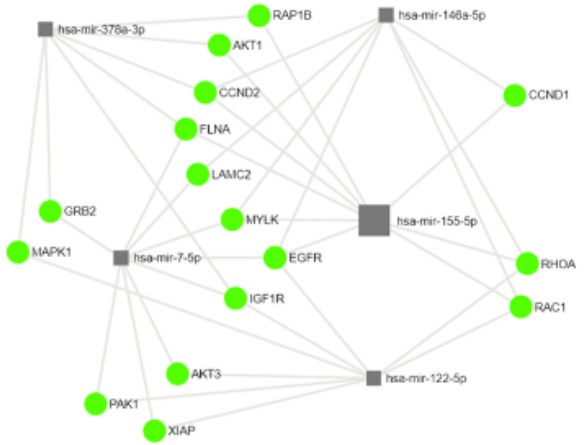

Focal adhesion Adj Pval: 5.95e-7

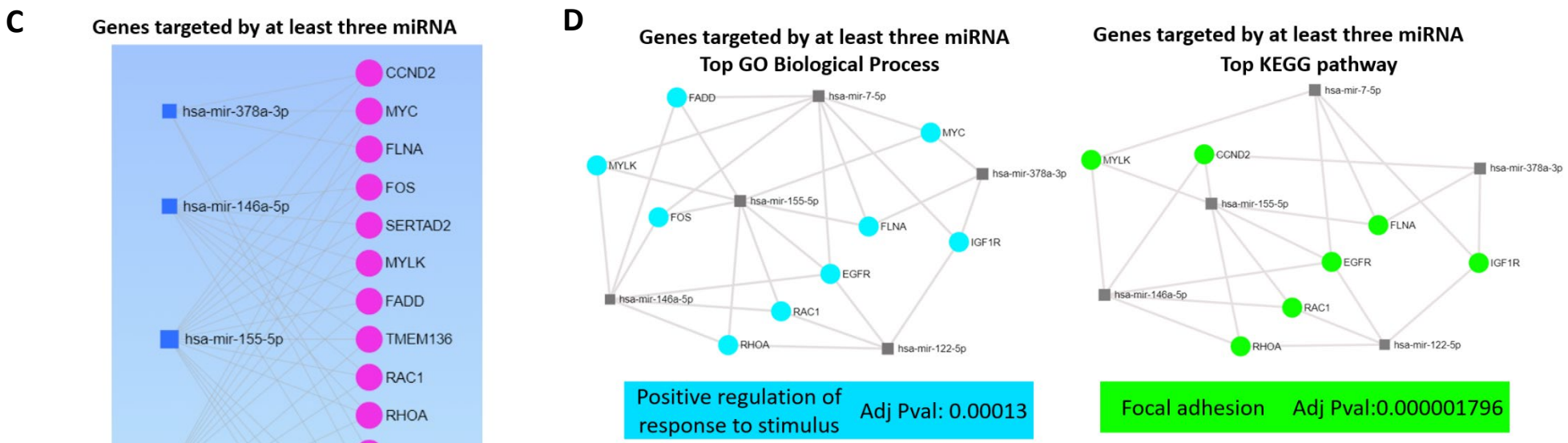

Figure 5.7 EV miRNA upregulated in response to IAV have shared gene targets

A) Diagram of functional analyses steps of significantly upregulated miRNA (miR-378a-3p, miR-7-5p, miR-146a-5p, miR-155-5p and miR-122-5p). Target genes were identified using miRTarBase v8.0. B) Top GO biological processes and KEGG pathway associated with target genes based on miRNet analyses of genes targeted by at least two miRNA. C) Network of genes targeted by at least 3 miRNA. D) Top GO biological process and KEGG pathways based on miRNet analyses of genes targeted by at least 3 miRNA.

5.3 Discussion

Infected respiratory epithelial cells release EVs with pathological characteristics and have been proposed to participate in the immune response (264). The export and transfer of miRNAs via EVs has been suggested as a mechanism that can alter biological processes in recipient cells, thereby modulating disease (228). A single miRNA can regulate many genes within any individual cell via binding to the 3' UTR of the target mRNA (105). Previous studies report that miRNA play a role to fine-tune the immune response by targeting key regulatory molecules (265). This chapter addresses the aim of completing functional analyses of miRNA cargo of EVs released from ALI cultured bronchial epithelial cells in response to infection with IAV.

Identifying which gene sets or pathways that particular miRNA regulate is a key question to address in functional miRNA studies. The miRNA network visualisation analytics platform, miRNet and miRNA target database, miRTarBase was used to explore experimentally validated target genes of EV miRNA altered in response to IAV (miR-122-5p, miR-155-5p, miR-146a-5p, miR-7-5p, miR-378a-3p and miR-505-5p). The results of the *in silico* analysis identified 2348 target genes for the six EV miRNA altered in response to IAV. The top three GO biological processes were ageing, response to UV and epidermal growth factor signalling pathway. These processes are all associated with damage and damage response which aligns with the observations in this thesis and other studies that IAV results in damage to the airway epithelium.

Many of the genes associated with the top two biological functions identified for EV miRNA altered in response to IAV are related to the DNA damage response. Indeed the DNA damage response has been suggested to contribute to IAV associated damage is direct induction of DNA damage and altered regulation of DNA damage pathways (266). Genes, such as MSH2 and MSH6, that function in DNA mismatch repair were identified in the top biological processes reported in this chapter. Furthermore a number of caspase genes involved in regulating cell death were shown to be targeted by the EV miRNA identified in this thesis to be altered in response to IAV (267). In addition, genes targeted by two or more of the miRNA increased in EVs in response to IAV were revealed to be associated with wound healing. Suggesting these EV miRNA may regulate events that restore integrity to a damaged tissue, following an injury. Though further work is required to investigate whether this would have a beneficial or negative impact on the host. The top KEGG pathway associated with genes targeted by more than one miRNA was focal adhesion. Studies have shown focal adhesion kinases to be important in wound healing process (268). This may support function of these miRNA in damage associated response to IAV.

As mentioned previously one of the top biological functions associated with the target genes of EV miRNA altered in response to IAV was the epidermal growth factor signalling pathway. Indeed, the gene identified to be targeted by the most EV miRNA in this chapter was EGFR. Network analyses revealed EGFR to be targeted by four of the EV miRNA upregulated in response to influenza, including miR-155, miR-122, miR-7 and miR-146a. EGFR activation has been described as a double-edged sword in influenza infection. EGFR signalling has been shown to support tissue regrowth during respiratory infection (269). However, it has also been suggested to promote viral replication through increased virion uptake or suppression of cytokine expression (269). Therefore further work is required to understand the function of miRNA regulation of EGFR in response to IAV.

In silico analyses also suggested EV miRNAs altered in response to IAV target genes involved in immune cell development and T cell signalling. The function of miRNA as key regulators of immune cell development and function has been widely suggested (270). In monocytes, macrophages and myeloid dendritic cells, miR-155 increases substantially following activation by a variety of inflammatory stimuli. In addition miR-155 plays a central role in regulating Akt-dependent polarization of macrophages (271). Furthermore, miR-155 is required for efficient CD4+ T cell activation during anti-viral defence (272). Further work is required to investigate if release of miR-155 in EVs from IAV infected epithelial cells can mediate activation of immune cells such as macrophages in response to IAV.

Strongly validated target genes shared by multiple miRNA altered in response to IAV include *FADD*, *SOCS1* and *NFKB*. These gene have previously been shown to be involved in the viral immune response (273,274). IAV has been shown to activate FADD to drive apoptosis of infected cells and protects the host (273). FLNA was identified as a target of three of the EV miRNA identified in this thesis to be upregulated in response to IAV (miR-378a, mR-7 and miR-155). FLNA is an actin-binding protein previously shown to be involved in regulating multiple signalling pathways and involved in the IAV replication cycle (275). These results further suggest a function of EV miRNA in modulating the response to IAV. However, one major limitation of investigating the function of miRNA through *in silico* analyses is that validation of all miRNA targets still remains incomplete and in some cases biased towards most prevalent areas of research such as cancer.

5.4 Summary

A better understanding of IAV–host interaction is required for the development of sustainable and effective anti-influenza strategies. Many of the identified target genes of these miRNAs are involved in damage response, apoptosis and immune cell activation and differentiation pathways further

suggesting that these miRNAs are involved in immune response to IAV. Therefore, the EV miRNA identified in this study may be used to develop immune-modulating therapies that strengthen the host defences against influenza viruses and counteract immune dysfunction in ageing and COPD.

6 Functional analyses of microRNA altered in epithelial EVs in response to IAV

6.1 Introduction

To further understand the relationship between miRNA and response to IAV, this chapter reports the correlation of expression of viral RNA or anti-viral immune genes, and miRNA. In addition, given miR-155 was to most upregulated EV miRNA in response to IAV that could be detected by RT qPCR, the impact of transfection of miR-155 mimic and inhibitors on IAV infection of bronchial epithelial cells and immune response was investigated.

6.2 Results

6.2.1 Correlation of PBEC miRNA and immune gene expression

To further investigate the immune function of EV miRNA altered in response to IAV the correlation of levels of miRNA with viral RNA or immune gene expression (*CXCL10*, *IFNB1*, *ISG15* and *SOCS1*) was investigated. For this analyses healthy and COPD samples were combined. In the infected PBEC samples the following significant correlation were observed for cellular miRNA: *CXCL10* and miR-146a, *IFNB1* and miR-155 or miR-146a, *ISG15* and miR-146a, *SOCS1* and miR-7 or miR-505 (**Figure 6.1A**). Similarly, the following significant correlations were observed for EV miRNA: *CXCL10* and miR-146a, *IFNB1* and miR-146a, *ISG15* and miR-146a (**Figure 6.1B**). Unlike cellular miRNA EV miR-7 correlated significantly with viral RNA.

A **IAV infected PBEC - Cell miRNA**

		miR-155-5p	miR-146a-5p	miR-7-5p	miR-378a-3p	miR-505-5p
CXCL10	r	0.7855	-0.8612	0.3148	-0.1076	0.2756
	p	0.0641	0.0276	0.5434	0.8392	0.5971
IFNB1	r	0.9495	-0.9034	0.7115	-0.1791	0.5497
	p	0.0038	0.0135	0.1128	0.7343	0.2585
ISG15	r	0.9622	-0.8039	0.7322	-0.2484	0.4611
	p	0.0021	0.0539	0.0979	0.6351	0.3573
SOCS1	r	0.7659	-0.4784	0.8231	-0.5893	0.8864
	p	0.0758	0.3371	0.0442	0.2183	0.0186
Viral RNA	r	0.3831	-0.7937	0.1687	-0.1912	0.6494
	p	0.4535	0.0595	0.7493	0.7168	0.1628

B **IAV infected PBEC - EV miRNA**

		miR-155-5p	miR-146a-5p	miR-7-5p	miR-378a-3p	miR-505-5p
CXCL10	r	0.03774	-0.8902	0.6533	-0.4349	0.44
	p	0.9434	0.0174	0.1595	0.3888	0.3826
IFNB1	r	0.5389	-0.9556	0.7835	-0.3902	0.2517
	p	0.2699	0.0029	0.0652	0.4444	0.6305
ISG15	r	0.5621	-0.9268	0.5974	-0.4349	-0.02053
	p	0.2456	0.0078	0.2105	0.3888	0.9692
SOCS1	r	0.5833	-0.6588	0.4687	-0.2782	0.3273
	p	0.2242	0.1548	0.3484	0.5935	0.5266
Viral RNA	r	0.1227	-0.6555	0.8215	-0.4867	0.5737
	p	0.8169	0.1575	0.045	0.3276	0.2338

Figure 6.1 Correlation observed between miRNA and viral RNA or anti-viral immune genes

A) Table displaying Pearson correlation coefficient (r) and p-value (p) calculated for expression of cellular miRNA and immune gene expression or viral RNA levels for IAV infected PBEC (n=6). B) Table displaying Pearson correlation coefficient and p-value calculated for expression of EV miRNA and immune gene expression or viral RNA levels for IAV infected PBEC (n=6).

6.3 Transfection of miR-155 mimic and inhibitor in BCi epithelial cells

Given the time and resources available it was not possible to complete transfection experiments to further investigate the function of all the miRNA altered in EVs in response to IAV. miR-155 was chosen for transfection studies given it was the second highest upregulated EV miRNA in response to IAV. In addition, the most upregulated miRNA, miR-122 was not of a suitable abundance to be detected by RT-qPCR. A control mimic and inhibitor were used to ensure to control for non-specific changes in gene expression. Submerged BCi cells were transfected with 10nM of either miR-155 mimic or inhibitor or control mimic or inhibitor for 48 h. Cells were then infected with IAV at MOI 0.3 for a further 24 h. Transfection of miRNA mimics not only allows the investigation of target gene and

function of miR-155 in response to IAV but also simulates a situation in which miR-155 may be transferred in EVs to other cells. Successful transfection of miR-155 mimic was confirmed by the detection of significantly greater levels of miR-155 in the miR-155 mimic transfected samples (**Figure 6.2A**). Significant levels of viral RNA were detected in the control, miR-155 mimic and inhibitor samples. Significantly less viral RNA was detected for miR-155 mimic transfected samples compared to control mimic samples (**Figure 6.2B**).

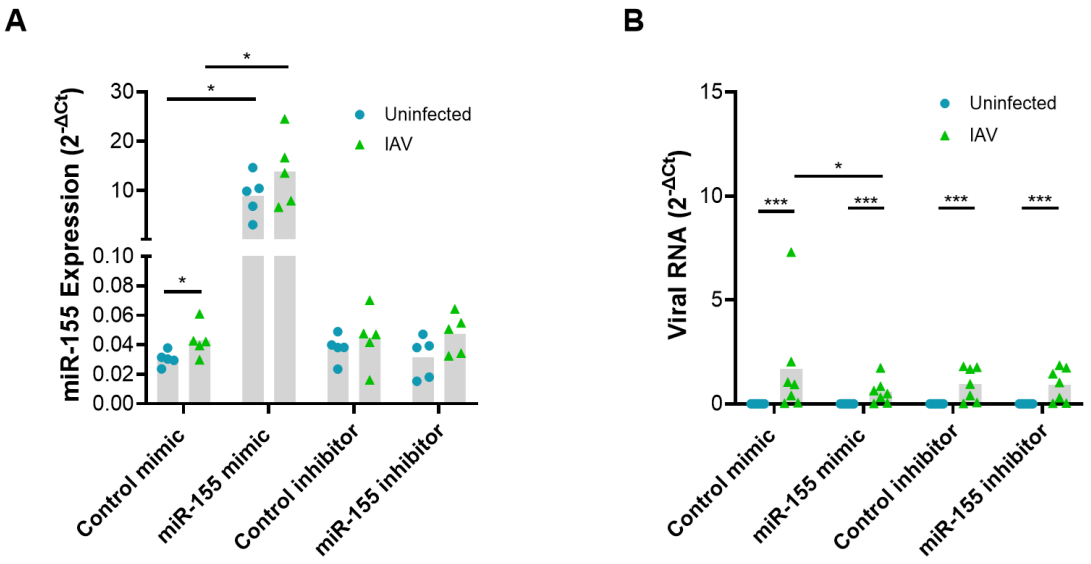

Figure 6.2 Successful infection and transfection of submerged BCi

*Submerged BCi transfected with 10 nM of either control mimic, miR-155 mimic, control inhibitor or miR-155 inhibitor for 48 h. Then infected with IAV for 24 h. An uninfected control was also completed. The level of A) miR-155 or B) viral RNA was then detected via RT-qPCR. Normality determined by Shapiro-Wilk test. Paired t-test *P<0.05, ***p<0.001*

6.4 Regulation of anti-viral immune genes following transfection with miR-155 mimic

As observed for ALI BCi, infection of submerged BCi with IAV at MOI 0.3 for 24 h resulted in increased level of expression of immune genes including *CXCL10*, *IFNB1*, *SOCS1* and *ISG15*. Transfection of submerged BCi with miR-155 mimic resulted in a slight reduction of expression of *CXCL10* in uninfected BCi (**Figure 6.3A**). In IAV infected BCi, miR-155 mimic transfection significantly reduced expression of immune genes including *CXCL10*, *ISG15* and *SOCS1* (**Figure 6.3B**). This experiment was also completed using RNA mimic with no lipofectamine to support these

observations were associated miRNA mimics being taken up into the cell and not with free miRNA mimics (**Figure 6.3C-D**). In these experiments no significant differences in expression of immune genes were observed.

6.5 Regulation of anti-viral immune genes following transfection with miR-155 inhibitor

Transfection with miR-155 inhibitor induced a significant increase in the expression of *CXCL10* in uninfected BCi (**Figure 6.4**). Furthermore, significantly lower levels of *IFNB1* were detected in infected BCi. No changes in SOCS or ISG15 expression were observed following transfection with the miR-155 inhibitor.

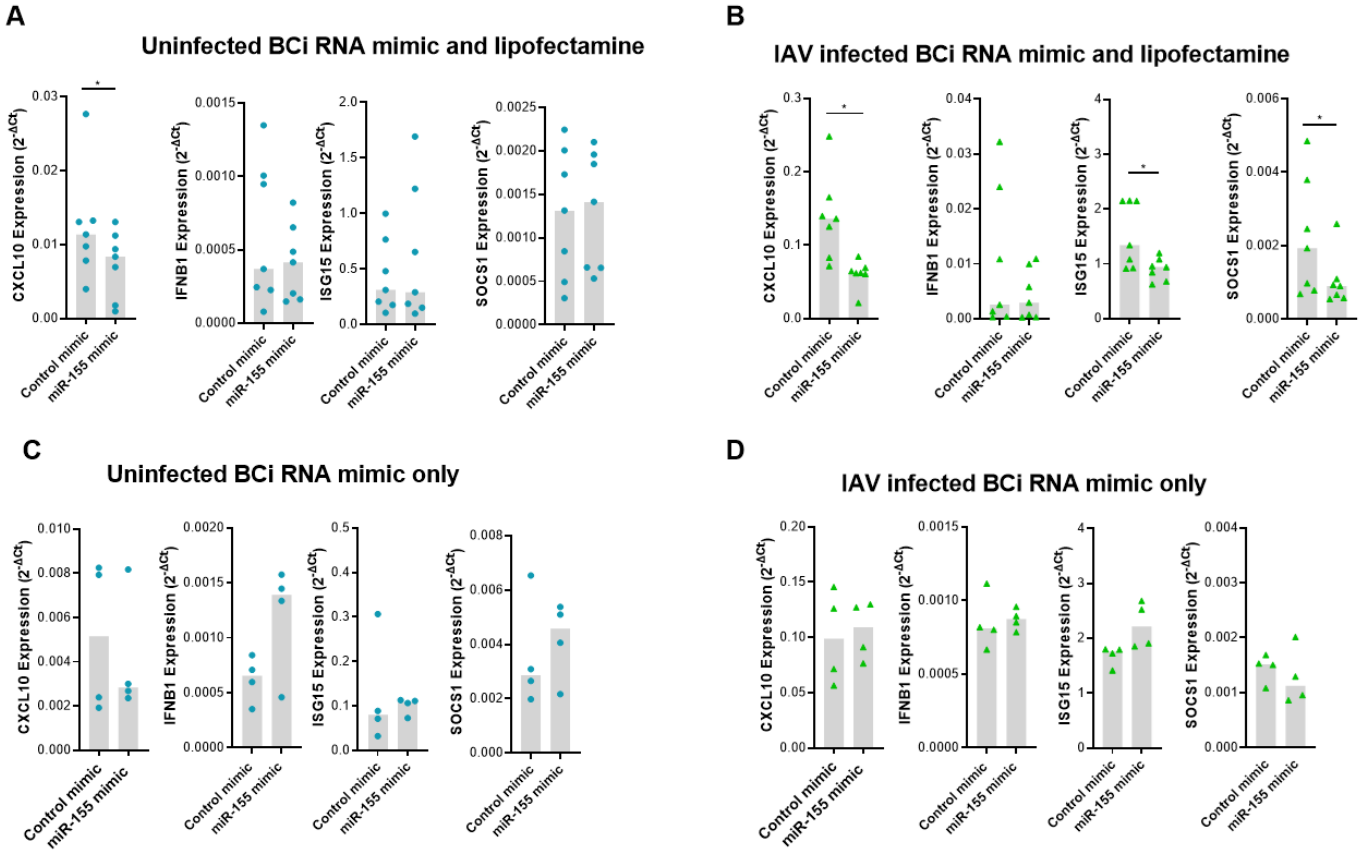

Figure 6.3 Changes in anti-viral immune response on transfection with miR-155 mimic

*Submerged BCi transfected with 10 nM of either control mimic or miR-155 mimic plus lipofectamine for 48 hours and either A) uninfected or B) infected with IAV for 24 hours. Submerged BCi transfected with 10 nM of either control mimic or miR-155 mimic without lipofectamine for 48 hours and either C) uninfected or D) infected with IAV for 24 hours. Gene expression was then detected via RT-qPCR. Normality determined by Shapiro-Wilk test. Non-parametric data displayed with medium and analysed using Wilcoxon test. *P<0.05, ***p<0.001*

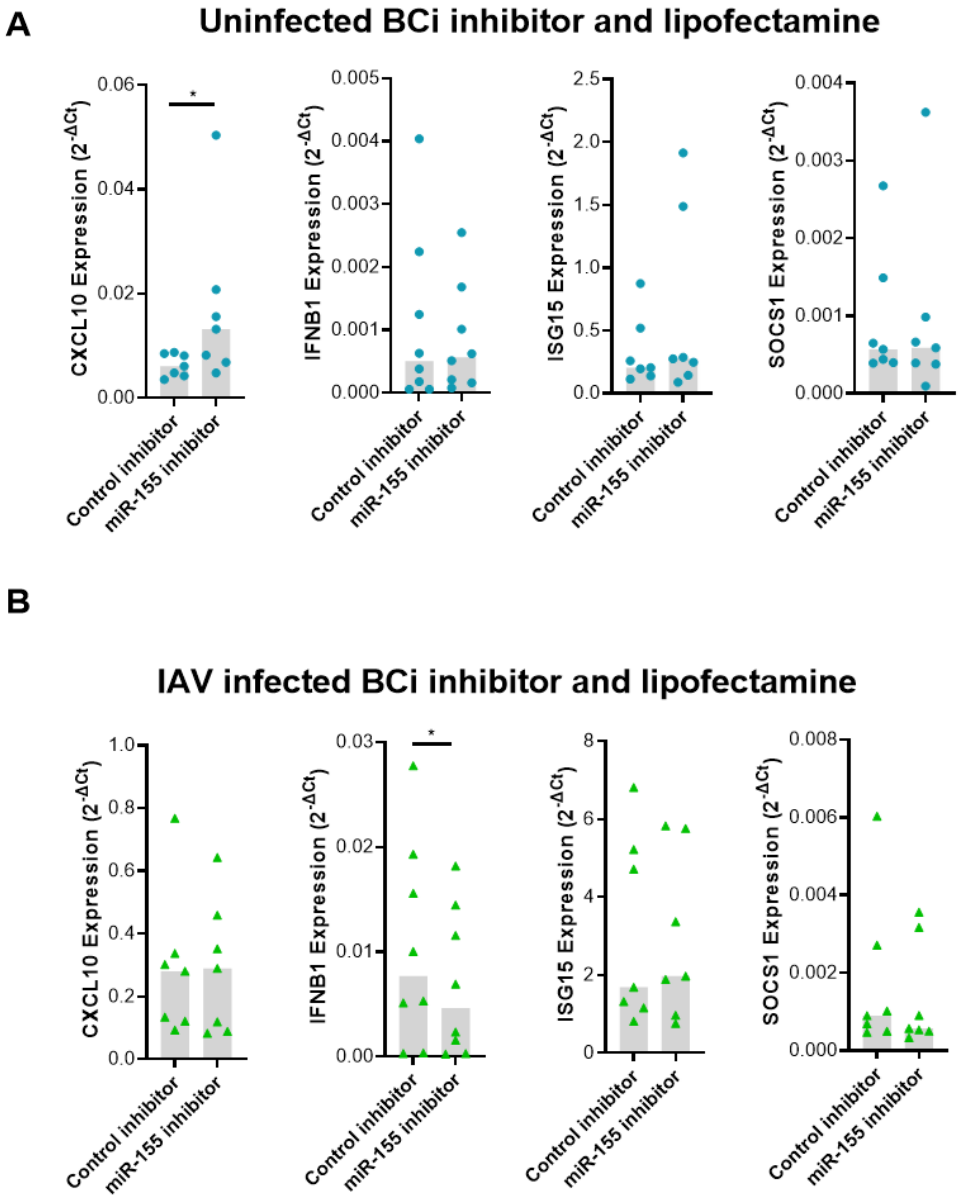

Figure 6.4 Changes in anti-viral immune response on transfection with miR-155 inhibitor

*Submerged BCi transfected with 10 nM of either control inhibitor or miR-155 inhibitor plus lipofectamine for 48 hours. Samples were the either A) uninfected or B) infected with IAV for 24 hours. Gene expression was then detected via RT-qPCR. Normality determined by Shapiro-Wilk test. Non-parametric data displayed with medium and analysed using Wilcoxon test *P<0.05*

6.6 ALI transfection with miR-155 mimic

Interestingly it was observed that miR-155 expression was significantly higher in submerged BCi epithelial cells compared to ALI cultured BCi epithelial cells (**Figure 6.5A**). ALI BCi cells were transfected by applying 100 nM to apical and basal compartments for 4 hours. The following day ALI cells were then infected as described previously for 24h with IAV. Successful transfection of ALI was achieved as demonstrated by increased levels of miR-155 detected via qPCR (**Figure 6.5B**). However, no changes in level of viral RNA or immune response were detected between control mimic transfected cells and miR-155 mimic transfected cells (**Figure 6.5C-D)**.

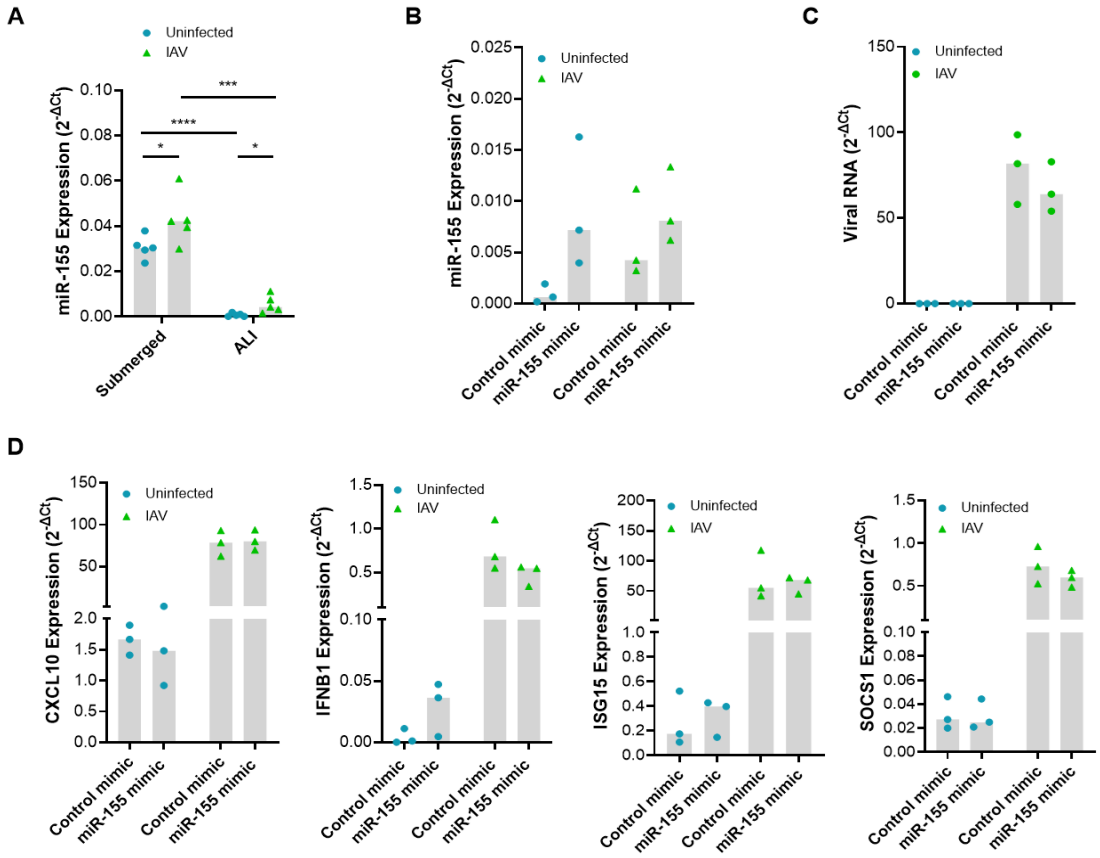

Figure 6.5 Transfection of ALI cultured BCi with miR-155 inhibitor

*A) Cellular miR-155 in uninfected or infected submerged cultured BCi or ALI cultured BCi. ALI cultured BCi transfected with control mimic or miR-155 then either uninfected or infected with IAV. Level of C) viral RNA or D) immune gene expression. Gene expression was then detected via RT-qPCR. Normality determined by Shapiro-Wilk test. Non-parametric data displayed with medium and analysed using Wilcoxon test. *P<0.05*

6.7 Regulation of oxidative stress in epithelial cells following transfection with miR-155 mimic and inhibitor

The results of this thesis suggest EV miRNA may function to regulate damage response to IAV. Recently *in vitro* transfection of miR-155 mimic into BEAS-2B cells was shown to significantly decrease FOXO3a protein expression, accompanied by the reduced SOD2 and catalase expressions, promoting oxidative stress (251). The expression of SOD2 was therefore investigated in this thesis in response to transfection with miR-155 mimic and inhibitor. The results suggest increased cell death and reduced level of SOD2 antioxidant 24 h following transfection with miR-155 mimic (**Figure 6.6A-B**). However, following removal of transfection media and then completion of IAV infection experiment no significant difference in the level of cell death was observed (**Figure 6.6C**), although significantly reduced levels of antioxidant SOD2 was still observed in miR-155 mimic transfected samples for both uninfected and IAV infected cells (**Figure 6.6D**). No change in the expression of SOD2 was observed following transfection with the miR-155 inhibitor (**Figure 6.6E**).

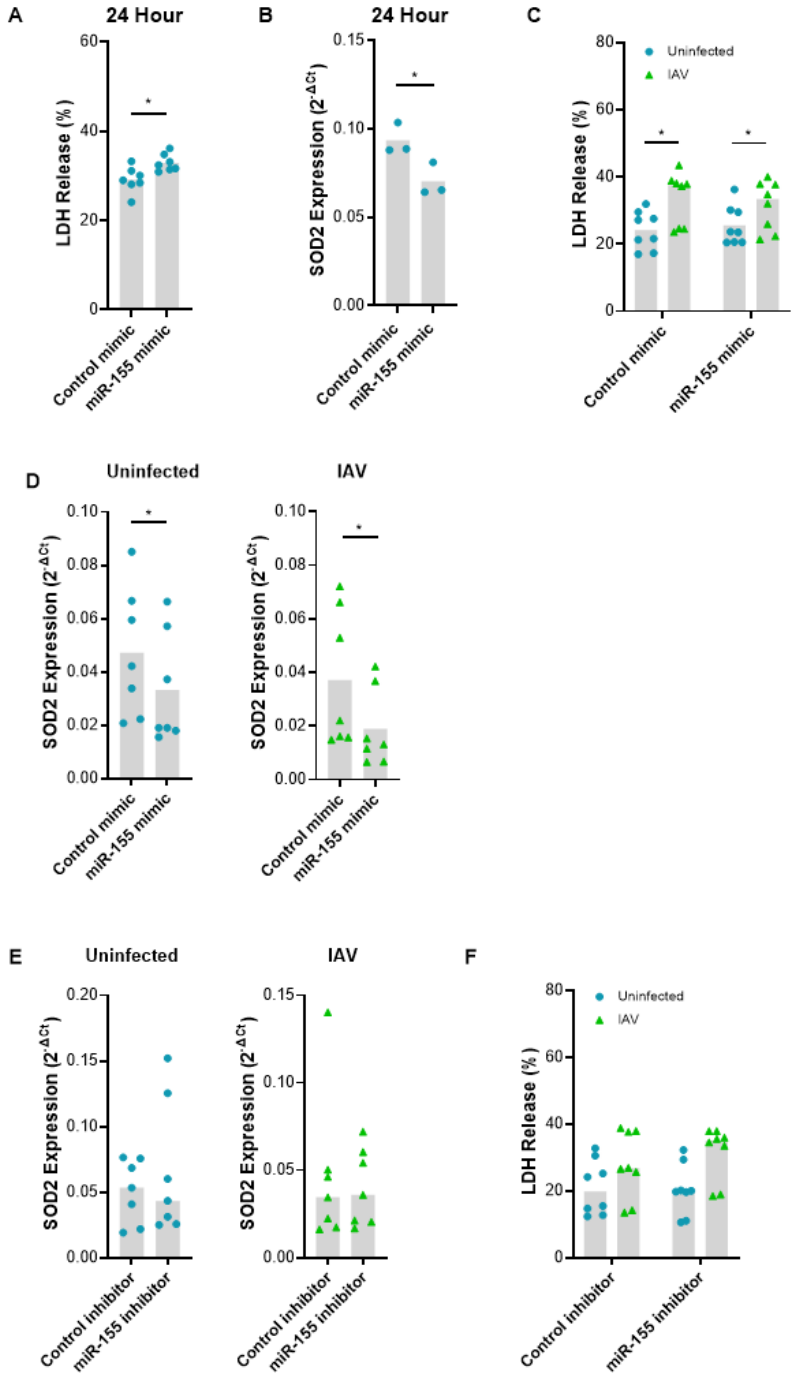

Figure 6.6 Changes in cell death and antioxidant in response on transfection with miR-155 inhibitor

*A) LDH release or B) SOD2 expression of submerged BCi transfected with 10 nM of either control mimic or miR-155 mimic for 24 hours. C) LDH release or D) SOD2 expression of submerged BCi transfected with 10 nM of either control mimic or miR-155 mimic for 48 hours the either uninfected or infected with IAV for 24 hours. D) LDH release or E) SOD2 expression of submerged BCi transfected with 10 nM of either control inhibitor or miR-155 inhibitor for 48 hours the either uninfected or infected with IAV for 24 hours. Gene expression was then detected via RT-qPCR. Normality determined by Shapiro-Wilk test. Non-parametric data displayed with medium and analysed using Wilcoxon test *P<0.05*

6.8 Discussion

Investigating the correlation of miRNA levels following infection with IAV and expression of anti-viral genes revealed a positive significant correlation with miR-155 and *IFNB1* or *ISG15* but a negative correlation with miR-146a and *IFNB1* or *CXCL10*. This aligns with previous literature that has suggested miR-155 and miR-146a form a combined positive and negative auto regulatory loop to control precise NF-κB activity during inflammatory stimuli. While miR-155 expression potentiates NF-κB, leading to both an overactive acute inflammatory response and chronic inflammation, miR-146a has been suggested as a slower response that mediates repression of NF-κB activation (276). This may suggest these miRNAs are good markers of the status of the immune response. However, it is not possible to distinguish if this correlation is due to regulation of immune genes by miRNA or is dependent on the pathways that regulate the levels of miRNA.

The next step was to validate the miRNA-mRNA targets using a lipofectamine transfection system which can efficiently deliver miRNA mimics into *in vitro* cultured mammalian cells. It is a fast, easy, and economical way to gain insights into the functions of miRNAs. Furthermore, use of this agent provides a model for EV delivery machinery. Measurement of downstream target gene expression with RT-qPCR can be used to validate the predicted targets of the differentially expressed miRNA. Given the time and resources available it was not possible to complete transfection experiments to further investigate the function of all the miRNA altered in EVs in response to IAV. miR-155 was chosen for transfection studies given it was the second highest upregulated EV miRNA in response to IAV below miR-122 which was not of a suitable abundance to be detected by RT-qPCR. Previous literature suggests miR-155, upregulates IFN signalling downstream of IFNAR through repression of *SOCS1*, an ISG that limits IFNAR signal transduction. In macrophages, miR-155 was shown to target the *SOCS1* 3' UTR, enhancing STAT1 phosphorylation and ISG expression while reducing viral replication (277). In this study transfection of BCi with miR-155 did result in a significant decrease in *SOCS1* and viral RNA. However, unexpectedly a decrease in *CXCL10* and *ISG15* was also observed contradicting previous studies that have suggested miR-155 enhances ISG expression.

A recent study suggested that although miR-155 is considered a pro-inflammatory mediator, it may also have anti-inflammatory effects. They found that miR-155 acted as an anti-inflammatory mediator in the initial stage of LPS-induced inflammatory response mainly through repressing TAB2 protein translation, and as a pro-inflammatory mediator by down-regulating SOCS1 in the later stages (278). In addition, miR-155-3p was shown to promote type I IFN production by inhibiting the negative regulator IRAK3, while miR-155-5p was shown to restrict type I IFN by targeting the positive regulator TAB2 (279). They suggested, miR-155-3p and miR-155-5p help to

ensure robust, early induction of IFN and inhibit prolonged, deleterious expression of this inflammatory cytokine. Furthermore other studies have shown expression of CXCL10 and CCL2 to be significantly decreased in macrophages when treated with EV miR-155 (280). Whether miR-155 released from bronchial epithelial cells in EVs in response to IAV can regulate the immune response in neighbouring cells remains unclear and requires further investigation. Furthermore, future studies should investigate the effect of miR-155 mimic on protein expression and not just gene expression. In addition, other targets such as expression of other cytokines, such as IL-2, IL-4, IL-6 and TNF regulated by SOCS1 should be investigated.

Additionally, miR-155 overexpression has also been suggested to contribute to viral infection-induced tissue damage. Using a mouse model of lung injury induced by influenza infection it was found that lung inflammation was significantly inhibited in miR-155 knockout mice (235). In a cell model, overexpression of miR-155 significantly aggravated LPS-induced lung epithelial cell damage and inflammatory factor production, while inhibition of miR-155 was resistant to LPS-induced lung epithelial cell injury and inflammatory factor production (281). Recently in vitro transfection of miR-155 mimic into Beas-2B was shown to significantly decreased FOXO3a protein expression, accompanied by the reduced SOD2 and catalase (CAT) expressions, promoting PM2.5-evoked oxidative stress (251). Furthermore hypoxia-induced miR-155 overexpression in extracellular vesicles has been shown to target FOXO3 (238). The results of this thesis support role of miR-155 in cell death and to reduce expression of SOD2 antioxidant.

One of the major limitations with this study is that transient transfection of miRNA mimics can alter gene expression in a non-specific manner or fail to efficiently suppress target gene expression (282). Furthermore, given it has been estimated that mammalian cells often express 100–200 different species of miRNAs with a total amount of 1–2 $\times 10^5$ copies of mature miRNAs in a cell transient transfection of high concentrations of miRNA mimics into mammalian cells may not represent any mammalian miRNAs under physiological or pathological conditions (282,283). In this study efforts were made to reduce this limitation such as miRNA mimics were used at 10 nM lower than the 25 or 100 nM that are commonly used. Another limitation of this study is that experiments were carried out in cell culture systems that cannot fully capture the spatial and physiological complexity of the whole respiratory tract. Therefore, further *in vitro* co-culture and *in vivo* studies are required.

6.9 Summary

The results of this chapter show a positive significant correlation with miR-155 and *IFNB1* or *ISG15* but a negative correlation with miR-146a and *IFNB1* or *CXCL10*. Furthermore, transfection of BCi

with miR-155 did result in a significant decrease in *SOCS1* and viral RNA. However, unexpectedly a decrease in *CXCL10* and *ISG15* was also observed contradicting previous studies that have suggested miR-155 enhances ISG expression. In addition the results of this thesis support role of miR-155 in cell death and to reduce expression of SOD2 antioxidant. However there are limitations with transient transfection and therefore further functional studies are required.

7 Summary discussion and future work

7.1 Overview

Influenza has caused millions of deaths throughout history. Despite the development and implementation of strategies to combat influenza, such as the influenza vaccine, it continues to be one of the most common respiratory viruses. Lung epithelial cells are the primary target and first line of defence against influenza. The immune and inflammatory response to influenza must be tightly regulated to provide viral clearance but avoid excessive damage. EVs have been reported as biomarkers of the biological status of the cell as well as a mechanism for transferring immune and inflammatory signals through cellular cargo such miRNA (284,285). However, to date there have been no studies that fully characterise miRNA profile of EV released from bronchial epithelial cells in response to IAV. Given the role of miRNAs in modulating gene expression in disease they have recently been suggested as potential therapeutic targets by modulating expression using mimics or inhibitors.

Thus, the primary aim of PhD was to understand the targets and functions of EV miRNA released from bronchial epithelial cells in response to IAV with the hypothesis being that the microRNA cargo of extracellular vesicles released from bronchial epithelial cells is altered following infection with IAV promoting the anti-viral immune response.

In summary, the results of the sequencing completed in this thesis demonstrate 5 miRNA to be increased with logFC > 0.6 (miR-122-5p, miR-155-5p, miR-146a-5p, miR-7-5p, miR-378a-3p) and 1 decreased with logFC < -0.6 (miR-505-5p) in EVs released from ALI BCi in response to IAV. Validation of these miRNA with qPCR using both ALI cultured BCi and PBEC support an increase in miR-155, miR-146a, miR-7 and miR-378a in EVs in response to IAV. Furthermore, analyses of PBEC samples suggest changes in EV miRNA in response to IAV may be dysregulated as a result of COPD or ageing. Functional analyses of the target genes of miRNA altered in EVs in response to IAV were significantly enriched in the influenza A pathway. Furthermore, target genes were identified to be involved in pathways associated with damage response, apoptosis and immune cell activation and differentiation pathways. Therefore, the results of this thesis support the hypothesis that EV miRNA of bronchial epithelial cells are altered in response to IAV. Furthermore, the results support EV miRNA may have a function in modulating anti-viral immune response, however further studies are required to determine if the transfer of EV miRNA can modulate the anti-viral response to IAV.

A summary of the aims addressed in this thesis are detailed below.

1) Establish air-liquid interface bronchial epithelial cell model for IAV infection and isolation of EVs

To address the first aim of this study a suitable *in vitro* culture model was established for the characterisation of EVs released by bronchial epithelial cells.

The human airway epithelium is composed of a variety of cell types including ciliated and secretory goblet cells. The majority of previous studies investigating infection with IAV use cancerous, submerged epithelial monolayer models whereas this thesis uses non-cancerous BCi bronchial epithelial cell line that when cultured under ALI differentiates into a pseudostratified layer and therefore more closely mimics *in vivo* infection conditions (122,127,197). Experiments were completed using BCi cells rather than primary bronchial epithelial cells due to the availability of primary cells during the COVID pandemic. To model EVs released in the lung, EVs were isolated from the apical air-exposed surface of ALI cultured BCi. Previous studies have demonstrated that ALI cultured epithelial cells release EVs into the apical secretions (286).

Isolation of pure EV subpopulations remains a challenge and therefore it is important to characterise the isolated EV population according to ISEV guidelines. In this thesis a range of techniques were utilised to characterise the isolated EV population. Membrane bound vesicles with typical EV morphology were visualised with TEM (215). Analysis of protein markers using western blot and ExoView fluorescence imaging demonstrated a heterogenous population of small EVs with an average diameter of around 60 nm and the presence of CD9, CD63 and CD81 tetraspanins that are commonly associated with EVs. In addition, similar EV characteristics between isolated and non-isolated EVs were observed using ExoView. Given Exoview combines EV capture and analysis, it does not require isolated samples. Therefore, it is a very useful tool especially considering a large amount of EVs are lost during the isolation process.

CD9 was demonstrated to be the predominant tetraspanin. Interestingly out of the three tetraspanins CD63 had the least colocalisation. In particular, there was only a low level of colocalisation between CD63 and CD81. On the other hand, there were few CD81 positive only EVs with the majority of CD81 positive EVs also containing CD9. Other studies have reported changes in the EV population with infection. For example, HSV-1 infection causes major alterations in the biogenesis of EVs, including an increase in their number and an increase in the CD63-positive population of EVs. Furthermore, CD63 was shown to negatively impact infection and therefore the authors proposed the activation of antiviral responses in cells receiving CD63-positive EVs released by infected cells (287). It would be interesting in future studies to complete ExoView characterisation of EVs from uninfected compared to IAV infected epithelial cells to identify changes in tetraspanin markers and EV biogenesis. It was not possible to use ExoView in

this thesis for EVs released in IAV infection as this technology was not available locally and therefore, the samples were sent to NanoView who did not accept infected samples.

While it would have been interesting to investigate the presence of miRNA in EVs over different conditions of IAV infection, due to the costs associated with sequencing it was only possible to investigate one infection condition. IAV infection of epithelial cells has been widely shown to induce apoptosis or necrosis of airway epithelial cells (192). The results of this thesis support IAV results in epithelial cell death and disruption to barrier function. Previous studies have suggested substantial loss of ciliated cells as a result of infection with IAV (288). However, it has also been suggested that basal cells can differentiate to compensate the loss of infected cells (288). The time points in this thesis were not long enough to investigate any potential recovery of damage following influenza. A low infectious dose with a 24 h infection period was chosen to minimise levels of cell death and the release of apoptotic bodies. However, it was not possible in this study to establish an infection model to ensure EV were released from living cells rather than apoptotic bodies released during cell death. Therefore, further work is required to investigate EVs released from living cells compared to dying cells in response to IAV.

It was important that the culture conditions taken forward for sequencing demonstrated substantial activation of the innate immune response in epithelial cell following infection with IAV. The results of this thesis demonstrate an increase in *IFNB1* expression and IFN-stimulated genes such as *ISG15* which are the first line of defence against viral infection and *CXCL10* which helps to inhibit viral replication through the recruitment of immune cells (54). Increased expression of these antiviral genes have been widely demonstrated in response to IAV (208). Infection of ALI cultured BCi with IAV at 3.6 x 10^6 IU/ml for 24 h was identified as the most suitable condition to take forward for EV miRNA-sequencing. This was because infection of ALI cultured BCi with IAV at 3.6 x 10^6 IU/ml induced a substantial increase in immune gene expression at 24 h without high levels of cell death and disruption to barrier function. Previous studies have shown significant differences in miRNA profile of EVs 24 hours after viral infection (161,164).

2) Compare EV miRNA released from IAV infected bronchial epithelial to non-infected control

To address the second aim of this thesis, miRNA sequencing was completed to compare miRNA profiles of EVs released from uninfected compared to IAV infected bronchial epithelial cells. In total 13 significantly different EV miRNA with FDR of less than 0.01 were identified. Of these 13 miRNAs, 5 miRNAs had a logFC > 0.6 (miR-122-5p, miR-155-5p, miR-146a-5p, miR-7-5p, miR-378a-3p) and 1 had logFC < -0.6 (miR-505-5p). Overall, the levels of fold change observed for these miRNAs were relatively low. Other studies have reported log2FC greater than 4 for EV miRNA released from epithelial cells in response to stimuli including viral infection and cigarette smoke

extract (161,289). This may be due to the low infectious dose used in this study. However several miRNA profiling studies have suggested even subtle changes in miRNA levels, can have a significant impact on the biology of the cell (290).

This thesis demonstrated that the top 10 most abundant miRNA make up around 60% of all miRNA reads. This supports previous studies that have shown a small number (<20) of miRNAs accounts for > 80% of all cellular miRNAs (243). By determining the most abundant miRNA, defined as miRNA present in levels of more than 3 SD above average, we can see that the majority of abundant miRNA are not significantly altered with IAV infection. The exception being miR-103a-3p, miR-191-5p and miR-146a-5p. These miRNAs had a very small log2FC of 0.4, 0.5 and 0.8 respectively. However, given the abundance of these miRNAs, even a small change may have a significant impact on target protein levels. On the other hand, miRNA of low abundance may require a higher fold change to translate into a measurable biological phenotype. For example, miR-155-5p is observed at lower abundance but has much greater fold change in response to IAV. Furthermore, even if EV are of too low abundance to have biological effect they shouldn't be discounted as less abundant miRNAs may still serve as specific biomarkers for a disease.

Analyses of changes of EV miRNA (miR-122-5p, miR-155-5p, miR-146a-5p, miR-7-5p, miR-378a-3p and miR-505-5p) in response to IAV was completed using RT-qPCR to verify the sequencing data. ALI cultured PBECs were also used to validate changes in EV miRNA. Overall, the changes in EV miRNA observed in BCi were also observed in PBEC cells supporting the use of BCi cells as a model for bronchial epithelial cells. Overall, the differences observed by RT-qPCR were smaller and less significant compared to sequencing. Furthermore, some miRNAs were below the detection limit of qPCR. This may suggest RT-qPCR used in this thesis had lower sensitivity and specificity. The expression of miR-122-5p was not detected by qPCR. Both BCi and PBEC ALI models support a strong significant increase of miR-155 in EVs. A small increase in EV miR-146a, miR-7 and miR-378 was observed in PBEC EVs by qPCR. Furthermore, qPCR did not support change in miR-505 in EVs in response to IAV.

The results of this thesis support presence of both EV and non-EV extracellular miRNA. For example, increased levels of miR-155 was observed in EVs as well as non-EV samples in response to IAV. Despite the fact miRNA is also present in the extracellular space not associated with EVs it is thought that EVs are relatively stable and protect miRNA from degradation due to the presence of extracellular RNases. Furthermore, in this thesis an increase in miR-146a, miR-7 and miR-378a was observed in PBEC EVs in response to IAV but not in non-EV samples. Previous studies have reported differences between non-EV and EV associated miRNA in biofluids in response to infectious diseases (120). This highlights the potential different function of EV miRNA as a

mechanism of intercellular communication and biomarker of disease compared to cell-free miRNA.

Overall, the levels of EV miRNA were observed to largely reflect the cellular profile supporting, to at least some degree, that the level of EV miRNA is dependant of the level of cellular miRNA. However, on examination of the ratio of EV miRNA to cellular miRNA it does appear that some miRNA may be more preferentially packaged into EVs than others. For example, the relative level of miR-155, miR-7 and miR-378 was comparable between EVs and cells. On the other hand, the relative levels of mirR-146a and miR-505 were higher in EVs compared to cells, providing some support for the presence of a sorting mechanism. In addition, supporting the presence of a sorting mechanism is that while an increase in miR-146 and miR-378 was observed for PBEC EVs in response to IAV, no increase was observed on the cellular level. However, further studies are required to determine whether these miRNAs are selectively packaged into EVs and the potential mechanisms which may modulate this.

3) Compare EV miRNA of healthy and COPD primary epithelial cells in response to IAV

COPD exacerbations cause significant morbidity and mortality worldwide and are associated with increased airway inflammation usually triggered by bacterial and viral infections (249). As discussed previously COPD patients have been demonstrated to have a dysregulated immune response. Furthermore exacerbations triggered by viral infections are usually associated with hypersusceptibility of airway inflammatory response, more severe symptoms, and delayed recovery compared to those without viral infections (152). However, the underlying molecular mechanisms of the hypersusceptibility of airway inflammatory response induced by IAV in COPD patients remain unclear.

Previous studies profiling of EVs from plasma have successfully identified markers of AECOPD exacerbation (291)**.** This present study investigated whether changes in EV miRNA in response to IAV were altered in COPD epithelial cells compared to healthy epithelial cells. It was observed that changes in EV miRNA were dysregulated in COPD epithelial cells in response to IAV. A lower miR-155 EV response was observed for COPD. Furthermore, no increase in miR-146, miR-378 or miR-7 response was observed. These observations may suggest a potential mechanism for immune dysfunction that is observed in COPD resulting in increased susceptibility to infection. However, these changes require validation using larger sample size to enable analyses of statistical significance and samples isolated from healthy and COPD patients to encompass all aspects of the clinical disease pathology.

Infected patients who are older have higher risks of developing severe complications and higher mortality from influenza. There is accumulating evidence that ageing induces a state of chronic inflammation, that may simultaneously contribute to the development of multiple age-related chronic diseases such as COPD, CVD and osteoporosis (254–256). This process, known as inflammaging, is characterised by significantly higher levels of circulating pro-inflammatory markers (254). Ageing has been shown to alter many of the miRNA investigated in this thesis (292). Interestingly, when grouping patients into 41-65 and over 65 age groups the results suggested differences in EV miRNA response. The levels of EV miR-146a and miR-378 were elevated in PBEC of the over 65 patient group in the uninfected samples. Furthermore, an increase in miR-7 was observed for the under 65 patient group but not the over 65 patient group. One recent study identified four miRNAs (miR-7-5p, miR-24-3p, miR-145-5p and miR-223-3p) that were downregulated in elderly people and associated with anti-viral response to SARS-CoV-2 (257). In addition, they showed that EVs from the serum of young people can significantly inhibit SARS-CoV-2 infection and reduce viral load. These observations suggest EV miRNA altered with age may contribute to altered immune response and may be useful in the development of therapeutics. However, these observations require further investigation in a larger cohort that can separate patients into under 65 healthy, under 65 COPD, over 65 healthy and over 65 COPD.

4) Identify the biologically significant targets of these differentially expressed miRNA and validate these in-vitro

Under physiological condition, respiratory cells and immune cells are thought to release protective EVs to defend against endogenous stress and maintain respiratory homeostasis. In response to noxious stimuli respiratory cells release EVs containing various cytokines, chemokines, miRNA, or proteins to transfer immune and inflammatory signals (161,162).

Analyses of the genes targets of miRNA altered in response to IAV revealed the KEGG influenza A pathway to be significantly enriched. A range of processes were targeted. These include IFN and ISG that have been widely shown to play a key role in the anti-viral immune defence. Other cytokines and chemokines, such as IL-6 and IL-8 that are upregulated in response to IAV were also suggested as potential targets of miRNA altered in response to IAV (56). The miRNA also may target genes involved in processes such as viral protein export and nucleocytoplasmic transport that are important for viral replication. Strongly validated target genes shared by multiple miRNA altered in response to IAV include *FADD*, *SOCS1* and *NFKB* that are involved in antiviral immune responses (273,274). Furthermore, IAV has been shown to activate FADD to drive apoptosis of infected cells and protects the host (273). Another target protein identified was FLNA, an actin-

binding protein previously shown to be involved in regulating multiple signalling pathways and involved in the IAV replication cycle (275).

Investigating the correlation of miRNA levels following infection with IAV and expression of anti-viral genes revealed a positive significant correlation with miR-155 and *IFNB1* or *ISG15* but a negative correlation with miR-146a and *IFNB1* or *CXCL10*. The function of EV miR-155 delivered locally to other epithelial cells as a paracrine mechanism was also investigated via transfection. Transfection of miR-155 mimic reduced expression of IFN stimulated genes. Therefore, the transfer of miR-155 via EVs may not be useful at priming other epithelial cells anti-viral immune response. The following significant correlation were observed for EV miRNA: CXCL10 and miR-146a, IFNB1 and miR-146a, ISG15 and miR-146a, miR-7 and viral RNA. This may suggest these EV miR-146a as good marker of the status of the immune response or EV miR-7 as marker of level of viral infection.

The inflammatory response plays an essential role in host defense and immune responses but can become a run-away cascade, which can cause collateral damage in tissues. Studies have reported that miR-155 expression correlates with pulmonary lung damage (235). In support of this, in this thesis the increase in miR-155 expression was higher at 48 h compared to 24 h. At this point destruction of tight junction and cell death was observed. It is not possible to say that miR-155 directly promotes cell death at this point but it may suggest it is a good marker of tissue damage. A number of studies have suggested miR-155 deficiency protects epithelial cells from telomeric and genomic DNA damage in tissue injury (293). Another possible idea is that miR-155 was identified to be higher in basal monolayer epithelial cultures. Therefore, the increase in miR-155 with infection may be related to the loss of ciliated cells and the attempt of the epithelium to replicate basal epithelial cells to repair the damage.

In addition, miR-155 has been suggested to play a crucial role in the pathogenesis and severity of COVID-19 (294). Increased miR-155 expression level has been detected in COVID-19 patients compared to controls, in severe compared to moderate COVID-19 patients, and in non-survival compared to those COVID-19 patients who survived. miR-155 expression level also had significant correlations with clinicopathological characteristics of COVID-19 patients such as C-reactive protein (CRP), mortality, lymphocytes and neutrophils percentages (294). Therefore, it may be miR-155 may be a useful marker of severity of viral infections.

The top biological process associated with miRNA altered in response to IAV was ageing. The worldwide ageing population presents a major challenge for health care services given the prevalence of many chronic diseases dramatically increases with age (295,296). Cellular senescence, defined as irreversible cell cycle arrest, has also been suggested to contribute to

inflammaging. This process is driven by a variety of mechanisms including the DNA damage response and age-related telomere attrition that activate the senescence-associated secretory phenotype (SASP) wherein cells release high levels of pro-inflammatory factors (297). Interestingly when separating EV miRNA based on age, we observed some significant differences. Though surprisingly miR-146 was show to be higher in our ageing population where as other studies have reported an age-related decline in miR-146 (298,299). Other studies have shown miR-7 up-regulation in aged cells reduced the expression of EGFR protein via degradation of its mRNA, but it may also interact with the mRNA of downstream targets of the EGFR-dependent signaling pathway such as MAPK/ERK, CaMKII, Rho-GTPase, PI3K, Akt and mTOR that is important to wound healing (300). In support of this the top associated biological process with these miRNA target genes was 'wound healing'.

7.2 Translational impact of the study

The findings of this study may have important applications for developing and designing further EV studies or therapeutics for influenza. The translational impact of this work is discussed below.

To my knowledge, this is the first study to identify changes in miRNA in EVs from ALI differentiated bronchial epithelial cells in response to IAV. EVs have been identified as novel disease biomarkers given, they reflect the physiological state of the parent cells and as well as being highly stable in biofluids (301). EV miRNAs have been widely described as potential biomarkers. However, given this thesis investigates EVs released from lung epithelial cells it may be that the miRNA identified here are not very useful biomarkers. Biofluids such as plasma are more useful for identifying biomarkers as it can more easily be obtained compared to samples from the lung. Therefore, further work is required to see if changes in EV miRNA observed in this thesis are reflected in BALF and plasma samples of people with influenza. Furthermore, based on the functional analyses completed it seems unlikely that any of the miRNA detected in this thesis are specific markers of influenza, though potentially the relative combination of these miRNA may be useful markers to determine immune status and damage in response to IAV. Especially given that there was a significant correlation of immune genes and EV miRNA.

Molecular engineering techniques have been employed to modify EV cargo for therapeutic use to deliver therapeutic molecules, including miRNA (302). EVs offer advantages over synthetic liposomes and nanovesicles that have had issues regarding biocompatibility and safety (303). EVs provide the ideal transportation method for therapeutic miRNA cargo given they protect miRNA from digestion and degradation whilst evading the host immune surveillance system due to their surface markers reflecting host cell origin. Several previously published reports have

demonstrated the therapeutic effects of EV miRNA (including miR-146a) at alleviating lung injury using *in vivo* models of ARDS (304). Therefore, the modification of EVs to overexpress specific miRNAs may be useful for developing therapeutic treatments to reduce damage associated with viral infections. Therapeutic EVs can be engineered to display an affinity tag for efficient downstream purification to allow large-scale purification of engineered vesicles. This thesis identified EV miRNA altered in response to IAV to target genes involved in pathways associated with immune and damage response. Therefore, manipulation of these EV miRNA either with mimics or inhibitors could result in a significant impact on IAV pathological processes. Furthermore, given EV miRNA was suggested to be dysregulated with age and COPD they may be modulated to combat the immune dysfunction observed in ageing and COPD.

7.3 Strengths and Limitations

The strengths and limitations of this thesis have been discussed throughout. One of the major strengths is the use of ALI cultured differentiated BCi epithelial cells and primary epithelial cells from both healthy and COPD patients that more closely mimics *in vivo* infection conditions. However, a larger sample size of the primary PBECs would have been beneficial to increase the power of the results especially given the heterogeneity and complexity of COPD. Furthermore, future work to investigate if these changes in EV miRNA can be detected *in vivo* are required. EVs should be isolated from healthy and IAV patient biofluids. Preferably BAL fluid and serum though it may be challenging to obtain BAL fluid from influenza infected patients. These EVs may be separated based on parent cell type given EVs have been shown to contain proteins from parent cell type for example EPCAM and TSPAN8 have been described as epithelial cell EV markers (305).

Another strength is that this study used small RNA sequencing to determine complete EV profile of small RNA. Though another limitation of the results in this thesis regarding investigating the function of EV miR155 using mimics is that potential targets were not investigated on the protein level. However, the results of this thesis provide a useful basis for more detailed functional studies. In addition, these miRNAs were investigated by qPCR in EVs as well as cellular and non-EV samples. This was important to determine if changes in miRNA in response were EV specific.

A further limitation of this study is that EVs overlap in size to IAV and therefore are likely to be co-isolated using isolation mechanism used in this study. This makes it particularly difficult to do functional characterisation of the EV miRNA cargo. Future studies potentially investigating other isolation methods for the separation of EVs or the use of neuraminidase inhibitors that prevent the release of viral particles from host cells, thereby halting the spread of infection may overcome this. Such investigations will be further discussed in the following section.

7.4 Future Work

7.4.1 Investigation of EV transfer and uptake

EVs have been suggested to transfer their cargo into target cells through direct fusion with the plasma membrane or endocytosis. When the EVs are taken up and internalised by the target cell, the contents of EVs are released into the cytoplasm of recipient cells through re-fusion with the plasma membrane. Using pharmacological inhibitors, it has been demonstrated that epithelial cells are exclusively dependent on the clathrin and caveolin dependent endocytotic pathway, whereas alveolar macrophage uptake may involve a significant phagocytic component (306). One of the major limitations of this thesis is that it did not demonstrate that EV miRNA released from bronchial epithelial cells can be taken up and have an effect on other cells. Therefor future work is required to validate transfer and uptake of the EV miRNA.

Previous studies have used fluorescent membrane labelled EVs to investigate uptake of EVs by individual cells by flow cytometry and confocal microscopy (306). Joshi et al demonstrated that after endocytosis of green fluorescent protein labelled EVs into HEK293 cells, internalised EVs fused with the membrane of endosomes/lysosomes resulting in EV cargo exposure to the cell cytosol (307). Transfer should be considered to other epithelial cells but also to immune cells. Indeed miR-155 has been shown to contribute to macrophage polarisation. Therefore increased levels of miR-155 in EVs may be transferred to macrophages and lead to polarisation and recruitment of macrophages in influenza virus infection (308). Previous studies have created an *in vitro* system composed of primary alveolar macrophages and lung epithelial cells (306). This co-culture system enables exploration of the dynamics and mechanisms of EV-mediated communication between different types of cells from the lung. In a co-culture system it has been shown that substantial amounts of EVs are internalised by alveolar macrophages, but less by epithelial cells (306). However, upon increasing EV numbers, alveolar macrophages appeared to become saturated and unable to internalise any further EVs, while epithelial cells started taking up EVs to almost a similar extent as alveolar macrophages. This suggests there may be increased uptake efficiency of the epithelial cells at higher EV concentrations.

7.4.2 Separation EVs and IAV

Another of the major limitations of this study is that EVs and IAVs are of a similar size and therefore will be co-isolated by size exclusion chromatography. This impacts the ability to investigate transfer of EV miRNA given that isolated EVs could not be applied to uninfected cells given it would not be possible to determine if changes in the recipient cells were due to the EVs or

IAV particles. Given that IAV particles have been suggested not to contain EV marker CD63, a second step using CD63 antibody based immuno-magnetic isolation has previously been used to solve this (161). However, this will only select for a specific subset of EVs. Another study recently reported a two-step chromatographic purification method. In the first step, virus-like particles and extracellular vesicles were collected and separated from smaller impurities in a flow-through chromatography using a column packed with core-shell beads. The collected flow-through was further purified using heparin affinity chromatography based on binding ability of proteins at different salt concentrations (309). However, depending on their molecular makeup, it might not capture all EV populations due to the broad binding affinity of heparin to various proteins. Furthermore, the elution conditions need to be carefully optimised to balance efficient release and preserved biological activity of EVs.

Another method that could be used to further investigate the transfer of EV miRNA is by adding a neuraminidase inhibitor, such as oseltamivir. Neuraminidase cleaves sialic acid residues on the surface of the infected cell which allows new virions to be released (310). Therefore, using a neuraminidase inhibitor would allow the isolation of EVs using SEC as described in this thesis without contamination with IAV. These isolated EVs could then be incubated with other uninfected cells to investigate changes in miRNA levels of the recipient cell and functional effect such as promotion of anti-viral response or damage associated response.

7.4.3 Analyses of other EV cargo

While the purpose of this thesis was to investigate EV miRNA, it will be important to consider a wide range of other EV cargo exists that may have a function in response to IAV. Studies investigating the multiple cargo types are required to get a better idea of the overall function of EVs in response to IAV and to identify if miRNA cargo are a major contributor to this function.

For example, EVs have shown to carry MHC class I and MHC class II complexes that can stimulate CD4+ and CD8+ T cells directly as well as indirectly through an interaction with antigen-presenting cells. Peptide–MHC complexes of EVs attached or fused to APC surfaces may be directly presented to T cells or internalized where the peptide-MHC complexes can be degraded by the APCs and can be used as a source of peptides to indirectly interact with T cells. Single-EV microarray imaging technology from NanoView has been used previously to directly determine the MHC-I or MHCII level of EVs (334). EVs from patients with mild COVID-19 symptoms had higher levels of the MHC class II receptor, which is responsible for antigen presentation to CD4+ T helper cells (311). Furthermore, studies are required to determine if EVs transfer IAV fragments. EVs of mild COPD

patients have detectable SARS-CoV-2-S-derived fragments that may act to activate immune response in recipient cell (311).

There are a wide number of studies that report the function of protein cargo of EVs (312). Previous studies completing proteomic characterisation of EVs released from human macrophages upon influenza infection revealed EVs can also directly transfer pro-inflammatory cytokines to target cells (111). Mass spectrometry has been widely used as a technique to profile the proteome of EVs (198). Bottom-up proteomics approaches which involve the proteolytic digestion of proteins before mass spectrometry analysis have enabled the identification of thousands of proteins in EVs.

7.5 Summary

EV miRNA identified in this study may be used to develop immune-modulating therapies that strengthen the host defences against influenza viruses and reduce tissue damage associated with viral infections especially in those with immune dysfunction such as the elderly and COPD patients. However, this requires further research to determine efficiency of EV miRNA transfer and uptake as well as determining recipient cell type. In addition, further functional studies are required to validate function of these miRNA in IAV infection to ensure no deleterious effects are observed.

References

1. Martini M, Gazzaniga V, Bragazzi NL, Barberis I. The Spanish Influenza Pandemic: a lesson from history 100 years after 1918. J Prev Med Hyg [Internet]. 2019 Mar;60(1):E64–7. Available from: http://www.ncbi.nlm.nih.gov/pubmed/31041413

2. Kawaoka Y, Krauss S, Webster RG. Avian-to-human transmission of the PB1 gene of influenza A viruses in the 1957 and 1968 pandemics. J Virol [Internet]. 1989 Nov;63(11):4603–8. Available from: https://journals.asm.org/doi/10.1128/jvi.63.11.4603-4608.1989

3. Lakdawala SS, Lamirande EW, Suguitan AL, Wang W, Santos CP, Vogel L, et al. Eurasian-Origin Gene Segments Contribute to the Transmissibility, Aerosol Release, and Morphology of the 2009 Pandemic H1N1 Influenza Virus. Fouchier RAM, editor. PLoS Pathog [Internet]. 2011 Dec 29;7(12):e1002443. Available from: https://dx.plos.org/10.1371/journal.ppat.1002443

4. Mallah SI, Ghorab OK, Al-Salmi S, Abdellatif OS, Tharmaratnam T, Iskandar MA, et al. COVID-19: breaking down a global health crisis. Ann Clin Microbiol Antimicrob [Internet]. 2021 Dec 18;20(1):35. Available from: https://ann-clinmicrob.biomedcentral.com/articles/10.1186/s12941-021-00438-7

5. Horman WSJ, Nguyen THO, Kedzierska K, Bean AGD, Layton DS. The Drivers of Pathology in Zoonotic Avian Influenza: The Interplay Between Host and Pathogen. Front Immunol [Internet]. 2018 Aug 8;9(AUG):1–13. Available from: https://www.frontiersin.org/article/10.3389/fimmu.2018.01812/full

6. Tanner H, Boxall E, Osman H. Respiratory viral infections during the 2009–2010 winter season in Central England, UK: incidence and patterns of multiple virus co-infections. Eur J Clin Microbiol Infect Dis [Internet]. 2012 Nov 8;31(11):3001–6. Available from: http://link.springer.com/10.1007/s10096-012-1653-3

7. Chen L, Han X, Bai L, Zhang J. Clinical characteristics and outcomes in adult patients hospitalized with influenza, respiratory syncytial virus and human metapneumovirus infections. Expert Rev Anti Infect Ther [Internet]. 2021 Jun 3;19(6):787–96. Available from: https://www.tandfonline.com/doi/full/10.1080/14787210.2021.1846520

8. Keech M, Beardsworth P. The impact of influenza on working days lost: a review of the literature. Pharmacoeconomics [Internet]. 2008;26(11):911–24. Available from:

http://www.ncbi.nlm.nih.gov/pubmed/18850761

9. Iuliano AD, Roguski KM, Chang HH, Muscatello DJ, Palekar R, Tempia S, et al. Estimates of global seasonal influenza-associated respiratory mortality: a modelling study. Lancet (London, England) [Internet]. 2018 Mar 31;391(10127):1285–300. Available from: http://www.ncbi.nlm.nih.gov/pubmed/29248255

10. Xu X, Blanton L, Elal AIA, Alabi N, Barnes J, Biggerstaff M, et al. Update: Influenza Activity in the United States During the 2018-19 Season and Composition of the 2019-20 Influenza Vaccine. MMWR Morb Mortal Wkly Rep [Internet]. 2019 Jun 21;68(24):544–51. Available from: http://www.ncbi.nlm.nih.gov/pubmed/31220057

11. McLean S, Hoogendoorn M, Hoogenveen RT, Feenstra TL, Wild S, Simpson CR, et al. Projecting the COPD population and costs in England and Scotland: 2011 to 2030. Sci Rep [Internet]. 2016 Oct 1;6(1):31893. Available from: http://www.nature.com/articles/srep31893

12. Raherison C, Girodet P-O. Epidemiology of COPD. Eur Respir Rev [Internet]. 2009 Dec 1;18(114):213–21. Available from: http://err.ersjournals.com/cgi/doi/10.1183/09059180.00003609

13. Finch D, Lange P, Halpin D, O'Donnell D, MacNee W. Diagnosis, assessment, and phenotyping of COPD: beyond FEV1. Int J Chron Obstruct Pulmon Dis [Internet]. 2016 Feb;11:3. Available from: https://www.dovepress.com/diagnosis-assessment-and-phenotyping-of-copd-beyond-fev1-peer-reviewed-article-COPD

14. Hogg JC, Chu F, Utokaparch S, Woods R, Elliott WM, Buzatu L, et al. The nature of small-airway obstruction in chronic obstructive pulmonary disease. N Engl J Med [Internet]. 2004 Jun 24;350(26):2645–53. Available from: http://www.ncbi.nlm.nih.gov/pubmed/15215480

15. Stanojevic S, Wade A, Stocks J, Hankinson J, Coates AL, Pan H, et al. Reference ranges for spirometry across all ages: a new approach. Am J Respir Crit Care Med [Internet]. 2008 Feb 1;177(3):253–60. Available from: http://www.ncbi.nlm.nih.gov/pubmed/18006882

16. Hadzic S, Wu C-Y, Avdeev S, Weissmann N, Schermuly RT, Kosanovic D. Lung epithelium damage in COPD – An unstoppable pathological event? Cell Signal [Internet]. 2020 Apr;68(January):109540. Available from: https://linkinghub.elsevier.com/retrieve/pii/S0898656820300176

17. Wan ES, Silverman EK. Genetics of COPD and Emphysema. Chest [Internet]. 2009

Sep;136(3):859–66. Available from: https://linkinghub.elsevier.com/retrieve/pii/S0012369209605572

18. Stoller JK, Aboussouan LS. A Review of α 1 -Antitrypsin Deficiency. Am J Respir Crit Care Med [Internet]. 2012 Feb 1;185(3):246–59. Available from: https://www.atsjournals.org/doi/10.1164/rccm.201108-1428CI

19. Linden D, Guo-Parke H, Coyle P V., Fairley D, McAuley DF, Taggart CC, et al. Respiratory viral infection: a potential "missing link" in the pathogenesis of COPD. Eur Respir Rev [Internet]. 2019 Mar 31;28(151):180063. Available from: http://err.ersjournals.com/lookup/doi/10.1183/16000617.0063-2018

20. Singanayagam A, Loo S-L, Calderazzo M, Finney LJ, Trujillo Torralbo M-B, Bakhsoliani E, et al. Antiviral immunity is impaired in COPD patients with frequent exacerbations. Am J Physiol Cell Mol Physiol [Internet]. 2019 Dec 1;317(6):L893–903. Available from: https://www.physiology.org/doi/10.1152/ajplung.00253.2019

21. Schneider D, Ganesan S, Comstock AT, Meldrum CA, Mahidhara R, Goldsmith AM, et al. Increased Cytokine Response of Rhinovirus-infected Airway Epithelial Cells in Chronic Obstructive Pulmonary Disease. Am J Respir Crit Care Med [Internet]. 2010 Aug 1;182(3):332–40. Available from: https://www.atsjournals.org/doi/10.1164/rccm.200911-1673OC

22. Perera WR, Hurst JR, Wilkinson TMA, Sapsford RJ, Müllerova H, Donaldson GC, et al. Inflammatory changes, recovery and recurrence at COPD exacerbation. Eur Respir J [Internet]. 2007 Mar;29(3):527–34. Available from: http://www.ncbi.nlm.nih.gov/pubmed/17107990

23. Wilkinson TMA, Aris E, Bourne S, Clarke SC, Peeters M, Pascal TG, et al. A prospective, observational cohort study of the seasonal dynamics of airway pathogens in the aetiology of exacerbations in COPD. Thorax [Internet]. 2017 Oct;72(10):919–27. Available from: https://thorax.bmj.com/lookup/doi/10.1136/thoraxjnl-2016-209023

24. Ivey KS, Edwards KM, Talbot HK. Respiratory Syncytial Virus and Associations With Cardiovascular Disease in Adults. J Am Coll Cardiol [Internet]. 2018 Apr 10;71(14):1574–83. Available from: http://www.ncbi.nlm.nih.gov/pubmed/29622165

25. Allard R, Leclerc P, Tremblay C, Tannenbaum T-N. Diabetes and the severity of pandemic influenza A (H1N1) infection. Diabetes Care [Internet]. 2010 Jul;33(7):1491–3. Available from: http://www.ncbi.nlm.nih.gov/pubmed/20587722

26. Goto T, Shimada YJ, Faridi MK, Camargo CA, Hasegawa K. Incidence of Acute Cardiovascular Event After Acute Exacerbation of COPD. J Gen Intern Med [Internet]. 2018 Sep 8;33(9):1461–8. Available from: http://link.springer.com/10.1007/s11606-018-4518-3

27. Smeeth L, Thomas SL, Hall AJ, Hubbard R, Farrington P, Vallance P. Risk of myocardial infarction and stroke after acute infection or vaccination. N Engl J Med [Internet]. 2004 Dec 16;351(25):2611–8. Available from: http://www.ncbi.nlm.nih.gov/pubmed/15602021

28. MOHAN A, CHANDRA S, AGARWAL D, GULERIA R, BROOR S, GAUR B, et al. Prevalence of viral infection detected by PCR and RT-PCR in patients with acute exacerbation of COPD: A systematic review. Respirology [Internet]. 2010 Apr;15(3):536–42. Available from: https://onlinelibrary.wiley.com/doi/10.1111/j.1440-1843.2010.01722.x

29. Liao K-M, Chen Y-J, Shen C-W, Ou S-K, Chen C-Y. The Influence of Influenza Virus Infections in Patients with Chronic Obstructive Pulmonary Disease. Int J Chron Obstruct Pulmon Dis [Internet]. 2022 Sep;Volume 17(August):2253–61. Available from: https://www.dovepress.com/the-influence-of-influenza-virus-infections-in-patients-with-chronic-o-peer-reviewed-fulltext-article-COPD

30. Huang H-H, Chen S-J, Chao T-F, Liu C-J, Chen T-J, Chou P, et al. Influenza vaccination and risk of respiratory failure in patients with chronic obstructive pulmonary disease: A nationwide population-based case-cohort study. J Microbiol Immunol Infect [Internet]. 2019 Feb;52(1):22–9. Available from: https://linkinghub.elsevier.com/retrieve/pii/S1684118217301974

31. Weeks JR, Staples KJ, Spalluto CM, Watson A, Wilkinson TMA. The Role of Non-Typeable Haemophilus influenzae Biofilms in Chronic Obstructive Pulmonary Disease. Front Cell Infect Microbiol [Internet]. 2021;11(August):720742. Available from: http://www.ncbi.nlm.nih.gov/pubmed/34422683

32. Santos S, Marín A, Serra-Batlles J, de la Rosa D, Solanes I, Pomares X, et al. Treatment of patients with COPD and recurrent exacerbations: the role of infection and inflammation. Int J Chron Obstruct Pulmon Dis [Internet]. 2016 Mar;11(1):515. Available from: https://www.dovepress.com/treatment-of-patients-with-copd-and-recurrent-exacerbations-the-role-o-peer-reviewed-article-COPD

33. Viniol C, Vogelmeier CF. Exacerbations of COPD. Eur Respir Rev [Internet]. 2018 Mar 31;27(147):170103. Available from: http://err.ersjournals.com/lookup/doi/10.1183/16000617.0103-2017

34. Osman KL, Jefferies JMC, Woelk CH, Devos N, Pascal TG, Mortier M, et al. Patients with Chronic Obstructive Pulmonary Disease harbour a variation of Haemophilus species. Sci Rep [Internet]. 2018 Oct 3;8(1):14734. Available from: https://www.nature.com/articles/s41598-018-32973-3

35. Sethi S, Murphy TF. Infection in the Pathogenesis and Course of Chronic Obstructive Pulmonary Disease. N Engl J Med [Internet]. 2008 Nov 27;359(22):2355–65. Available from: http://www.nejm.org/doi/abs/10.1056/NEJMra0800353

36. Taubenberger JK, Morens DM. The Pathology of Influenza Virus Infections. Annu Rev Pathol Mech Dis [Internet]. 2008 Feb 1;3(1):499–522. Available from: https://www.annualreviews.org/doi/10.1146/annurev.pathmechdis.3.121806.154316

37. Krammer F, Smith GJD, Fouchier RAM, Peiris M, Kedzierska K, Doherty PC, et al. Influenza. Nat Rev Dis Prim [Internet]. 2018 Jun 28;4(1):3. Available from: https://www.nature.com/articles/s41572-018-0002-y

38. Abdelwhab EM, Abdel-Moneim AS. Orthomyxoviruses. In: Malik YS, Singh RK, Yadav MP, editors. Recent Advances in Animal Virology [Internet]. Singapore: Springer Singapore; 2019. p. 351–78. Available from: http://link.springer.com/10.1007/978-981-13-9073-9_19

39. Dane H, Duffy C, Guelbenzu M, Hause B, Fee S, Forster F, et al. Detection of influenza D virus in bovine respiratory disease samples, UK. Transbound Emerg Dis [Internet]. 2019 Sep 7;66(5):2184–7. Available from: https://onlinelibrary.wiley.com/doi/10.1111/tbed.13273

40. Palese P, Schulman JL. Mapping of the influenza virus genome: identification of the hemagglutinin and the neuraminidase genes. Proc Natl Acad Sci [Internet]. 1976 Jun 1;73(6):2142–6. Available from: https://pnas.org/doi/full/10.1073/pnas.73.6.2142

41. Bouvier NM, Palese P. The biology of influenza viruses. Vaccine [Internet]. 2008 Sep 12;26(5):D49–53. Available from: https://linkinghub.elsevier.com/retrieve/pii/S0264410X08009377

42. Stevens J, Blixt O, Glaser L, Taubenberger JK, Palese P, Paulson JC, et al. Glycan Microarray Analysis of the Hemagglutinins from Modern and Pandemic Influenza Viruses Reveals Different Receptor Specificities. J Mol Biol [Internet]. 2006 Feb;355(5):1143–55. Available from: https://linkinghub.elsevier.com/retrieve/pii/S0022283605013707

43. Dou D, Revol R, Östbye H, Wang H, Daniels R. Influenza A Virus Cell Entry, Replication, Virion Assembly and Movement. Front Immunol [Internet]. 2018 Jul 20;9(JUL):1–17.

Available from: https://www.frontiersin.org/article/10.3389/fimmu.2018.01581/full

44. Lakadamyali M, Rust MJ, Zhuang X. Endocytosis of influenza viruses. Microbes Infect [Internet]. 2004 Aug;6(10):929–36. Available from: https://linkinghub.elsevier.com/retrieve/pii/S1286457904001753

45. Li S, Sieben C, Ludwig K, Höfer CT, Chiantia S, Herrmann A, et al. pH-Controlled Two-Step Uncoating of Influenza Virus. Biophys J [Internet]. 2014 Apr;106(7):1447–56. Available from: https://linkinghub.elsevier.com/retrieve/pii/S0006349514002240

46. Brunotte L, Flies J, Bolte H, Reuther P, Vreede F, Schwemmle M. The Nuclear Export Protein of H5N1 Influenza A Viruses Recruits Matrix 1 (M1) Protein to the Viral Ribonucleoprotein to Mediate Nuclear Export. J Biol Chem [Internet]. 2014 Jul;289(29):20067–77. Available from: https://linkinghub.elsevier.com/retrieve/pii/S0021925820476562

47. Hiemstra PS, McCray PB, Bals R. The innate immune function of airway epithelial cells in inflammatory lung disease. Eur Respir J [Internet]. 2015 Apr;45(4):1150–62. Available from: http://erj.ersjournals.com/lookup/doi/10.1183/09031936.00141514

48. Gao W, Li L, Wang Y, Zhang S, Adcock IM, Barnes PJ, et al. Bronchial epithelial cells: The key effector cells in the pathogenesis of chronic obstructive pulmonary disease? Respirology [Internet]. 2015 Jul;20(5):722–9. Available from: https://onlinelibrary.wiley.com/doi/10.1111/resp.12542

49. Rawlins EL, Ostrowski LE, Randell SH, Hogan BLM. Lung development and repair: Contribution of the ciliated lineage. Proc Natl Acad Sci [Internet]. 2007 Jan 9;104(2):410–7. Available from: https://pnas.org/doi/full/10.1073/pnas.0610770104

50. Rogers DF. The airway goblet cell. Int J Biochem Cell Biol [Internet]. 2003 Jan;35(1):1–6. Available from: https://linkinghub.elsevier.com/retrieve/pii/S1357272502000833

51. BOERS JE, AMBERGEN AW, THUNNISSEN FBJM. Number and Proliferation of Clara Cells in Normal Human Airway Epithelium. Am J Respir Crit Care Med [Internet]. 1999 May 1;159(5):1585–91. Available from: https://www.atsjournals.org/doi/10.1164/ajrccm.159.5.9806044

52. BOERS JE, AMBERGEN AW, THUNNISSEN FBJM. Number and Proliferation of Clara Cells in Normal Human Airway Epithelium. Am J Respir Crit Care Med [Internet]. 1999 May 1;159(5):1585–91. Available from:

https://www.atsjournals.org/doi/10.1164/ajrccm.159.5.9806044

53. Plasschaert LW, Žilionis R, Choo-Wing R, Savova V, Knehr J, Roma G, et al. A single-cell atlas of the airway epithelium reveals the CFTR-rich pulmonary ionocyte. Nature [Internet]. 2018 Aug 1;560(7718):377–81. Available from: http://www.nature.com/articles/s41586-018-0394-6

54. Chen X, Liu S, Goraya MU, Maarouf M, Huang S, Chen J-L. Host Immune Response to Influenza A Virus Infection. Front Immunol [Internet]. 2018 Mar 5;9(MAR):1–13. Available from: http://journal.frontiersin.org/article/10.3389/fimmu.2018.00320/full

55. Ehre C, Worthington EN, Liesman RM, Grubb BR, Barbier D, O'Neal WK, et al. Overexpressing mouse model demonstrates the protective role of Muc5ac in the lungs. Proc Natl Acad Sci [Internet]. 2012 Oct 9;109(41):16528–33. Available from: https://pnas.org/doi/full/10.1073/pnas.1206552109

56. Benam KH, Denney L, Ho L-P. How the Respiratory Epithelium Senses and Reacts to Influenza Virus. Am J Respir Cell Mol Biol [Internet]. 2019 Mar;60(3):259–68. Available from: https://www.atsjournals.org/doi/10.1165/rcmb.2018-0247TR

57. Denney L, Ho LP. The role of respiratory epithelium in host defence against influenza virus infection. Biomed J [Internet]. 2018;41(4):218–33. Available from: https://doi.org/10.1016/j.bj.2018.08.004

58. Ryan LK, Dai J, Yin Z, Megjugorac N, Uhlhorn V, Yim S, et al. Modulation of human β-defensin-1 (hBD-1) in plasmacytoid dendritic cells (PDC), monocytes, and epithelial cells by influenza virus, Herpes simplex virus, and Sendai virus and its possible role in innate immunity. J Leukoc Biol [Internet]. 2011 Aug;90(2):343–56. Available from: http://doi.wiley.com/10.1189/jlb.0209079

59. Chong KT, Thangavel RR, Tang X. Enhanced expression of murine β-defensins (MBD-1, -2,-3, and -4) in upper and lower airway mucosa of influenza virus infected mice. Virology [Internet]. 2008 Oct;380(1):136–43. Available from: https://linkinghub.elsevier.com/retrieve/pii/S0042682208004807

60. Pizzolla A, Smith JM, Brooks AG, Reading PC. Pattern recognition receptor immunomodulation of innate immunity as a strategy to limit the impact of influenza virus. J Leukoc Biol [Internet]. 2017 Apr;101(4):851–61. Available from: http://doi.wiley.com/10.1189/jlb.4MR0716-290R

61. Ioannidis I, Ye F, McNally B, Willette M, Flaño E. Toll-Like Receptor Expression and Induction of Type I and Type III Interferons in Primary Airway Epithelial Cells. J Virol [Internet]. 2013 Mar 15;87(6):3261–70. Available from: https://journals.asm.org/doi/10.1128/JVI.01956-12

62. Guillot L, Le Goffic R, Bloch S, Escriou N, Akira S, Chignard M, et al. Involvement of Toll-like Receptor 3 in the Immune Response of Lung Epithelial Cells to Double-stranded RNA and Influenza A Virus. J Biol Chem [Internet]. 2005 Feb;280(7):5571–80. Available from: https://linkinghub.elsevier.com/retrieve/pii/S0021925819630590

63. Wisskirchen C, Ludersdorfer TH, Müller DA, Moritz E, Pavlovic J. The Cellular RNA Helicase UAP56 Is Required for Prevention of Double-Stranded RNA Formation during Influenza A Virus Infection. J Virol [Internet]. 2011 Sep;85(17):8646–55. Available from: https://journals.asm.org/doi/10.1128/JVI.02559-10

64. Iwasaki A, Pillai PS. Innate immunity to influenza virus infection. Nat Rev Immunol [Internet]. 2014 May 25;14(5):315–28. Available from: http://www.nature.com/articles/nri3665

65. Lund JM, Alexopoulou L, Sato A, Karow M, Adams NC, Gale NW, et al. Recognition of single-stranded RNA viruses by Toll-like receptor 7. Proc Natl Acad Sci [Internet]. 2004 Apr 13;101(15):5598–603. Available from: https://pnas.org/doi/full/10.1073/pnas.0400937101

66. Liu G, Park H-S, Pyo H-M, Liu Q, Zhou Y. Influenza A Virus Panhandle Structure Is Directly Involved in RIG-I Activation and Interferon Induction. Lyles DS, editor. J Virol [Internet]. 2015 Jun;89(11):6067–79. Available from: https://journals.asm.org/doi/10.1128/JVI.00232-15

67. Goffic R Le, Balloy V, Lagranderie M, Alexopoulou L, Escriou N, Flavell R, et al. Detrimental Contribution of the Toll-Like Receptor (TLR)3 to Influenza A Virus–Induced Acute Pneumonia. Levine B, editor. PLoS Pathog [Internet]. 2006 Jun 9;2(6):e53. Available from: https://dx.plos.org/10.1371/journal.ppat.0020053

68. Uematsu S, Akira S. Toll-like receptors and type I Interferons. J Biol Chem [Internet]. 2007;282(21):15319–24. Available from: http://dx.doi.org/10.1074/jbc.R700009200

69. Pillai PS, Molony RD, Martinod K, Dong H, Pang IK, Tal MC, et al. Mx1 reveals innate pathways to antiviral resistance and lethal influenza disease. Science [Internet]. 2016 Apr 22;352(6284):463–6. Available from: http://www.ncbi.nlm.nih.gov/pubmed/27102485

70. Crotta S, Davidson S, Mahlakoiv T, Desmet CJ, Buckwalter MR, Albert ML, et al. Type I and Type III Interferons Drive Redundant Amplification Loops to Induce a Transcriptional Signature in Influenza-Infected Airway Epithelia. Kawaoka Y, editor. PLoS Pathog [Internet]. 2013 Nov 21;9(11):e1003773. Available from: https://dx.plos.org/10.1371/journal.ppat.1003773

71. Kuriakose T, Kanneganti T-D. Regulation and functions of NLRP3 inflammasome during influenza virus infection. Mol Immunol [Internet]. 2017;86(10):56–64. Available from: http://www.ncbi.nlm.nih.gov/pubmed/28169000

72. Allen IC, Scull MA, Moore CB, Holl EK, McElvania-TeKippe E, Taxman DJ, et al. The NLRP3 Inflammasome Mediates In Vivo Innate Immunity to Influenza A Virus through Recognition of Viral RNA. Immunity [Internet]. 2009 Apr;30(4):556–65. Available from: https://linkinghub.elsevier.com/retrieve/pii/S1074761309001393

73. O'Neill LAJ, Bowie AG. The family of five: TIR-domain-containing adaptors in Toll-like receptor signalling. Nat Rev Immunol [Internet]. 2007 May;7(5):353–64. Available from: https://www.nature.com/articles/nri2079

74. Koff JL, Shao MXG, Ueki IF, Nadel JA. Multiple TLRs activate EGFR via a signaling cascade to produce innate immune responses in airway epithelium. Am J Physiol Cell Mol Physiol [Internet]. 2008 Jun;294(6):L1068–75. Available from: https://www.physiology.org/doi/10.1152/ajplung.00025.2008

75. Jung HE, Lee HK. Host Protective Immune Responses against Influenza A Virus Infection. Viruses [Internet]. 2020 May 3;12(5):504. Available from: https://www.mdpi.com/1999-4915/12/5/504

76. Yang M, Wang C, Yang S, Leu C, Chen S. IL-6 ameliorates acute lung injury in influenza virus infection. Nat Publ Gr [Internet]. 2017;(September 2016):1–11. Available from: http://dx.doi.org/10.1038/srep43829

77. Pharo EA, Williams SM, Boyd V, Sundaramoorthy V, Durr PA, Baker ML. Host-Pathogen Responses to Pandemic Influenza H1N1pdm09 in a Human Respiratory Airway Model. Viruses [Internet]. 2020 Jun 24;12(6):5–7. Available from: http://www.ncbi.nlm.nih.gov/pubmed/32599823

78. Yuan J, Liu Z, Lim T, Zhang H, He J, Walker E, et al. CXCL10 Inhibits Viral Replication Through Recruitment of Natural Killer Cells in Coxsackievirus B3-Induced Myocarditis. Circ Res [Internet]. 2009 Mar 13;104(5):628–38. Available from:

https://www.ahajournals.org/doi/10.1161/CIRCRESAHA.108.192179

79. Rampart M, Van Damme J, Zonnekeyn L, Herman AG. Granulocyte chemotactic protein/interleukin-8 induces plasma leakage and neutrophil accumulation in rabbit skin. Am J Pathol [Internet]. 1989 Jul;135(1):21–5. Available from: http://www.ncbi.nlm.nih.gov/pubmed/2672824

80. Deshmane SL, Kremlev S, Amini S, Sawaya BE. Monocyte Chemoattractant Protein-1 (MCP-1): An Overview. J Interf Cytokine Res [Internet]. 2009 Jun;29(6):313–26. Available from: http://www.liebertpub.com/doi/10.1089/jir.2008.0027

81. Belisle SE, Tisoncik JR, Korth MJ, Carter VS, Proll SC, Swayne DE, et al. Genomic Profiling of Tumor Necrosis Factor Alpha (TNF-α) Receptor and Interleukin-1 Receptor Knockout Mice Reveals a Link between TNF-α Signaling and Increased Severity of 1918 Pandemic Influenza Virus Infection. J Virol [Internet]. 2010 Dec 15;84(24):12576–88. Available from: https://journals.asm.org/doi/10.1128/JVI.01310-10

82. DeBerge MP, Ely KH, Enelow RI. Soluble, but Not Transmembrane, TNF-α Is Required during Influenza Infection To Limit the Magnitude of Immune Responses and the Extent of Immunopathology. J Immunol [Internet]. 2014 Jun 15;192(12):5839–51. Available from: https://journals.aai.org/jimmunol/article/192/12/5839/92563/Soluble-but-Not-Transmembrane-TNF-Is-Required

83. Farag NS, Breitinger U, Breitinger HG, El Azizi MA. Viroporins and inflammasomes: A key to understand virus-induced inflammation. Int J Biochem Cell Biol [Internet]. 2020 Mar 22;122(3):105738. Available from: https://www.mdpi.com/1999-4915/13/3/522

84. Xiao H, Killip MJ, Staeheli P, Randall RE, Jackson D. The Human Interferon-Induced MxA Protein Inhibits Early Stages of Influenza A Virus Infection by Retaining the Incoming Viral Genome in the Cytoplasm. J Virol [Internet]. 2013 Dec;87(23):13053–8. Available from: https://journals.asm.org/doi/10.1128/JVI.02220-13

85. Farag NS, Breitinger U, Breitinger HG, El Azizi MA. Viroporins and inflammasomes: A key to understand virus-induced inflammation. Int J Biochem Cell Biol [Internet]. 2020;122(January):105738. Available from: http://www.ncbi.nlm.nih.gov/pubmed/32156572

86. Feehan J, Tripodi N, Apostolopoulos V. The twilight of the immune system: The impact of immunosenescence in aging. Maturitas [Internet]. 2021;147(January):7–13. Available from: https://doi.org/10.1016/j.maturitas.2021.02.006

87. Shao W, Li X, Goraya M, Wang S, Chen J-L. Evolution of Influenza A Virus by Mutation and Re-Assortment. Int J Mol Sci [Internet]. 2017 Aug 7;18(8):1650. Available from: http://www.mdpi.com/1422-0067/18/8/1650

88. van de Sandt CE, Kreijtz JHCM, Rimmelzwaan GF. Evasion of Influenza A Viruses from Innate and Adaptive Immune Responses. Viruses [Internet]. 2012 Sep 3;4(9):1438–76. Available from: http://www.mdpi.com/1999-4915/4/9/1438

89. Hsu AC-Y. Influenza Virus: A Master Tactician in Innate Immune Evasion and Novel Therapeutic Interventions. Front Immunol [Internet]. 2018 Apr 12;9(APR):1–11. Available from: http://journal.frontiersin.org/article/10.3389/fimmu.2018.00743/full

90. Hussain M, Galvin H, Haw TY, Nutsford A, Husain M. Drug resistance in influenza A virus: the epidemiology and management. Infect Drug Resist [Internet]. 2017 Apr;Volume 10:121–34. Available from: https://www.dovepress.com/drug-resistance-in-influenza-a-virus-the-epidemiology-and-management-peer-reviewed-article-IDR

91. Tavares LP, Teixeira MM, Garcia CC. The inflammatory response triggered by Influenza virus: a two edged sword. Inflamm Res [Internet]. 2017 Apr 15;66(4):283–302. Available from: http://link.springer.com/10.1007/s00011-016-0996-0

92. Théry C, Witwer KW, Aikawa E, Alcaraz MJ, Anderson JD, Andriantsitohaina R, et al. Minimal information for studies of extracellular vesicles 2018 (MISEV2018): a position statement of the International Society for Extracellular Vesicles and update of the MISEV2014 guidelines. J Extracell Vesicles [Internet]. 2018 Dec 1;7(1):1535750. Available from: https://www.tandfonline.com/doi/full/10.1080/20013078.2018.1535750

93. Johnstone RM, Adam M, Hammond JR, Orr L, Turbide C. Vesicle formation during reticulocyte maturation. Association of plasma membrane activities with released vesicles (exosomes). J Biol Chem [Internet]. 1987 Jul 5;262(19):9412–20. Available from: http://www.ncbi.nlm.nih.gov/pubmed/3597417

94. Kowal J, Tkach M, Théry C. Biogenesis and secretion of exosomes. Curr Opin Cell Biol [Internet]. 2014 Aug;29(1):116–25. Available from: https://linkinghub.elsevier.com/retrieve/pii/S095506741400057X

95. Akers JC, Gonda D, Kim R, Carter BS, Chen CC. Biogenesis of extracellular vesicles (EV): exosomes, microvesicles, retrovirus-like vesicles, and apoptotic bodies. J Neurooncol [Internet]. 2013 May 2;113(1):1–11. Available from: http://link.springer.com/10.1007/s11060-013-1084-8

96. Gandham S, Su X, Wood J, Nocera AL, Alli SC, Milane L, et al. Technologies and Standardization in Research on Extracellular Vesicles. Trends Biotechnol [Internet]. 2020 Oct;38(10):1066–98. Available from: https://linkinghub.elsevier.com/retrieve/pii/S0167779920301633

97. Liangsupree T, Multia E, Riekkola ML. Modern isolation and separation techniques for extracellular vesicles. J Chromatogr A [Internet]. 2021;1636:461773. Available from: https://doi.org/10.1016/j.chroma.2020.461773

98. Zhang H, Freitas D, Kim HS, Fabijanic K, Li Z, Chen H, et al. Identification of distinct nanoparticles and subsets of extracellular vesicles by asymmetric flow field-flow fractionation. Nat Cell Biol [Internet]. 2018 Mar 19;20(3):332–43. Available from: http://dx.doi.org/10.1038/s41556-018-0040-4

99. Simons M, Raposo G. Exosomes – vesicular carriers for intercellular communication. Curr Opin Cell Biol [Internet]. 2009 Aug;21(4):575–81. Available from: https://linkinghub.elsevier.com/retrieve/pii/S0955067409000775

100. Raposo G, Stoorvogel W. Extracellular vesicles: Exosomes, microvesicles, and friends. J Cell Biol [Internet]. 2013 Feb 18;200(4):373–83. Available from: https://rupress.org/jcb/article/200/4/373/37234/Extracellular-vesicles-Exosomes-microvesicles-and

101. Trappe A, Donnelly SC, McNally P, Coppinger JA. Role of extracellular vesicles in chronic lung disease. Thorax [Internet]. 2021 Oct;76(10):1047–56. Available from: https://thorax.bmj.com/lookup/doi/10.1136/thoraxjnl-2020-216370

102. Admyre C, Grunewald J, Thyberg J, Gripenbäck S, Tornling G, Eklund A, et al. Exosomes with major histocompatibility complex class II and co-stimulatory molecules are present in human BAL fluid. Eur Respir J [Internet]. 2003 Oct;22(4):578–83. Available from: http://erj.ersjournals.com/lookup/doi/10.1183/09031936.03.00041703

103. Caby M-P, Lankar D, Vincendeau-Scherrer C, Raposo G, Bonnerot C. Exosomal-like vesicles are present in human blood plasma. Int Immunol [Internet]. 2005 Jul 1;17(7):879–87. Available from: http://academic.oup.com/intimm/article/17/7/879/675097/Exosomallike-vesicles-are-present-in-human-blood

104. Aiello A, Giannessi F, Percario ZA, Affabris E. An emerging interplay between extracellular vesicles and cytokines. Cytokine Growth Factor Rev [Internet]. 2020 Feb;51:49–60. Available from: https://linkinghub.elsevier.com/retrieve/pii/S1359610119301534

105. O'Brien J, Hayder H, Zayed Y, Peng C. Overview of MicroRNA Biogenesis, Mechanisms of Actions, and Circulation. Front Endocrinol (Lausanne) [Internet]. 2018 Aug 3;9(AUG):1–12. Available from: https://www.frontiersin.org/article/10.3389/fendo.2018.00402/full

106. Denli AM, Tops BBJ, Plasterk RHA, Ketting RF, Hannon GJ. Processing of primary microRNAs by the Microprocessor complex. Nature [Internet]. 2004 Nov 11;432(7014):231–5. Available from: http://www.ncbi.nlm.nih.gov/pubmed/15531879

107. Hwang H-W, Mendell JT. MicroRNAs in cell proliferation, cell death, and tumorigenesis. Br J Cancer [Internet]. 2006 Mar 21;94(6):776–80. Available from: http://www.nature.com/articles/6603023

108. Yao S. MicroRNA biogenesis and their functions in regulating stem cell potency and differentiation. Biol Proced Online [Internet]. 2016;18(1):1–10. Available from: http://dx.doi.org/10.1186/s12575-016-0037-y

109. Chandan K, Gupta M, Sarwat M. Role of Host and Pathogen-Derived MicroRNAs in Immune Regulation During Infectious and Inflammatory Diseases. Front Immunol [Internet]. 2020 Jan 24;10(January):1–14. Available from: https://www.frontiersin.org/article/10.3389/fimmu.2019.03081/full

110. Friedman RC, Farh KK-H, Burge CB, Bartel DP. Most mammalian mRNAs are conserved targets of microRNAs. Genome Res [Internet]. 2009 Jan;19(1):92–105. Available from: http://genome.cshlp.org/lookup/doi/10.1101/gr.082701.108

111. Cypryk W, Lorey M, Puustinen A, Nyman TA, Matikainen S. Proteomic and Bioinformatic Characterization of Extracellular Vesicles Released from Human Macrophages upon Influenza A Virus Infection. J Proteome Res [Internet]. 2017 Jan 6;16(1):217–27. Available from: https://pubs.acs.org/doi/10.1021/acs.jproteome.6b00596

112. Fujita Y, Araya J, Ito S, Kobayashi K, Kosaka N, Yoshioka Y, et al. Suppression of autophagy by extracellular vesicles promotes myofibroblast differentiation in COPD pathogenesis. J Extracell Vesicles [Internet]. 2015 Jan 1;4(1):28388. Available from: https://www.tandfonline.com/doi/full/10.3402/jev.v4.28388

113. Benedikter BJ, Wouters EFM, Savelkoul PHM, Rohde GGU, Stassen FRM. Extracellular vesicles released in response to respiratory exposures: implications for chronic disease. J Toxicol Environ Heal - Part B Crit Rev [Internet]. 2018;21(3):142–60. Available from: https://doi.org/10.1080/10937404.2018.1466380

114. Groot M, Lee H. Sorting Mechanisms for MicroRNAs into Extracellular Vesicles and Their Associated Diseases. Cells [Internet]. 2020 Apr 22;9(4):1–16. Available from: http://www.ncbi.nlm.nih.gov/pubmed/32331346

115. Koppers-Lalic D, Hackenberg M, Bijnsdorp I V., van Eijndhoven MAJ, Sadek P, Sie D, et al. Nontemplated Nucleotide Additions Distinguish the Small RNA Composition in Cells from Exosomes. Cell Rep [Internet]. 2014 Sep;8(6):1649–58. Available from: https://linkinghub.elsevier.com/retrieve/pii/S2211124714007037

116. Villarroya-Beltri C, Gutiérrez-Vázquez C, Sánchez-Cabo F, Pérez-Hernández D, Vázquez J, Martin-Cofreces N, et al. Sumoylated hnRNPA2B1 controls the sorting of miRNAs into exosomes through binding to specific motifs. Nat Commun [Internet]. 2013 Dec 20;4(1):2980. Available from: http://www.nature.com/articles/ncomms3980

117. Gibbings DJ, Ciaudo C, Erhardt M, Voinnet O. Multivesicular bodies associate with components of miRNA effector complexes and modulate miRNA activity. Nat Cell Biol [Internet]. 2009 Sep 16;11(9):1143–9. Available from: http://www.nature.com/articles/ncb1929

118. Guiot J, Struman I, Louis E, Louis R, Malaise M, Njock M-S. Exosomal miRNAs in Lung Diseases: From Biologic Function to Therapeutic Targets. J Clin Med [Internet]. 2019 Aug 29;8(9):1–17. Available from: http://www.ncbi.nlm.nih.gov/pubmed/31470655

119. Valadi H, Ekström K, Bossios A, Sjöstrand M, Lee JJ, Lötvall JO. Exosome-mediated transfer of mRNAs and microRNAs is a novel mechanism of genetic exchange between cells. Nat Cell Biol [Internet]. 2007 Jun 7;9(6):654–9. Available from: http://www.nature.com/articles/ncb1596

120. Zhang D, Lee H, Wang X, Groot M, Sharma L, Dela Cruz CS, et al. A potential role of microvesicle-containing miR-223/142 in lung inflammation. Thorax [Internet]. 2019 Sep;74(9):865–74. Available from: https://thorax.bmj.com/lookup/doi/10.1136/thoraxjnl-2018-212994

121. Song L, Liu H, Gao S, Jiang W, Huang W. Cellular MicroRNAs Inhibit Replication of the H1N1 Influenza A Virus in Infected Cells. J Virol [Internet]. 2010 Sep;84(17):8849–60. Available from: https://journals.asm.org/doi/10.1128/JVI.00456-10

122. Khongnomnan K, Makkoch J, Poomipak W, Poovorawan Y, Payungporn S. Human miR-3145 inhibits influenza A viruses replication by targeting and silencing viral PB1 gene. Exp Biol Med [Internet]. 2015 Dec 15;240(12):1630–9. Available from:

http://journals.sagepub.com/doi/10.1177/1535370215589051

123. Wang R, Zhang Y-Y, Lu J-S, Xia B-H, Yang Z-X, Zhu X-D, et al. The highly pathogenic H5N1 influenza A virus down-regulated several cellular MicroRNAs which target viral genome. J Cell Mol Med [Internet]. 2017 Nov;21(11):3076–86. Available from: https://onlinelibrary.wiley.com/doi/10.1111/jcmm.13219

124. Dong C, Sun X, Guan Z, Zhang M, Duan M. Modulation of influenza A virus replication by microRNA-9 through targeting MCPIP1. J Med Virol [Internet]. 2017;89(1):41–8. Available from: http://www.ncbi.nlm.nih.gov/pubmed/27322373

125. Terrier O, Textoris J, Carron C, Marcel V, Bourdon J-C, Rosa-Calatrava M. Host microRNA molecular signatures associated with human H1N1 and H3N2 influenza A viruses reveal an unanticipated antiviral activity for miR-146a. J Gen Virol [Internet]. 2013 May 1;94(5):985–95. Available from: https://www.microbiologyresearch.org/content/journal/jgv/10.1099/vir.0.049528-0

126. Rosenberger CM, Podyminogin RL, Diercks AH, Treuting PM, Peschon JJ, Rodriguez D, et al. miR-144 attenuates the host response to influenza virus by targeting the TRAF6-IRF7 signaling axis. Lopez CB, editor. PLOS Pathog [Internet]. 2017 Apr 5;13(4):e1006305. Available from: https://dx.plos.org/10.1371/journal.ppat.1006305

127. Buggele WA, Johnson KE, Horvath CM. Influenza A Virus Infection of Human Respiratory Cells Induces Primary MicroRNA Expression. J Biol Chem [Internet]. 2012 Sep;287(37):31027–40. Available from: https://linkinghub.elsevier.com/retrieve/pii/S0021925820630496

128. Gui S, Chen X, Zhang M, Zhao F, Wan Y, Wang L, et al. Mir-302c mediates influenza A virus-induced IFNβ expression by targeting NF-κB inducing kinase. FEBS Lett [Internet]. 2015 Dec 21;589(24PartB):4112–8. Available from: http://doi.wiley.com/10.1016/j.febslet.2015.11.011

129. Fang J, Hao Q, Liu L, Li Y, Wu J, Huo X, et al. Epigenetic Changes Mediated by MicroRNA miR29 Activate Cyclooxygenase 2 and Lambda-1 Interferon Production during Viral Infection. J Virol [Internet]. 2012 Jan 15;86(2):1010–20. Available from: https://journals.asm.org/doi/10.1128/JVI.06169-11

130. Zhang X, Dong C, Sun X, Li Z, Zhang M, Guan Z, et al. Induction of the cellular miR-29c by influenza virus inhibits the innate immune response through protection of A20 mRNA. Biochem Biophys Res Commun [Internet]. 2014;450(1):755–61. Available from:

http://dx.doi.org/10.1016/j.bbrc.2014.06.059

131. Guan Z, Shi N, Song Y, Zhang X, Zhang M, Duan M. Induction of the cellular microRNA-29c by influenza virus contributes to virus-mediated apoptosis through repression of antiapoptotic factors BCL2L2. Biochem Biophys Res Commun [Internet]. 2012;425(3):662–7. Available from: http://dx.doi.org/10.1016/j.bbrc.2012.07.114

132. Buggele WA, Krause KE, Horvath CM. Small RNA Profiling of Influenza A Virus-Infected Cells Identifies miR-449b as a Regulator of Histone Deacetylase 1 and Interferon Beta. Pekosz A, editor. PLoS One [Internet]. 2013 Sep 26;8(9):e76560. Available from: https://dx.plos.org/10.1371/journal.pone.0076560

133. Xia B, Lu J, Wang R, Yang Z, Zhou X, Huang P. miR-21-3p Regulates Influenza A Virus Replication by Targeting Histone Deacetylase-8. Front Cell Infect Microbiol [Internet]. 2018 May 25;8(MAY):1–12. Available from: https://www.frontiersin.org/article/10.3389/fcimb.2018.00175/full

134. Gao S, Li J, Song L, Wu J, Huang W. Influenza A virus-induced downregulation of miR-26a contributes to reduced IFNα/β production. Virol Sin [Internet]. 2017 Aug 30;32(4):261–70. Available from: http://link.springer.com/10.1007/s12250-017-4004-9

135. Fan N, Wang J. MicroRNA 34a contributes to virus-mediated apoptosis through binding to its target gene Bax in influenza A virus infection. Biomed Pharmacother [Internet]. 2016 Oct;83:1464–70. Available from: http://dx.doi.org/10.1016/j.biopha.2016.08.049

136. Othumpangat S, Noti JD, Beezhold DH. Lung epithelial cells resist influenza A infection by inducing the expression of cytochrome c oxidase VIc which is modulated by miRNA 4276. Virology [Internet]. 2014 Nov;468–470(1):256–64. Available from: http://www.ncbi.nlm.nih.gov/pubmed/25203353

137. Othumpangat S, Noti JD, Blachere FM, Beezhold DH. Expression of non-structural-1A binding protein in lung epithelial cells is modulated by miRNA-548an on exposure to influenza A virus. Virology [Internet]. 2013 Dec;447(1–2):84–94. Available from: http://www.ncbi.nlm.nih.gov/pubmed/24210102

138. Hu Y, Jiang L, Lai W, Qin Y, Zhang T, Wang S, et al. MicroRNA-33a disturbs influenza A virus replication by targeting ARCN1 and inhibiting viral ribonucleoprotein activity. J Gen Virol [Internet]. 2016 Jan 1;97(1):27–38. Available from: https://www.microbiologyresearch.org/content/journal/jgv/10.1099/jgv.0.000311

139. Chen X, Zhou L, Peng N, Yu H, Li M, Cao Z, et al. MicroRNA-302a suppresses influenza A virus-stimulated interferon regulatory factor-5 expression and cytokine storm induction. J Biol Chem [Internet]. 2017;292(52):21291–303. Available from: http://dx.doi.org/10.1074/jbc.M117.805937

140. Rosenberger CM, Podyminogin RL, Navarro G, Zhao G-W, Askovich PS, Weiss MJ, et al. miR-451 Regulates Dendritic Cell Cytokine Responses to Influenza Infection. J Immunol [Internet]. 2012 Dec 15;189(12):5965–75. Available from: https://journals.aai.org/jimmunol/article/189/12/5965/86029/miR-451-Regulates-Dendritic-Cell-Cytokine

141. Zhang N, Ma Y, Tian Y, Zhou Y, Tang Y, Hu S. Downregulation of microRNA-221 facilitates H1N1 influenza A virus replication through suppression of type-IFN response by targeting the SOCS1/NF-κB pathway. Mol Med Rep [Internet]. 2021 May 6;24(1):497. Available from: http://www.spandidos-publications.com/10.3892/mmr.2021.12136

142. Lin X, Yu S, Ren P, Sun X, Jin M. Human microRNA-30 inhibits influenza virus infection by suppressing the expression of SOCS1, SOCS3, and NEDD4. Cell Microbiol [Internet]. 2020 May 26;22(5):1–15. Available from: https://onlinelibrary.wiley.com/doi/10.1111/cmi.13150

143. Bamunuarachchi G, Yang X, Huang C, Liang Y, Guo Y, Liu L. <scp>MicroRNA</scp> -206 inhibits influenza A virus replication by targeting tankyrase 2. Cell Microbiol [Internet]. 2021 Feb 4;23(2). Available from: https://onlinelibrary.wiley.com/doi/10.1111/cmi.13281

144. Yang X, Zhao C, Bamunuarachchi G, Wang Y, Liang Y, Huang C, et al. miR-193b represses influenza A virus infection by inhibiting Wnt/β-catenin signalling. Cell Microbiol [Internet]. 2019 May 25;21(5):e13001. Available from: https://onlinelibrary.wiley.com/doi/10.1111/cmi.13001

145. Huang SY, Huang CH, Chen CJ, Chen TW, Lin CY, Lin Y Te, et al. Novel Role for miR-1290 in Host Species Specificity of Influenza A Virus. Mol Ther - Nucleic Acids [Internet]. 2019;17(September):10–23. Available from: https://doi.org/10.1016/j.omtn.2019.04.028

146. Zhang F, Lin X, Yang X, Lu G, Zhang Q, Zhang C. MicroRNA-132-3p suppresses type I IFN response through targeting IRF1 to facilitate H1N1 influenza A virus infection. Biosci Rep [Internet]. 2019 Dec 20;39(12):1–11. Available from: http://www.ncbi.nlm.nih.gov/pubmed/31746331

147. Guo M, Li F, Ji J, Liu Y, Liu F, Zhao Y, et al. Inhibition of miR-93 promotes interferon effector

signaling to suppress influenza A infection by upregulating JAK1. Int Immunopharmacol [Internet]. 2020;86(May):106754. Available from: https://doi.org/10.1016/j.intimp.2020.106754

148. Wu W, Wang C, Xia C, Liu S, Mei Q. MicroRNA let-7 Suppresses Influenza A Virus Infection by Targeting RPS16 and Enhancing Type I Interferon Response. Front Cell Infect Microbiol [Internet]. 2022 Jul 7;12(July):1–15. Available from: https://www.frontiersin.org/articles/10.3389/fcimb.2022.904775/full

149. Zheng B, Zhou J, Wang H. Host microRNAs and exosomes that modulate influenza virus infection. Virus Res [Internet]. 2020;279(January):197885. Available from: https://doi.org/10.1016/j.virusres.2020.197885

150. García-Valero J, Olloquequi J, Montes JF, Rodríguez E, Martín-Satué M, Texidó L, et al. Deficient pulmonary IFN-β expression in COPD patients. Singanayagam A, editor. PLoS One [Internet]. 2019 Jun 6;14(6):e0217803. Available from: https://dx.plos.org/10.1371/journal.pone.0217803

151. Hsu ACY, Dua K, Starkey MR, Haw T-J, Nair PM, Nichol K, et al. MicroRNA-125a and -b inhibit A20 and MAVS to promote inflammation and impair antiviral response in COPD. JCI Insight [Internet]. 2017 Apr 6;2(7):e90443. Available from: https://insight.jci.org/articles/view/90443

152. Tu Y-H, Guo Y, Ji S, Shen J-L, Fei G-H. The Influenza A Virus H3N2 Triggers the Hypersusceptibility of Airway Inflammatory Response via Activating the lncRNA TUG1/miR-145-5p/NF-κB Pathway in COPD. Front Pharmacol [Internet]. 2021 Feb 22;12(February):1–10. Available from: https://www.frontiersin.org/articles/10.3389/fphar.2021.604590/full

153. Pua HH, Happ HC, Gray CJ, Mar DJ, Chiou N-T, Hesse LE, et al. Increased Hematopoietic Extracellular RNAs and Vesicles in the Lung during Allergic Airway Responses. Cell Rep [Internet]. 2019 Jan;26(4):933-944.e4. Available from: https://linkinghub.elsevier.com/retrieve/pii/S2211124719300026

154. Parker D, Prince A. Innate immunity in the respiratory epithelium. Am J Respir Cell Mol Biol [Internet]. 2011 Aug;45(2):189–201. Available from: http://www.ncbi.nlm.nih.gov/pubmed/21330463

155. Eltom S, Dale N, Raemdonck KRG, Stevenson CS, Snelgrove RJ, Sacitharan PK, et al. Respiratory Infections Cause the Release of Extracellular Vesicles: Implications in Exacerbation of Asthma/COPD. Chan RW, editor. PLoS One [Internet]. 2014 Jun

27;9(6):e101087. Available from: https://dx.plos.org/10.1371/journal.pone.0101087

156. Soni S, Wilson MR, O'Dea KP, Yoshida M, Katbeh U, Woods SJ, et al. Alveolar macrophage-derived microvesicles mediate acute lung injury. Thorax [Internet]. 2016 Nov;71(11):1020–9. Available from: https://thorax.bmj.com/lookup/doi/10.1136/thoraxjnl-2015-208032

157. Mills JT, Schwenzer A, Marsh EK, Edwards MR, Sabroe I, Midwood KS, et al. Airway Epithelial Cells Generate Pro-inflammatory Tenascin-C and Small Extracellular Vesicles in Response to TLR3 Stimuli and Rhinovirus Infection. Front Immunol [Internet]. 2019 Aug 21;10(August):1–12. Available from: https://www.frontiersin.org/article/10.3389/fimmu.2019.01987/full

158. Sun L, Wang X, Zhou Y, Zhou R, Ho W, Li J. Exosomes contribute to the transmission of anti-HIV activity from TLR3-activated brain microvascular endothelial cells to macrophages. Antiviral Res [Internet]. 2016 Oct;134:167–71. Available from: https://linkinghub.elsevier.com/retrieve/pii/S0166354216301383

159. Kesimer M, Scull M, Brighton B, DeMaria G, Burns K, O'Neal W, et al. Characterization of exosome-like vesicles released from human tracheobronchial ciliated epithelium: a possible role in innate defense. FASEB J [Internet]. 2009 Jun 3;23(6):1858–68. Available from: https://onlinelibrary.wiley.com/doi/10.1096/fj.08-119131

160. Cocozza F, Névo N, Piovesana E, Lahaye X, Buchrieser J, Schwartz O, et al. Extracellular vesicles containing ACE2 efficiently prevent infection by SARS-CoV-2 Spike protein-containing virus. J Extracell Vesicles [Internet]. 2020 Dec 28;10(2). Available from: https://onlinelibrary.wiley.com/doi/10.1002/jev2.12050

161. Chahar HS, Corsello T, Kudlicki AS, Komaravelli N, Casola A. Respiratory Syncytial Virus Infection Changes Cargo Composition of Exosome Released from Airway Epithelial Cells. Sci Rep [Internet]. 2018 Jan 10;8(1):387. Available from: https://www.nature.com/articles/s41598-017-18672-5

162. Liu Y-M, Tseng C-H, Chen Y-C, Yu W-Y, Ho M-Y, Ho C-Y, et al. Exosome-delivered and Y RNA-derived small RNA suppresses influenza virus replication. J Biomed Sci [Internet]. 2019 Dec 15;26(1):58. Available from: https://jbiomedsci.biomedcentral.com/articles/10.1186/s12929-019-0553-6

163. Maemura T, Fukuyama S, Kawaoka Y. High Levels of miR-483-3p Are Present in Serum Exosomes Upon Infection of Mice With Highly Pathogenic Avian Influenza Virus. Front Microbiol [Internet]. 2020 Feb 11;11(February):1–8. Available from:

https://www.frontiersin.org/article/10.3389/fmicb.2020.00144/full

164. Maemura T, Fukuyama S, Sugita Y, Lopes TJS, Nakao T, Noda T, et al. Lung-Derived Exosomal miR-483-3p Regulates the Innate Immune Response to Influenza Virus Infection. J Infect Dis [Internet]. 2018 Apr 11;217(9):1372–82. Available from: https://academic.oup.com/jid/article/217/9/1372/4823229

165. Testa JS, Apcher GS, Comber JD, Eisenlohr LC. Exosome-driven antigen transfer for MHC class II presentation facilitated by the receptor binding activity of influenza hemagglutinin. J Immunol [Internet]. 2010 Dec 1;185(11):6608–16. Available from: https://www.ncbi.nlm.nih.gov/pmc/articles/PMC3624763/pdf/nihms412728.pdf

166. Smith VL, Cheng Y, Bryant BR, Schorey JS. Exosomes function in antigen presentation during an in vivo Mycobacterium tuberculosis infection. Sci Rep [Internet]. 2017 Mar 6;7(1):43578. Available from: https://www.nature.com/articles/srep43578

167. Bhatnagar S, Schorey JS. Exosomes Released from Infected Macrophages Contain Mycobacterium avium Glycopeptidolipids and Are Proinflammatory. J Biol Chem [Internet]. 2007 Aug;282(35):25779–89. Available from: https://linkinghub.elsevier.com/retrieve/pii/S0021925820746533

168. Scheller N, Herold S, Kellner R, Bertrams W, Jung AL, Janga H, et al. Proviral MicroRNAs Detected in Extracellular Vesicles From Bronchoalveolar Lavage Fluid of Patients With Influenza Virus–Induced Acute Respiratory Distress Syndrome. J Infect Dis [Internet]. 2019 Jan 29;219(4):540–3. Available from: https://academic.oup.com/jid/article/219/4/540/5098403

169. Altan-Bonnet N. Extracellular vesicles are the Trojan horses of viral infection. Curr Opin Microbiol [Internet]. 2016 Aug;32:77–81. Available from: http://dx.doi.org/10.1016/j.mib.2016.05.004

170. Bruce EA, Stuart A, McCaffrey MW, Digard P. Role of the Rab11 pathway in negative-strand virus assembly. Biochem Soc Trans [Internet]. 2012 Dec 1;40(6):1409–15. Available from: https://portlandpress.com/biochemsoctrans/article/40/6/1409/66731/Role-of-the-Rab11-pathway-in-negative-strand-virus

171. Hutchinson EC, Charles PD, Hester SS, Thomas B, Trudgian D, Martínez-Alonso M, et al. Conserved and host-specific features of influenza virion architecture. Nat Commun [Internet]. 2014 Dec 17;5(1):4816. Available from: http://www.nature.com/articles/ncomms5816

172. Benedikter BJ, Bouwman FG, Vajen T, Heinzmann ACA, Grauls G, Mariman EC, et al. Ultrafiltration combined with size exclusion chromatography efficiently isolates extracellular vesicles from cell culture media for compositional and functional studies. Sci Rep [Internet]. 2017 Nov 10;7(1):15297. Available from: https://www.nature.com/articles/s41598-017-15717-7

173. Lee H, Zhang D, Zhu Z, Dela Cruz CS, Jin Y. Epithelial cell-derived microvesicles activate macrophages and promote inflammation via microvesicle-containing microRNAs. Sci Rep [Internet]. 2016;6:35250. Available from: http://dx.doi.org/10.1038/srep35250

174. Héliot A, Landkocz Y, Roy Saint-Georges F, Gosset P, Billet S, Shirali P, et al. Smoker extracellular vesicles influence status of human bronchial epithelial cells. Int J Hyg Environ Health [Internet]. 2017 Apr;220(2):445–54. Available from: https://linkinghub.elsevier.com/retrieve/pii/S1438463916302772

175. He S, Chen D, Hu M, Zhang L, Liu C, Traini D, et al. Bronchial epithelial cell extracellular vesicles ameliorate epithelial–mesenchymal transition in COPD pathogenesis by alleviating M2 macrophage polarization. Nanomedicine Nanotechnology, Biol Med [Internet]. 2019 Jun;18:259–71. Available from: https://linkinghub.elsevier.com/retrieve/pii/S1549963419300723

176. Burke H, Cellura D, Freeman A, Hicks A, Ostridge K, Watson A, et al. Pulmonary EV miRNA profiles identify disease and distinct inflammatory endotypes in COPD. Front Med [Internet]. 2022 Dec 15;9(December):1–13. Available from: https://www.frontiersin.org/articles/10.3389/fmed.2022.1039702/full

177. Neudecker V, Brodsky KS, Clambey ET, Schmidt EP, Packard TA, Davenport B, et al. Neutrophil transfer of miR-223 to lung epithelial cells dampens acute lung injury in mice. Sci Transl Med [Internet]. 2017 Sep 20;9(408). Available from: http://www.ncbi.nlm.nih.gov/pubmed/28931657

178. Ismail N, Wang Y, Dakhlallah D, Moldovan L, Agarwal K, Batte K, et al. Macrophage microvesicles induce macrophage differentiation and miR-223 transfer. Blood [Internet]. 2013 Feb 7;121(6):984–95. Available from: https://ashpublications.org/blood/article/121/6/984/31436/Macrophage-microvesicles-induce-macrophage

179. Chiou N-T, Kageyama R, Ansel KM. Selective Export into Extracellular Vesicles and Function of tRNA Fragments during T Cell Activation. Cell Rep [Internet]. 2018 Dec;25(12):3356-

3370.e4. Available from: https://linkinghub.elsevier.com/retrieve/pii/S0031938416312148

180. Tsukamoto H, Kouwaki T, Oshiumi H. Aging-Associated Extracellular Vesicles Contain Immune Regulatory microRNAs Alleviating Hyperinflammatory State and Immune Dysfunction in the Elderly. iScience [Internet]. 2020;23(9):101520. Available from: https://doi.org/10.1016/j.isci.2020.101520

181. Watson A, Spalluto CM, McCrae C, Cellura D, Burke H, Cunoosamy D, et al. Dynamics of IFN-β Responses during Respiratory Viral Infection. Insights for Therapeutic Strategies. Am J Respir Crit Care Med [Internet]. 2020 Jan 1;201(1):83–94. Available from: https://www.atsjournals.org/doi/10.1164/rccm.201901-0214OC

182. Reynolds S, Lunn K, Beegan R, Tear V, Monk PD. Antiviral biomarkers are upregulated in sputum cells following administration of inhaled interferon beta to COPD patients. In: Airway pharmacology and treatment [Internet]. European Respiratory Society; 2019. p. OA263. Available from: http://erj.ersjournals.com/lookup/doi/10.1183/13993003.congress-2019.OA263

183. Harris JR. Negative staining of thinly spread biological samples. Methods Mol Biol [Internet]. 2007;369(1):107–42. Available from: http://www.ncbi.nlm.nih.gov/pubmed/17656749

184. Robinson MD, Oshlack A. A scaling normalization method for differential expression analysis of RNA-seq data. Genome Biol [Internet]. 2010;11(3):R25. Available from: http://www.ncbi.nlm.nih.gov/pubmed/20196867

185. Robinson MD, McCarthy DJ, Smyth GK. edgeR: a Bioconductor package for differential expression analysis of digital gene expression data. Bioinformatics [Internet]. 2010 Jan 1;26(1):139–40. Available from: https://academic.oup.com/bioinformatics/article-lookup/doi/10.1093/bioinformatics/btp616

186. Andersen CL, Jensen JL, Ørntoft TF. Normalization of Real-Time Quantitative Reverse Transcription-PCR Data: A Model-Based Variance Estimation Approach to Identify Genes Suited for Normalization, Applied to Bladder and Colon Cancer Data Sets. Cancer Res [Internet]. 2004 Aug 1;64(15):5245–50. Available from: https://aacrjournals.org/cancerres/article/64/15/5245/511517/Normalization-of-Real-Time-Quantitative-Reverse

187. Walters MS, Gomi K, Ashbridge B, Moore MAS, Arbelaez V, Heldrich J, et al. Generation of a human airway epithelium derived basal cell line with multipotent differentiation

capacity. Respir Res [Internet]. 2013 Dec 3;14(1):135. Available from: https://respiratory-research.biomedcentral.com/articles/10.1186/1465-9921-14-135

188. Pezzulo AA, Starner TD, Scheetz TE, Traver GL, Tilley AE, Harvey B-G, et al. The air-liquid interface and use of primary cell cultures are important to recapitulate the transcriptional profile of in vivo airway epithelia. Am J Physiol Cell Mol Physiol [Internet]. 2011 Jan;300(1):L25–31. Available from: https://www.physiology.org/doi/10.1152/ajplung.00256.2010

189. Michi AN, Proud D. A toolbox for studying respiratory viral infections using air-liquid interface cultures of human airway epithelial cells. Am J Physiol Cell Mol Physiol [Internet]. 2021 Jul 1;321(1):L263–79. Available from: https://journals.physiology.org/doi/10.1152/ajplung.00141.2021

190. Martínez-Baz I, Casado I, Navascués A, Portillo ME, Guevara M, Ezpeleta C, et al. Chronic obstructive pulmonary disease and influenza vaccination effect in preventing outpatient and inpatient influenza cases. Sci Rep [Internet]. 2022;12(1):1–9. Available from: https://doi.org/10.1038/s41598-022-08952-0

191. Arroyo JD, Chevillet JR, Kroh EM, Ruf IK, Pritchard CC, Gibson DF, et al. Argonaute2 complexes carry a population of circulating microRNAs independent of vesicles in human plasma. Proc Natl Acad Sci [Internet]. 2011 Mar 22;108(12):5003–8. Available from: https://pnas.org/doi/full/10.1073/pnas.1019055108

192. Mori I, Komatsu T, Takeuchi K, Nakakuki K, Sudo M, Kimura Y. In vivo induction of apoptosis by influenza virus. J Gen Virol [Internet]. 1995 Nov 1;76(11):2869–73. Available from: https://www.microbiologyresearch.org/content/journal/jgv/10.1099/0022-1317-76-11-2869

193. Brennan K, Martin K, FitzGerald SP, O'Sullivan J, Wu Y, Blanco A, et al. A comparison of methods for the isolation and separation of extracellular vesicles from protein and lipid particles in human serum. Sci Rep [Internet]. 2020 Jan 23;10(1):1039. Available from: https://www.nature.com/articles/s41598-020-57497-7

194. Yao X, Gordon EM, Figueroa DM, Barochia A V., Levine SJ. Emerging Roles of Apolipoprotein E and Apolipoprotein A-I in the Pathogenesis and Treatment of Lung Disease. Am J Respir Cell Mol Biol [Internet]. 2016 Aug;55(2):159–69. Available from: https://www.atsjournals.org/doi/10.1165/rcmb.2016-0060TR

195. Uhlén M, Fagerberg L, Hallström BM, Lindskog C, Oksvold P, Mardinoglu A, et al. Tissue-

based map of the human proteome. Science (80-) [Internet]. 2015 Jan 23;347(6220). Available from: https://www.science.org/doi/10.1126/science.1260419

196. Bartel S, Deshane J, Wilkinson T, Gabrielsson S. Extracellular Vesicles as Mediators of Cellular Cross Talk in the Lung Microenvironment. Front Med. 2020;7(August):1–8.

197. Jantaratrirat S, Boonarkart C, Ruangrung K, Suptawiwat O, Auewarakul P. Microparticle Release from Cell Lines and Its Anti-Influenza Activity. Viral Immunol [Internet]. 2018 Jul;31(6):447–56. Available from: https://www.liebertpub.com/doi/10.1089/vim.2017.0201

198. Ax E, Jevnikar Z, Cvjetkovic A, Malmhäll C, Olsson H, Rådinger M, et al. T2 and T17 cytokines alter the cargo and function of airway epithelium-derived extracellular vesicles. Respir Res [Internet]. 2020 Dec 19;21(1):155. Available from: https://respiratory-research.biomedcentral.com/articles/10.1186/s12931-020-01402-3

199. Gutierrez MJ, Gomez JL, Perez GF, Pancham K, Val S, Pillai DK, et al. Airway Secretory microRNAome Changes during Rhinovirus Infection in Early Childhood. Larcombe A, editor. PLoS One [Internet]. 2016 Sep 19;11(9):e0162244. Available from: https://dx.plos.org/10.1371/journal.pone.0162244

200. Hiemstra PS, Grootaers G, van der Does AM, Krul CAM, Kooter IM. Human lung epithelial cell cultures for analysis of inhaled toxicants: Lessons learned and future directions. Toxicol Vitr [Internet]. 2018;47(September 2017):137–46. Available from: https://doi.org/10.1016/j.tiv.2017.11.005

201. Upadhyay S, Palmberg L. Air-Liquid Interface: Relevant In Vitro Models for Investigating Air Pollutant-Induced Pulmonary Toxicity. Toxicol Sci [Internet]. 2018 Jul 1;164(1):21–30. Available from: https://academic.oup.com/toxsci/article/164/1/21/4925479

202. Reddel RR, Ke Y, Gerwin BI, McMenamin MG, Lechner JF, Su RT, et al. Transformation of human bronchial epithelial cells by infection with SV40 or adenovirus-12 SV40 hybrid virus, or transfection via strontium phosphate coprecipitation with a plasmid containing SV40 early region genes. Cancer Res [Internet]. 1988 Apr 1;48(7):1904–9. Available from: http://www.ncbi.nlm.nih.gov/pubmed/2450641

203. Li M, Liao L, Tian W. Extracellular Vesicles Derived From Apoptotic Cells: An Essential Link Between Death and Regeneration. Front Cell Dev Biol [Internet]. 2020 Oct 2;8(October):1–12. Available from: https://www.frontiersin.org/article/10.3389/fcell.2020.573511/full

204. Atkin-Smith GK, Duan M, Chen W, Poon IKH. The induction and consequences of Influenza A virus-induced cell death. Cell Death Dis [Internet]. 2018;9(10). Available from: http://dx.doi.org/10.1038/s41419-018-1035-6

205. Ye C, Li H, Bao M, Zhuo R, Jiang G, Wang W. Alveolar macrophage - derived exosomes modulate severity and outcome of acute lung injury. Aging (Albany NY) [Internet]. 2020 Apr 7;12(7):6120–8. Available from: http://www.ncbi.nlm.nih.gov/pubmed/32259794

206. Lee N, Wong CK, Chan PKS, Chan MCW, Wong RYK, Lun SWM, et al. Cytokine Response Patterns in Severe Pandemic 2009 H1N1 and Seasonal Influenza among Hospitalized Adults. Zimmer J, editor. PLoS One [Internet]. 2011 Oct 13;6(10):e26050. Available from: https://dx.plos.org/10.1371/journal.pone.0026050

207. Bian J-R, Nie W, Zang Y-S, Fang Z, Xiu Q-Y, Xu X-X. Clinical aspects and cytokine response in adults with seasonal influenza infection. Int J Clin Exp Med [Internet]. 2014;7(12):5593–602. Available from: http://www.ncbi.nlm.nih.gov/pubmed/25664078

208. Hsu ACY, Parsons K, Barr I, Lowther S, Middleton D, Hansbro PM, et al. Critical Role of Constitutive Type I Interferon Response in Bronchial Epithelial Cell to Influenza Infection. Thiel V, editor. PLoS One [Internet]. 2012 Mar 2;7(3):e32947. Available from: https://dx.plos.org/10.1371/journal.pone.0032947

209. Hayney MS, Henriquez KM, Barnet JH, Ewers T, Champion HM, Flannery S, et al. Serum IFN-γ-induced protein 10 (IP-10) as a biomarker for severity of acute respiratory infection in healthy adults. J Clin Virol [Internet]. 2017;90(January):32–7. Available from: http://www.ncbi.nlm.nih.gov/pubmed/28334685

210. Spurrell JCL, Wiehler S, Zaheer RS, Sanders SP, Proud D. Human airway epithelial cells produce IP-10 (CXCL10) in vitro and in vivo upon rhinovirus infection. Am J Physiol Cell Mol Physiol [Internet]. 2005 Jul;289(1):L85–95. Available from: https://www.physiology.org/doi/10.1152/ajplung.00397.2004

211. Perng YC, Lenschow DJ. ISG15 in antiviral immunity and beyond. Nat Rev Microbiol [Internet]. 2018;16(7):423–39. Available from: http://dx.doi.org/10.1038/s41579-018-0020-5

212. Pothlichet J, Chignard M, Si-Tahar M. Cutting Edge: Innate Immune Response Triggered by Influenza A Virus Is Negatively Regulated by SOCS1 and SOCS3 through a RIG-I/IFNAR1-Dependent Pathway. J Immunol. 2008;180(4):2034–8.

213. Dienz O, Rud JG, Eaton SM, Lanthier PA, Burg E, Drew A, et al. Essential role of IL-6 in protection against H1N1 influenza virus by promoting neutrophil survival in the lung. Mucosal Immunol [Internet]. 2012 May;5(3):258–66. Available from: http://www.ncbi.nlm.nih.gov/pubmed/22294047

214. Paquette SG, Banner D, Zhao Z, Fang Y, Huang SSH, León AJ, et al. Interleukin-6 Is a Potential Biomarker for Severe Pandemic H1N1 Influenza A Infection. Poehlmann S, editor. PLoS One [Internet]. 2012 Jun 5;7(6):e38214. Available from: https://dx.plos.org/10.1371/journal.pone.0038214

215. Lee H, Abston E, Zhang D, Rai A, Jin Y. Extracellular Vesicle: An Emerging Mediator of Intercellular Crosstalk in Lung Inflammation and Injury. Front Immunol [Internet]. 2018 Apr 30;9(APR). Available from: http://journal.frontiersin.org/article/10.3389/fimmu.2018.00924/full

216. Dogrammatzis C, Saleh S, Deighan C, Kalamvoki M. Diverse Populations of Extracellular Vesicles with Opposite Functions during Herpes Simplex Virus 1 Infection. J Virol [Internet]. 2021 Feb 24;95(6). Available from: http://www.ncbi.nlm.nih.gov/pubmed/33361424

217. Kowal J, Arras G, Colombo M, Jouve M, Morath JP, Primdal-Bengtson B, et al. Proteomic comparison defines novel markers to characterize heterogeneous populations of extracellular vesicle subtypes. Proc Natl Acad Sci [Internet]. 2016 Feb 23;113(8):E968–77. Available from: https://pnas.org/doi/full/10.1073/pnas.1521230113

218. Kudryavtsev I, Kalinina O, Bezrukikh V, Melnik O, Golovkin A. The Significance of Phenotyping and Quantification of Plasma Extracellular Vesicles Levels Using High-Sensitivity Flow Cytometry during COVID-19 Treatment. Viruses [Internet]. 2021 Apr 27;13(5). Available from: http://www.ncbi.nlm.nih.gov/pubmed/33925492

219. Vickers KC, Palmisano BT, Shoucri BM, Shamburek RD, Remaley AT. MicroRNAs are transported in plasma and delivered to recipient cells by high-density lipoproteins. Nat Cell Biol [Internet]. 2011;13(4):423–35. Available from: http://dx.doi.org/10.1038/ncb2210

220. The Human Protein Atlas [Internet]. Available from: https://www.proteinatlas.org/

221. Jeppesen DK, Fenix AM, Franklin JL, Higginbotham JN, Zhang Q, Zimmerman LJ, et al. Reassessment of Exosome Composition. Cell [Internet]. 2019 Apr;177(2):428-445.e18. Available from: https://linkinghub.elsevier.com/retrieve/pii/S0092867419302120

222. Webber J, Clayton A. How pure are your vesicles? J Extracell Vesicles [Internet]. 2013 Jan

14;2(1):19861. Available from: https://www.tandfonline.com/doi/full/10.3402/jev.v2i0.19861

223. Nolte-'t Hoen ENM, Buermans HPJ, Waasdorp M, Stoorvogel W, Wauben MHM, 't Hoen PAC. Deep sequencing of RNA from immune cell-derived vesicles uncovers the selective incorporation of small non-coding RNA biotypes with potential regulatory functions. Nucleic Acids Res [Internet]. 2012 Oct;40(18):9272–85. Available from: https://academic.oup.com/nar/article-lookup/doi/10.1093/nar/gks658

224. Mei Y, Wang Y, Kumari P, Shetty AC, Clark D, Gable T, et al. A piRNA-like small RNA interacts with and modulates p-ERM proteins in human somatic cells. Nat Commun [Internet]. 2015 Nov 22;6(1):7316. Available from: http://www.nature.com/articles/ncomms8316

225. Wang C, Lin H. Roles of piRNAs in transposon and pseudogene regulation of germline mRNAs and lncRNAs. Genome Biol [Internet]. 2021 Dec 8;22(1):27. Available from: https://genomebiology.biomedcentral.com/articles/10.1186/s13059-020-02221-x

226. Kok MGM, de Ronde MWJ, Moerland PD, Ruijter JM, Creemers EE, Pinto-Sietsma SJ. Small sample sizes in high-throughput miRNA screens: A common pitfall for the identification of miRNA biomarkers. Biomol Detect Quantif [Internet]. 2018;15(December 2017):1–5. Available from: https://doi.org/10.1016/j.bdq.2017.11.002

227. Othumpangat S, Lindsley WG, Beezhold DH, Kashon ML, Burrell CN, Mubareka S, et al. Differential Expression of Serum Exosome microRNAs and Cytokines in Influenza A and B Patients Collected in the 2016 and 2017 Influenza Seasons. Pathogens [Internet]. 2021 Feb 2;10(2):149. Available from: https://www.mdpi.com/2076-0817/10/2/149

228. Chen J, Hu C, Pan P. Extracellular Vesicle MicroRNA Transfer in Lung Diseases. Front Physiol [Internet]. 2017 Dec 12;8(DEC). Available from: http://journal.frontiersin.org/article/10.3389/fphys.2017.01028/full

229. Schindler VEM, Alhamdan F, Preußer C, Hintz L, Alashkar Alhamwe B, Nist A, et al. Side-Directed Release of Differential Extracellular Vesicle-associated microRNA Profiles from Bronchial Epithelial Cells of Healthy and Asthmatic Subjects. Biomedicines [Internet]. 2022 Mar 7;10(3):622. Available from: https://www.mdpi.com/2227-9059/10/3/622

230. Chakrabortty SK, Prakash A, Nechooshtan G, Hearn S, Gingeras TR. Extracellular vesicle-mediated transfer of processed and functional RNY5 RNA. RNA [Internet]. 2015 Nov;21(11):1966–79. Available from:

http://rnajournal.cshlp.org/lookup/doi/10.1261/rna.053629.115

231. Driedonks TAP, van der Grein SG, Ariyurek Y, Buermans HPJ, Jekel H, Chow FWN, et al. Immune stimuli shape the small non-coding transcriptome of extracellular vesicles released by dendritic cells. Cell Mol Life Sci [Internet]. 2018;75(20):3857–75. Available from: https://doi.org/10.1007/s00018-018-2842-8

232. Ge Y, Liu K, Chi Y, Zhu X, Wu T, Zhao K, et al. Exosomal microRNA expression profiles derived from A549 human lung cells in response to influenza A/H1N1pdm09 infection. Virology [Internet]. 2022;574(July):9–17. Available from: https://doi.org/10.1016/j.virol.2022.07.009

233. Santangelo L, Bordoni V, Montaldo C, Cimini E, Zingoni A, Battistelli C, et al. Hepatitis C virus direct-acting antivirals therapy impacts on extracellular vesicles microRNAs content and on their immunomodulating properties. Liver Int [Internet]. 2018 Oct;38(10):1741–50. Available from: http://www.ncbi.nlm.nih.gov/pubmed/29359389

234. Jopling C. Liver-specific microRNA-122. RNA Biol [Internet]. 2012;9(2):1–6. Available from: http://www.ncbi.nlm.nih.gov/pmc/articles/PMC3346312/%0Ahttp://www.ncbi.nlm.nih.gov/pmc/articles/PMC3346312/pdf/rna-9-137.pdf

235. Woods PS, Doolittle LM, Rosas LE, Nana-Sinkam SP, Tili E, Davis IC. Increased expression of microRNA-155-5p by alveolar type II cells contributes to development of lethal ARDS in H1N1 influenza A virus-infected mice. Virology [Internet]. 2020;545(3):40–52. Available from: http://www.ncbi.nlm.nih.gov/pubmed/32308197

236. Gutierrez MJ, Perez G, Pancham K, Huseni S, Nino G. Exosomal Mir-155 Secretion during Rhinovirus Infection in EARLY Childhood. J Allergy Clin Immunol [Internet]. 2015;135(2):AB150. Available from: http://dx.doi.org/10.1016/j.jaci.2014.12.1428

237. De Smet EG, Van Eeckhoutte HP, Avila Cobos F, Blomme E, Verhamme FM, Provoost S, et al. The role of miR-155 in cigarette smoke-induced pulmonary inflammation and COPD. Mucosal Immunol [Internet]. 2020;13(3):423–36. Available from: http://dx.doi.org/10.1038/s41385-019-0241-6

238. Meng L, Xing Z, Guo Z, Qiu Y, Liu Z. Hypoxia-induced microRNA-155 overexpression in extracellular vesicles promotes renal cell carcinoma progression by targeting FOXO3. Aging (Albany NY) [Internet]. 2021 Apr 15;13(7):9613–26. Available from: https://www.aging-us.com/lookup/doi/10.18632/aging.202706

239. Hu J, Huang S, Liu X, Zhang Y, Wei S, Hu X. miR-155: An Important Role in Inflammation Response. J Immunol Res [Internet]. 2022;2022:7437281. Available from: http://www.ncbi.nlm.nih.gov/pubmed/35434143

240. Luo H, Liang H, Chen Y, Chen S, Xu Y, Xu L, et al. miR-7-5p overexpression suppresses cell proliferation and promotes apoptosis through inhibiting the ability of DNA damage repair of PARP-1 and BRCA1 in TK6 cells exposed to hydroquinone. Chem Biol Interact [Internet]. 2018;283(December 2017):84–90. Available from: https://doi.org/10.1016/j.cbi.2018.01.019

241. Yuan W, Liang X, Liu Y, Wang H. Mechanism of miR-378a-3p enriched in M2 macrophage-derived extracellular vesicles in cardiomyocyte pyroptosis after MI. Hypertens Res [Internet]. 2022 Apr 26;45(4):650–64. Available from: https://www.nature.com/articles/s41440-022-00851-1

242. Zhang F, Sun X, Zhu Y, Qin W. Downregulation of miR-146a inhibits influenza A virus replication by enhancing the type I interferon response in vitro and in vivo. Biomed Pharmacother [Internet]. 2019;111(December 2018):740–50. Available from: https://doi.org/10.1016/j.biopha.2018.12.103

243. Landgraf P, Rusu M, Sheridan R, Sewer A, Iovino N, Aravin A, et al. A Mammalian microRNA Expression Atlas Based on Small RNA Library Sequencing. Cell [Internet]. 2007 Jun;129(7):1401–14. Available from: https://linkinghub.elsevier.com/retrieve/pii/S0092867407006046

244. Polikepahad S, Knight JM, Naghavi AO, Oplt T, Creighton CJ, Shaw C, et al. Proinflammatory role for let-7 microRNAS in experimental asthma. J Biol Chem [Internet]. 2010 Sep 24;285(39):30139–49. Available from: http://www.ncbi.nlm.nih.gov/pubmed/20630862

245. Schwarzenbach H, da Silva AM, Calin G, Pantel K. Data Normalization Strategies for MicroRNA Quantification. Clin Chem [Internet]. 2015 Nov 1;61(11):1333–42. Available from: https://academic.oup.com/clinchem/article/61/11/1333/5611589

246. Sastre B, Cañas JA, Rodrigo-Muñoz JM, del Pozo V. Novel Modulators of Asthma and Allergy: Exosomes and MicroRNAs. Front Immunol [Internet]. 2017 Jul 21;8(JUL):1–14. Available from: http://journal.frontiersin.org/article/10.3389/fimmu.2017.00826/full

247. Adeloye D, Chua S, Lee C, Basquill C, Papana A, Theodoratou E, et al. Global and regional estimates of COPD prevalence: Systematic review and meta-analysis. J Glob Health [Internet]. 2015;5(2):020415. Available from:

http://www.ncbi.nlm.nih.gov/pubmed/26755942%0Ahttp://www.pubmedcentral.nih.gov/articlerender.fcgi?artid=PMC4693508

248. Zhou X, Li Q, Zhou X. Exacerbation of Chronic Obstructive Pulmonary Disease. Cell Biochem Biophys [Internet]. 2015 Nov 23;73(2):349–55. Available from: http://link.springer.com/10.1007/s12013-015-0605-9

249. Kwak HJ, Park DW, Kim JE, Park MK, Koo GW, Park TS, et al. Prevalence and Risk Factors of Respiratory Viral Infections in Exacerbations of Chronic Obstructive Pulmonary Disease. Tohoku J Exp Med [Internet]. 2016;240(2):131–9. Available from: https://www.jstage.jst.go.jp/article/tjem/240/2/240_131/_article

250. Yin T, Zhu Z, Mei Z, Feng J, Zhang W, He Y, et al. Analysis of viral infection and biomarkers in patients with acute exacerbation of chronic obstructive pulmonary disease. Clin Respir J [Internet]. 2018 Mar;12(3):1228–39. Available from: https://onlinelibrary.wiley.com/doi/10.1111/crj.12656

251. Li J, Wang J, Li Y, Zhao P, Tian Y, Liu X, et al. Effective-component compatibility of Bufei Yishen formula protects COPD rats against PM2.5-induced oxidative stress via miR-155/FOXO3a pathway. Ecotoxicol Environ Saf [Internet]. 2021 Nov 10;228:112918. Available from: http://www.ncbi.nlm.nih.gov/pubmed/34773846

252. Akbas F, Coskunpinar E, Aynacı E, Müsteri Oltulu Y, Yildiz P. ANALYSIS OF SERUM MICRO-RNAs AS POTENTIAL BIOMARKER IN CHRONIC OBSTRUCTIVE PULMONARY DISEASE. Exp Lung Res [Internet]. 2012 Jul 3;38(6):286–94. Available from: http://www.tandfonline.com/doi/full/10.3109/01902148.2012.689088

253. Chen B-B, Li Z-H, Gao S. Circulating miR-146a/b correlates with inflammatory cytokines in COPD and could predict the risk of acute exacerbation COPD. Medicine (Baltimore) [Internet]. 2018 Feb;97(7):e9820. Available from: http://www.ncbi.nlm.nih.gov/pubmed/29443743

254. Singh T, Newman AB. Inflammatory markers in population studies of aging. Ageing Res Rev [Internet]. 2011;10(3):319–29. Available from: http://dx.doi.org/10.1016/j.arr.2010.11.002

255. John-Schuster G, Günter S, Hager K, Conlon TM, Eickelberg O, Yildirim AÖ. Inflammaging increases susceptibility to cigarette smoke-induced COPD. Oncotarget [Internet]. 2016 May 24;7(21):30068–83. Available from: https://www.oncotarget.com/lookup/doi/10.18632/oncotarget.4027

256. Ferrucci L, Fabbri E. Inflammageing: chronic inflammation in ageing, cardiovascular disease, and frailty. Nat Rev Cardiol [Internet]. 2018;15(9):505–22. Available from: http://dx.doi.org/10.1038/s41569-018-0064-2

257. Wang Y, Zhu X, Jiang XM, Guo J, Fu Z, Zhou Z, et al. Decreased inhibition of exosomal miRNAs on SARS-CoV-2 replication underlies poor outcomes in elderly people and diabetic patients. Signal Transduct Target Ther [Internet]. 2021;6(1). Available from: http://dx.doi.org/10.1038/s41392-021-00716-y

258. Lee H, Li C, Zhang Y, Zhang D, Otterbein LE, Jin Y. Caveolin-1 selectively regulates microRNA sorting into microvesicles after noxious stimuli. J Exp Med [Internet]. 2019 Sep 2;216(9):2202–20. Available from: https://rupress.org/jem/article/216/9/2202/120717/Caveolin1-selectively-regulates-microRNA-sorting

259. Turchinovich A, Weiz L, Langheinz A, Burwinkel B. Characterization of extracellular circulating microRNA. Nucleic Acids Res [Internet]. 2011 Sep;39(16):7223–33. Available from: https://academic.oup.com/nar/article-lookup/doi/10.1093/nar/gkr254

260. Clément T, Salone V, Rederstorff M. Dual Luciferase Gene Reporter Assays to Study miRNA Function. In: Methods in Molecular Biology [Internet]. 2015. p. 187–98. Available from: https://link.springer.com/content/pdf/10.1007%2F978-1-4939-2547-6.pdf%0Ahttp://link.springer.com/10.1007/978-1-4939-2547-6

261. Su S-F, Chang Y-W, Andreu-Vieyra C, Fang JY, Yang Z, Han B, et al. miR-30d, miR-181a and miR-199a-5p cooperatively suppress the endoplasmic reticulum chaperone and signaling regulator GRP78 in cancer. Oncogene [Internet]. 2013 Sep 26;32(39):4694–701. Available from: http://www.ncbi.nlm.nih.gov/pubmed/23085757

262. Wolfenson H, Lavelin I, Geiger B. Dynamic Regulation of the Structure and Functions of Integrin Adhesions. Dev Cell [Internet]. 2013 Mar;24(5):447–58. Available from: https://linkinghub.elsevier.com/retrieve/pii/S153458071300124X

263. Rao TC, Ma VP-Y, Blanchard A, Urner TM, Grandhi S, Salaita K, et al. EGFR activation attenuates the mechanical threshold for integrin tension and focal adhesion formation. J Cell Sci [Internet]. 2020 Jul 10;133(13). Available from: http://www.ncbi.nlm.nih.gov/pubmed/32546532

264. Tahyra ASC, Calado RT, Almeida F. The Role of Extracellular Vesicles in COVID-19 Pathology. Cells [Internet]. 2022 Aug 11;11(16):2496. Available from:

https://www.mdpi.com/2073-4409/11/16/2496

265. Jia Y, Wei Y. Modulators of MicroRNA Function in the Immune System. Int J Mol Sci [Internet]. 2020 Mar 29;21(7):2357. Available from: https://www.mdpi.com/1422-0067/21/7/2357

266. Li N, Parrish M, Chan TK, Yin L, Rai P, Yoshiyuki Y, et al. Influenza infection induces host DNA damage and dynamic DNA damage responses during tissue regeneration. Cell Mol Life Sci [Internet]. 2015 Aug;72(15):2973–88. Available from: http://www.ncbi.nlm.nih.gov/pubmed/25809161

267. Brentnall M, Rodriguez-Menocal L, De Guevara RL, Cepero E, Boise LH. Caspase-9, caspase-3 and caspase-7 have distinct roles during intrinsic apoptosis. BMC Cell Biol [Internet]. 2013 Dec 9;14(1):32. Available from: https://bmcmolcellbiol.biomedcentral.com/articles/10.1186/1471-2121-14-32

268. Ma K, Kwon SH, Padmanabhan J, Duscher D, Trotsyuk AA, Dong Y, et al. Controlled Delivery of a Focal Adhesion Kinase Inhibitor Results in Accelerated Wound Closure with Decreased Scar Formation. J Invest Dermatol [Internet]. 2018;138(11):2452–60. Available from: https://doi.org/10.1016/j.jid.2018.04.034

269. Mitchell HD, Eisfeld AJ, Stratton KG, Heller NC, Bramer LM, Wen J, et al. The Role of EGFR in Influenza Pathogenicity: Multiple Network-Based Approaches to Identify a Key Regulator of Non-lethal Infections. Front Cell Dev Biol [Internet]. 2019 Sep 20;7(SEP):1–14. Available from: https://www.frontiersin.org/article/10.3389/fcell.2019.00200/full

270. Baltimore D, Boldin MP, O'Connell RM, Rao DS, Taganov KD. MicroRNAs: new regulators of immune cell development and function. Nat Immunol [Internet]. 2008 Aug;9(8):839–45. Available from: http://www.ncbi.nlm.nih.gov/pubmed/18645592

271. Wang N, Liang H, Zen K. Molecular mechanisms that influence the macrophage m1-m2 polarization balance. Front Immunol [Internet]. 2014;5(NOV):614. Available from: http://www.ncbi.nlm.nih.gov/pubmed/25506346

272. Goncalves-Alves E, Saferding V, Schliehe C, Benson R, Kurowska-Stolarska M, Brunner JS, et al. MicroRNA-155 Controls T Helper Cell Activation During Viral Infection. Front Immunol [Internet]. 2019;10(JUN):1367. Available from: http://www.ncbi.nlm.nih.gov/pubmed/31275315

273. Oltean T, Van San E, Divert T, Vanden Berghe T, Saelens X, Maelfait J, et al. Viral dosing of

influenza A infection reveals involvement of RIPK3 and FADD, but not MLKL. Cell Death Dis [Internet]. 2021;12(5). Available from: http://dx.doi.org/10.1038/s41419-021-03746-0

274. Thompson MR, Kaminski JJ, Kurt-Jones EA, Fitzgerald KA. Pattern recognition receptors and the innate immune response to viral infection. Viruses [Internet]. 2011 Jun;3(6):920–40. Available from: http://www.ncbi.nlm.nih.gov/pubmed/21994762

275. Sharma A, Batra J, Stuchlik O, Reed MS, Pohl J, Chow VTK, et al. Influenza A Virus Nucleoprotein Activates the JNK Stress-Signaling Pathway for Viral Replication by Sequestering Host Filamin A Protein. Front Microbiol [Internet]. 2020 Sep 25;11(September):1–17. Available from: https://www.frontiersin.org/article/10.3389/fmicb.2020.581867/full

276. Mann M, Mehta A, Zhao JL, Lee K, Marinov GK, Garcia-Flores Y, et al. An NF-κB-microRNA regulatory network tunes macrophage inflammatory responses. Nat Commun [Internet]. 2017;8(1). Available from: http://dx.doi.org/10.1038/s41467-017-00972-z

277. Wang P, Hou J, Lin L, Wang C, Liu X, Li D, et al. Inducible microRNA-155 Feedback Promotes Type I IFN Signaling in Antiviral Innate Immunity by Targeting Suppressor of Cytokine Signaling 1. J Immunol [Internet]. 2010 Nov 15;185(10):6226–33. Available from: https://journals.aai.org/jimmunol/article/185/10/6226/82847/Inducible-microRNA-155-Feedback-Promotes-Type-I

278. Liu Y, Wan X, Yuan Y, Huang J, Jiang Y, Zhao K, et al. Opposite effects of miR-155 in the initial and later stages of lipopolysaccharide (LPS)-induced inflammatory response. J Zhejiang Univ B [Internet]. 2021 Jul 29;22(7):590–8. Available from: https://link.springer.com/10.1631/jzus.B2000826

279. Zhou H, Huang X, Cui H, Luo X, Tang Y, Chen S, et al. miR-155 and its star-form partner miR-155* cooperatively regulate type I interferon production by human plasmacytoid dendritic cells. Blood [Internet]. 2010 Dec 23;116(26):5885–94. Available from: https://ashpublications.org/blood/article/116/26/5885/28246/miR155-and-its-starform-partner-miR155

280. Li X, Wang S, Mu W, Barry J, Han A, Carpenter RL, et al. Reactive oxygen species reprogram macrophages to suppress antitumor immune response through the exosomal miR-155-5p/PD-L1 pathway. J Exp Clin Cancer Res [Internet]. 2022;41(1):1–19. Available from: https://doi.org/10.1186/s13046-022-02244-1

281. Zech A, Ayata CK, Pankratz F, Meyer A, Baudiß K, Cicko S, et al. MicroRNA-155 modulates

P2R signaling and Th2 priming of dendritic cells during allergic airway inflammation in mice. Allergy [Internet]. 2015 Sep;70(9):1121–9. Available from: https://onlinelibrary.wiley.com/doi/10.1111/all.12643

282. Jin HY, Gonzalez-Martin A, Miletic A V., Lai M, Knight S, Sabouri-Ghomi M, et al. Transfection of microRNA Mimics Should Be Used with Caution. Front Genet [Internet]. 2015 Dec 2;6(DEC):1–23. Available from: http://journal.frontiersin.org/Article/10.3389/fgene.2015.00340/abstract

283. Janas MM, Wang B, Harris AS, Aguiar M, Shaffer JM, Subrahmanyam YVBK, et al. Alternative RISC assembly: Binding and repression of microRNA–mRNA duplexes by human Ago proteins. RNA [Internet]. 2012 Nov;18(11):2041–55. Available from: http://rnajournal.cshlp.org/lookup/doi/10.1261/rna.035675.112

284. Fujita Y, Kadota T, Araya J, Ochiya T, Kuwano K. Extracellular Vesicles: New Players in Lung Immunity. Am J Respir Cell Mol Biol [Internet]. 2018 May;58(5):560–5. Available from: https://www.atsjournals.org/doi/10.1165/rcmb.2017-0293TR

285. Chan BD, Wong W, Lee MM, Cho WC, Yee BK, Kwan YW, et al. Exosomes in Inflammation and Inflammatory Disease. Proteomics [Internet]. 2019 Apr 22;19(8):1800149. Available from: https://onlinelibrary.wiley.com/doi/10.1002/pmic.201800149

286. Bartel S, La Grutta S, Cilluffo G, Perconti G, Bongiovanni A, Giallongo A, et al. Human airway epithelial extracellular vesicle miRNA signature is altered upon asthma development. Allergy [Internet]. 2020 Feb 2;75(2):346–56. Available from: https://onlinelibrary.wiley.com/doi/10.1111/all.14008

287. Dogrammatzis C, Deschamps T, Kalamvoki M. Biogenesis of Extracellular Vesicles during Herpes Simplex Virus 1 Infection: Role of the CD63 Tetraspanin. J Virol [Internet]. 2019 Jan 15;93(2):1–15. Available from: http://www.ncbi.nlm.nih.gov/pubmed/30355691

288. Wu N-H, Yang W, Beineke A, Dijkman R, Matrosovich M, Baumgärtner W, et al. The differentiated airway epithelium infected by influenza viruses maintains the barrier function despite a dramatic loss of ciliated cells. Sci Rep [Internet]. 2016 Dec 22;6(July):39668. Available from: http://www.ncbi.nlm.nih.gov/pubmed/28004801

289. Corsello T, Kudlicki AS, Garofalo RP, Casola A. Cigarette Smoke Condensate Exposure Changes RNA Content of Extracellular Vesicles Released from Small Airway Epithelial Cells. Cells [Internet]. 2019 Dec 17;8(12):1652. Available from: https://www.mdpi.com/2073-4409/8/12/1652

290. Li Y, Chan EY, Li J, Ni C, Peng X, Rosenzweig E, et al. MicroRNA Expression and Virulence in Pandemic Influenza Virus-Infected Mice. J Virol [Internet]. 2010 Mar 15;84(6):3023–32. Available from: https://journals.asm.org/doi/10.1128/JVI.02203-09

291. Jung AL, Møller Jørgensen M, Bæk R, Griss K, Han M, Auf Dem Brinke K, et al. Surface Proteome of Plasma Extracellular Vesicles as Biomarkers for Pneumonia and Acute Exacerbation of Chronic Obstructive Pulmonary Disease. J Infect Dis [Internet]. 2020 Jan 2;221(2):325–35. Available from: http://www.ncbi.nlm.nih.gov/pubmed/31617573

292. Ong J, Woldhuis RR, Boudewijn IM, van den Berg A, Kluiver J, Kok K, et al. Age-related gene and miRNA expression changes in airways of healthy individuals. Sci Rep [Internet]. 2019;9(1):1–8. Available from: http://dx.doi.org/10.1038/s41598-019-39873-0

293. Yin Q, Zhao Y-J, Ni W-J, Tang T-T, Wang Y, Cao J-Y, et al. MiR-155 deficiency protects renal tubular epithelial cells from telomeric and genomic DNA damage in cisplatin-induced acute kidney injury. Theranostics [Internet]. 2022;12(10):4753–66. Available from: http://www.ncbi.nlm.nih.gov/pubmed/35832084

294. Haroun RA-H, Osman WH, Amin RE, Hassan AK, Abo-Shanab WS, Eessa AM. Circulating plasma miR-155 is a potential biomarker for the detection of SARS-CoV-2 infection. Pathology [Internet]. 2022 Feb;54(1):104–10. Available from: http://www.ncbi.nlm.nih.gov/pubmed/34838331

295. Watson A, Wilkinson TMA. Respiratory viral infections in the elderly. Ther Adv Respir Dis [Internet]. 2021;15:1–17. Available from: https://doi.org/10.1177/1753466621995050

296. Espeland MA, Crimmins EM, Grossardt BR, Crandall JP, Gelfond JAL, Harris TB, et al. Clinical Trials Targeting Aging and Age-Related Multimorbidity. J Gerontol A Biol Sci Med Sci [Internet]. 2017 Mar 1;72(3):355–61. Available from: http://www.ncbi.nlm.nih.gov/pubmed/28364543

297. Fulop T, Larbi A, Dupuis G, Le Page A, Frost EH, Cohen AA, et al. Immunosenescence and Inflamm-Aging As Two Sides of the Same Coin: Friends or Foes? Front Immunol [Internet]. 2018 Jan 10;8(JAN). Available from: http://journal.frontiersin.org/article/10.3389/fimmu.2017.01960/full

298. Mensà E, Giuliani A, Matacchione G, Gurău F, Bonfigli AR, Romagnoli F, et al. Circulating miR-146a in healthy aging and type 2 diabetes: Age- and gender-specific trajectories. Mech Ageing Dev [Internet]. 2019;180(March):1–10. Available from: https://doi.org/10.1016/j.mad.2019.03.001

299. Vasa-Nicotera M, Chen H, Tucci P, Yang AL, Saintigny G, Menghini R, et al. MiR-146a is modulated in human endothelial cell with aging. Atherosclerosis [Internet]. 2011;217(2):326–30. Available from: http://dx.doi.org/10.1016/j.atherosclerosis.2011.03.034

300. Koltai E, Bori Z, Osvath P, Ihasz F, Peter S, Toth G, et al. Master athletes have higher miR-7, SIRT3 and SOD2 expression in skeletal muscle than age-matched sedentary controls. Redox Biol [Internet]. 2018;19(April):46–51. Available from: https://doi.org/10.1016/j.redox.2018.07.022

301. Sundar IK, Li D, Rahman I. Small RNA-sequence analysis of plasma-derived extracellular vesicle miRNAs in smokers and patients with chronic obstructive pulmonary disease as circulating biomarkers. J Extracell Vesicles [Internet]. 2019;8(1). Available from: https://doi.org/10.1080/20013078.2019.1684816

302. Klyachko NL, Arzt CJ, Li SM, Gololobova OA, Batrakova E V. Extracellular Vesicle-Based Therapeutics: Preclinical and Clinical Investigations. Pharmaceutics [Internet]. 2020 Dec 1;12(12):1171. Available from: https://www.mdpi.com/1999-4923/12/12/1171

303. Munir J, Yoon JK, Ryu S. Therapeutic miRNA-Enriched Extracellular Vesicles: Current Approaches and Future Prospects. Cells [Internet]. 2020 Oct 11;9(10):1–33. Available from: http://www.ncbi.nlm.nih.gov/pubmed/33050562

304. Abraham A, Krasnodembskaya A. Mesenchymal stem cell-derived extracellular vesicles for the treatment of acute respiratory distress syndrome. Stem Cells Transl Med [Internet]. 2020 Jan;9(1):28–38. Available from: http://www.ncbi.nlm.nih.gov/pubmed/31647191

305. Sun H, Burrola S, Wu J, Ding W-Q. Extracellular Vesicles in the Development of Cancer Therapeutics. Int J Mol Sci [Internet]. 2020 Aug 24;21(17):1–22. Available from: http://www.ncbi.nlm.nih.gov/pubmed/32847103

306. Soni S, O'Dea KP, Abe E, Khamdan M, Shah S V., Sarathchandra P, et al. Microvesicle-Mediated Communication Within the Alveolar Space: Mechanisms of Uptake by Epithelial Cells and Alveolar Macrophages. Front Immunol [Internet]. 2022;13(April):853769. Available from: http://www.ncbi.nlm.nih.gov/pubmed/35572508

307. Joshi BS, de Beer MA, Giepmans BNG, Zuhorn IS. Endocytosis of Extracellular Vesicles and Release of Their Cargo from Endosomes. ACS Nano [Internet]. 2020 Apr 28;14(4):4444–55. Available from: https://pubs.acs.org/doi/10.1021/acsnano.9b10033

308. Pasca S, Jurj A, Petrushev B, Tomuleasa C, Matei D. MicroRNA-155 Implication in M1 Polarization and the Impact in Inflammatory Diseases. Front Immunol [Internet]. 2020;11(April):625. Available from: http://www.ncbi.nlm.nih.gov/pubmed/32351507

309. Reiter K, Aguilar PP, Wetter V, Steppert P, Tover A, Jungbauer A. Separation of virus-like particles and extracellular vesicles by flow-through and heparin affinity chromatography. J Chromatogr A [Internet]. 2019;1588:77–84. Available from: https://doi.org/10.1016/j.chroma.2018.12.035

310. Shtyrya YA, Mochalova L V, Bovin N V. Influenza virus neuraminidase: structure and function. Acta Naturae [Internet]. 2009 Jul;1(2):26–32. Available from: http://www.ncbi.nlm.nih.gov/pubmed/22649600

311. Pesce E, Manfrini N, Cordiglieri C, Santi S, Bandera A, Gobbini A, et al. Exosomes Recovered From the Plasma of COVID-19 Patients Expose SARS-CoV-2 Spike-Derived Fragments and Contribute to the Adaptive Immune Response. Front Immunol [Internet]. 2021;12(January):785941. Available from: http://www.ncbi.nlm.nih.gov/pubmed/35111156

312. Coppinger JA, Cagney G, Toomey S, Kislinger T, Belton O, McRedmond JP, et al. Characterization of the proteins released from activated platelets leads to localization of novel platelet proteins in human atherosclerotic lesions. Blood [Internet]. 2004 Mar 15;103(6):2096–104. Available from: http://www.ncbi.nlm.nih.gov/pubmed/14630798

Appendix

Unsupervised filtering was performed using the following code:

```
counts <- read.csv("miRNA_countsRAW.csv",header = TRUE, row.name=1)

Filter <- 5

keep_tags <- rowSums(counts>10)>=Filter

counts_filtered<-counts[keep_tags,]

CPM<-cpm(counts_filtered)

dim(counts)

[1] 2632    10

dim(counts_filtered)

[1] 320   10
```

Violin plots were generated in R (v 4.1.1) using the following code:

```
cpm.log2<-cpm(counts, log=TRUE)

log2.cpm.df <- as_tibble(cpm.log2)

log2.cpm.df.melt <- melt(log2.cpm.df)

Log2.cpm.df.melt <- as_tibble(log2.cpm.df.melt)


par(cex=0.6,mar=c(5,10,10,15))

ggplot(Log2.cpm.df.melt, aes(x=variable, y=value, fill=variable)) +

  geom_violin(trim = FALSE, show.legend = FALSE) +

  ggtitle("Raw Violin Plot") +

  xlab("Sample") +

  ylab("log2CPM") +

  stat_summary(fun = "median", geom = "point", shape = 95, size = 10, color = "black", show.legend =
FALSE) +

  theme_bw(base_size = 20)
```

The presence of outliers was further investigated using IQR/Median plots using the following code:

```
Condition <-factor(Experimental_Design[,"Condition"],levels=c("Non_infected","Infected"))


col.cell <- c("orange","blue")[Condition]


IQR<-apply(CPM, 2, IQR)

Median<-apply(CPM, 2, median)

diff1<-mean(Median)-min(Median)

diff2<-max(Median)-mean(Median)

diff3<-mean(IQR)-min(IQR)

diff4<-max(IQR)-mean(IQR)


Xlim=c(mean(Median)-2*diff1,mean(Median)+2*diff2)

Ylim=c(mean(IQR)-2*diff3,mean(IQR)+2*diff4)


#  Make boxes for StDev.

Median_mean<-mean(Median)

c_sd1_mean<-sd(Median)

c_sd2_mean<-2*sd(Median)

c_sd3_mean<-3*sd(Median)

IQR_mean<-mean(IQR)

c_sd1_IQR<-sd(IQR)

c_sd2_IQR<-2*sd(IQR)

c_sd3_IQR<-3*sd(IQR)


x0_c<-Median_mean-c_sd1_mean

y0_c<-IQR_mean-c_sd1_IQR
```

```
x1_c<-Median_mean+c_sd1_mean

y1_c<-IQR_mean+c_sd1_IQR


x0_c.2<-Median_mean-c_sd2_mean

y0_c.2<-IQR_mean-c_sd2_IQR

x1_c.2<-Median_mean+c_sd2_mean

y1_c.2<-IQR_mean+c_sd2_IQR


x0_c.3<-Median_mean-c_sd3_mean

y0_c.3<-IQR_mean-c_sd3_IQR

x1_c.3<-Median_mean+c_sd3_mean

y1_c.3<-IQR_mean+c_sd3_IQR


plot(Median, IQR, main="IQR vs. Median TMM normaliztion CPM", type="n", xlim=Xlim,ylim=Ylim,
col=col.cell)

text(Median, IQR, labels=names(IQR),col=col.cell, cex=0.5)


segments(x0_c,y0_c, x1=x1_c, y1=y0_c, col="blue")

segments(x0_c,y0_c, x1=x0_c, y1=y1_c, col="blue")

segments(x1_c,y0_c, x1=x1_c, y1=y1_c, col="blue")

segments(x0_c,y1_c, x1=x1_c, y1=y1_c, col="blue")


segments(x0_c.2,y0_c.2, x1=x1_c.2, y1=y0_c.2, col="red")

segments(x0_c.2,y0_c.2, x1=x0_c.2, y1=y1_c.2, col="red")

segments(x1_c.2,y0_c.2, x1=x1_c.2, y1=y1_c.2, col="red")

segments(x0_c.2,y1_c.2, x1=x1_c.2, y1=y1_c.2, col="red")


segments(x0_c.3,y0_c.3, x1=x1_c.3, y1=y0_c.3, col="green")
```

```
segments(x0_c.3,y0_c.3, x1=x0_c.3, y1=y1_c.3, col="green")

segments(x1_c.3,y0_c.3, x1=x1_c.3, y1=y1_c.3, col="green")

segments(x0_c.3,y1_c.3, x1=x1_c.3, y1=y1_c.3, col="green")
```

The following code performs the TMM normalisation and generates a list of normalisation factors for each sample:

```
design <-model.matrix(~Condition)

eds<-DGEList(counts=counts_filtered,genes=rownames(counts_filtered))

eds<-calcNormFactors(eds,method="TMM")

eds<-estimateDisp(eds,design)
```

The PCA and plots were generated using the rgl package in R (v 3.8.2) using the function "prcomp" on the filtered CPM, using the following code:

```
CPM<-cpm(eds)

tCPM<-t(CPM)

pca<-prcomp(tCPM)


PC1<-pca$x[,1]

PC2<-pca$x[,2]

PC3<-pca$x[,3]

PCA_details<-cbind(PC1,PC2,PC3)


pca3d(pca, group=Condition, show.ellipses = TRUE, ellipse.ci=0.95, radius =4, axes.color =
"mistyrose4", palette=c(4,3), show.plane = FALSE, show.scale=FALSE, legend="topright")
```

Differential expression analysis was completed using edgeR method using the following code:

```
fit<-glmFit(eds, design)

colnames(fit)

lrt<-glmLRT(fit, coef=2)

colnames(fit)
```

```
topTags(lrt)

all_tags<-as.data.frame(topTags(lrt,n=nrow(eds)))

#  Rename first column

colnames(all_tags)[1]<-"Genes"

#  Generate summary of differentially expressed gene count and give names.

Summary<-summary(de <-decideTestsDGE(lrt))

rownames(Summary)<-c("Down-Regulated","Neither","Up-Regulated")

colnames(Summary)<-"Gene_count"

Summary

o <- order(lrt$table$PValue)

counts_per_M<-cpm(eds[o[1:length(o)],])

#  Merge everything into one object

all_results_EDGER<-cbind(all_tags,counts_per_M)

DE_results_EDGER<-all_results_EDGER[all_results_EDGER[,"FDR"]<=0.01,]
```